~~CONFIDENTIAL~~

MPR-SAT-FE-64-19
December 30, 1964
(Supersedes MPR-SAT-FE-64-17)

CLASSIFICATION CHANGED
TO - UNCLASSIFIED
By authority of E.O. No. 11652 Date 1/22/74
Changed by C. W. Kirkland

SATURN

MARSHALL SPACE FLIGHT CENTER — HUNTSVILLE, ALABAMA

RESULTS OF THE SEVENTH SATURN I LAUNCH VEHICLE TEST FLIGHT [U]

SA 7

~~Group 4~~
~~Downgraded at 3 year intervals;~~
~~declassified after 12 years~~

NATIONAL AERONAUTICS AND SPACE ADMINISTRATION

NASA

~~CONFIDENTIAL~~

RRF

[redacted]

This document contains information affecting the national defense of the United States within the meaning of the Espionage Law, Title 18, U.S.C., Sections 793 and 794 as amended. The revelation of its contents in any manner to an unauthorized person is prohibited by law.

C69-2739

GEORGE C. MARSHALL SPACE FLIGHT CENTER

MPR-SAT-FE-64-19

RESULTS OF THE SEVENTH SATURN I LAUNCH VEHICLE TEST FLIGHT

By Saturn Flight Evaluation Working Group

ABSTRACT

This report presents the results of the Early Engineering Evaluation of the SA-7 test flight. Third of the Block II Series, SA-7 was the second of the Saturn class vehicles to carry an Apollo Boilerplate, BP-15, Payload. The performance of each major vehicle system is discussed with special emphasis on malfunctions and deviations.

Test flight of SA-7 proved the capability of all vehicle systems. This was the first complete flight test utilizing the ST-124 for both stages and the second to demonstrate the closed loop performance of the path guidance during S-IV burn. The performance of the guidance system was successful and the insertion velocity was very near the expected value. All missions of the flight were successfully accomplished.

Any questions or comments pertaining to the information contained in this report are invited and should be directed to:

Director, George C. Marshall Space Flight Center
Huntsville, Alabama
Attention: Chairman, Saturn Flight Evaluation Working Group, R-AERO-F (Phone 876-2701)

~~CONFIDENTIAL~~

GEORGE C. MARSHALL SPACE FLIGHT CENTER

MPR-SAT-FE-64-19

January 31, 1966

(Supersedes MPR-SAT-64-17)

RESULTS OF THE SEVENTH SATURN I LAUNCH VEHICLE TEST FLIGHT

SATURN FLIGHT EVALUATION
WORKING GROUP

~~CONFIDENTIAL~~

ACKNOWLEDGEMENT

Contributions to this report were made by various elements of MSFC, John F. Kennedy Space Center, Douglas Aircraft Company, Chrysler Corporation, Rocketdyne and Pratt & Whitney. Without the joint efforts and assistance of these elements, this integrated report would not have been possible. The Saturn Flight Evaluation Working Group is especially indebted to the following for their major contributions:

John F. Kennedy Space Center
Douglas Aircraft Company
Chrysler Corporation Space Division
Pratt & Whitney
Rocketdyne

George C. Marshall Space Flight Center

Research and Development Operations

Aero-Astrodynamics Laboratory

Aero-Astrophysics Office
Aerodynamics Division
Flight Evaluation and Operations Studies Division

Astrionics Laboratory

Electrical Systems Integration Division
Flight Dynamics Branch
Guidance and Control Division
Instrumentation and Communications Division

Computation Laboratory

R& D Applications Division

Propulsion and Vehicle Engineering Laboratory

Propulsion Division
Structures Division
Vehicle Systems Division

TABLE OF CONTENTS

TABLE OF CONTENTS (Cont'd)

TABLE OF CONTENTS (Cont'd)

TABLE OF CONTENTS (Cont'd)

TABLE OF CONTENTS (Concluded)

LIST OF ILLUSTRATIONS

LIST OF ILLUSTRATIONS (Cont'd)

LIST OF ILLUSTRATIONS (Cont'd)

LIST OF ILLUSTRATIONS (Cont'd)

LIST OF ILLUSTRATIONS (Concluded)

LIST OF TABLES

ABBREVIATIONS AND SYMBOLS

Abbreviation	Definition
AGC	Automatic Gain Control
AOS	Assumption of Signal
BP	Boiler Plate
CDR	Command Destruct Receiver
CM	Command Module
CO	Cutoff
CSM	Combustion Stability Monitor
DDAS	Digital Data Acquisition System
DOD	Department of Defense
DTS	Data Transmission System
EBW	Exploding Bridge Wire
E. F.	Earth Fixed
EMF	Electro Motive Force
EMR	Engine Mixture Ratio
ETR	Eastern Test Range
GLOTRAC	Global Tracking System
GSE	Ground Support Equipment
IECO	Inboard Engine Cutoff
IETD	Inboard Engine Thrust Decay
IGOR	Intercept Ground Optical Recording
IP	Impact Position
LES	Launch Escape System
LOS	Loss of Signal
MISTRAM	Missile Trajectory Measurement System
MOTS	Minitrack Optical Tracking Station
MSFN	Manned Space Flight Network
MSL	Main Structure Level
NORAD	North American Air Defense Command
NPSH	Net Positive Suction Head
NPV	Non-Propulsive Vent
OECO	Outboard Engine Cutoff
OETD	Outboard Engine Thrust Decay
PAFB	Patrick Air Force Base
PAM	Pulse Amplitude Modulated
PCM	Pulse Code Modulated
PDM	Pulse Duration Modulated
PRA	Patrick Air Force Base, 1963 Reference Atmosphere
PU	Propellant Utilization
RC	Rough Combustion
RCS	Reaction Control System
ROTI	Recording Optical Tracking Instrument
RPS	Repeated Pressure Surges
RSS	Range Safety Signal
SAO	Smithsonian Astrophysical Observatory
SM	Service Module
SOX	Solid Oxygen
STADAN	Space Tracking and Data Acquisition Network
T/M	Telemetry
USA	Umbilical Swing Arm
VCO	Voltage Controlled Oscillator

CONVERSION FACTORS TO INTERNATIONAL SYSTEM OF UNITS OF 1960

Parameter	Multiply	By	To Obtain
acceleration	ft/s^2	3.048×10^{-1} (exact)	m/s^2
area	$in.^2$	6.4516×10^{-4} (exact)	m^2
barometer pressure	mbs	1.00×10^{-2} (exact)	N/cm^2
density	$slugs/ft^3$	$5.153788185 \times 10^{2}$	kg/m^3
energy	BTU	1.0543503×10^{3} (thermal chemical)	watt-s
mass flow rate	lb s/ft	4.5359237×10^{-1} (exact)	kg/s
force	lb	4.448221615	N (newton)
heating rate	BTU/ft^2-s	1.1348931 (thermal chemical)	$watt/cm^2$
impulse	lb-s	4.448221615	N-s
length	ft	3.048×10^{-1} (exact)	m
	in.	2.54×10^{-2} (exact)	m
mass	$lb\ s^2/ft$	4.5359237×10^{-1} (exact)	kg
moment	lb-ft	1.355817948	N-m
moment of inertia	$lb\text{-}ft\text{-}s^2$	1.355817948	$kg\text{-}m^2$
power	BTU/hr	2.9287508×10^{-4}	kw
pressure	$lb/in.^2$	$6.894757293 \times 10^{-1}$	N/cm^2
specific weight	lb/ft^3	1.57087468×10^{2}	N/m^3
temperature	°F+459.67	$5.555555556 \times 10^{-1}$	°K
velocity	ft/s	3.048×10^{-1} (exact)	m/s
volume	ft^3	$2.8316846592 \times 10^{-2}$ (exact)	m^3

NOTE: $g_o = 9.80665\ m/s^2$ (exact)

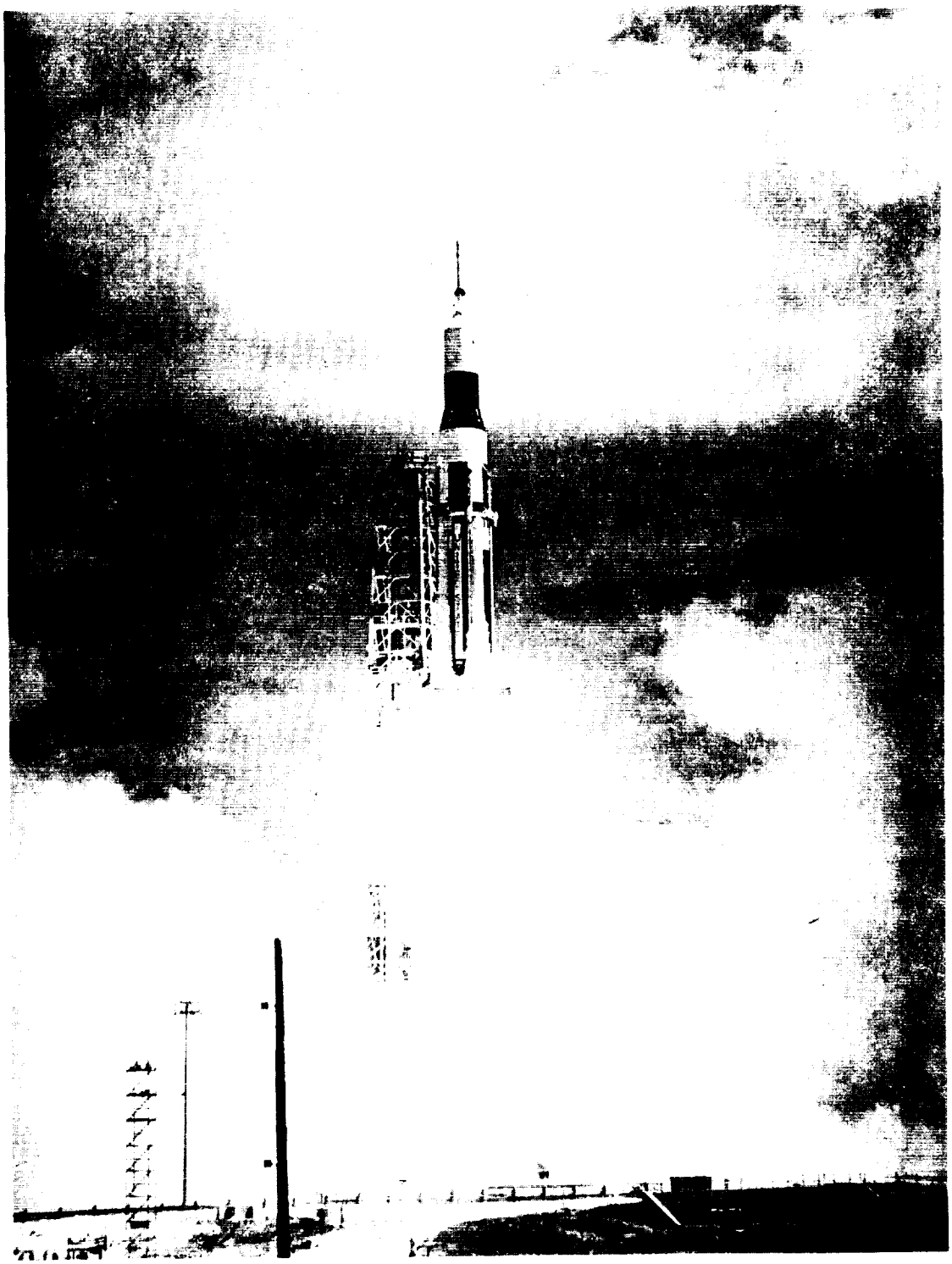

GEORGE C. MARSHALL SPACE FLIGHT CENTER

MPR-SAT-FE-64-19

RESULTS OF THE SEVENTH SATURN I LAUNCH VEHICLE TEST FLIGHT

By Saturn Flight Evaluation Working Group

SECTION I. FLIGHT TEST SUMMARY

1.1 FLIGHT TEST RESULTS

Saturn launch vehicle SA-7, third of the Block II vehicles, was launched at 11:22 AM EST on September 18, 1964. The flight test was a complete success with all missions being achieved.

SA-7 was the third Saturn vehicle launched from Complex 37B at Cape Kennedy and represents the second launch of a Saturn/Apollo configuration. The countdown of SA-7 was interrupted by four holds that lasted for a total of two hours and 42 minutes. The first hold came at T-245 minutes of the countdown and was caused by inadvertent firex system activation on the service structure during air conditioning duct removal. The hold lasted for 69 minutes. At T-30 minutes a scheduled 20-minute hold was extended 4 minutes when the S-IV LOX pressurizing regulator indicated a malfunction. The third hold, at T-12 minutes, lasted for 20 minutes. The hold resulted from a malfunctioning of the S-I hydraulic pump temperature OK interlock which prevented S-I hydraulic pumps from being turned on. The final hold was a range safety hold. Grand Turk Radar was operating intermittently. This hold was called at T-5 minutes; it lasted for 49 minutes. The count was recycled to T-13 minutes, resumed, and continued through launch.

The actual flight path of SA-7 deviated from nominal due to high S-I stage performance. Total velocity was 39.4 m/s higher than nominal at OECO and 1.8 m/s higher than nominal at S-IV cutoff. At S-IV cutoff the actual altitude was 0.99 km lower than nominal and the range was 13.72 km longer than nominal. The cross range velocity deviated 3.5 m/s to the left of nominal at S-IV cutoff. The S-IV payload at orbital insertion (S-IV cutoff + 10 sec) had a space-fixed velocity 2.8 m/s greater than nominal, a perigee altitude of 180.21 km and an apogee altitude of 231.10 km, giving a predicted lifetime of 3.8 days, 0.6 days longer than nominal. The extrapolated orbit based on data for an epoch of 10:57 Z, September 22, reached the estimated breakup altitude of 86 km at approximately 11:50 Z, September 22, at coordinates of 21.7 degrees S latitude and 56.4 degrees E longitude. The theoretical ballistic impact time is approximately 12:00 Z, September 22, at coordinates of 26.4 degrees latitude and 69.0 degrees E longitude.

The performance of both the S-I and S-IV stage propulsion systems was satisfactory for the SA-7 flight test. SA-7 was the third Saturn vehicle to employ H-1 engines at a thrust level of 836,000 N (188,000 lb_f) to provide thrust for the S-I stage. The vehicle longitudinal thrust of the S-I stage averaged between 0.92 percent (engine analysis) and 1.24 percent (flight simulation) higher than predicted. Vehicle specific impulse averaged between 0.71 percent (engine analysis) and 0.90 percent (flight simulation) higher than predicted. The performance of all subsystems was as expected for the flight test.

SA-7 also represented the third Saturn flight test of the RL10A-3 engine for the S-IV stage. The vehicle longitudinal thrust determined by engine analysis was approximately equal to predicted thrust, and the thrust determined by flight simulation was 0.89 percent lower than predicted. From engine analysis, the specific impulse was 0.02 percent higher than predicted, but was 0.98 percent lower than predicted based upon flight simulation. The performance of all S-IV subsystems was as expected for the flight test.

The overall performance of the SA-7 Guidance and Control System was satisfactory. The ST-124 system, along with control rate gyros, provided attitude and rate control for both stages. Partial load relief was accomplished by control accelerometers active in the control loop from 35 to 100 seconds. Vehicle response to all signals was properly executed including the roll maneuver, pitch program and path guidance during the S-IV stage flight. The counterclockwise roll moment, due to the unbalanced aerodynamic forces caused by the S-I turbine exhaust ducts, resulted in a roll attitude error of -3.5 degrees near 60 seconds. A large aerodynamic moment in both the pitch and yaw was required to simulate the telemetered control parameters during the S-I stage flight. The source of this moment has not been isolated.

Separation was executed smoothly with small control deviations experienced in the pitch and yaw plane. A larger than expected ullage rocket misalignment produced a significant roll deviation of 6.0 degrees. The ullage rocket misalignment in roll required to simulate this deviation was approximately 1.2 degrees compared to a 3σ RMS value for the four rockets of 1.4-degree.

Path guidance was initiated at 17.2 seconds after separation. Performance of the adaptive guidance mode in the pitch plane and delta minimum in yaw was satisfactory in achieving insertion conditions very near those desired.

A misalignment of the ST-124 stabilized platform occurred during the holddown period after ignition of S-I stage engines. The cause of this condition was traced to a high vibration of the leveling pendulums. This vibration of the pendulums is believed to have driven the platform out of alignment before it became space-fixed at liftoff. The total measured ST-124 guidance system space-fixed velocity at S-IV cutoff was 7806.0 m/s (7806.0 m/s was programmed for velocity cutoff). The total velocity at cutoff from tracking was 7807.8 m/s. Most of this deviation is due to the problem mentioned above.

The maximum bending moment experienced during the flight of SA-7 occurred at 74.7 seconds and indicated a maximum of approximately 30 percent of the design moment. Second mode bending frequencies were noted for a short period after separation, with the frequency gradually decreasing to near first mode prior to LES jettison. First mode bending was excited for a short period of time following LES jettison.

The vibration levels on the S-I stage were among the lowest ever exhibited by the Saturn vehicle. The S-IV vibrations were about the same as previously observed.

No unexpected environments were indicated for the SA-7 flight. Surface pressures and temperatures on the S-I and S-IV stages were in good agreement with past results. S-I stage base thermal environment was similar to previous flight results indicating maximum heating to the outer region. Simulation of the flame shield total heat rate indicated a level of 30-40 watts/cm^2 after approximately 70 seconds. This verifies that no convective cooling is present in this area as would be expected. Engine compartment temperatures indicated that no fires existed in the S-I base. Compartment pressures and loading on SA-7 were in good agreement with expected levels.

The S-I and Instrument Unit electrical systems operated satisfactorily during the boost and orbital phase of flight. All mission requirements were met. The life of the F6 and P1 telemeters was 129 minutes.

All S-IV electrical systems functioned properly. All power requirements were satisfactorily met, and sequenced commands were received and executed at the correct times.

Overall reliability of the SA-7 measuring system was 99.35 percent; this includes 8 measurement malfunctions that resulted in total loss of information. Operation of the three airborne tape recorders (one in the S-I, one in the IU and one in the S-IV stage) was very satisfactory. The playback records were free of retro flame attenuation effects. The passenger fire detection system, flown for the first time on SA-7, operated satisfactorily. No fires were indicated.

Ninety-one cameras provided optical coverage for launch of SA-7. Nine of the instruments failed due to a power failure on camera station 4.

Recovery of the 8 onboard cameras was impossible because of Hurricane Gladys. Two cameras were subsequently recovered after having been washed up on the beaches at San Salvador and Eleuthera Islands.

The Boilerplate Apollo Spacecraft (BP-15) performance was highly satisfactory with all spacecraft mission test objectives being fulfilled by the time of orbital insertion, and additional data were obtained by telemetry through the Manned Space Flight Network until the end of effective battery life during the fourth orbital pass.

1.2 TEST OBJECTIVES

The objectives of the SA-7 flight test were as follows:

1. Launch Vehicle Propulsion, Structural, Guidance and Control Flight Test with Boilerplate Apollo Payload - Achieved

2. First Complete Flight Test (Both Stages) Utilization of the ST-124 Platform System - Achieved

3. Second Flight to Demonstrate the Closed Loop Performance of the Path Guidance Scheme during S-IV burn using the ST-124 Guidance System - Achieved

4. Third Live Test of S-IV Stage - Achieved

5. Third Flight Test of Instrument Unit - Achieved

6. Demonstrate Physical Compatability of Launch Vehicle and the Second Apollo Boilerplate under Preflight, Launch and Flight Conditions - Achieved

7. Second Test of Guidance Velocity Cutoff (S-IV Stage) - Achieved

8. Third Test of S-I/S-IV Separation - Achieved

9. Third Launch From Complex 37B - Achieved

10. First Flight of Active ASC-15 Time Tilt Polynomial for S-I - Achieved

11. First Complete Flight Test (Both Stages) Using Control Rate Gyros in Closed Loop - Achieved

12. First Flight Test Demonstration of the Spacecraft's Alternate LES Tower Jettison Mode Utilizing the Launch Escape Motor and Pitch Control Motor-Achieved

13. First Test of the S-IV Stage Non-Propulsive Venting System - Achieved

14. First Test of S-I Engine Area Fire Detection System (Passenger Only) - Achieved

15. First Test Without S-IV LOX Tank Backup Pressurization System - Achieved

16. Recovery of 8 Movie Cameras Which View LOX Sloshing, Separation, Chilldown, etc - Not Achieved*

17. Third Orbital Flight of Burned Out S-IV Stage and Instrument Unit; Second Orbital Flight of Burned Out S-IV Stage, Instrument Unit and Apollo Boilerplate; Approximate Weight 17,700 kg(39,100 lbm) - Achieved.

* Two cameras were subsequently recovered after having been washed up on the beaches at San Salvador and Eleuthera Islands.

TABLE 1-I. TIMES OF EVENTS

Event	Range Time			Predicted		
	Actual	Pred	Act-Pred	Time From First Motion	Time From Guid Zero (Ti)	Time From OECO (TB3)
First Motion	0.06			0		
LO Signal (Umb Disc)	0.26			-		
Guidance Detects LO	0.27	0.27	0	-		
Guidance Computes Zero Time	0.33	0.33	0	-	0	
Brakes Released	10.96	10.96	0	-	10.63	
Load Ladders & Roll Command	11.28	11.28	0	-	10.95	
Pitch Command	12.88	12.88	0	-	12.55	
Roll Completed	26.4	26.35	0.05	-	26.02	
Lock Modules	136.59	136.59	0	-	136.26	
Level Sense	139.54	138.93	0.56	138.87	-	-8.0*
IECO	141.54	140.93	0.61	140.87	-	-6.0*
OECO	147.64	146.93	0.71	146.87	-	0
Ullage Rockets Ignite	148.34	147.63	0.71	-	-	0.7
Separation	148.44	147.73	0.71	-	-	0.8
Open S-IV Accumulators	149.24	148.53	0.71	-	-	1.6
S-IV Start	150.14	149.43	0.71	-	-	2.5
Jettison Ullage Rockets & LES	160.44	159.73	0.71	-	-	12.8
Introduce Guidance	165.67			-	-	18.19-18.89
Introduce Misalignment Corr.	172.07			-	-	23.95-24.65
Guidance Cutoff Signal	621.375	619.35	2.015	619.3	-	

*Time Base 2 (Low Level Sense)

SECTION II. INTRODUCTION

Saturn launch vehicle SA-7 was launched at 11:22 AM EST on September 18, 1964, from Saturn Launch Complex 37B, Eastern Test Range, Cape Kennedy, Florida. SA-7 was the seventh vehicle to be flight tested in the Saturn I R&D program and represents the third of the Block II series. The major mission of this test was to evaluate the performance of the complete launch vehicle system (two live stages) and to place into orbit the Apollo Boilerplate, BP-15, payload configuration. SA-7 represented the second flight test of the Apollo Boilerplate with a Saturn I Launch Vehicle.

This report presents the results of the Early Engineering Evaluation of the SA-7 test flight. Performance of each major vehicle system is discussed with special emphasis on malfunctions and deviations.

This report is published by the Saturn Flight Evaluation Working Group which is made up of representatives from all of Marshall Space Flight Center Laboratories, John F. Kennedy Space Center, MSFC's prime contractors for the S-I stage (Chrysler) and S-IV stage (Douglas Aircraft Company) and engine contractors (Rocketdyne and Pratt & Whitney). Therefore, the report represents the official MSFC position at this time. This report will not be followed by a similarly integrated report unless continued analysis and/or new evidence should prove the conclusion presented here partially or entirely wrong. Final evaluation reports may, however, be published by the MSFC Laboratories and the stage contractors covering some of the major systems and/or special subjects as required.

SECTION III. LAUNCH OPERATIONS

3.1 SUMMARY

Apollo/Saturn Vehicle SA-7 was launched from Pad 37B at Cape Kennedy, Florida. Ground support equipment and launch complex performance was satisfactory. Swing arm 3 was disconnected by mechanical release (swing arm rotation) instead of by the umbilical connector pneumatic system operation as it should have. Only minor damage normally encountered in a Saturn launch was sustained by these facilities.

The countdown of SA-7 was interrupted by four holds that lasted for a total of two hours and 42 minutes. The first hold came at T-245 minutes of the countdown and was caused by inadvertent firex system activation on the service structure during air conditioning duct removal. The hold lasted for 69 minutes. At T-30 minutes a scheduled 20-minute hold was extended 4 minutes when the S-IV LOX pressurizing regulator indicated a malfunction. The third hold, at T-12 minutes, lasted for 20 minutes. The hold resulted from a malfunctioning of the S-I hydraulic pump temperature OK interlock which prevented S-I hydraulic pumps from being turned on. The final hold was a range safety hold. Grand Turk Radar was operating intermittently. This hold was called at T-5 minutes; it lasted for 49 minutes. The count was recycled to T-13 minutes, resumed, and continued through launch.

The total propellant load based on delta pressure readings corrected for fuel tank temperature readings and environmental conditions was 520 kg (1147 lbm) less than the total load determined by discrete level probe data.

A number of problems concerning ETR instrumentation were encountered during the SA-7 countdown.

3.2 PRELAUNCH MILESTONES

Between June 7 and June 15, 1964, all stages arrived at KSC. A chronological summary of events and preparations leading to the launch of SA-7 is shown in Table 3-I.

3.3 ATMOSPHERIC CONDITIONS

At 11:22 AM EST, September 18, 1964, a high pressure cell of 1024 mb located in the Virginia-North Carolina area extended to the south and southwest dominating the eastern Gulf, Florida and upper Eastern Test Range areas. Surface winds in the vicinity of the launch site were easterly, 3 to 6.2 m/s. Cloudiness in the late hours of countdown and launch consisted of slowly developing cumulus clouds over the

TABLE 3-I PRELAUNCH MILESTONES

June 7, 1964	S-I and IU arrive at KSC via barge. Service Module and adapter arrive via aircraft.
June 8, 1964	IU and spacecraft adapter fit check.
June 9, 1964	S-I erection.
June 12, 1964	S-IV stage arrived via aircraft. S-I umbilical connections completed.
June 15, 1964	Command Module arrives via aircraft.
June 16, 1964	Integrated GSE-test completed.
June 17, 1964	S-IV weight and balance operation.
June 19, 1964	S-IV erection. IU erected for drill marking.
June 22, 1964	IU erected after drill operation completed. Swing arm qualification test completed.
June 23, 1964	Power applied to S-IV stage. IU umbilical connection.
June 24, 1964	S-I turbo pump torque test.
June 25, 1964	Power applied to IU.
June 26, 1964	Spacecraft erected. A crack in the LOX dome on one of the S-I engines was discovered. This problem resulted in all S-I engines being replaced.
July 7, 1964	S-I and IU power transfer test.
July 16, 1964	LOX simulation and malfunction test.

TABLE 3-I CONCLUDED

July 31, 1964	Last of the engine replacements (due to cracked LOX domes) was checked out electrically.
August 4, 1964	S-I and S-IV full pressure test.
August 6, 1964	Electrical mate of S-I, S-IV and IU.
August 7, 1964	Spacecraft electrical mate to launch vehicle. EBW and CDR test.
August 12, 1964	Sequence malfunction test.
August 17, 1964	Spacecraft LES erected.
August 19, 1964	All systems vehicle overall test.
August 27, 1964	Hurricane Cleo passed the area and launch complex was secured.
August 29, 1964	Plug drop and swing arm overall test.
September 3, 1964	Simulated flight test. A LES tower bolt failure was determined to be stress corrosion. The tower was removed to a remote area.
September 4, 1964	All tower bolts were exchanged and the LES reinstalled on the vehicle.
September 9, 1964	Hurricane Dora passed the area and the complex required complete securing.
September 12, 1964	RP-1 loading.
September 14, 15, 1964	Countdown demonstration test.
September 17, 1964	Launch countdown begun.
September 18, 1964	LAUNCH

mainland with a few convective cells over the Atlantic drifting westward in over the launch site. Radar scan information showed that the cells had tops to 3657 m and were slowly dissipating as they passed over the coastline. A high pressure ridge oriented NE-SW over the eastern Gulf area produced generally northeasterly winds aloft over the launch site.

At 11:00 AM EST, Hurricane Gladys was located at 26.4° N. 67.6° W. or approximately 644 km on a bearing of 032 degrees from Grand Turk. Gladys was moving toward the west northwest at 4 m/s. Highest winds were estimated at 56.6 m/s, or a little less, near the center with hurricane force winds extending out 145 km to the northeast and 72 km to the southwest. Gales extended outward 346 km in the northeast semicircle and 241 km to the southwest of the center.

Because of the condition of the seas in the vicinity of the recovery area, camera capsule recovery was not attempted. However, two of the eight cameras were discovered approximately 50 days after launch.

The following are specific observations at launch:

1. Pressure - 1017.3 mean sea level in millibars

2. Temperature - 303°K

3. Dewpoint - 295°K

4. Relative Humidity - 64%

5. Surface Winds - From the easterly direction at 3.4 m/s.

6. Cloud Coverage - One cumulus cloud at 823 m base, five alto-cumulus clouds at an estimated height of 3352 m base, and one cirrus cloud at an unknown height.

7. Precipitation - Showers in the vicinity of Hurricane Gladys.

3.4 COUNTDOWN

The Saturn/Apollo launch countdown is divided into two parts, each performed at different time intervals. Part I, begins at T-1035 minutes and

proceeds to T-545 minutes. Part II picks up at T-545 minutes and continues through launch.

3.4.1 COUNTDOWN, PART II

Part II of the countdown was picked up at 11:25 PM EST, September 17, 1964, at T-545 minutes and was continuous until T-245 minutes, when a hold was caused by inadvertent firex system activation on the service structure during air-conditioning duct removal. The water entered one S-IV umbilical connector which, in turn, produced erroneous indications of S-IV engine exciter firing. Power was removed from the S-IV stage and moisture dried from the connector. After reconnection all indications were normal and the count was picked up 69 minutes later.

The count was then continuous until T-30 minutes when a scheduled hold was initiated. During this scheduled 21-minute hold, the S-IV LOX pressurizing regulator indicated a malfunction. Analysis of the problem indicated normal and satisfactory operation. By this time, the hold had been extended four minutes longer than scheduled. The count progressed to T-12 minutes when it was again interrupted because of malfunctioning S-I hydraulic pump temperature OK interlock, which prevented S-I hydraulic pumps from being turned on. Since measurements indicated normal temperature, the interlock was jumpered in a blockhouse distributor. Hold time was 20 minutes.

The count was resumed at T-12 minutes and progressed to T-5 minutes when a range safety hold was called because of intermittent operation of the Grand Turk radar. Due to S-IV LOX bubbling and spacecraft battery lifetime constraints, the count was recycled to T-13 minutes. During the hold, difficulty was encountered with the swing arm hydraulic test. This problem was corrected without adding to the range hold by a jumper in a blockhouse distributor. After 49 minutes, the radar problem was corrected, and the count resumed and continued through liftoff which occurred at 1122:43.26 EST.

3.4.2 COUNTDOWN PROBLEM AREAS

The major difficulties encountered during the SA-7 countdown are listed in Table 3-II. Figure 3-1 shows hold time versus count time.

A number of the problems listed in Table 3-II concerned Eastern Test Range, ETR, instrumentation. These items are marked with an asterisk in Table 3-II.

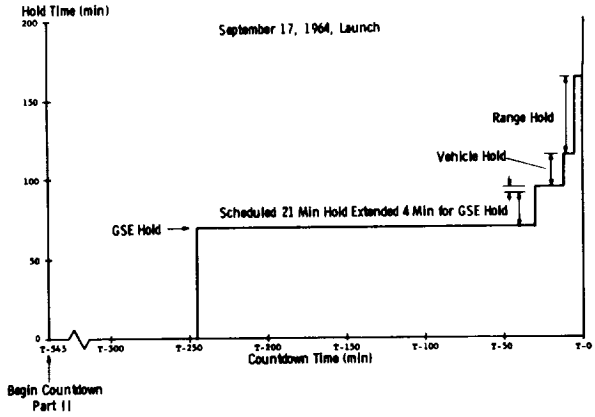

FIGURE 3-1. HOLD TIME VERSUS COUNT TIME

3.5 PROPELLANT LOADING

There were no propellant transfer system problem areas or malfunctions in the SA-7 launch countdown.

3.5.1 S-I STAGE

The S-I stage LOX tanks were loaded to a predetermined weight. The fuel weight was to be adjusted to compensate for variations in bulk fuel specific weight at launch. A fuel specific weight check was made at T-25 minutes on the initial countdown. At this time, S-I tank temperature indicated the average bulk fuel specific weight to be 99.55 percent of nominal 7935.9 N/m^3 (50.519 lb/ft^3). To account for the anticipated increase in specific weight between that time and ignition, the fuel correction was based on a fuel specific weight of 99.58 percent. A correction of -0.090 N/cm^2 (-0.130 psi) was dialed into the fuel level computer and the semi-automatic loading system began to correct the fuel load.

At T-10 minutes, fuel tank temperatures indicated the average bulk fuel specific weight to be 7907.3 N/m^3 (50.337 lb/ft^3). Allowing for a slight temperature decrease during the remaining time of countdown, the fuel specific weight at T-3 minutes was 7908.9 N/m^3 (50.347 lb/ft^3). LOX tank temperature indicated the mean LOX specific weight to be 11,061 N/m^3 (70.41 lb/ft^3). Based on these specific weights and recorded wind conditions, the average delta pressure readings show the propellant weights at T-3 minutes to be 277,951 kg (612,777 lb) of LOX and 123,530 kg (272,337 lb) of fuel.

Discrete probe activation times were telemetered during the flight. Analysis of these data gives an

TABLE 3-II. SPECIFIC PROBLEM AREAS DURING COUNTDOWN

1.	T-795 Minutes:	Initial S-IV LH_2 tank gas sample contained excessive moisture necessitating several tank-purge cycles. As a result, the start of S-IV ordnance installation was delayed approximately 80 minutes.
2.	T-740 Minutes:	The vacuum jacket on LH_2 skid inlet line would not hold vacuum. Investigation proved the inner line to be intact. The leak in the vacuum jacket could not be located. All welds and fittings in the jacket were coated with sealant to minimize the leakage problem. No delay resulted.
3.	T-365 Minutes:	Inadvertent firex system activation on the service structure drenched the S-IV stage. Water entered one electrical umbilical connector which, in turn, produced erroneous indications of engine #1 and helium heater igniter exciter firing. Power was removed from the S-IV stage and the connector was dried. Associated circuitry was functionall· checked. The above resulted in a hold at T-245 min of 69 min duration.
4.	T-357 Minutes:	S-I fuel depletion sensor #1 gave an indication of depletion. Since the sensor was one of two redundant probes, fuel bay #2 was reopened and the probe electrically disconnected. No delay resulted.
5.	T-220 Minutes:	S-IV fire detection system indicated fire at the S-IV LH_2 skid during S-IV LOX loading. The indication was determined to be erroneous and the result of corrosion in a connector in the resistance wire circuitry. The system was not considered usable for launch and was not used further. No delays resulted.
6.	T-120 Minutes:	*The 91.18 radar at Antigua was reported non-operational with a 24 hour estimated repair time. The MPS-26 radar also located at Antigua was being dismantled and therefore could not be utilized as a backup system. However, the Grand Turk radar was still operational and it was decided to continue preparations for launch. The Antigua station is the primary station for cutoff and orbital insertion data.
7.	T-37 Minutes:	S-IV cold helium regulator outlet pressure appeared to exceed red-line values. Several functional cycles were accomplished to verify indications before it was discovered that the problem was one of data misinterpretation only. This problem delayed resuming the count at T-30 for approximately 5 minutes.
8.	T-30 Minutes:	*The C-Band 5.16 radar at San Salvador was experiencing interference due to a commercial ship with its navigation radar operating within the C-Band. It was determined that Grand Turk Radar (7.18) would provide the necessary data. No delay resulted.
9.	T-19 Minutes:	*For a period of approximately four minutes the Valkaria Mistram site was non-operational. However, at T-15 it was reported operational. Since SA-7 was using a new Azusa antenna, which lowered the confidence in obtaining Azusa data, the loss of Valkaria Mistram site posed a potential loss of range safety and metric data.
10.	T-12 Minutes:	The S-I auxiliary hydraulic pumps were turned on for the initiation of steering commands. Pumps #1 and #2 came on satisfactorily. When pump #3 was turned on, the motor temperature OK relay dropped out. In turn, the OK-to-start hydraulic pumps lights went out and pumps #1 and #2 shut down. This is the normal sequence for the stated malfunction. Since measurements indicated normal temperatures, the OK-to-start hydraulic pumps indication interlock was removed from the circuit by means of a jumper.
		*During the same time frame, the IU C-Band beacon readout from the range indicated marginal performance for metric data. The beacon readout improved with time and was termed "Go". The total hold time was 20 minutes.
11.	T-8 Minutes:	During the automatic bleed test of the umbilical swing arms the panel operator actuated the "Auto Test" switch for an excessive length of time. The electrical system locked itself in, requiring that a jumper be installed to unlock the system and to prevent the test from running continuously. This was accomplished during the Range Safety hold that followed.
12.	T-5 Minutes:	*Grand Turk radar (7.18) operation became intermittent, resulting in a Range Safety hold. Due to S-IV LOX bubbling and spacecraft battery constraints, the count was recycled to T-13 minutes. The total duration of hold was 49 minutes.
		*During the above Range Safety hold, the Data Transmission System (DTS) for the IGOR's and ROTI's was reported non-operational. This presented a potential loss of optical coverage since focusing data and angular tracking data are transmitted to these cameras from the radars by this system. This system was reported operational just prior to resuming count.
		*During the period of preparing the vehicle to resume count, the Azusa Mk II lost its zero reference. This system was to provide powered flight range safety and metric data. At 11:05 EST the system had obtained zero set and was again operational.

*ETR Instrumentation Problems

accurate indication of propellant volume flow rates. Using specific weights determined from tank temperatures, the propellant load corresponding to these flow rates was 277,862 kg (613,582 lb) of LOX and 124,139 kg (273,679 lb) of fuel. This load is considered to be the best estimate of the actual propellant loaded. Approximately 340 kg (752 lbm) in the engine fuel jackets are not included in the above load. The total weights are reflected in the ignition weights shown in the mass tables in Section IV.

The upper portion of Figure 3-2 is a fuel specific weight versus temperature curve for SA-7 with applicable prelaunch and flight data included. The lower portion of Figure 3-2 shows the launch day predicted and indicated propellant loads versus fuel specific weight with applicable weight information included.

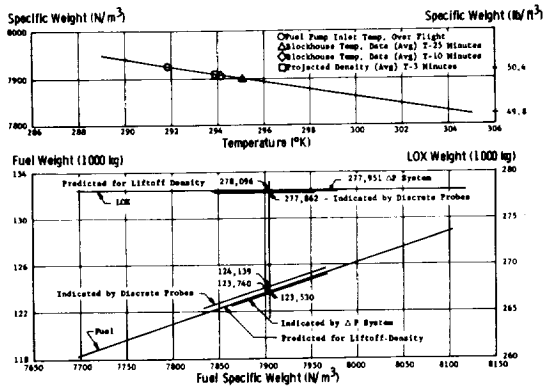

FIGURE 3-2. S-I STAGE PROPELLANT TANKING PARAMETERS

Temperatures experienced in the outer LOX tanks were approximately 1°K higher than the center tank temperatures. The higher temperatures resulted in a lower mean LOX specific weight than predicted. Reconstructed flow rate data, in conjunction with mean specific weight, indicated that LOX was shortloaded by 234 kg (516 lb). Reconstruction of flow rate and discrete level probe data indicated that fuel was overloaded by 609 kg (1342 lb) when compared to the ΔP loading system. The total propellant load based on delta pressure readings from the loading system was 520 kg (1147 lb) less than the total load determined by discrete level probe data. This difference is within the specification value of ±0.25 percent of total propellant tanked.

3.5.2 S-IV STAGE

3.5.2.1 LOX

The oxidizer system was successfully loaded with LOX by cooling down and filling in two phases: (1) main fill, and (2) replenish. The automated LOX loading system, in conjunction with the LOX supply pump, was successfully utilized for loading the LOX tank. Loading of LOX into the S-IV stage was initiated 5 hours and 47 minutes prior to liftoff.

The LOX vent valves remained open throughout the loading operation. The LOX transfer line had been precooled for approximately 12 minutes prior to the initiation of LOX main fill. The LOX main fill line pressure reached a maximum of 141 N/cm^2 (205 psi) and stabilized at approximately 139 N/cm^2 (202 psi). At approximately the 10 percent level, a stabilized loading rate of 745 gpm was reached. This loading rate was maintained until the 98 percent mass level was reached at 25 minutes and 30 seconds after initiation of the LOX transfer line precool. The loading system then closed the main LOX fill valve as scheduled. After the cooldown of the S-I and S-IV LOX replenish systems was completed, the cycle replenishing operation was initiated. During this operation, the LOX in the tank was allowed to boil off to the 99.5 percent level. It was then replenished to the 99.75 percent mass level at a rate of approximately 200 gpm. This replenishing cycle continued until tank prepressurization was initiated. The LOX tank was pressurized during loading of the LH_2 tank. After LH_2 fill was completed, the LOX tank vent valves were opened and the LOX replenishing cycle was resumed. The cycle was continued until the start of the 150-second automatic count. At this time the tank was again pressurized, and the final LOX replenishing was completed. The LOX load at S-I ignition command was 38,225 kg (84,271 lbm).

3.5.2.2 LH_2

The fuel system was satisfactorily loaded with LH_2 by cooling down and filling in four stages: (1) initial fill, (2) main fill, (3) replenish, and (4) reduced replenish. The automatic fuel-loading system was successfully utilized for loading the LH_2 tank. Loading of LH_2 into the S-IV stage was initiated 3 hours, 16 minutes and 13 seconds before liftoff.

The LH_2 transfer line had been precooled for approximately 5 minutes prior to the initiation of LH_2 initial fill. The LH_2 transfer line cooldown was accomplished through the helium precool heat exchanger and the stage LH_2 tank. The LH_2 initial fill was accomplished with an LH_2 transfer line pressure of 17.2 N/cm^2 (25 psi) and with the LH_2 tank vents open. The stage loading was initiated at approximately 430 gpm. During this initial fill operation, the LH_2 tank ullage pressure was monitored; however, the tank pressure did not decrease below the prefill ambient pressure.

At approximately the 15 percent mass level, main fill was initiated, and the loading rate was increased to approximately 1960 gpm. When the 95.5 percent level was reached at approximately 30 minutes after initiation of LH_2 precool, the main fill valve closed automatically. LH_2 replenish continued with normal automatic operation until pickup of the 99.25 percent mass level. Reduced replenish was then initiated to increase the LH_2 mass level cycling between the 99.25 and the 99.5 percent level.

During the 150-second automatic count, the automatic loading system was used to complete the final replenish operation to the 100 percent mass indication. The LH_2 load at S-I ignition command was 7,772 kg (17,134 lbm).

3.6 HOLDDOWN

3.6.1 COMBUSTION STABILITY MONITOR

The S-I stage Combustion Stability Monitor and all associated recording equipment performed satisfactorily during the launch.

Measurement	Engine	Maximum G_{rms}	Average G_{rms}
XE57-1	1	35	15
XE57-2	2	36	15
XE57-3	3	>100	15
XE57-4	4	32	15
XE57-5	5	30	15
XE57-6	6	20	18
XE57-7	7	20	15
XE57-8	8	25	13

See Section VI, Propulsion, for additional information concerning the combustion stability monitor on engine 3.

3.6.2 FIRE DETECTION MONITOR

The S-I stage Fire Detection Monitor and all associated recording equipment performed satisfactorily during launch. No temperature rise was noted.

3.7 GROUND SUPPORT EQUIPMENT

3.7.1 ELECTRICAL SUPPORT EQUIPMENT

The electrical support equipment responded and performed as designed during the SA-7 countdown and automatic sequence. A switch jumper was installed to bypass the vehicle engine 3 hydraulic-temperature OK switch which malfunctioned. This jumper was removed after launch sequence start by opening the switch. This interlock is not required after launch sequence start, and the jumper would have prevented the four hydraulic pumps from being deenergized at "all engines running." An additional "momentary" jumper was necessary at T-8 minutes to unlatch a circuit in the swing arm hydraulic systems. This circuit will be modified for SA-9.

3.7.2 COMPUTER

Power to the RCA 110 Computer was applied at 9:50 PM, August 17, 1964, to perform preventive maintenance checks, computer verification tests, and system interface checkout tests. At approximately 11:00 PM, the operational launch programs were loaded into the computer to support the launch countdown.

The computer was in operation for approximately 14.5 hours in support of the launch. At T-245 minutes, the paper tape reader did not function properly. A backup system was utilized, after which the test progressed satisfactorily.

3.7.3 MECHANICAL GROUND SUPPORT EQUIPMENT

The active ground support equipment including the launcher, engine service platform, holddown arms, firing accessories, umbilical swing arms, environmental control system, and pneumatic distribution system sustained the launch of SA-7 with less damage than in any previous Saturn launch. The added reinforcement, shielding and insulation of the ground support equipment protected the systems to the extent that no assembly was damaged beyond repair, as known at this time. As was expected, equipment above and below the launcher sustained only minor damage.

No significant damage was noted to the launcher, engine service platform, or main structure of the firing accessories. Electrical cables, pneumatic flex lines water quench hoses, and cryogenic and fuel flex hoses and bellows were burned beyond repair, but generally only portions of these were completely destroyed. An inspection of the holddown arms revealed that no appreciable damage was sustained by them.

The environmental control system sustained the launch with negligible damage. Insulation covers that were blown from several places on the launcher and boattail ECS ducts during the launch of SA-6 sustained negligible damage during the SA-7 launch because of better shielding provisions.

A visual inspection of the Umbilical Swing Arm (USA) system revealed blast damage in the following areas: Access platform roofs blown off on USA Nos. 1, 2 and 3, access platform door and door housing blown loose on USA 2, accumulator pressure gauge damaged at USA No. 1 Control Panel, frayed housing retract lanyards on USA Nos. 3 and 4. Minor damage occurred on umbilical arms 1 and 3 A/C duct insulation.

A frayed section of the Q-ball retract cable was noted. The camera purge pressure gauge in valve panel 9 was damaged. No damage was observed on the umbilical tower pneumatic systems. Insulation on the spacecraft cooling system (Water/Glycol) supply and return lines was burned away in the area of the umbilical 11 m (35 ft) level.

A review of the launch records available to date indicates that all active ground support equipment systems performed within design specifications. One deficiency was noted.

Only three of the four swing arms functioned properly. The LH_2 vent line on arm 3 did not disconnect as it should have when the umbilical pneumatic system operated. Instead, arm 3 disconnected when the mechanical release was actuated by the swing arm rotation. This malfunction was observed in the SA-7 film analysis. The film clearly showed that the pneumatic disconnect did not operate, and consequently there was a hydraulic lanyard disconnect during launch. At the time of the IU umbilical separation, an initial movement of the vent disconnect was observed indicating that there was some pneumatic pressure on the pneumatic cylinders. This initial movement indicated that some pneumatic force was exerted. However, it has been concluded that the complete opening of the solenoid valve, for the duration of time required, did not take place.

The film analysis also indicates that venting occurred through the LOX umbilical drain lines for from 4 to 5 seconds after liftoff. This has been attributed to a configuration change since the S-IV umbilical drain was connected to the S-I vent. The S-I vent lines were not precooled, and therefore resulted in a LOX boil when the LOX flowed into the lines. This caused a 13.8 N/cm^2 (20 psi) back pressure. The effect of this back pressure was the venting observed in the film.

Damage normally encountered by these facilities was sustained by the launch of SA-7. Wiring, relays and transformers were damaged in the elevator equipment at the northeast corner of the launch pedestal.

The flame deflector sustained minor damage and can be used for the third time. The majority of the damage was to tubing that served communication equipment, cameras, etc. The third and fourth levels of the umbilical tower sustained minor damage to gauges, relief valves and tubing of the GN_2 hazard proofing system.

3.8 LAUNCH FACILITY MEASUREMENTS

3.8.1 BLOCKHOUSE REDLINE VALUES

Blockhouse redline values are limits placed on certain critical engine and vehicle parameters to indicate safe ignition and launch conditions. The measurements are monitored in the blockhouse during countdown. Since these specified limits apply to parameters which are critical to vehicle performance and, in turn, mission success, the countdown procedure may be halted if any redline system value falls outside its assigned limits. Whether launch procedure is halted or continues depends upon the validity placed in the indicated measurement value and the danger imposed by the value in question. If the value poses a threat to vehicle performance, launch will be delayed until the problem is corrected.

All redline values were within the required limits, and no holds were necessary because of redline parameters.

3.8.2 SOUND LEVEL MEASUREMENTS

Sound pressure levels recorded during SA-7 launch were generally in agreement with those of SA-6. There was no evidence of sound focusing during this launch. This was in agreement with rawinsonde information which gave no evidence of thermal gradients that could result in focusing.

Sound level measurements were made in three regions defined by relative distance of the transducer from the launcher. These regions are termed "Far Field," "Mid Field," and "Near Field." In addition, three recording stations were located in the AGCS rooms at LC-37.

The maximum "Far Field" (Cape Kennedy area) sound level measured was 113 db, recorded by the station located at Hangar D.

The maximum "Mid Field," 365.8 m (1200 ft) radius from vehicle, sound level measured was 156 db, recorded at stations 25K05 located 64 m (210 ft) 178 degrees azimuth, 66 degrees angular coordinates.

The maximum "Near Field" (umbilical tower) sound level measured was 164 db. All "Near Field" transducers are located on the umbilical tower from approximately the 12 m (41 ft) level to the 77.1 m (253 ft) level.

All acoustical db levels are referenced to 0.002 microbar (0 db).

SECTION IV. MASS CHARACTERISTICS

4.1 VEHICLE MASS

The total vehicle mass was approximately 519,600 kg (1,145,400 lbm) at S-I ignition, 65,500 kg (144,400 lbm) at S-IV ignition and 17,760 kg (39,160 lbm) in orbit. The orbital payload included approximately 1300 kg (2860 lbm) ballast. Approximate booster propellant mainstage consumption during S-I powered flight (ignition to OECO) was 397,900 kg (877,200 lbm). The approximate S-IV stage propellant (mainstage) consumption was 44,600 kg (98,350 lbm) during powered flight (see Figs. 4-1 and 4-2). Table 4-I is a vehicle mass breakdown at significant flight events. A flight sequence mass summary is given in Table 4-II. The predicted masses presented in this section are those presented in Reference 1.

4.2 VEHICLE CENTER OF GRAVITY AND MOMENTS OF INERTIA

Longitudinal and radial center of gravity and roll and pitch moments of inertia are given in Table 4-III. These parameters are plotted versus burning time in Figures 4-1 and 4-2.

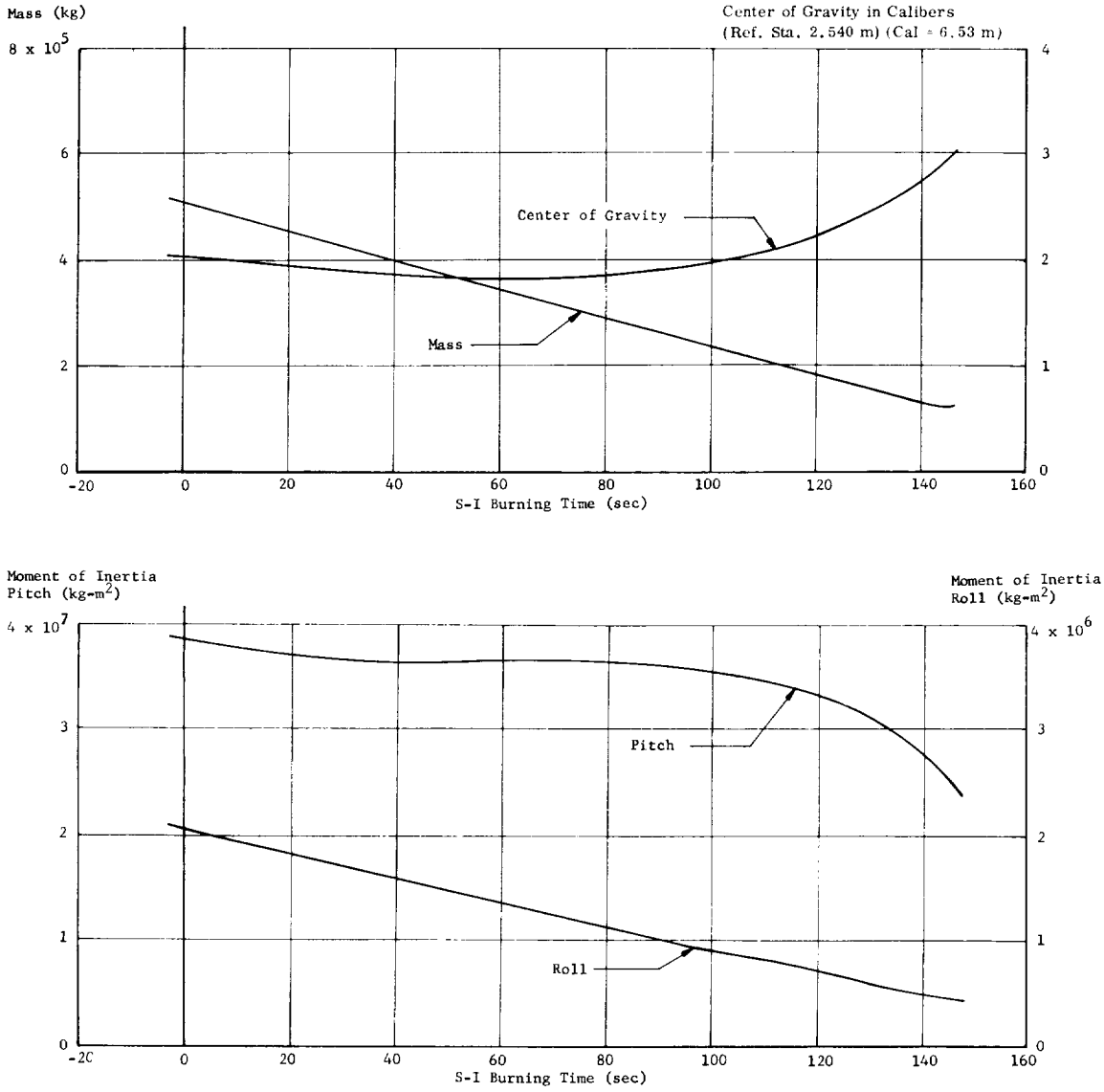

FIGURE 4-1. VEHICLE MASS, CENTER OF GRAVITY AND MASS MOMENT OF INERTIA

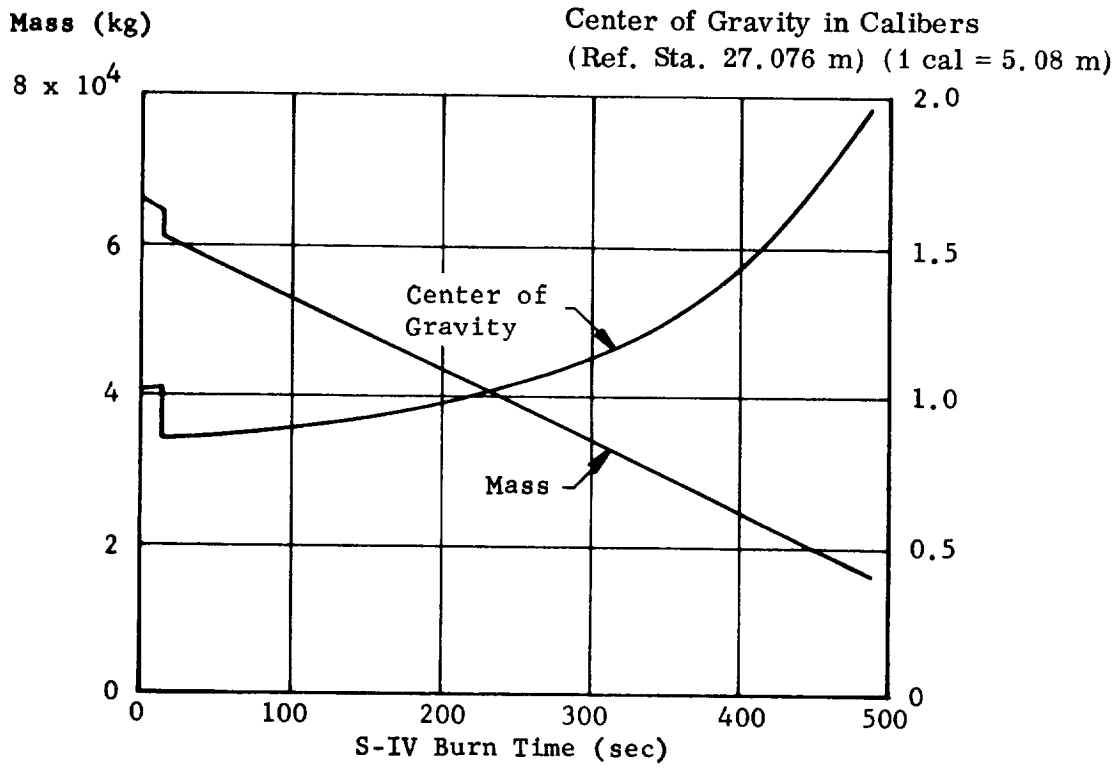

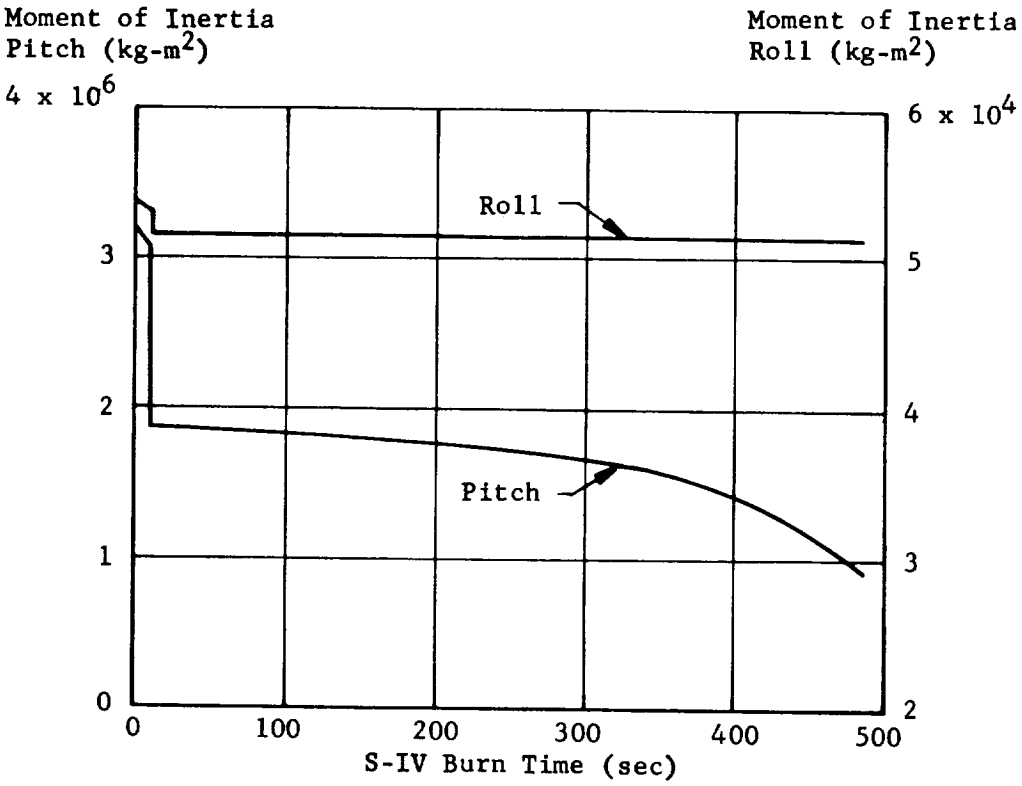

FIGURE 4-2. VEHICLE MASS, CENTER OF GRAVITY AND MASS MOMENT OF INERTIA

TABLE 4-I. VEHICLE MASSES

EVENT	IGNITION COMMAND		FIRST MOTION		OUTBOARD ENGINE CUTOFF		SEPARATION		S-IV STAGE IGNITION COMMAND		S-IV STAGE CUTOFF		S-IV STAGE END OF THRUST DECAY	
	Pred*	Actual	Pred*	Actual	Pred*	Actual	Pred*	Actual	Pred*	Actual	Pred*	Actual	Pred*	Actual
RANGE TIME (sec)	-3.04	-3.06	0	0.06	146.93	147.64	147.73	148.44	149.43	150.14	619.35	621.38	621.67	624.0
MASS (kg)														
S-I Stage, Dry	48,761	48,784	48,761	48,784	48,761	48,784	48,761	48,784						
LOX	278,096	277,862	273,202	273,033	1,769	1,991	1,469	1,682						
RP-1	121,817	124,479	120,417	123,061	2,778	2,453	2,410	2,072						
LOX Ullage Gas (GOX & He)	56	58	66	66	1,787	1,680	1,787	1,680						
Helium	3	3	3	3	3	3	3	3						
Hydraulic Oil	13	13	13	13	13	13	13	13						
Retro Rocket Propellant	614	614	614	614	614	614	614	614						
Frost	454	454	454	454	0	0	0	0						
Oronite	14	14	14	16	0	0	0	0						
N_2	386	381	385	381	305	308	298	302						
Total S-I Stage	450,214	452,662	443,929	448,423	56,030	55,846	55,355	55,150						
S-I/S-IV Interstage	1,087	1,111	1,087	1,111	958	982	958	982						
S-IV Stage, Dry	6,135	6,145	6,135	6,145	6,135	6,145	6,135	6,145	6,135	6,145	6,135	6,145	6,135	6,145
LOX	38,195	38,225	38,195	38,225	38,157	38,178	38,153	38,173	38,144	38,163	88	1,001	64	977
LH_2	7,722	7,772	7,722	7,772	7,612	7,664	7,609	7,662	7,604	7,657	32	209	26	203
LOX Ullage Gas (GOX & He)	15	11	15	11	16	16	16	16	16	16	104	105	104	105
LH_2 Ullage Gas (GH_2 & He)	11	14	11	14	13	16	14	16	14	16	69	55	69	55
Other Helium	59	61	59	61	58	60	58	60	58	60	21	22	21	22
Ullage Rocket Propellant	110	110	110	110	110	110	106	108	44	44	0	0	0	0
Ullage Rocket Cases	127	126	127	126	127	126	127	126	127	126	0	0	0	0
Frost	41	77	41	77	0	12	0	0	0	0	0	0	0	0
Total S-IV Stage	52,415	52,541	52,415	52,541	52,228	52,327	52,218	52,306	52,142	52,249	6,449	7,537	6,419	7,507
Vehicle Instrument Unit	2,465	2,441	2,465	2,441	2,463	2,440	2,463	2,440	2,463	2,440	2,457	2,433	2,457	2,433
Payload Assembly	7,816	7,814	7,816	7,814	7,816	7,814	7,816	7,814	7,816	7,814	7,816	7,814	7,816	7,814
LES & Q-BALL	2,994	2,997	2,994	2,997	2,994	2,997	2,994	2,997	2,994	2,997				
First Flight Stage Total	516,991	519,566	510,706	515,327	122,689	122,606	121,804	121,689						
Second Flight Stage Total							65,491	65,554	65,415	65,500	16,722	17,784	16,692	17,754
MASS (lbm)														
S-I Stage, Dry	107,500	107,550	107,500	107,550	107,500	107,550	107,500	107,550						
LOX	613,098	612,582	602,308	601,935	3,901	4,389	3,240	3,709						
RP-1	268,561	274,431	265,473	271,304	6,125	5,408	5,313	4,569						
LOX Ullage Gas (GOX & He)	123	128	145	147	3,939	3,704	3,939	3,704						
Helium	6	6	6	6	6	6	6	6						
Hydraulic Oil	28	28	28	28	28	28	28	28						
Retro Rocket Propellant	1,353	1,353	1,353	1,353	1,353	1,353	1,353	1,353						
Frost	1,000	1,000	1,000	1,000	0	0	0	0						
Oronite	32	32	32	32	0	0	0	0						
N_2	850	840	850	840	672	681	657	666						
Total S-I Stage	992,551	997,950	978,695	984,195	123,524	123,119	122,036	121,585						
S-I/S-IV Interstage	2,396	2,449	2,396	2,449	2,113	2,166	2,113	2,166						
S-IV Stage, Dry	13,526	13,547	13,526	13,547	13,526	13,547	13,526	13,547	13,526	13,547	13,526	13,547	13,526	13,547
LOX	84,206	84,271	84,206	84,271	84,122	84,167	84,113	84,157	84,094	84,135	193	2,207	140	2,154
LH_2	17,024	17,134	17,024	17,134	16,782	16,897	16,776	16,892	16,765	16,881	70	460	57	447
LOX Ullage Gas (GOX & He)	33	25	33	25	35	36	35	36	35	36	228	231	228	231
LH_2 Ullage Gas (GH_2 & He)	25	31	25	31	29	35	30	35	30	35	153	121	153	121
Other Helium	130	134	130	134	127	132	127	132	127	132	47	49	47	49
Ullage Rocket Propellant	243	243	243	243	243	243	235	238	97	146	0	0	0	0
Ullage Rocket Cases	279	277	279	277	279	277	279	277	279	277	0	0	0	0
Frost	90	170	90	170	0	27	0	0	0	0	0	0	0	0
Total S-IV Stage	115,556	115,832	115,556	115,832	115,143	115,361	115,121	115,314	114,953	115,189	14,217	16,615	14,151	16,549
Vehicle Instrument Unit	5,434	5,382	5,434	5,382	5,430	5,378	5,430	5,378	5,430	5,378	5,416	5,364	5,416	5,364
Payload Assembly	17,232	17,228	17,232	17,228	17,232	17,228	17,232	17,228	17,232	17,228	17,232	17,228	17,232	17,228
LES & Q-BALL	6,600	6,607	6,600	6,607	6,600	6,607	6,600	6,607	6,600	6,607				
First Flight Stage Total	1,139,769	1,145,448	1,125,913	1,131,693	270,042	269,859	268,532	268,278						
Second Flight Stage Total							144,383	144,527	144,215	144,402	36,865	39,207	36,799	39,141

Notes:
1. GOX vented accounted for.
2. No GH_2 vented from RP-1 containers (S-I Stage).
3. Ignition weight includes jacket prefill (predicted-located in containers).
4. Predicted RP-1 weights based on density of 799.3 kg/m^3 (49.90 lb/ft^3), actual RP-1 weights based on 806.5 kg/m^3 (50.35 lb/ft^3).
5. Fuel consumed includes 17 kg/s (37.5 lbm/s) lube RP-1 flow per engine.
6. S-IV propellant consumed includes 11 kg (24 lbm) for helium heater consumption.

*Predicted weights are those reported in R-P&VE-VAW-64-59

TABLE 4-II. SA-7 FLIGHT SEQUENCE MASS SUMMARY

MASS HISTORY	ACTUAL		PREDICTED	
	kg	(lbm)	kg	(lbm)
S-I Stage @ Ground Ignition	452,662	997,950	450,214	992,551
S-I/S-IV Interstage @ Ground Ignition	1,111	2,449	1,087	2,396
S-IV Stage @ Ground Ignition	52,541	115,832	52,415	115,556
Vehicle Instrument Unit @ Ground Ignition	2,441	5,382	2,465	5,434
Payload @ Ground Ignition	10,811	23,835	10,810	23,832
1st Flight Stage @ Ground Ignition	519,566	1,145,448	516,991	1,139,769
S-I Thrust Buildup Propellants	-6,239	-13,755	-6,285	-13,856
1st Flight Stage @ First Motion	513,327	1,131,693	510,706	1,125,913
S-I Mainstage Propellants	-388,830	-857,224	-386,157	-851,332
S-I Frost	-454	-1,000	-454	-1,000
S-IV Frost	-65	-143	-41	-90
S-I Fuel Additive	-253	-559	-252	-556
S-I Lube Oil (Oronite)	-14	-32	-14	-32
S-I N_2 for S-IV Tail Purge	-53	-116	-61	-134
S-I N_2 for Camera Purge	-19	-43	-20	-43
S-I/S-IV Interstage N_2	-128	-283	-128	-283
Vehicle Instrument Unit N_2	-2	-4	-2	-4
S-IV Chilldown LOX	-42	-93	-38	-84
S-IV Chilldown LH_2	-107	-235	-108	-239
S-I IETD Propellants	-954	-2,102	-941	-2,074
1st Flight Stage @ Cutoff Signal	122,406	269,859	122,489	270,042
S-I N_2 for S-IV Tail Purge	-6	-14	-6	-14
S-I OETD Propellants (To Separation)	-689	-1,519	-668	-1,473
Camera Purge N_2	-1	-1	-1	-1
S-IV Chilldown LOX	-5	-10	-4	-9
S-IV Chilldown LH_2	-2	-5	-2	-5
S-IV Ullage Rocket Propellants	-2	-5	-4	-8
S-IV Frost	-12	-27		
1st Flight Stage @ Separation	121,689	268,278	121,804	268,532
S-I Stage @ Separation	-55,150	-121,585	-55,356	-122,036
S-I/S-IV Interstage @ Separation	-982	-2,166	-958	-2,113
S-IV Chilldown LOX	-10	-22	-8	-19
S-IV Chilldown LH_2	-5	-11	-5	-11
S-IV Ullage Rocket Propellants	-42	-92	-62	-138
2nd Flight Stage @ Ignition	65,500	144,402	65,415	144,215
S-IV Mainstage Propellants *	-44,509	-98,126	-45,511	-100,335
S-IV Helium Heater Propellants	-11	-24	-11	-24
S-IV Ullage Rocket Propellants	-66	-146	-44	-97
S-IV Ullage Rocket Cases	-126	-277	-126	-279
S-IV Helium, Pneumatic	-1	-1	-1	-1
Vehicle Instrument Unit N_2	-6	-14	-6	-14
Launch Escape System	-2,997	-6,607	-2,994	-6,600
2nd Flight Stage @ Cutoff Signal **	17,784	39,207	16,722	36,865
S-IV Thrust Decay Propellants	-11	-24	-11	-24
S-IV Propellant Below Pump Inlets	-19	-42	-19	-42
2nd Flight Stage @ End of Thrust Decay	17,754	39,141	16,692	36,799
S-IV Stage @ End of Thrust Decay	-7,507	-16,549	-6,419	-14,151
Vehicle Instrument Unit	-2,433	-5,364	-2,457	-5,416
Payload	7,814	17,228	7,816	17,232

* Includes Thrust Buildup Propellants
** Predicted Values are for a Depletion Cutoff

Note: IETD - Inboard Engine Thrust Decay
OETD - Outboard Engine Thrust Decay

TABLE 4-III. MASS CHARACTERISTICS COMPARISON

EVENT		RANGE TIME	MASS		LONGITUDINAL C.G. (X-Sta)		RADIAL C. G.		ROLL MOMENT OF INERTIA		PITCH MOMENT OF INERTIA	
		sec	kg lb	% Dev	meters inches	Dev	meters inches	Dev	$kg\text{-}m^2$	% Dev	$kg\text{-}m^2$	% Dev
S-I Stage, Dry	Pred*	N/A	48,761 107,500		9.53 375.3		0.0206 0.81		335,093		3,798,802	
	Actual	N/A	48,784 107,550	0.05	9.53 375.3	0.0 0.0	0.0206 0.81	0.0 0.0	335,200	0.03	3,800,617	0.05
S-I/S-IV Interstage	Pred*	N/A	958 2,113		26.88 1,058.1		0.1334 5.25		7,649		5,884	
	Actual	N/A	982 2,166	2.44	26.94 1,060.7	0.06 2.60	0.1334 5.25	0.0 0.0	7,852	2.58	6,013	2.14
S-IV Stage, Dry Without Ullage Rocket Cases	Pred*	N/A	6,135 13,526		30.03 1,182.3		0.1984 7.81		25,595		75,511	
	Actual	N/A	6,145 13,547	0.16	30.04 1,182.6	0.01 0.30	0.1984 7.81	0.0 0.0	25,626	0.12	75,607	0.13
Vehicle Instrument Unit	Pred*	N/A	2,431 5,360		37.59 1,479.9		0.0665 2.62		4,609		2,942	
	Actual	N/A	2,408 5,308	0.96	37.59 1,479.9	0.0 0.0	0.0665 2.62	0.0 0.0	4,597	0.26	2,899	1.48
Payload Assembly With L.E.S. & Q-Ball	Pred*	N/A	10,810 23,832		47.07 1,853.3		0.0500 1.97		20,888		231,437	
	Actual	N/A	10,811 23,835	0.01	47.07 1,853.0	0.0 0.30	0.0498 1.96	0.0002 0.01	20,871	0.08	230,649	0.34
Payload Assembly Without L.E.S. & Q-Ball	Pred*	N/A	7,816 17,232		44.76 1,762.1		0.0709 2.79		20,496		67,176	
	Actual	N/A	7,814 17,228	0.03	44.75 1,762.0	0.01 0.10	0.0706 2.78	0.0003 0.01	20,517	0.10	67,161	0.02
1st Flight Stage at Ignition	Pred*	N/A	516,991 1,139,769		16.05 632.0		0.0056 0.22		2,104,507		38,834,334	
	Actual	N/A	519,566 1,145,448	0.50	16.06 632.2	0.01 0.2	0.0048 0.19	0.0008 0.03	2,118,795	0.67	38,917,740	0.21
1st Flight Stage at First Motion	Pred*	N/A	510,706 1,125,913		15.96 628.3		0.0056 0.22		2,071,164		38,706,848	
	Actual	N/A	513,327 1,131,693	0.51	15.99 629.5	0.03 1.2	0.0048 0.19	0.0008 0.03	2,084,962	0.66	38,804,394	0.25
1st Flight Stage at OECO	Pred*	N/A	122,489 270,042		22.08 869.5		0.0218 0.86		437,377		23,859,579	
	Actual	N/A	122,406 269,859	0.07	22.11 870.4	0.03 0.9	0.0218 0.86	0.0 0.0	437,072*	0.07	23,831,866	0.12
1st Flight Stage at Separation	Pred*	N/A	121,804 268,532		22.17 873.0		0.0218 0.86		434,435		23,673,253	
	Actual	N/A	121,689 268,278	0.09	22.20 874.0	0.03 1.0	0.0218 0.86	0.0 0.0	433,591	0.19	23,638,116	0.15
2nd Flight Stage at Ignition	Pred*	N/A	65,415 144,215		32.82 1,292.0		0.0305 1.20		53,485		3,184,219	
	Actual	N/A	65,500 144,402	0.13	32.81 1,291.9	0.01 0.1	0.0295 1.16	0.001 0.04	53,740	0.47	3,180,189	0.13
2nd Flight Stage at CO	Pred**	N/A	16,722 36,865		37.41 1,472.7		0.1054 4.15		51,132		1,028,070	
	Actual	N/A	17,784 39,207	5.97	37.40 1,472.6	0.01 0.1	0.1044 4.11	0.001 0.04	51,171	0.08	1,018,372	0.95
2nd Flight Stage at End of Thrust Decay	Pred**	N/A	16,692 36,799		37.42 1,473.2		0.1057 4.16		51,132		1,016,096	
	Actual	N/A	17,754 39,141	5.98	37.42 1,473.2	0.0 0.0	0.1046 4.12	0.0011 0.04	51,142	0.02	1,015,145	0.09
S-I & S-I/S-IV Interstage at Separation	Pred*	N/A	56,313 124,149		9.80 385.7		0.0130 0.51		380,498		4,446,335	
	Actual	N/A	56,132 123,751	0.32	9.80 386.0	0 0.30	0.0137 0.54	0.0007 0.03	379,477	0.27	4,453,733	0.17

NOTE: Percent Deviation = Deviation ÷ Actual x 100

*Predicted weights are those reported in R-P&VE-VAW-64-59.
**Predicted values of 2nd flight stage CO & engine thrust decay are for a depletion cutoff.

SECTION V. TRAJECTORY

5.1 SUMMARY

The actual trajectory of SA-7 deviated from nominal because of high S-I stage performance. Total velocity was 39.4 m/s higher than nominal at OECO and 1.8 m/s higher than nominal at S-IV cutoff. At S-IV cutoff the actual altitude was 0.99 km lower than nominal and the range was 13.72 km longer than nominal. The cross range velocity deviated 3.5 m/s to the left of nominal at S-IV cutoff.

A theoretical free flight trajectory of the separated S-I booster indicates that the impact ground range was 58.5 km longer than nominal. Impact, assuming the tumbling booster remained intact, occurred at 536.8 seconds range time.

The S-IV payload at orbital insertion (S-IV cutoff + 10 sec) had a space-fixed velocity 2.8 m/s greater than nominal, a perigee altitude of 180.21 km and an apogee altitude of 234.10 km, giving a predicted lifetime of 3.8 days, 0.6 days longer than nominal. The extrapolated orbit based on data for an epoch of 10:57 Z, September 22, reached the estimated breakup altitude of 86 km at approximately 11:50 Z, September 22, at coordinates of 21.7 degrees south latitude and 56.4 degrees east longitude. The theoretical ballistic impact time is approximately 12:00 Z, September 22, at coordinates of 26.4 degrees south latitude and 69.0 degrees east longitude.

5.2 TRAJECTORY ANALYSIS

Tracking data were available from first motion through insertion. All tracking systems experienced difficulty in maintaining track during the S-I cutoff and separation sequence. The reduced metric tracking data showed discrepancies between the various tracking systems of 200 to 400 m in position components.

SA-7 was the fourth engineering test of the MISTRAM tracking system and the second engineering test of the GLOTRAC system on a Saturn vehicle. The most comprehensive tracking coverage was obtained from the MISTRAM system. Reliable data, with less than 5 m random error, were obtained from 50 to 500 seconds. The GLOTRAC system had some difficulty with the San Salvador transmitter; therefore, reduced metric data were obtained only from 170 to 403 seconds. The random error in this data was also less than 5 meters.

An engineering test of the radar altimeter was flown on SA-7. According to the altimeter reliability signal, valid data were obtained from 164 to 795 seconds with only a few short dropouts. The random error in the altimeter data was 75 meters. A possible bias was indicated in the altimeter output of approximately 100 meters.

5.3 TRAJECTORY COMPARISON WITH NOMINAL

Actual and nominal altitude, range, and cross range (Z_e) are compared graphically in Figure 5-1 for the S-I phase of flight and in Figure 5-2 for the S-IV phase. Actual and nominal total earth-fixed velocities are shown graphically in Figure 5-3. Comparisons of actual and nominal parameters at the three cutoff events are shown in Table 5-I. The nominal trajectory is presented in Reference 2.

Altitude and range were greater than nominal during S-I burn. The actual earth-fixed velocity was 39.4 m/s greater than nominal at OECO. This excess velocity can be attributed to the high performance and longer burning time of the S-I stage.

The longitudinal acceleration was lower than nominal for the first 45 seconds of S-I flight and higher than nominal for the remainder of S-I stage operation (Fig. 5-4).

The S-IV stage cutoff 2.02 seconds later than nominal and, combined with the 0.71 second late S-I stage cutoff, resulted in a 1.31 seconds longer burning time of the S-IV stage. Total acceleration during S-IV burn averaged 2 percent lower than nominal as a result of low S-IV stage performance. This low performance and a steeper trajectory with more gravitational losses resulted in a S-IV stage velocity gain of 37.6 m/s less than nominal in 1.31 seconds longer burning time.

The actual space-fixed velocity at the S-IV cutoff signal given by the guidance computer (621.375 sec) was 7807.8 m/s, compared to the predicted velocity of 7806.0 m/s. The actual velocity is based on the powered flight trajectory, which matches the velocity at insertion deduced from orbital tracking. The deviation was due principally to guidance errors identified after the flight.

The range was greater than nominal during S-IV burn. The altitude was greater than nominal to 566 seconds and less than nominal for the remainder of the flight. The apex altitude reached during S-IV burn was 4.4 km higher than nominal; however, by S-IV cutoff this deviation was reduced to 0.99 km lower than nominal. Approximately 0.28 km of the low cutoff altitude can be attributed to low S-IV stage performance. The remaining 0.71 km can be attributed to guidance errors. Mach number and dynamic

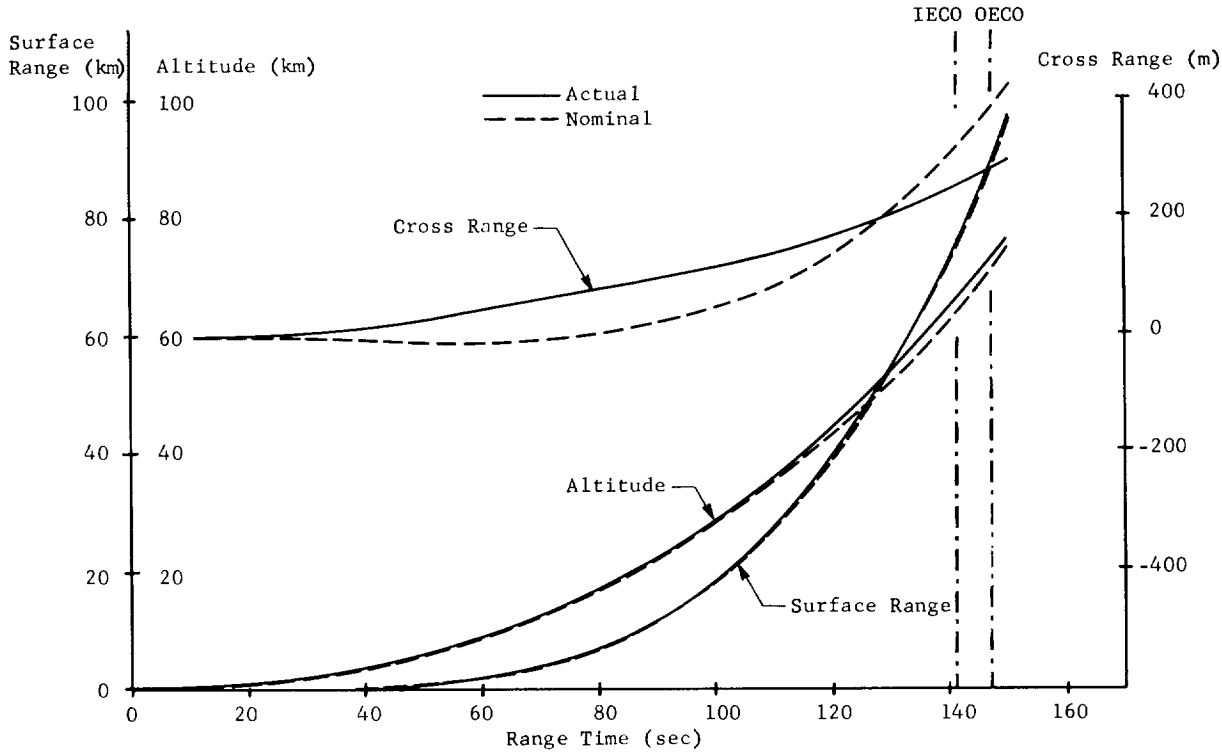

FIGURE 5-1. S-I TRAJECTORY

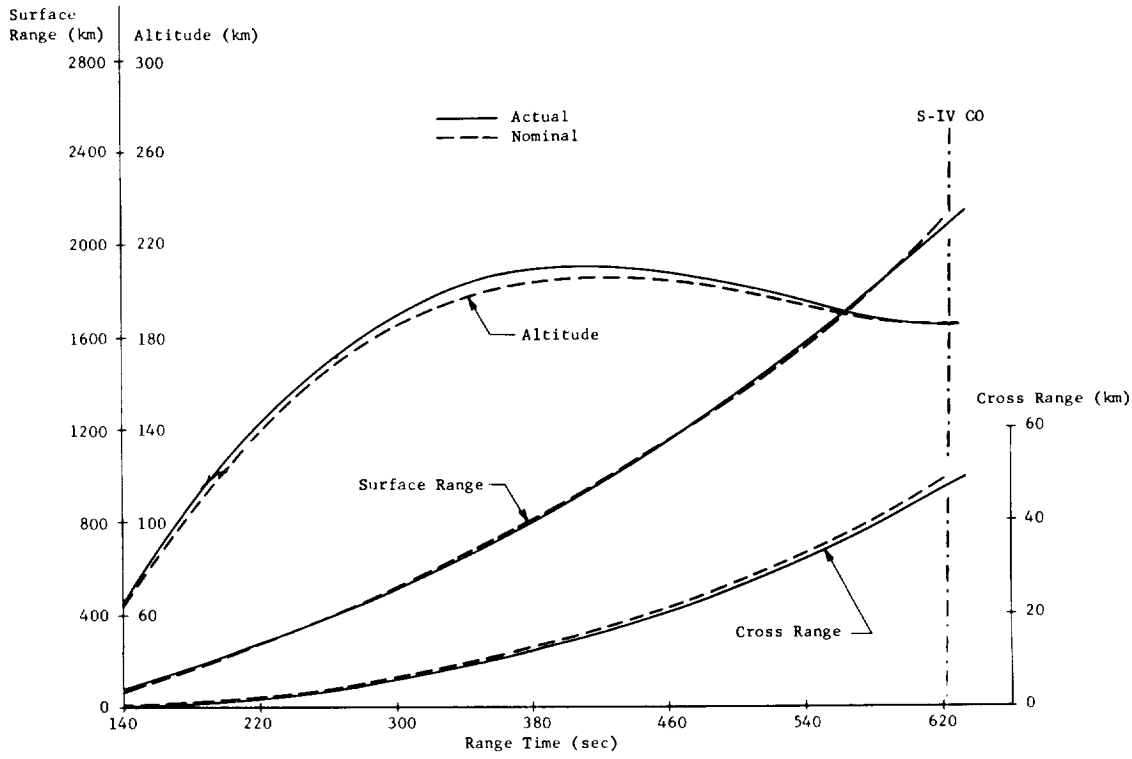

FIGURE 5-2. S-IV TRAJECTORY

TABLE 5-I. CUTOFF CONDITIONS

PARAMETER	IECO			OECO			S-IV CO (Guidance Signal)		
	Actual	Nominal	Act-Nom	Actual	Nominal	Act-Nom	Actual	Nominal	Act-Nom
Range Time (sec)	141.54	140.93*	0.61	147.64	146.93*	0.71	621.375	619.35*	2.025
Altitude (km)	65.65	63.86	1.79	72.90	70.71	2.21	184.33	185.32	-0.99
Range (km)	75.87	75.20	0.67	89.95	88.93	1.02	2084.84	2071.12	13.72
Cross Range, Z_c (km)	0.25	0.31	-0.06	0.29	0.38	-0.09	47.38	48.82	-1.44
Cross Range Velocity, $\dot{Z}_c$ (m/s)	5.9	11.0	-5.1	7.4	12.8	-5.4	218.0	221.5	-3.50
Earth-Fixed Velocity (m/s)	2534.3	2494.9	39.4	2697.4	2658.0	39.4	7403.2	7401.4	1.8
Earth-Fixed Velocity Vector Elevation (deg)	27.61	26.92	0.69	26.49	25.78	0.71	0.07	0.07	0.00
Earth-Fixed Velocity Vector Azimuth (deg)	105.43	105.56	-0.13	105.52	105.65	-0.13	115.10	115.08	0.02
Space-Fixed Velocity (m/s)	2895.8	2858.1	37.7	3062.0	3024.2	37.8	7807.8	7806.0	1.8
Longitudinal Acceleration (m/s^2)	57.81	56.90	0.91	30.23	30.68	-0.45	22.21	22.24	-0.03

*Based on First Motion Time of 0.06 sec.

Earth-Fixed Velocity Accuracy
OECO ± 0.5 m/s
S-IV CO ± 1.0 m/s

Altitude Accuracy
OECO ± 30 m
S-IV CO ± 100 m

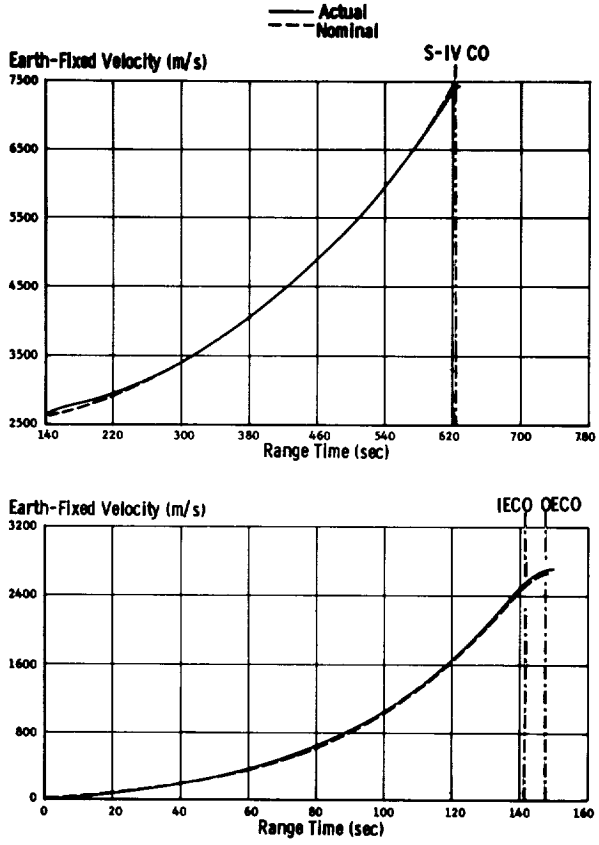

FIGURE 5-3. EARTH-FIXED VELOCITY

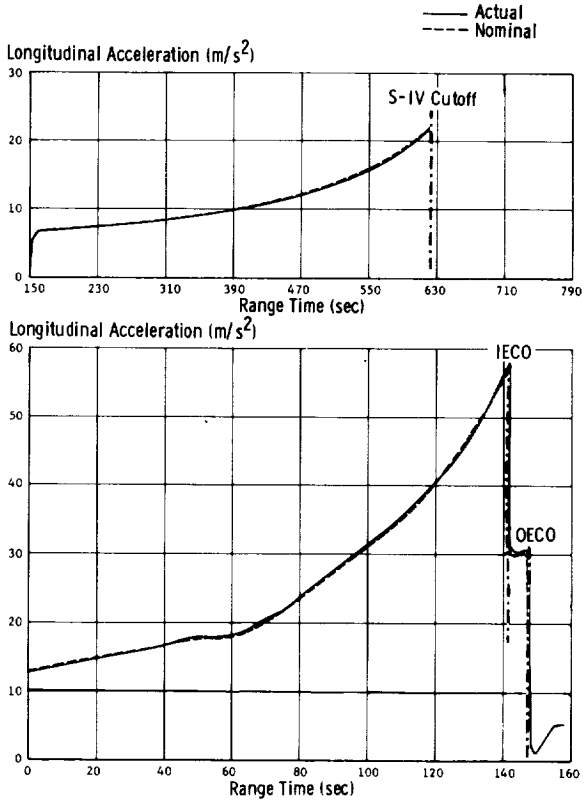

FIGURE 5-4. LONGITUDINAL ACCELERATION

pressure are shown in Figure 5-5. These parameters were calculated using measured meteorological data to an altitude of 27 km. Above this altitude the U. S. Standard Reference Atmosphere was used.

A comparison of actual and nominal parameters at significant event times is given in Table 5-II. Apex is given for both the S-IV stage and the discarded S-I stage. It should be noted that loss of telemetry signal and impact apply only to the discarded S-I stage.

The S-IV cutoff signal was given by the guidance computer at 621.375 seconds; however, the solenoids for the propellant valves on the S-IV stage do not receive the signal until 0.022 seconds later. The velocity increments imparted to the vehicle from the terminating

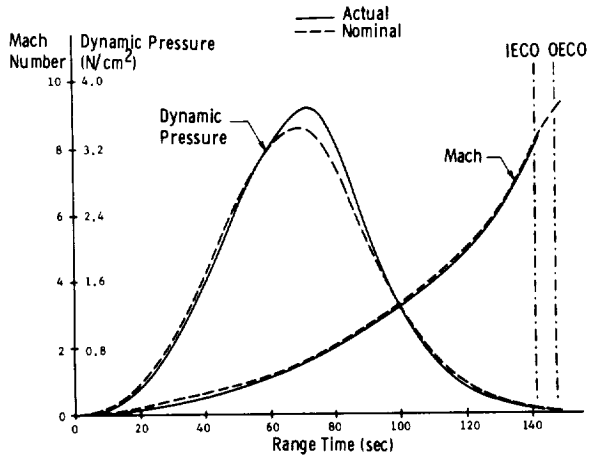

FIGURE 5-5. MACH NUMBER AND DYNAMIC PRESSURE

TABLE 5-II. SIGNIFICANT EVENTS

Event	Parameter	Actual	Nominal	Act-Nom
First Motion	Range Time (sec) Longitudinal Acceleration (m/s^2)	0.062 12.68	0.062 12.90	- -0.22
Mach One	Range Time (sec) Altitude (km)	55.245 7.18	55.03 7.26	0.215 -0.08
Maximum Dynamic Pressure	Range Time (sec) Dynamic Pressure (N/cm^2) Altitude (km)	73.0 3.680 13.53	70.0 3.447 12.46	3.0 0.233 1.07
Maximum Longitudinal Acceleration (S-I Stage)	Range Time (sec) Acceleration (m/s^2)	141.660 57.93	140.932 56.90	0.728 1.08
Maximum Earth-Fixed Velocity (S-I Stage)	Range Time (sec) Velocity (m/s)	147.886 2703.7	147.762 2664.0	0.124 39.7
Apex (S-I Stage)	Range Time (sec) Altitude (km) Range (km) Earth-Fixed Velocity (m/s)	293.000 159.41 428.05 2360.1	284.062 147.15 409.14 2359.7	8.938 12.26 18.91 1.4
Apex (S-IV Stage)	Range Time (sec) Altitude (km) Range (km) Earth-Fixed Velocity (m/s)	408.0 210.35 914.44 4302.8	417.0 205.91 951.01 4388.5	-9.0 4.44 -36.57 -85.70
Loss of Telemetry (S-I Stage)	Range Time (sec) Altitude (km) Range (km) Total Acceleration (m/s^2) Evaluation Angle From Pad (deg)	464.3 38.6 828.27 -8.40 -1.028	464.3* 23.3 814.40 -65.00 -2.100	- 15.3 13.86 56.60 1.072
Impact (S-I Stage)	Range Time (sec) Range (km) Cross Range (km) Geodetic Latitude (deg) Longitude (deg)	536.800 883.66 12.40 26.0942 72.0617	598.362 825.15 12.60 26.2631 72.6164	-61.562 58.51 -0.20 -0.1689 -0.5547
Maximum Longitudinal Acceleration (S-IV Stage)	Range Time (sec) Acceleration (m/s^2)	621.425 22.22	619.355 22.23	2.070 -0.01
Maximum Earth-Fixed Velocity (S-IV Stage)	Range Time (sec) Velocity (m/s)	621.700 7405.8	619.355 7403.0	2.345 2.8

Note: *For Comparison Purposes Only.

thrust decays are shown in Table 5-III for the S-I and S-IV stage at OECO and S-IV guidance cutoff, respectively.

TABLE 5-III. VELOCITY GAIN AT CUTOFF

	Velocity Gain (m/s)	
	Actual	Nominal
S-I OECO	6.9	6.0
S-IV CO	2.7	1.6

A theoretical free flight trajectory was computed for the discarded S-I stage. A nominal tumbling drag coefficient was assumed for the dive phase. The calculated impact location relative to the launch site is shown in Figure 5-6. Table 5-IV presents booster impact position from RCA Preliminary IP Report, actual free flight trajectory, and nominal free flight trajectory.

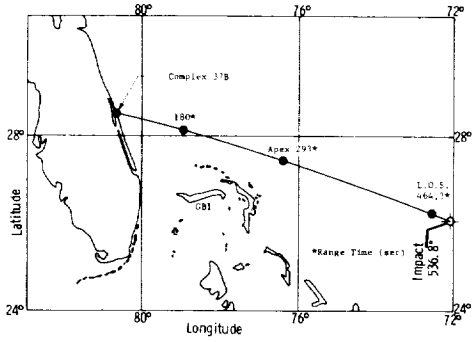

FIGURE 5-6. BOOSTER TRAJECTORY GROUND TRACK

TABLE 5-IV. BOOSTER IMPACT

Parameter	Preliminary IP Report	Actual (Calculated)	Nominal	Act-Nom
Surface Range* (km)	863.995	883.7	825.2	58.5
Cross Range (km)	-	12.4	12.6	-0.2
Geodetic Latitude (deg)	26.156	26.094	26.263	-0.169
Longitude (deg)	72.241	72.062	72.616	-0.554
Range Time (sec)	613.8	536.8	598.4	-61.6

*Surface Range is Measured from Launch Site

5.4 INSERTION CONDITIONS (S-IV CUTOFF + 10 SEC)

The orbital insertion conditions for SA-7 were determined by a differential correction procedure. Table 5-V shows a comparison between the actual and nominal orbital insertion elements.

TABLE 5-V. INSERTION ELEMENTS COMPARISON

	Actual	Nominal	Act-Nom
Time of Orbital Insertion (Range Time sec)	631.375	629.352	+2.023
Space-Fixed Velocity (m/s)	7810.44	7807.67	+2.77
Pitch Angle (deg)	89.97	89.93	0.04
Altitude (km)	184.35	185.34	-0.99
Ground Range (km)	2156.82	2143.07	13.75
Cross Range (km)	49.6	51.1	-1.5
Cross Range Velocity (m/s)	221.4	224.9	-3.5
Apogee Altitude (km)*	234.10	227.92	6.18
Perigee Altitude (km)*	180.21	180.95	-0.74
Period (min)	88.64	88.58	0.06
Inclination (deg)	31.75	31.76	-0.01
Excess Circular Velocity (m/s)	15.2	13.0	2.2
Lifetime (days)	3.8	3.2	0.6

*The Apogee and Perigee altitudes are referenced to a spherical earth radius of 6378.165 km.

The estimated accuracy of the velocity and position data are 0.4 m/s and 400 m respectively.

5.5 ORBITAL DECAY AND REENTRY

The SA-7 apogee and perigee altitudes from orbital insertion to reentry are shown in Figure 5-7. The orbital decay history was established by GSFC on a real time basis for the lifetime of the vehicle. The initial apogee and perigee decay rates respectively were 6 km/day and 3 km/day.

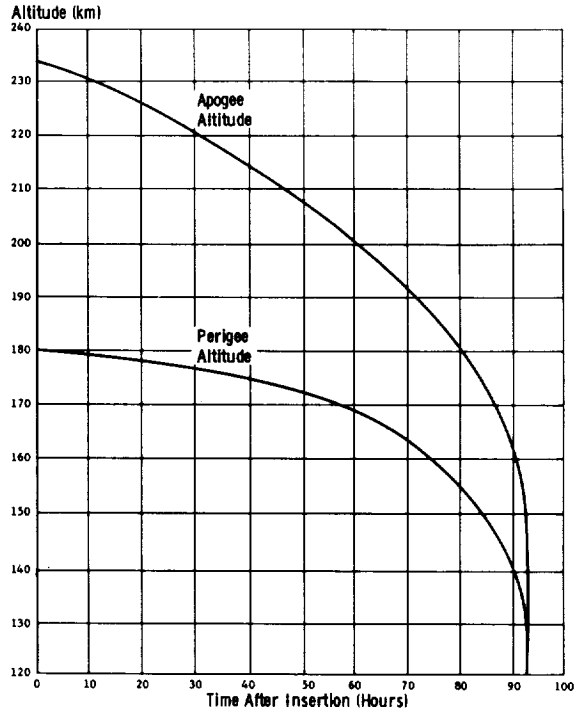

FIGURE 5-7. SA-7 APOGEE AND PERIGEE ALTITUDES

The final orbit and reentry of SA-7 is shown in Figure 5-8. The orbit reached the estimated breakup altitude of 86 km at approximately 11:50 Z, September 22, at coordinates of 21.7 degrees south latitude and 56.4 degrees east longitude (see Fig. 5-8). The theoretical ballistic impact time is approximately 12:00 Z, September 22, at coordinates 26.4 degrees south latitude and 69 degrees east longitude (southeast of Madagascar in the Indian Ocean). This reentry location is consistent with the fact that no signal was received from the Minitrack beacon after the KANO observation. Monitoring for the 136 mc beacon at Carnarvon and Woomera, Australia, and South Point, Hawaii, confirmed that the vehicle was no longer in orbit.

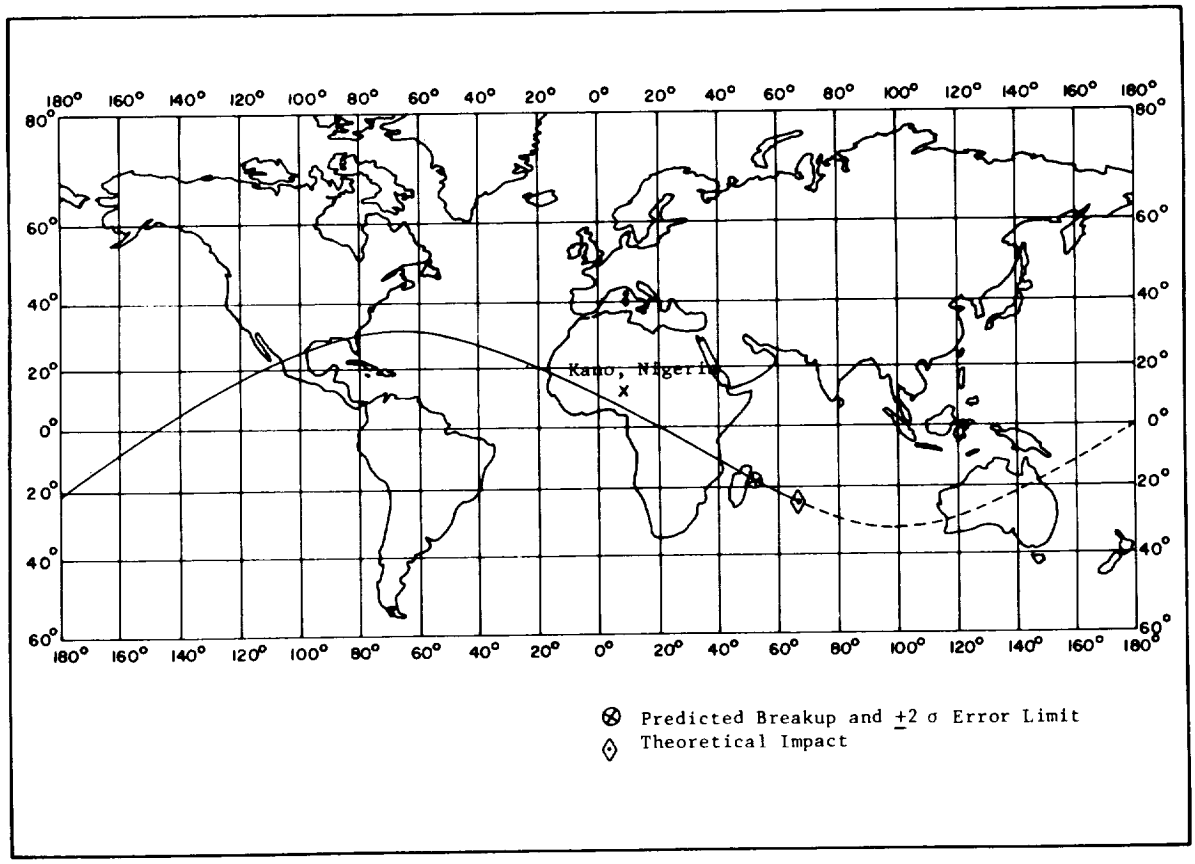

FIGURE 5-8. SA-7 FINAL ORBIT AND REENTRY

SECTION VI. PROPULSION

6.1 SUMMARY

The performance of both the S-I and S-IV stage propulsion systems was satisfactory for the SA-7 flight test. SA-7 was the third Saturn vehicle to employ H-1 engines at a thrust level of 836,000 N (188,000 lb_f) to provide thrust for the S-I stage. SA-7 also represented the third Saturn flight test of the RL10A-3 engine for the S-IV stage.

The vehicle longitudinal thrust of the S-I stage averaged between 0.92 percent (engine analysis) and 1.24 percent (flight simulation) higher than predicted. Vehicle specific impulse averaged between 0.71 percent (engine analysis) and 0.90 percent (flight simulation) higher than predicted. The performance of all pressurization systems, purge systems, hydraulic systems and other associated systems was as expected.

Propulsion performance of the S-IV stage was within design limits throughout the stage powered phase. From engine analysis the average vehicle longitudinal thrust was approximately equal to predicted and the stage specific impulse was 0.02 percent higher than predicted. The flight simulation method indicated the thrust and specific impulse were 0.89 percent and 0.98 percent respectively, lower than predicted. The performance of the individual engines, tank pressure systems, helium heater, hydraulic systems, PU system and the non-propulsive vent system were all within the expected values.

6.2 S-I STAGE PROPULSION SYSTEM

6.2.1 OVERALL STAGE PROPULSION PERFORMANCE

The propulsion system of the S-I stage performed satisfactorily. Ignition command was initiated -3.32 seconds before liftoff signal. Engine buildup was satisfactory except for large pressure disturbances in engine position 3 (see Para. 6.2.3). The chamber pressure buildup was otherwise normal with the engine starting sequence within expected tolerances of the prescribed 100 milliseconds delay between starting pairs. Figure 6-1 illustrates the thrust buildup of each engine. The largest deviation in the thrust buildup times of the engines that received ignition signal at the same time was 75 milliseconds (engines 2 and 4).

6.2.2 CLUSTER PERFORMANCE

Two separate analyses were employed in reconstructing the S-I stage all engine performance. The first method is an engine analysis, which uses telemetered parameters to compute clustered thrust, specific impulse, and mass flow. The second method is postflight simulation which uses the thrust and mass flow shapes obtained from the engine analysis and adjusts the levels to simulate the actual trajectory as closely as possible.

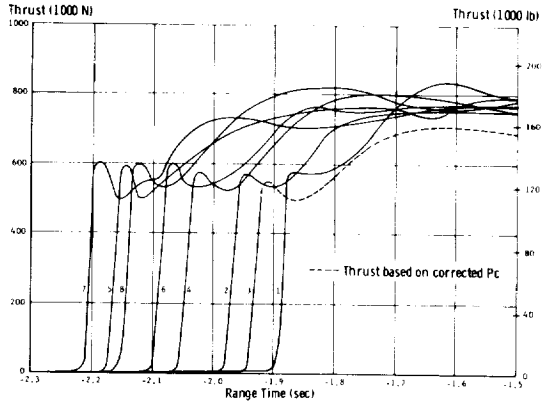

FIGURE 6-1. INDIVIDUAL ENGINE THRUST BUILDUP

6.2.2.1 ENGINE ANALYSIS

Vehicle longitudinal thrust (upper portion of Fig. 6-2) averaged approximately 0.7 percent higher than predicted. Vehicle specific impulse (lower portion of Fig. 6-2) averaged approximately 0.5 percent higher than predicted.

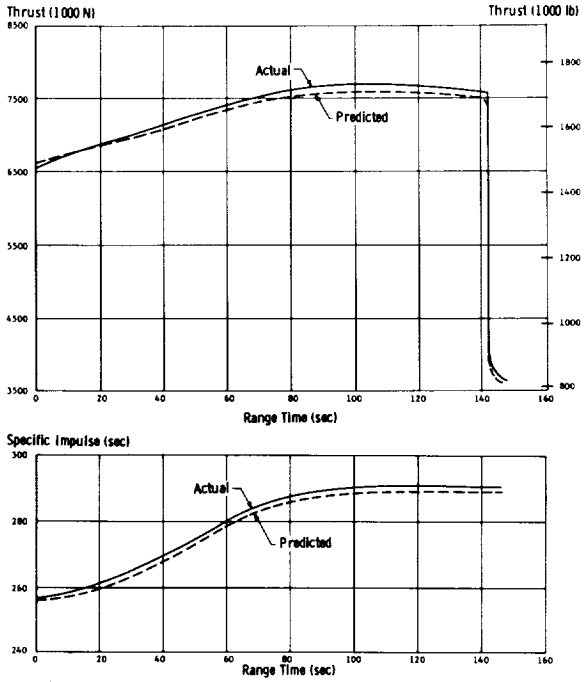

FIGURE 6-2. VEHICLE LONGITUDINAL THRUST AND SPECIFIC IMPULSE

Vehicle total propellant flow rate and mixture ratio are shown in Figure 6-3. Flight mixture ratio averaged approximately 2.2 percent lower than predicted.

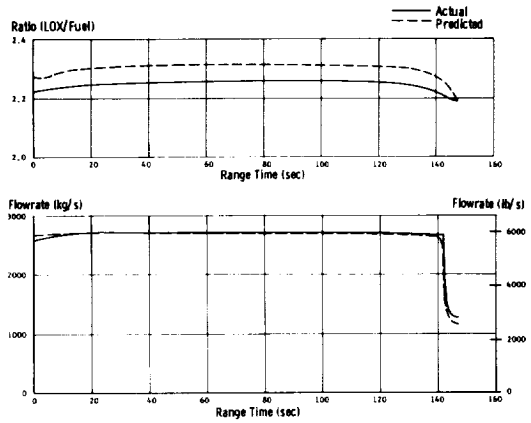

FIGURE 6-3. VEHICLE MIXTURE RATIO AND TOTAL FLOW RATE

The lower than predicted mixture ratio can be attributed to a higher than predicted fuel specific weight and a lower than predicted LOX specific weight.

Average S-I propulsion parameters for the SA-7 flight are summarized below:

Parameter	Propulsion Analysis	% Deviation Fm Predicted
Vehicle Longitudinal Thrust	6,792,844 N 1,527,092 lb_f	0.92
Vehicle Mass Loss Rate	2,693 kg/s 5,939 lbm/s	0.21
Vehicle Longitudinal Specific Impulse	257.1 sec	0.71

The engine cutoff sequence was normal for all engines. The cutoff sequence was initiated at 139.54 seconds by the liquid level sensor located in LOX tank 04. Inboard Engine Cutoff (IECO) occurred at 141.54 seconds, and Outboard Engine Cutoff (OECO) occurred at 147.64 seconds. A typical thrust decay of an outboard engine is presented in Figure 6-4.

6.2.2.2 FLIGHT SIMULATION

The vehicle longitudinal sea level specific impulse, vehicle longitudinal sea level thrust, and total liftoff weight were derived from the telemetered propulsion system measurements in a simulation of the tracked trajectory. A summarization of the average values and deviations of the flight simulation results from predicted and from the postflight engine analysis results are presented in Table 6-I.

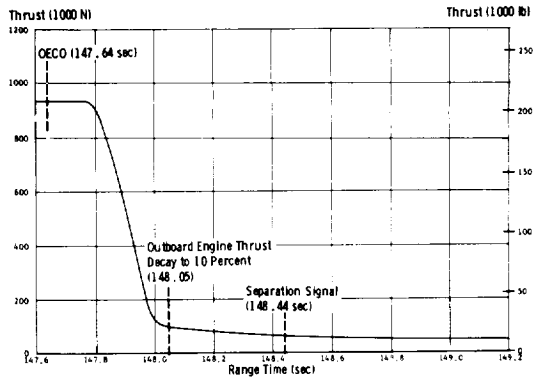

FIGURE 6-4. TYPICAL OUTBOARD ENGINE THRUST DECAY

TABLE 6-I. FLIGHT SIMULATION AVERAGE PROPULSION RESULTS

Parameter	Predicted	Flight Simulation	% Deviation From Predicted
First Motion	510,706 kg 1,125,910 lbm	513,327 kg 1,131,693 lbm	+0.51
Sea Level Thrust	6,730,640 N 1,513,108 lbf	6,815,342 N 1,532,150 lbf	+1.24
Flow Rate	2688.3 kg/s 5926.8 lb/s	269.79 kg/s 5947.8 lb/s	+0.35
Sea Level Specific Impulse	255.30 sec	257.6 sec	+0.90

The maximum deviations of the simulated trajectory from the tracking trajectory were 10 m/s in slant distance, 0.7 m/s in velocity and 0.05 m/s^2 in acceleration.

In analyses performed with the flight simulation method on Block I flights it has been assumed that the vehicle thrust and flow rate curve shapes as a function of time were known from the engine analysis based on the telemetered measurements. Only the absolute levels were considered in doubt. With the flights of the Saturn I Block II vehicles it has proven impossible to fit the trajectory with this assumption. Continued investigations have indicated a possible theory for the problem. Because of the clustered arrangement of the engines it is now theorized that the engines do not exhaust into an ambient atmospheric environment. Expansion rather takes place into a pressure field different from ambient caused by interference effects between the exhausts from the multiple engines.

The simulation method must now be used to solve for variations in thrust shape and drag shape simultaneously. This, of course, decreases the accuracy of the results. The exact amount of the degradation has not been determined as yet.

For this flight the simulation program was utilized in the normal manner with one significant exception; along with solving for the axial force coefficient, a variable multiplier was also determined which would change the shape of the local thrust curve to get a good fit to the observed tracking trajectory. This variable multiplier is presented in Figure 6-5 along with the indicated thrust correction that is computed from the telemetered base pressure measurements.

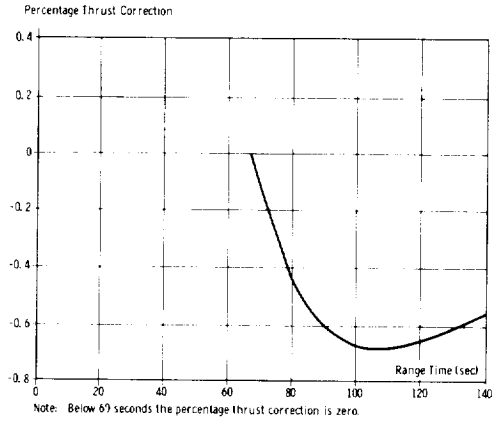

FIGURE 6-5. LOCAL THRUST CORRECTION DUE TO CLUSTER EFFECT

This procedure causes a certain lack of confidence in the uniqueness of the results when so much freedom in variation is allowed. However, certain consistencies in the results would also tend to build confidence. Also, the flight simulation gives a solution for the liftoff weight very close to the engine analysis results.

Results for the solution of the axial force coefficient are given in Figure 13-2 in Section XIII.

6.2.3 INDIVIDUAL ENGINE PERFORMANCE

Individual engine performance was satisfactory during mainstage operation. However, engine position 5 indicated a slightly lower thrust level during the first 30 seconds than observed on the other seven engines. This engine performed normally after 30 seconds and no hardware malfunction could be correlated with this lower thrust level from the available data.

During the time interval between S-I stage ignition and liftoff, engine position 3 combustion chamber pressure indicated large pressure disturbances which were substantiated by data from the thrust chamber dome combustion stability monitor longitudinal vibration measurement. Chamber pressure data (Fig. 6-6) indicated these pressure disturbances occurred between P_c prime and build up to 90 percent of rated thrust level. Chamber pressure during a normal build up is shown for comparison. Oscillograph data indicate the duration of the pressure disturbances was approximately 20 milliseconds. Combustion stability data indicated the frequency of vibration was within the range of 960 to 6000 Hz and equal to or greater than ± 100 g for 2.5 milliseconds (see Fig. 6-6). Flight data applicable to engine position 3 indicate the performance level of this engine was not degraded during S-I powered flight and no recurrence of the pressure disturbances after build up to 90 percent of rated thrust level.

Pressure disturbances during this period are defined as main propellant ignition pops. Pops are defined as short duration combustion chamber pressure disturbances which occur during the time interval from engine ignition signal and build up to 90 percent of rated thrust. Pressure disturbances which occur after 90 percent of rated thrust level are defined as repeated pressure surges (RPS) and rough combustion (RC) depending on the predominant frequency of pressure disturbances. Pressure disturbances which occur at a predominant frequency of approximately 250 Hz are defined as RPS; RC is defined as pressure disturbances having a predominant frequency of 1200 Hz. Pops can trigger rough combustion, and the predominant frequency of pops are not consistent. Even though the predominant frequency of a pop is lower than the frequency range (960 to 6000 Hz) of the combustion stability monitor (CSM) measurement, the harmonics of the predominant frequency could be picked up by the CSM. To initiate S-I-7 stage cutoff the CSM must pick up a vibration frequency within 960 to 6000 Hz and vibration magnitude equal to or greater than ± 100 g for a sustained period of 100 milliseconds. Engine position 3 was within this range for only 2.5 milliseconds.

Rocketdyne data show that pops have occurred only four times during 2000 H-1 engine tests. The primary causes of these pressure disturbances are (a) residual fuel in the thrust chamber due to a slightly high ignitor fuel flow, (b) leaking "O" ring and (c) breaking up of carbon deposits on the injector. The chamber pressure measurement and thrust chamber dome vibration measurements were the only measurements which indicated engine position 3 pressure disturbances; however, this could be due to their high response rate in comparison to other measured parameters.

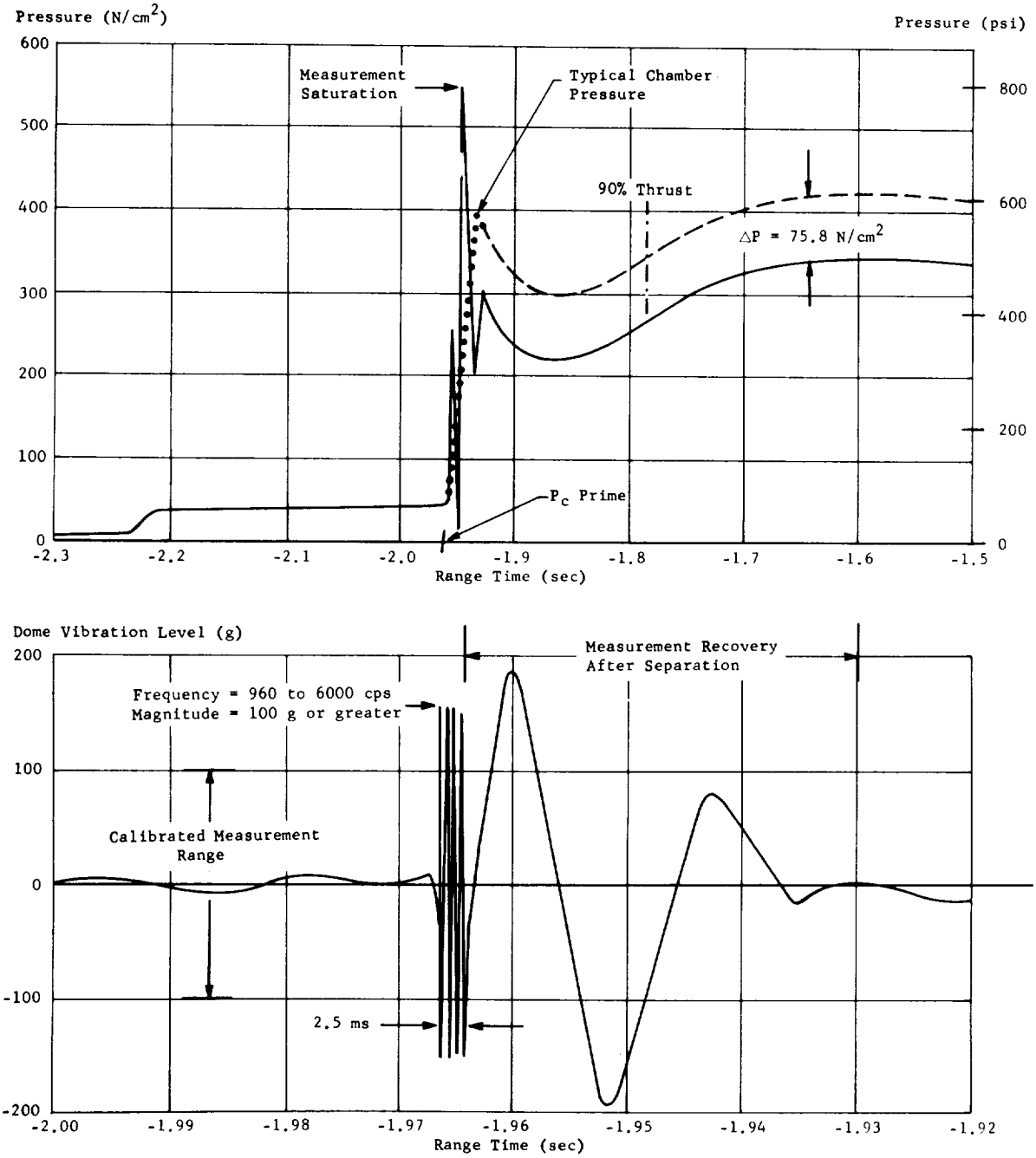

FIGURE 6-6. ENGINE 3 IGNITION COMBUSTION STABILITY

Individual engine thrust and specific impulse were calculated with the Saturn S-I stage propulsion system mathematical model. Input for the reconstruction was obtained from flight telemetry data and consisted of: propellant and vehicle weights, pump inlet conditions, propellant densities, and turbopump speeds.

In order to make a detailed analysis of engine performance it was necessary to establish a new prediction of the system performance, based on the actual flight propellant weights and densities. This new prediction is referred to as expected performance for discussion purposes. These expected data allow a clearer comparison of actual flight performance with predicted performance, since both data are based on common propellant densities. The flight fuel and LOX specific weights were significantly different than predicted; the fuel specific weight at launch was heavier than predicted and the LOX specific weight was lighter than predicted. The effects of the increased fuel density are twofold: the propellant loading system loads an additional amount of fuel in order to satisfy propellant depletion requirements, and burning time is increased because engine power levels are dropped and additional fuel must now be burned. The expected inboard engine cutoff time related to propellant load and fuel density which was reported by KSC was 142.5 seconds, or approximately 1.5 seconds longer than predicted. The effect of the warmer than predicted LOX is to increase burning time due to lower thrust levels and additional propellant consumption. The additional propellant consumption is obtained from the fuel bias which is loaded to provide a minimum residual with variations in flight mixture ratio. The warmer LOX causes a decrease in mixture ratio from that predicted and a portion of the bias is consumed. Therefore, the expected burning time considering the net effect caused by both density variations was 143.5 seconds. The actual cutoff time was 0.61 second later than predicted, but 1.96 seconds less than expected for the flight propellant densities. The shorter than expected burning was caused by higher than expected thrust levels.

A deviation between the average actual and predicted thrust levels and the average actual and expected thrust levels is shown in Table 6-II.

The average specific impulse for all eight engines was only 1.4 seconds higher than predicted, but was 1.64 seconds higher than expected. The cause of the engine performance being much higher than expected cannot be definitely established from the available

TABLE 6-II.

ENGINE THRUST LEVEL COMPARISON

Engine Position	Actual-Predicted (N)	(lbf)	Actual-Expected (N)	(lbf)
1	7,560	1,700	20,000	4,500
2	10,680	2,400	22,690	5,100
3	1,020	230	12,590	2,830
4	10,100	2,270	21,930	4,930
5	6,670	1,500	18,680	4,200
6	8,940	2,010	21,130	4,750
7	1,870	420	13,750	3,090
8	267	60	12,900	2,900

data. Figure 6-7 shows the engine-to-engine deviations in thrust and specific impulse. The largest deviation in thrust and specific impulse was observed on engine position 4.

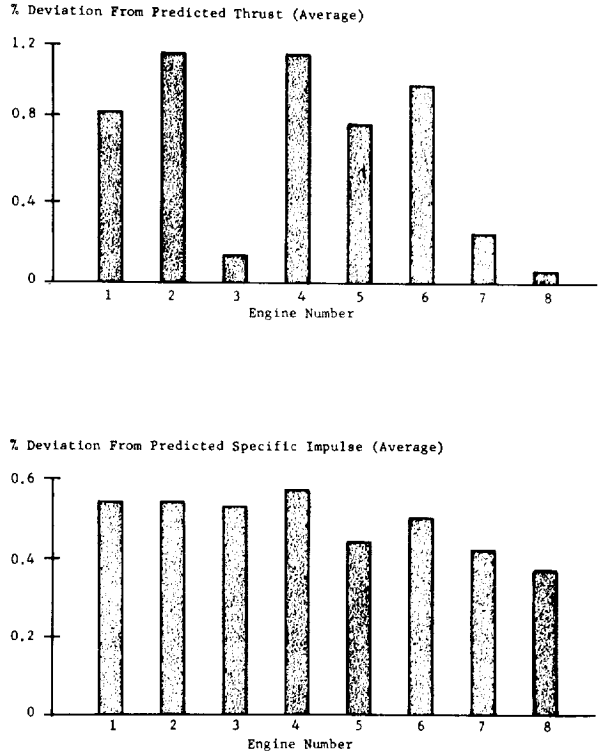

FIGURE 6-7. DEVIATIONS IN INDIVIDUAL ENGINE PERFORMANCE PARAMETERS (S-I)

The final flight performance prediction was based on data obtained from Rocketdyne single engine penalty

tests. Penalty static tests were conducted for all engines at Neosho test stand after the engines were removed from the stage for LOX dome and turbine seal replacements. The average penalty test data, at a 30-second time slice, showed thrust levels and engine specific impulses approximately 2000 lb and 1.5 seconds lower than those obtained during MSFC stage static test. Since the hardware changes were made at Neosho, penalty test data were used for prediction. However, MSFC test data contradicted the penalty test data used and indicated that the performance would be higher during flight. Only a 1.06 percent average engine thrust increase had been indicated by MSFC tests; however, some of the engines were as high as 2.2 percent in thrust during the stage tests.

The flight thrust levels were lower, or approximately as expected, for the first few seconds of flight, and then continuously diverged from the expected data until 20 to 30 seconds of flight when the difference became fairly constant. The continuously increasing difference between flight and expected thrust levels during the early portion of flight is a performance anomaly that cannot be explained from the available data. Since both the expected and flight data are based on approximately the same flight conditions, the difference should be approximately constant throughout the entire flight if the assumptions used in predicting performance are valid. A similar situation was indicated during the flight of SA-6. Possible explanations for the phenomenon are turbine exhaust effects or non-steady state engine performance; neither is considered when predicting performance.

6.3 S-I PRESSURIZATION SYSTEMS

6.3.1 FUEL TANK PRESSURIZATION SYSTEM

Fuel tank pressurization provides increased tank structural rigidity as well as adequate engine fuel pump inlet pressure. The system operated as expected with no major deviations from predicted performance.

The system is designed to maintain a constant ullage pressure of approximately 11 N/cm^2 gauge (16 psig) for the first 70 seconds of flight. The fuel container pressurizing switch opens and closes any of the three pressurizing valves which are active and keeps the tank pressure between 10.3 and 11.7 N/cm^2 gauge (15 and 17 psig). At 70 seconds, the flow of pressurant to the fuel tanks is terminated and the GN_2 remaining in the spheres is joined as one system and allowed to equalize with the GN_2 in the LOX-SOX spheres.

The pressure in the fuel tanks (Fig. 6-8) closely agreed with the pressure seen on past flights and the

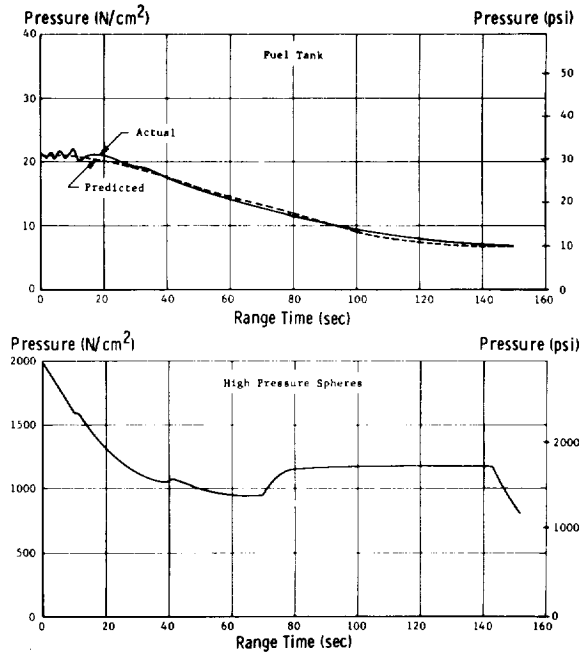

FIGURE 6-8. GAS PRESSURE IN FUEL TANK 3 AND HIGH PRESSURE SPHERES

predicted value. The fluctuations in pressure during system operation are normal and are due to the action of the fuel container pressurizing switch. These oscillations of pressure are transmitted to the fuel pumps but have a negligible effect on engine performance.

The 0.57 cubic meter (20 ft^3) sphere temperature and the nitrogen manifold gas temperature were normal during flight. The SA-7 fuel ullage gas temperature closely agreed with that of the SA-6 flight. The initial temperature in fuel tank was 294°K and decreased to a minimum of 270°K at 100 seconds. At this time aerodynamic heating effects were at a maximum and caused the temperature to increase to 276°K at the end of flight.

6.3.2 LOX TANK PRESSURIZATION SYSTEM

Pressurization of the LOX tanks provides increased tank structural rigidity and adequate LOX pump inlet pressures. Prelaunch pressurization is achieved with helium from a ground source. From vehicle ignition command to liftoff an increased helium flow is used to maintain adequate LOX tank pressure during engine start. Operation of the LOX tank pressurization system during prelaunch and flight was satisfactory.

Prelaunch pressurization of the 4.24 percent ullage was accomplished in 74 seconds. Predicted and measured LOX tank pressures during flight are shown in Figure 6-9. Center LOX tank and outboard LOX tank

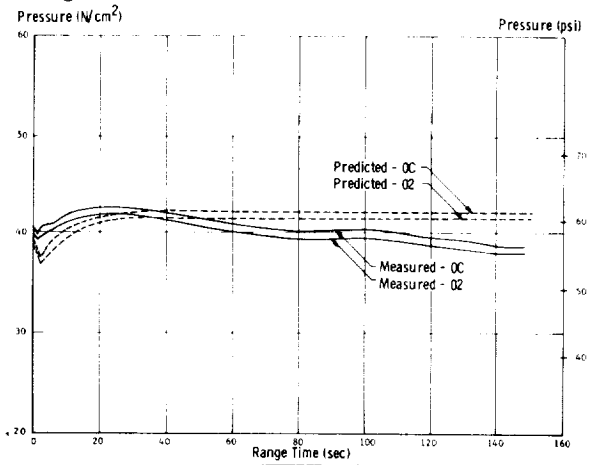

FIGURE 6-9. LOX TANK GAS PRESSURES

pressures averaged 2.4 N/cm^2 (3.5 psi) higher, at the beginning of flight, and 3.4 N/cm^2 (5 psi) lower, at the end of flight, than predicted. The center LOX tank pressure reached a maximum of 42.4 N/cm^2 (61.5 psi) at 25 seconds and had decreased to 38.6 N/cm^2 (56 psi) at 147 seconds. Although this is 0.7 N/cm^2 (1 psi) below the regulating range of the GOX Flow Control Valve (GFCV), it does not indicate abnormal system operation since the 0.7 N/cm^2 (1 psi) is within the measuring accuracy.

6.3.3 CONTROL PRESSURE SYSTEM

The pneumatic control pressure system supplies GN_2 at a regulated pressure of 517 ± 10 N/cm^2 gauge (750 ± 15 psig) for operation of the following: LOX tank pressure relief valves one and two, LOX vent valve, LOX replenishing control valve, suction line prevalve control valves, engine turbopump gearbox pressurization, and calorimeter and LOX pump seal purges. The SA-7 system was basically the same as the SA-6 system, except for the deletion of the engine compartment TV camera purge requirement. The control pressure system operated satisfactorily throughout the flight.

The supply sphere pressure was 1965 N/cm^2 (2850 psi) at liftoff and decreased to 1276 N/cm^2 (1850 psi) at 150 seconds. The final pressure compares well with the SA-5 level and is somewhat higher than SA-6 due to the TV camera purge on SA-6.

The regulated supply pressure was 527 N/cm^2 (765 psi) throughout S-I powered flight indicating satisfactory performance of the control pressure regulator.

6.3.4 LOX-SOX DISPOSAL SYSTEM

The LOX-SOX disposal system purges the S-I/S-IV interstage area with GN_2. The purge disperses LOX, SOX, or both from the S-IV engine thrust chambers during the chilldown cycle, and provides an inert environment prior to S-I/S-IV stage separation.

Successful operation of the LOX-SOX disposal system was indicated by the flight data. Pressure equalization between the 0.57 cubic meter (20 ft^3) triplex spheres occurred as scheduled at 70.5 seconds when the two systems were joined by a programmed signal. This equalization was shown by a rapid increase in sphere pressure to 1155 N/cm^2 (1675 psi) and a rapid decrease in plenum chamber temperature.

6.4 HYDROGEN VENT DUCT PURGE SYSTEM

The hydrogen vent duct purge system removes the chilldown hydrogen flowing through the S-IV stage plumbing at approximately 35 seconds prior to S-I/S-IV stage separation. The hydrogen exits the S-IV stage through three 12-inch diameter ducts that lead down the sides of the S-I/S-IV interstage and the S-I stage in line with stub fins II, III, and IV. Prior to launch, low-pressure helium from a ground source purges the three ducts. A helium triplex sphere assembly onboard the S-I stage supplies GHe for the purge after liftoff. This purge continues through the chilldown operation and S-I stage powered flight.

The sphere pressure and temperature at liftoff were 2040 N/cm^2 (2960 psi) and 297°K for SA-7 as compared to 2000 N/cm^2 (3000 psi) and 291°K for SA-6. The pressure at OECO was 440 N/cm^2 (640 psi) for SA-7 compared to 383 N/cm^2 (555 psi) for SA-6. The temperature of the gas in the sphere at OECO was 218°K. SA-7 hydrogen vent duct purge system operation was satisfactory and comparable to SA-6 system operation.

6.4.1 PROPELLANT UTILIZATION

Propellant utilization (the ratio of propellant used to propellant loaded) is an indication of the efficiency of a propulsion system in consuming the loaded propellant. Propellant utilization for the S-I stage was very close to predicted. The predicted and actual percent of loaded propellant utilized on the flight have been calculated from the vehicle weight data and are as follows:

	Predicted (%)	Actual (%)
Total	99.09	99.14
Fuel	98.21	98.53
LOX	99.48	99.41

LOX starvation cutoff of the outboard engines was attempted for the first time on SA-7. It was predicted that LOX starvation would occur when the LOX level reached the bottom of the outboard LOX container sumps. The backup timer was set to give outboard engine cutoff 6.1 seconds after inboard engine cutoff if starvation cutoff had not occurred.

The cutoff sequence was initiated by the uncovering of the LOX level cutoff probe in LOX tank 04 at 139.54 seconds. After a preset two-second delay, IECO occurred. OECO was initiated by the 6.1-second backup timer at 147.64 seconds indicating LOX starvation cutoff had not been accomplished.

It was predicted that OECO would occur from LOX starvation 5.64 seconds after IECO. This time interval was predicted on the basis of 0.33 m (13 in.) height differential between the center LOX tank and outboard LOX tank levels at IECO. The actual differential from probe data was 0.41 m (16 in.). This extra 7.62 cm (3 in.) represents approximately 435 kg (960 lbm) more LOX than predicted available to be burned between IECO and OECO. This helps to account for the backup timer cutoff since it represents approximately 0.5-second burn time for the four engines. The reconstructed residuals agree with probe data, verifying that LOX starvation was not accomplished.

The propellant residuals were determined utilizing continuous level probes located in the bottom of each propellant container, measuring the levels from 1.3 to 0.28 m (51.5 to 11.2) from the container bottom. The data from these probes were used in conjunction with reconstructed flowrates to determine the following propellant residuals:

	IECO		OECO		End of Thrust Decay	
	kg	lbm	kg	lbf	kg	lbm
LOX	7,812	17,222	1,991	4,389	1,633	3,600
Fuel	5,556	12,249	2,453	5,408	1,829	4,032

6.5 S-I HYDRAULIC SYSTEM

The four outboard H-1 engines, gimbal mounted on the stage thrust structure, provided engine thrust vectoring for vehicle attitude control and steering during operation of the S-I stage. Two hydraulic actuators were utilized to gimbal each engine in response to signals from the Flight Control Computer located in the Instrument Unit.

Four independent, closed-loop hydraulic systems provide power for gimbaling the outboard engines, both during engine firing and non-firing operations. This is accomplished without the use of an external pressurizing source. Hydraulic fluid flows to the actuators from the high pressure accumulator and returns to the low pressure reservoir. The electric motor driven auxiliary pump operates only during prelaunch checkout of the gimbaling system.

Performance of the hydraulic systems during S-I stage flight was satisfactory. Source pressures remained adequate throughout flight and the oil temperatures were well within their specified limits. The oil levels in the individual systems ran lower than predicted but remained within limits. Low accumulator GN_2 precharge pressures could account for these lower than predicted oil level values. Since the levels showed rising trends as the flight progressed, the possibility of an oil leak is unlikely. No threat to the performance of the individual hydraulic systems was posed by the lower than expected oil levels.

6.6 RETRO ROCKET PERFORMANCE

Four 151,240 N (34,000 lbf) thrust, solid propellant retro rockets provided the necessary retarding force on the S-I stage to prevent S-I/S-IV stage collision after separation. The retro rockets were mounted on the spider beam at the top of the S-I stage, 90 degrees apart and midway between the main fin positions. The nozzles were canted 12 degrees from the vehicle longitudinal axis to direct the thrust vector through the S-I stage center of percussion.

Retro rocket ignition occurred as planned. Combustion chamber pressure build up and decay appeared normal for all four retro rockets. The SA-7 onboard tape provided the specific data used in determining the trends. Erratic data for the middle portion of the burning period (149.10 to 150.10 sec) necessitated the use of curves derived from previous flights to establish the trend during this erratic data period. A typical chamber pressure for the retro rockets is shown in Figure 6-10.

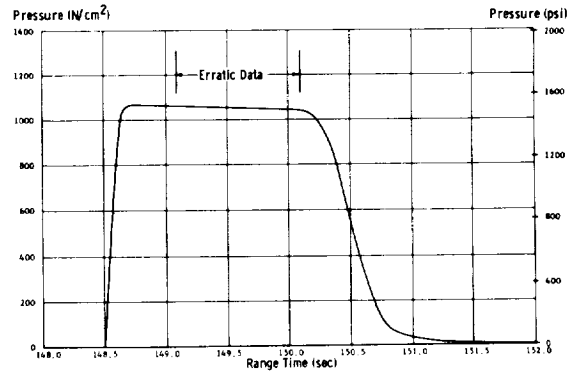

FIGURE 6-10. TYPICAL RETRO ROCKET COMBUSTION CHAMBER PRESSURE

Measured, calculated, and predicted performance values are shown in Table 6-III. The values obtained indicate higher combustion pressure and thrust levels than previous Block II vehicles along with correspondingly shorter burning times. High propellant grain temperatures appear to be the most probable cause for these high operating characteristics since combustion chamber pressure varies with temperature.

Retro rocket performance was exceptionally good. Proper operation prevented interaction of the S-I and S-IV stages.

6.7 S-IV STAGE PROPULSION SYSTEM

6.7.1 OVERALL S-IV STAGE PROPULSION PERFORMANCE

The performance of the S-IV propulsion system was within design limits throughout the S-IV-7 flight test. The performance of the individual engines, tank pressurization systems, helium heater, hydraulic systems, PU system, and the non-propulsive vent system were very close to predicted values.

6.7.2 CLUSTER PERFORMANCE

Two separate analyses were employed in reconstructing the S-IV stage six-engine performance.

The first method is an engine analysis, which uses the telemetered engine parameters to compute clustered thrust, specific impulse, and mass flow. A correction factor is used to account for the 6 degrees of engine cant angle to the vehicle center line, helium heater flow rates, helium heater thrust and chilldown vent thrust.

The second method is a postflight simulation, which uses the thrust and mass flow shapes obtained from the engine analysis and adjusts the levels to simulate the actual trajectory as closely as possible. In order to compare the postflight simulation results to the engine analysis results, a correction factor for base pressure must be applied.

TABLE 6-III. RETRO ROCKET PARAMETERS

Parameter	Retro Rockets					Predicted*
	1	2	3	4	Total	
Burning Time (sec)	2.15	2.20	2.15	2.25	----	2.15
Total Impulse (N-s) (lb-s)	323,610 72,750	341,400 76,750	328,060 73,750	351,410 79,000	1,344,480 302,250	331,400 74,500
Average Thrust (N) (lb)	150,514 33,837	155,181 34,886	152,583 34,302	157,169 35,333	615,447 138,358	154,130 34,650
Average Pressure (N/cm^2) (psi)	911 1,321	935 1,356	920 1,334	944 1,369	----	----
Firing Command (sec range time)	148.5	148.5	148.5	148.5		147.7

Definition of Terms:

1. Burning Time - Time interval between the intersection points on the zero thrust line described by a line tangent to the rise of thrust at the point of inflection extended to intersect the zero thrust line and by a line tangent to the decaying thrust curve at a point of reflection extended to intersect the zero thrust line.
2. Total Impulse - Area under thrust-versus-time curve.
3. Average Thrust - Total impulse divided by burning time.
4. Average Pressure - Area under pressure versus-time curve divided by burning time.

* Predicted values were based on a propellant grain temperature of 289°K and an altitude of 76,200 m (250,000 ft).

6.7.2.1 ENGINE ANALYSIS

S-IV-7 stage flight data analysis, which was based on an overall evaluation of burn time with respect to propellants loaded and on any possible error associated with these quantities, indicated that thrust and specific impulse deviated from predicted by 0.89 percent for thrust and 0.98 percent for specific impulse based upon flight simulation.

The engine analysis performance characteristics were reconstructed starting from LH_2 cooldown and continuing to engine cutoff. Three independent computer programs were used to gain statistical confidence in the reconstructed values and profiles.

Based on data obtained from the acceptance firing of the S-IV-7 stage, propellant depletion time has been predicted as 481.17 seconds burn time. The actual depletion time, determined by extrapolating from the propellant residuals remaining at command cutoff, would have been 482.5 seconds or approximately 1.3 seconds longer than predicted. The performance excursions were within the predicted bands and shapes.

Thrust, specific impulse, total propellant mass flow rate and engine mixture ratio determined from the engine analysis are presented in Figure 6-11.

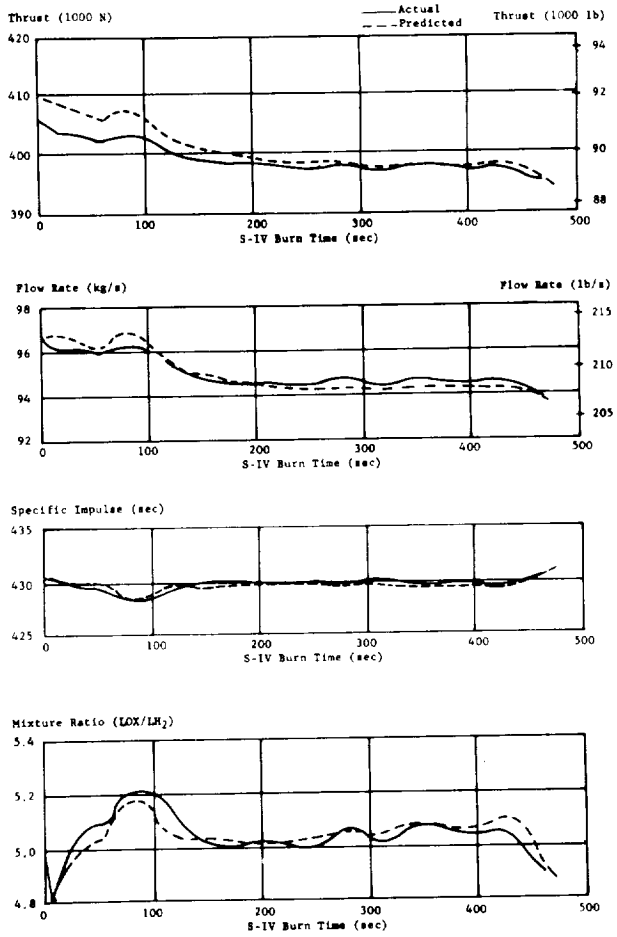

FIGURE 6-11. TOTAL S-IV STAGE PERFORMANCE (ENGINE ANALYSIS)

6.7.2.2 FLIGHT SIMULATION

Adjustment of the propulsion parameter histories obtained by engine analysis was accomplished by employing a six-degree-of-freedom trajectory simulation computer program incorporating a differential correction procedure. The ignition weight determined from the engine analysis was considered known. The results of the simulation indicate that the S-IV-7 stage performance was very close to the performances of previous S-IV stages, and was nearly a duplicate of S-IV-5 performance.

The simulation was obtained by varying vehicle thrust, mass flow, and pitch plane engine misalignment until the best fit of the actual trajectory parameters was obtained. The simulated trajectory matched the actual trajectory with a greater degree of accuracy than on any of the previous flights. The following average deviations existed:

1. Slant Range - 28 m
2. Earth-Fixed Velocity - 0.32 m/s
3. Altitude - 44 m

Since the actual was very close to the simulated trajectory, the only significant uncertainties in the results are those due to possible inaccuracies in postflight vehicle weight, in actual trajectory, and in thrust and mass flow shape from the engine analysis. It is estimated that these uncertainties could cause error of up to 0.3 percent in each of the propulsion parameters.

Table 6-IV compares the flight simulation and engine analysis results to predicted values. It can be seen that the S-IV-7 vehicle thrust and specific impulse were lower than predicted, and that the vehicle mass flow was nearly equal to predicted. As on previous flights, the vehicle specific impulse and thrust, as determined by the trajectory simulation technique, were somewhat less than those determined by engine analysis, indicating that the propulsion parameters determined from engine analysis are incompatible with the actual trajectory.

The flight simulation technique provides an accurate determination of a vehicle mass history, if the vehicle weight at any point of the trajectory is accurately known. The SA-7 flight simulation results completely verify the postflight vehicle mass history

TABLE 6-IV. S-IV-7 PROPULSION SYSTEM PERFORMANCE

Parameters			
	Predicted	Flight Simulation	Engine Analysis
Longitudinal Vehicle Thrust (N)	399,477	395,909	399,450
(lb_f)	89,806	89,004	89,800
Vehicle Mass Loss Rate (kg/s)	95.6	94.9	94.8
(lbm/s)	210.8	209.3	209.0
Longitudinal Vehicle Specific Impulse (sec)	429.5	425.3	429.6

Definition of Propulsion Parameters

Longitudinal Vehicle Thrust accounts for engine cant angle, and includes helium heater thrust and thrust originating at the cooldown vents due to leakage of LH_2 through the engine cooldown valves during engine operation. Ullage rocket thrust and predicted aerodynamic base drag (600.5 N or 135 lb_f thrust effect) are not included.
Vehicle Mass Loss Rate includes all stage weight flowrates, such as the sum of individual engine propellant weight flowrates, leakage of LH_2 through the cooldown valves, and helium heater propellant weight flow. Ullage rocket flowrate is not included.
Longitudinal Vehicle Specific Impulse is vehicle longitudinal thrust divided by vehicle mass loss rate.

*Average values between 90% S-IV thrust and S-IV cutoff.

obtained from the combination of propellant sensor data and stage weights. Using the actual initial mass as an initial condition for the flight simulation, it was determined that the S-IV cutoff mass derived from flight simulation was within 6.35 kg (14 lbm) of the actual S-IV cutoff mass measured during flight by capacitance probe data and point level sensor data.

6.7.3 INDIVIDUAL ENGINE PERFORMANCE

The six Pratt and Whitney RL10A-3 engines, which powered the S-IV stage, functioned satisfactorily during prestart, start, steady state, and cutoff. All engine events occurred as scheduled, and performance levels of all engines were consistent with performance levels established during acceptance testing.

6.7.3.1 ENGINE COOLDOWN

The engine cooldown period was 42.0 seconds for LH_2 and 10.1 seconds for LOX. The LOX consumption for cooldown was approximately 68.04 kg (150 lbm), or an average flow rate of 1.13 kg/s (2.5 lbm/s) per engine. The LH_2 consumption for cooldown was approximately 136 kg (250 lbm), or an average LH_2 flowrate of 0.454 kg/s (1.0 lbm/s) per engine.

6.7.3.2 START TRANSIENTS

Normal start transients were noted for all engines. The engine thrust buildup at the 90 percent level was achieved by all engines between 1.88 and 2.18 seconds after start command. For comparison, the chamber pressure transients at start are shown in Figure 6-12. The individual engine chamber pressure and the thrust overshoot during engine start transient were negligible. Engine thrust overshoot values were less than 5 percent on all engines.

6.7.3.3 STEADY STATE OPERATION

Satisfactory performance of the engines was demonstrated throughout the flight. Average engine specific impulse for the engines was 431.3 seconds with a mean total engine thrust level of 401,390 N (90,236 lb_f). Maximum and minimum mixture ratio levels during the flight were 5.28 and 4.80 respectively. The maximum mixture ratio occurred at a PU valve angle of -14 degrees while the minimum occurred at an angle of 21 degrees. Figure 6-13 shows the deviations from predicted thrust and specific impulse.

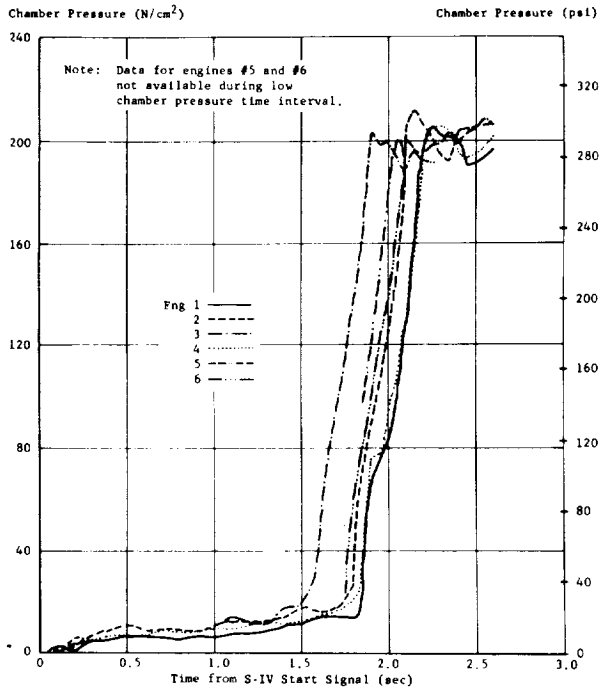

FIGURE 6-12. INDIVIDUAL ENGINE START TRANSIENTS

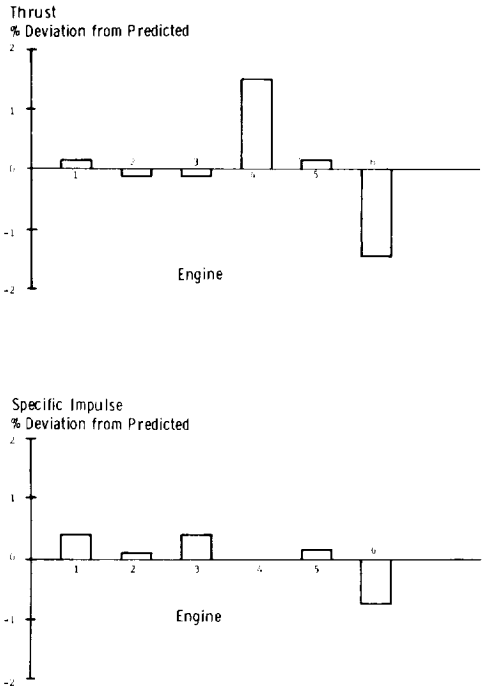

FIGURE 6-13. S-IV ENGINE DEVIATION FROM PREDICTED

6.7.3.4 CUTOFF TRANSIENTS

Engine cutoff was initiated by a guidance signal at 621.38 seconds. The six engine cluster experienced a smooth thrust decay and reached 5 percent within 0.128 to 0.152 seconds, as shown in Figure 6-14. The total cutoff impulse subsequent to guidance

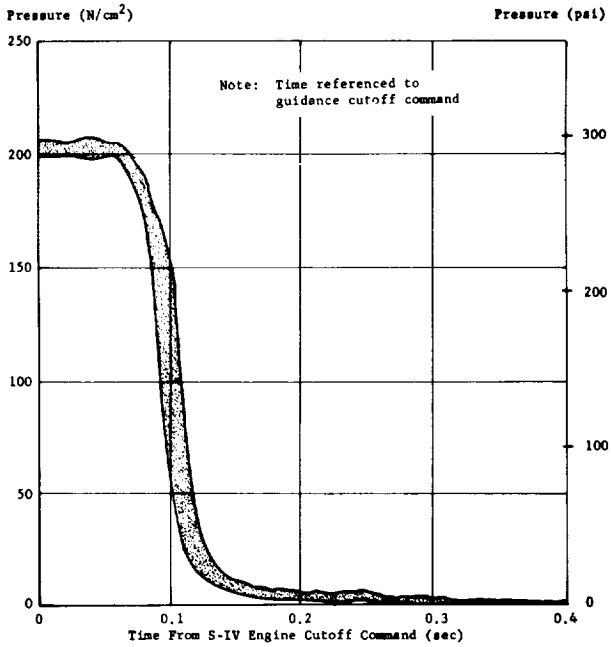

FIGURE 6-14. S-IV CUTOFF TRANSIENTS

cutoff signal from engine measurements was 50,803 N-s (11,421 lb_f-s), compared to a predicted nominal impulse of 29,038 N-s (6,528 lb_f-s) which was used in the predicted trajectory and does not include the 8,807 N-s (1,980 lb_f-s) due to relay time delay or the 2,224 N-s (500 lb_f-s) due to vent ducts. Analysis of velocity gains determined from guidance indicates a cutoff impulse of 49,375 N-s (11,100 lb_f-s)

An investigation of the continued higher than predicted cutoff impulse on the S-IV stage flights was made. Comparisons of flight and engine acceptance test data confirm the higher flight shutdown impulse in that they show 0.01 to 0.02 second slower decay characteristics for all engines during flight. Because of back EMF effects engine solenoid movements can be greatly affected by vehicle electrical circuits. Test runs at Pratt & Whitney Aircraft indicate that the 39-volt Zener Diodes used in the vehicle filter circuits at the engine solenoids cause delays in solenoid actuation times of approximately 0.008 second. This effect, as well as other electrical effects, is considered the most likely explanation of the increased cutoff impulse.

As a result of the investigation, it has been determined that the predicted value for cutoff impulse on the S-IV stage of SA-9 will be changed to 48,930 N-s (11,000 lb-s) not corrected for engine cant.

The following sketch illustrates the method used in determining the cutoff impulse of each engine.

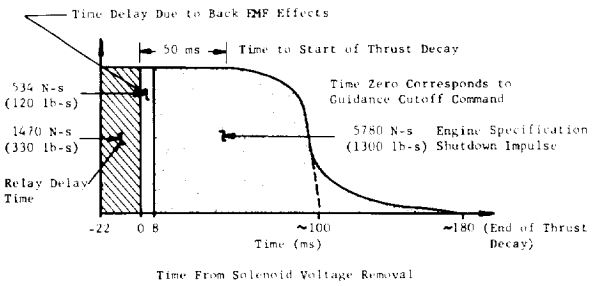

6.8 S-IV PRESSURIZATION SYSTEM

6.8.1 LH_2 TANK PRESSURIZATION

During the S-IV-7 flight, the LH_2 tank pressurization system performed satisfactorily. Figure 6-15 presents the LH_2 tank ullage pressures during prepressurization, S-I boost and S-IV flight.

The LH_2 pump inlet conditions were maintained within the engine specification requirements range throughout flight except for NPSP. The LH_2 tank was prepressurized with ground supplied helium from 11.0 N/cm^2 (15.9 psi) to 24.9 N/cm^2 (36.1 psi).

The ullage pressure decayed to 24.1 N/cm^2 (35.0 psi) at S-I liftoff. By the time of LH_2 prestart, the ullage pressure had decayed to 23.8 N/cm^2 (34.5 psi). The ullage pressure decreased during cooldown and was approximately 20.5 N/cm^2 (29.8 psi) at 140.0 seconds, at which time the ambient helium makeup was initiated by the LH_2 tank ullage pressure switch for the first time. The first makeup cycle lasted 3.5 seconds. Makeup was activated a second time at 150.0 seconds, and this cycle lasted approximately 3.0 seconds. Approximately 0.34 kg (0.74 lbm) of helium were used during makeup.

Inflight fuel tank pressurization is accomplished by GH_2 which is tapped off the engine supply downstream of the main fuel shutoff valve and routed through

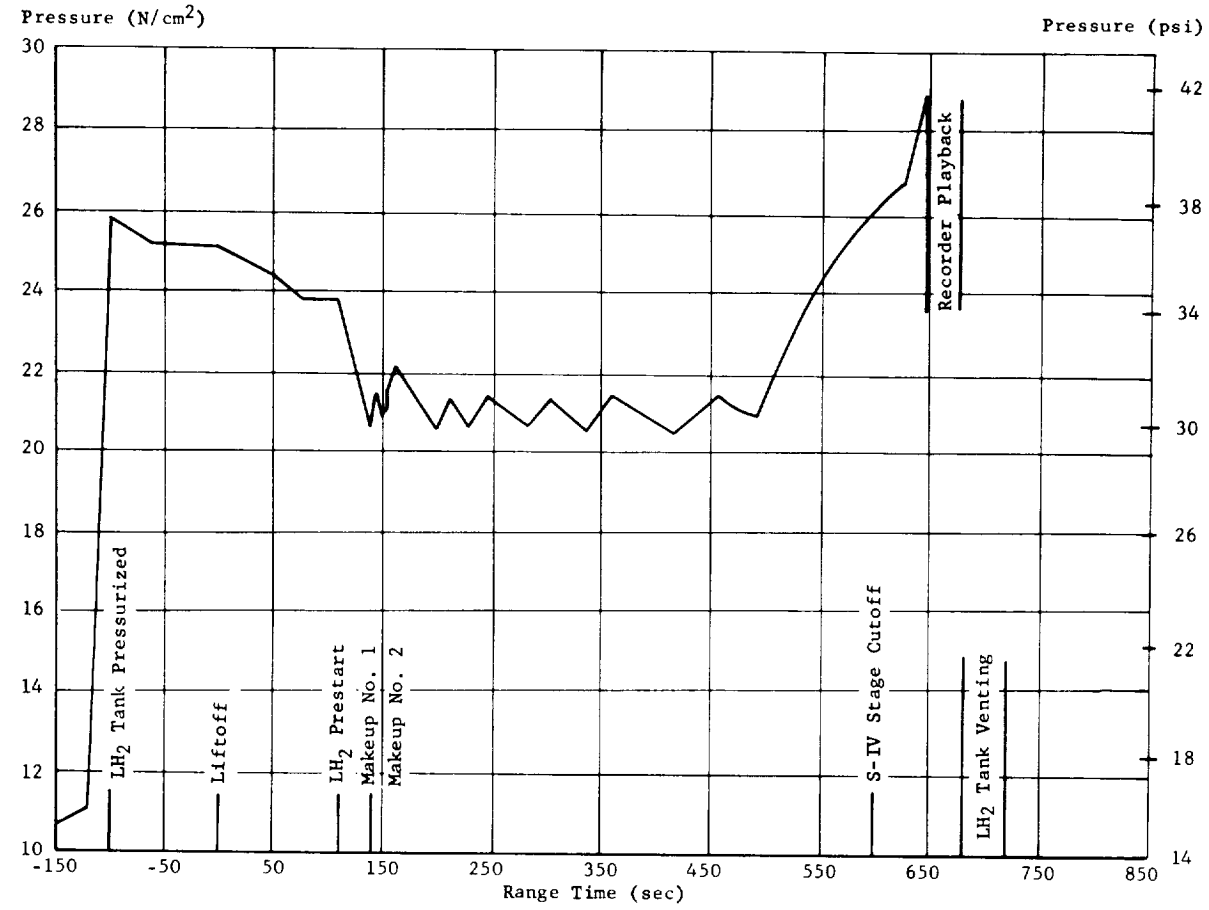

FIGURE 6-15. FUEL TANK ULLAGE PRESSURE DURING PREPRESSURIZATION S-I BOOST AND S-IV FLIGHT

the fuel tank pressurizing valve. Prior to initiation of step pressurization on signal from the propellant utilization system at 488.4 seconds, the LH_2 tank ullage pressure cycled between approximately 20.5 and 21.4 N/cm^2 (29.8 and 31.1 psi). The initiation of step pressurization opens the step pressure solenoid and the tank pressure is allowed to approach the vent setting. The ullage pressure increased from 20.8 N/cm^2 (30.2 psi) at initiation of step pressurization to 26.4 N/cm^2 (38.3 psi) at S-IV-7 stage cutoff.

The average pressurant temperature was approximately 186°K. The average pressurant flowrates obtained during normal, control and step were 0.051, 0.079 and 0.124 kg/s (0.113, 0.175 and 0.274 lbm/s), respectively. Average ullage temperature at cutoff was approximately 150°K. During the flight, 36.2 kg (79.9 lbm) of GH_2 was used to pressurize the tank, 19.7 kg (43.5 lbm) of which was used prior to step pressurization.

The performance of the non-propulsive vent system was as expected. See Section VIII for details on system performance.

6.8.1.1 LH_2 PUMP INLET CONDITIONS

Based on engine performance data, the LH_2 pump inlet conditions were adequate throughout the entire flight, even though minimum required conditions were not achieved for approximately 30 seconds (see Figure 6-16). Minimum NPSP was 4.8 N/cm^2 (7.0 psi) at initiation of step pressurization.

6.8.2 LOX TANK PRESSURIZATION

During the S-IV-7 stage flight, the LOX tank pressurization system operation was satisfactory. The LOX tank is pressurized with cold GHe from a ground source immediately prior to liftoff. During the S-IV powered phase pressure to LOX tank is provided by the helium heater. Figure 6-17 presents the LOX tank ullage pressure during prepressurization, S-I boost and S-IV flight.

Throughout flight, the engine total pump inlet pressures were above 31.7 N/cm^2 (46 psi) and the NPSP were well above the minimum required limit of 10.3 N/cm^2 (15 psi). At the initiation of automatic count (150 sec prior to liftoff), the LOX tank was prepressurized to approximately 33.0 N/cm^2 (47.9 psi) with about 1.9 kg (4.1 lbm) of ground supplied helium.

Between 120 and 100 seconds before liftoff, the LOX tank vent valve number 1 cycled 4 times. The LOX tank ullage pressure then decayed to about 30.1

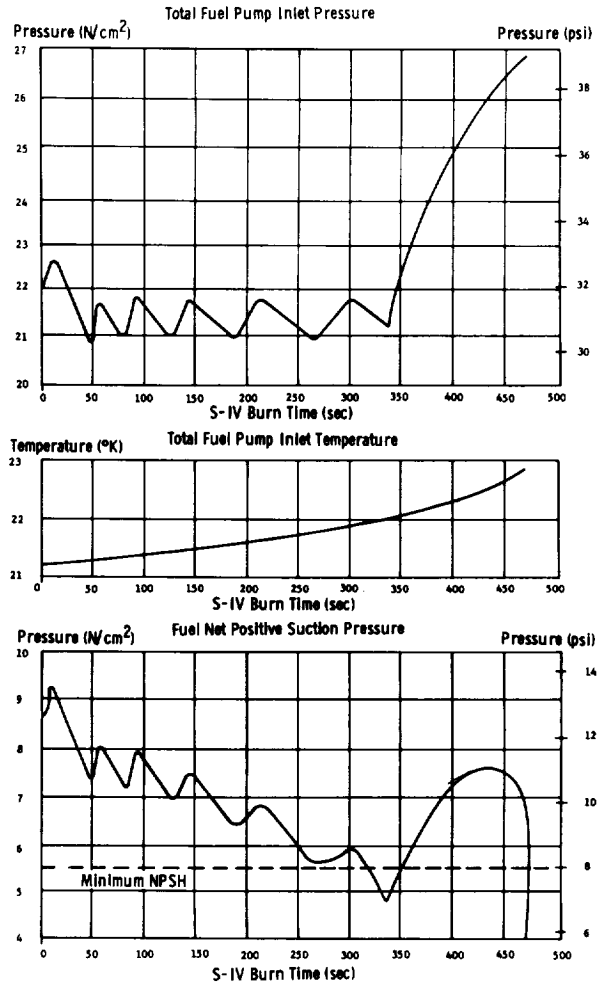

FIGURE 6-16. LH_2 PUMP INLET PARAMETERS

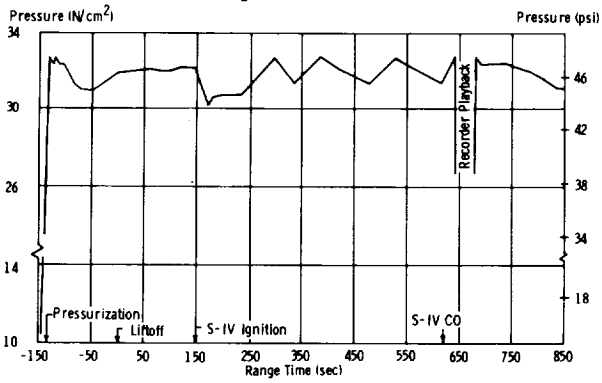

FIGURE 6-17. LOX TANK ULLAGE PRESSURE DURING PREPRESSURIZATION, S-I BOOST & S-IV FLIGHT

N/cm^2 (43.6 psi) at approximately 60 seconds before liftoff, after which it leveled off and began to increase. This pressure decay may have been due to flow from a vent valve pilot which remained unseated from the last vent until 60 seconds prior to liftoff.

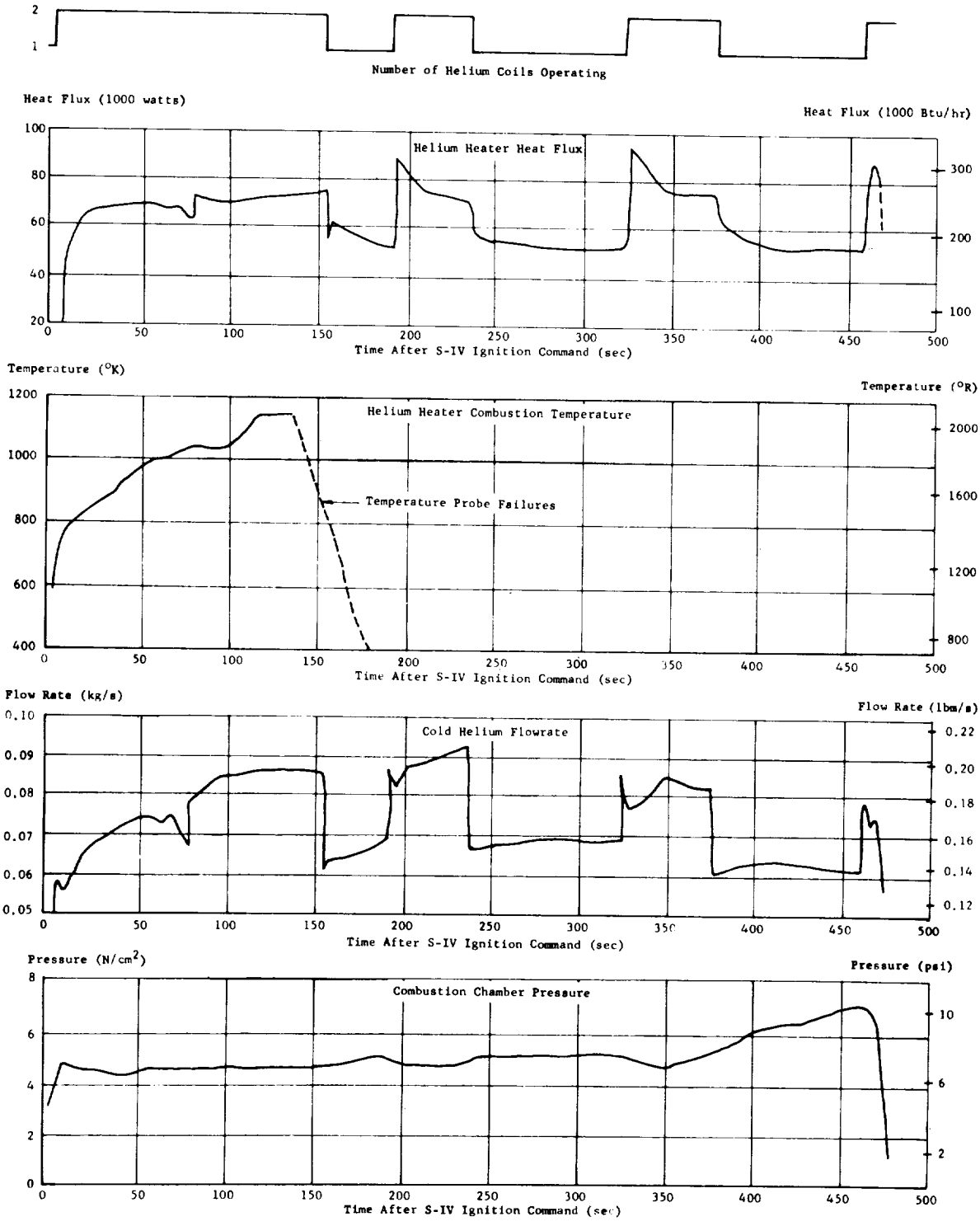

FIGURE 6-18. S-IV HELIUM HEATER PERFORMANCE

During S-I boost, the LOX tank ullage pressure remained relatively constant, which may be attributed to a balance between a pressure decrease due to propellant slosh and a pressure increase due to the vent valve purge.

As shown in Figure 6-18, the S-IV-7 flight demonstrated the successful operational capability of the helium heater as an integral component of the stage LOX tank pressurization system. Helium heater ignition was normal at the S-IV stage engine command, with the combustion temperature rising rapidly to above 556°K within three seconds. The combustion temperature continued to rise for 140 seconds of S-IV stage powered flight, reaching a maximum of 1144°K and then decreasing rapidly to off-scale. Investigation of other heater parameters, such as cold helium orifice inlet temperature and heat flux, shows that the combustion temperature drop was invalid, due to an instrumentation failure. Five seconds after S-IV stage engine cutoff, the combustion temperature rose sharply, showing the characteristic shape of the temperature transient after cutoff.

Helium heater heat flux was satisfactory for the full duration of the S-IV stage powered flight, averaging approximately 7.61 x 10^4 watts (260 x 10^3 Btu/hr) for two-coil mode and 5.42 x 10^4 watts (185 x 10^3 Btu/hr) for single-coil mode. The helium heater secondary coil control valve cycled 3.5 times during S-IV stage powered flight, with single-coil mode occurring during 45.5 percent of this time, and two-coil mode occurring during the remainder of the time. It is noted that the S-IV-7 was the first flight stage that did not incorporate the LOX tank pressurization backup system. The LOX tank pressure demands and the normal tank pressurization system operation were such that the backup system was not required.

The performance of the non-propulsive vent system was as expected. See Section VIII for details on system performance.

6.8.2.1 LOX PUMP INLET CONDITIONS

The LOX supply system delivered the necessary quantity of LOX to the engine pump inlets while maintaining the required conditions of pressure and temperature. The LOX pump inlet temperature stabilized at the bulk temperature of 90.4°K within 5 seconds after engine start. The temperature then slowly increased, maintaining an average of 91.81°K by the time of S-IV stage cutoff. The inlet conditions shown in Figure 6-19 were within the specified limits of temperature and pressure throughout S-IV operation. Cold helium bubbling was initiated at 488 seconds prior to liftoff and continued satisfactorily until its termination

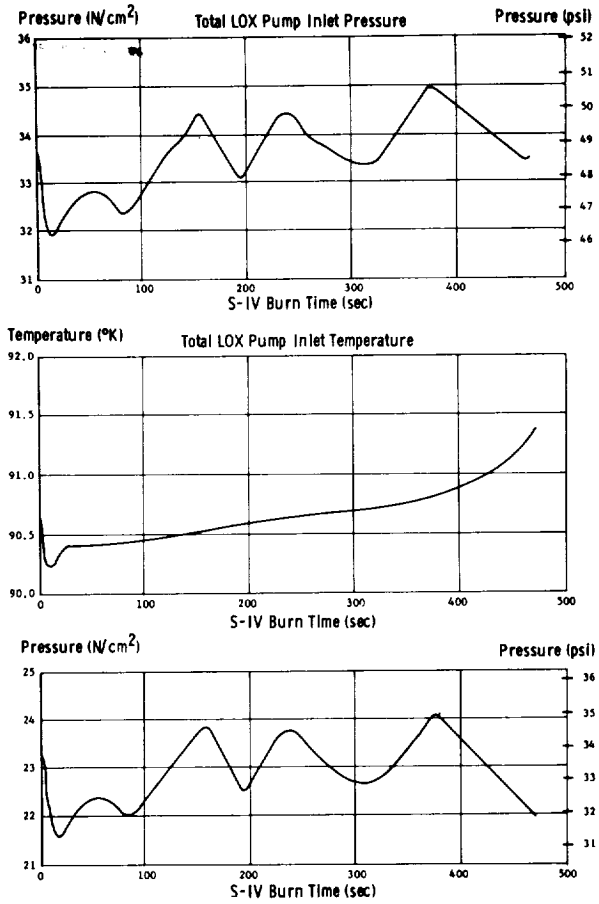

FIGURE 6-19. LOX PUMP INLET CONDITIONS

at 188 seconds prior to liftoff. The LOX pump inlet temperatures decreased in a normal manner and, at termination of cold helium bubbling, were within the range of 78.9° K to 81.4° K. This temperature range compared favorably with expected values. By prestart, the temperatures had increased to 92.2° K and 94.2° K, both of which were within the required limits of 90.3° K to 97.7° K. At engine start, the inlet temperatures were between 90.6° K and 91.1° K. A time-history of LOX pump inlet temperatures during the cold helium bubbling operation and the LOX pump cool-down period is presented in Figure 6-20.

6.8.3 COLD HELIUM SUPPLY

During S-IV stage flight, the cold helium supply was more than adequate. The pressure and temperature in the cold helium spheres at SA-7 liftoff were 2137 N/cm² (3100 psi) and 21.9°K respectively, indicating a helium mass of 57.4 kg (126.5 lbm). A lack of temperature data for the number 2 cold helium sphere during flight negates any determination of helium mass in the bottles after liftoff. However, the monitoring of pressure and temperature conditions at the LOX tank pressurization control orifice, during S-I boost and S-IV powered flight, verified that no

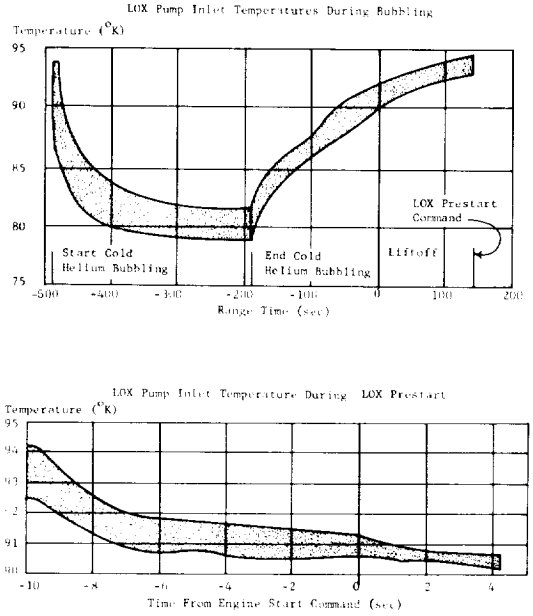

FIGURE 6-20. COLD HELIUM BUBBLING PERFORMANCE

makeup pressurization from the cold helium spheres was required prior to S-IV ignition. Based upon integration of the pressurization flow rate during S-IV burn, it was determined that 34.9 kg (77 lbm) of helium were consumed for LOX tank pressurization, leaving a residual of 22.5 kg (49.5 lbm) helium in the storage spheres.

6.8.4 CONTROL HELIUM SYSTEM

The S-IV-7 pneumatic control system operation was satisfactory during preflight checkout and flight. The control helium sphere was pressurized to approximately 2027 N/cm^2 (2940 psi); it decreased during S-I powered flight to about 1986 N/cm^2 (2880 psi) and reached approximately 1850 N/cm^2 (2690 psi) at S-IV engine cutoff. The sphere temperature ranged from a maximum of 292°K at liftoff to a minimum of 267°K at about 175 seconds after S-IV engine start. By the time of S-IV engine cutoff, the sphere temperature had increased to 268°K.

The control helium regulator outlet pressure varied between 344 and 327 N/cm^2 (499 and 474 psi) from liftoff to S-IV engine start command, after which time it stabilized at 330 N/cm^2 (478 psi). The change in regulator discharge pressure reflects the change in the ambient reference pressure.

6.9 S-IV PROPELLANT UTILIZATION SYSTEM

The propellant utilization (PU) system performed satisfactorily. The usable residuals above the pump inlets at command cutoff were 980 kg (2154 lbm) of LOX and 203 kg (447 lbm) of LH_2. If the S-IV-7 flight had been permitted to run to propellant depletion, the propellant utilization at depletion cutoff signal would have been 99.95 percent of the usable propellants loaded. The residual at depletion cutoff would have been 22.7 kg (50 lbm) of LH_2.

6.9.1 PROPELLANT MASS HISTORY

The propellant mass history at various event times is presented in the following table. The values are for total mass above the pump inlet.

Event	LOX		LH_2	
	kg	lbm	kg	lbm
First Motion	38,225	84,271	7,772	17,134
LH_2 Prestart	38,221	84,263	7,771	17,132
LOX Prestart	38,220	84,260	7,681	16,934
Ignition	38,163	84,135	7,657	16,881
PU Activation	37,903	83,562	7,600	16,755
Residual	977	2,154	203	447

The values in the table are based on separate studies of telemetered subsystem and engine propellant flow data.

6.9.2 SYSTEM RESPONSE

The PU system responded properly during S-IV-7 flight and provided the necessary PU valve movement to correct for the mass errors sensed by the system. Figure 6-21 shows the actual movement of the PU valve during S-IV stage flight.

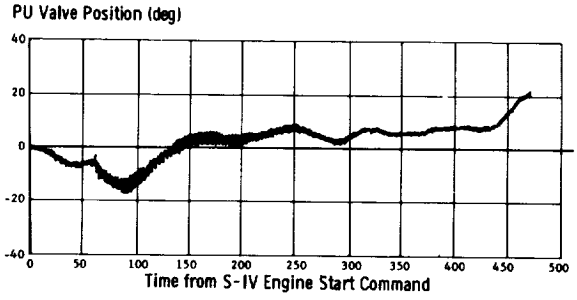

FIGURE 6-21. TYPICAL PROPELLANT UTILIZATION VALVE POSITION

At the time of PU system activation, the system sensed a positive equivalent LOX mass error (excess LOX 98.4 kg or 217 lbm) and positioned the PU valves, causing the engines to assume a higher mixture ratio. The factors primarily responsible for this PU valve excursion were non-linearities in the system and the initial LOX mass error sensed in the system. This initial mass error on SA-7 was within the accuracy of the loading system.

The average engine mixture ratio excursions during flight varied between 4.8 and 5.28, which are well within engine operational capabilities.

6.9.3 PU SYSTEM COMMAND

The PU system is designed to originate three commands:

1. The PU System Gain Change Command
2. The LH_2 Tank Step Pressure Command
3. The Arm All Engine Cutoff Command

The first two commands occurred at the proper times; the third was overridden by a signal from the IU.

The PU System Gain Change was scheduled to occur when the PU system indicated that the LOX mass had decreased to 33,513 kg (73,884 lbm). The command was observed to occur at 209.74 seconds (S-IV-7 stage engine start command was 150.14 sec). The LOX mass at this time was 33,467 kg (73,783 lbm), which was within the expected tolerance range.

The LH_2 Tank Step Pressure Command was scheduled to occur when the PU system indicated that the LOX mass had reached 11,476 kg (25,300 lbm). This command was observed to occur at 488.11 seconds, at which time the LOX mass was 11,378 kg (25,085 lbm). This mass value was within tolerance.

6.10 S-IV-7 HYDRAULIC SYSTEM

The S-IV hydraulic system's performance was satisfactory throughout the SA-7 flight. The sequence valves opened upon command, and the accumulators provided an adequate supply of high pressure oil to preposition the engines prior to engine start. When the engine driven pumps achieved a stabilized output, the accumulators bottomed in an oil filled position. This reaction was as expected. The accumulators are not required to absorb pump pulsations or pressure surges; system compliance provides the necessary damping.

Engine position control was maintained after engine cutoff for the following lengths of time:

Engines 1, 4, 5, & 6	22 sec minimum
Engine 2	21 sec
Engine 3	21.5 sec

Engines 1, 4, 5 & 6 still had a positive accumulator charge at the time (22 sec) noted; the onboard recorder playback interrupted the pertinent data transmission at that time, preventing an accurate placing of the accumulator fluid exhaustion point.

6.11 ULLAGE ROCKETS

Ullage rocket performance was satisfactory. The ullage rocket ignition command was given at 148.34 seconds. After ignition command the chamber pressure of rockets 3 and 4 began to increase immediately, while the chamber pressure increase of rockets 1 and 2 was delayed approximately 0.05 second. The chamber pressure rise rates, which were similar for all four rockets, required approximately 0.03 second to increase from 0 to 689 N/cm^2 (1,000 psi), representing a rate of approximately 23,000 $N/cm^2/s$ (33,000 psi/s). The chamber pressures during mainstage operations were nominal, averaging approximately 710 N/cm^2 (1,030 psi). The burn time above 90 percent thrust level, corresponding to chamber pressure of approximately 620 N/cm^2 (900 psi), was 3.7 seconds, which compares favorably with the required minimum of 3 seconds.

At burnout, the chamber pressures of all four rockets decreased simultaneously. Actual flight data compared with the manufacturer's data revealed an overall performance level that was slightly above the typical manufacturer-specified performance level for a grain temperature of 294°K. It should be noted that when the ullage rocket pressure sensing lines were installed, they were empty, not oil filled. Rocket thrust data, presented in Figure 6-22, show that the

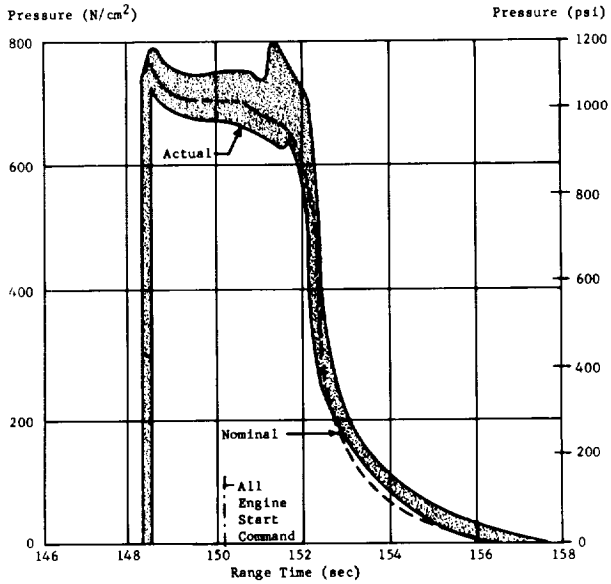

FIGURE 6-22. ULLAGE ROCKET CHAMBER PRESSURE

total longitudinal impulse (the impulse parallel to the axis of the stage) was 270,452 N-s (60,800 lb-s), which was within 0.5 percent of the predicted nominal.

Rocket jettison was satisfactory, with all rockets being jettisoned from 12.1 to 13.3 seconds after ullage rocket ignition command.

SECTION VII. GUIDANCE AND CONTROL

7.1 SUMMARY

The overall performance of the guidance and control system on SA-7 was satisfactory. The vehicle responded properly to the simultaneously executed roll and pitch programs which began shortly after liftoff. As expected, a counterclockwise roll moment, due to the unbalanced aerodynamic forces caused by the S-I turbine exhaust ducts, generated a vehicle roll attitude error (3.5 deg at 60 sec). Minor changes in pitch attitude and engine deflection were noted due to the change in control system gain coefficients at 110 seconds and due to a change in total thrust vector alignment at IECO. The roll torque due to the thrust vector misalignment caused only a 0.2-degree clockwise roll attitude error shortly after liftoff; after IECO the angle increased to 0.4 degree. These values are very small compared with SA-6 which experienced roll angles of 1 degree after liftoff and 3 degrees after IECO. These reduced roll angles are due primarily to the much smaller roll torque on SA-7 and secondarily to the fact that the roll gain was held constant throughout S-I powered flight (on SA-6 it was reduced by 50 percent at 110 sec).

A vehicle roll deviation of 5.9 degrees developed during S-I stage separation due to a much larger than expected misalignment of the S-IV ullage rockets. When the S-IV control system became effective about two seconds after separation, the roll angle was rapidly reduced. During this correction, the maximum roll rate of 5.6 deg/s was observed.

At path guidance initiation the vehicle's space-fixed velocity was about 1 percent higher than nominal. This condition caused the guidance system to issue a nose down pitch steering command correction which peaked at 4.5 degrees at 190 seconds. During this period (at 169 sec), the ST-124 platform issued a maximum nose up pitch attitude error signal of 2.3 degrees to the vehicle flight control system.

In the yaw plane, the computer data showed that the vehicle was to the left (-12.2 m/s and -460 m) at guidance initiation. Consequently, the guidance system issued maximum steering corrections of -5.7 deg χ_Y and 1.6 deg χ_X (nose right and CW viewed from rear). During this time (at 174 sec), the largest attitude error signals issued by the ST-124 to the vehicle flight control system were 2.4 degrees nose left yaw and 0.6-degree roll (CCW viewed from rear). The maximum yaw and roll attitudes resulting from the initiation of yaw plane guidance were 5.6 degrees nose left and 0.85-degree CW, occurring at 174 seconds.

The overall performance of the guidance system was satisfactory. At guidance initiation the computer indicated that the vehicle was to the left of the planned trajectory; 250 seconds later, these initial values of -12.2 m/s and -460 m reached 0 m/s and -190 m. However, due to the increasing S-IV stage center of gravity offset, the digital computer velocity increased to -0.4 m/s at 500 seconds and stabilized at that value through S-IV cutoff. The displacement from the reference trajectory measured at that time was -254 m (to the left).

The pitch plane steering misalignment correction term (χ_{ZC}) (introduced some 6 sec after guidance initiation) ranged from 1.0 degree to 1.4 degrees at the end of path guidance, well within the expected limits. At S-IV guidance cutoff command, the space-fixed velocity vector calculated by the digital computer was 7806.0 m/s and the altitude (calculated from computer data) was 184.6 km. These measured values compare favorably with the cutoff velocity presetting value of 7806.0 m/s and the precalculated altitude of 185.3 km. At S-IV cutoff command, the adjusted powered flight tracking data show that the actual space-fixed velocity was 7807.8 m/s (1.8 m/s larger than the velocity presetting) and the actual altitude was 184.3 km (1.0 km lower than the precalculated altitude).

The inertial velocity components measured by the ST-124 accelerometers are in agreement with those calculated by the digital computer. The predicted (based on the ST-124 system's 3σ errors) and measured inertial velocity component differences (i.e., accelerometer-tracking) at S-IV cutoff were:

Velocity Component	Predicted Difference (m/s)	Measured Difference (m/s)
Range	± 0.4	-1.0
Altitude	± 1.6	3.6
Cross Range	± 1.8	4.7

The measured differences are approximately two and one-half-times larger than those predicted for the SA-7 flight and are due principally to the development of large stabilized platform leveling errors after S-I ignition. The inertial velocity component differences (accelerometer-tracking) calculated using the laboratory measured ST-124 system errors (plus the pre-ignition range and cross range accelerometer leveling errors and the azimuth misalignment) fall well within the 3σ error bands.

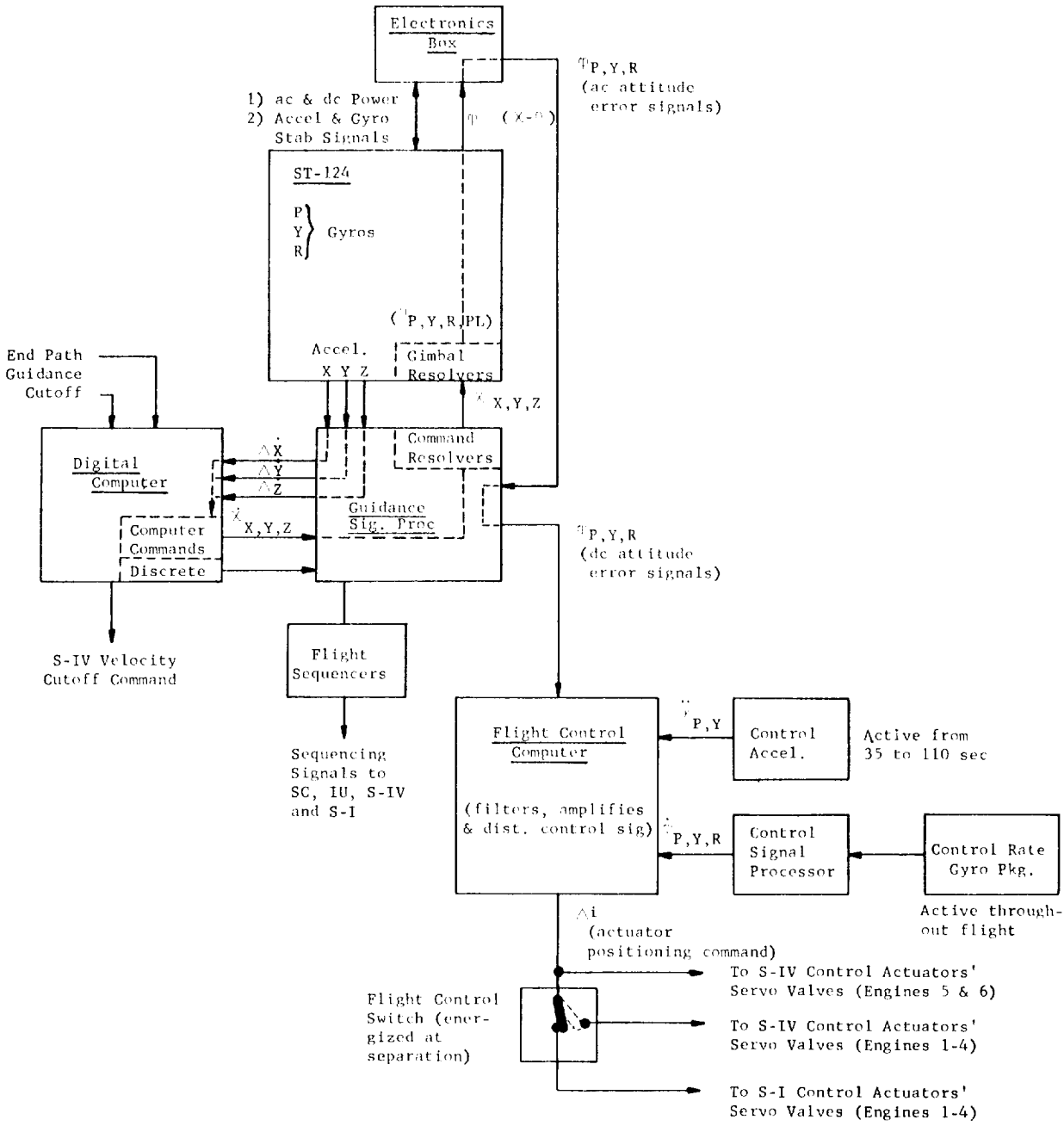

FIGURE 7-1. GUIDANCE AND CONTROL SYSTEM

7.2 SYSTEM DESCRIPTION

SA-7 was the first Saturn I vehicle to employ a fully active ST-124 guidance system. The principal functions of this system are to:

1. Generate attitude error signals for vehicle control and steering throughout flight.

2. Issue timed discretes to the Spacecraft, Instrument Unit, S-IV and S-I stages for sequencing vehicle events throughout the entire flight period.

3. Compute and issue steering commands for active path guidance during S-IV stage burn.

4. Terminate path guidance and initiate S-IV engine shutdown at the preselected space-fixed velocity.

The ST-124 guidance system consists of the ST-124 stabilized platform assembly and electronics box, the guidance signal processor and the digital computer. Figure 7-1 shows the interrelationship between the components of this system and their integration with the elements of the vehicle's control system. The operational periods of these major guidance and control system components are also indicated.

7.3 CONTROL ANALYSIS

7.3.1 S-I STAGE FLIGHT CONTROL

7.3.1.1 PITCH PLANE

Pitch plane deviations were small throughout S-I stage flight with maximum values observed in the Mach 1 to max Q region. The maximum deviations in the control parameters were:

Parameter	Magnitude	Range Time (sec)
Attitude Error (deg)	0.9	54.5
Angle-of-Attack (free stream) (deg)	-1.0	75.0
Angular Rate (deg/s)	-1.2	64.2
Normal Acceleration (m/s^2)	-0.8	75.0
Actuator Position (deg)	-1.6	75.0
Angle-of-Attack Dynamic Pressure Product ($deg\text{-}N/cm^2$)	3.7	75.0

This is the first flight in which the digital computer provided the pitch program. It utilized a five-term polynominal to generate the required vehicle pitch rate. The vehicle pitch commands were properly executed by the guidance and control system. The vehicle began to pitch over at 13.5 seconds; the program continued until 136.6 seconds where it was arrested at 66.75 degrees from the launch vertical.

First mode slosh frequencies (0.7 to 1.5 Hz) of the S-I propellants are indicated by the pitch angular rates during S-I stage flight. These slosh forces are largest during the max Q region; the resulting angular rates are ± 0.3 deg/s.

The pitch program was based on a zero wind profile. The largest pitch wind was 12 m/s observed during the max Q region. A wind velocity change of 4.7 m/s over a 650 m altitude increment caused the maximum angle-of-attack of 1 degree at 75.0 seconds (74.4 km altitude).

Figure 7-2 shows comparisons of the rawinsonde and angle-of-attack winds and angles-of-attack. The angle-of-attack winds which were calculated using the Q-ball angle-of-attack measuring system are in good agreement with rawinsonde winds. During the maximum dynamic pressure region (60 to 80 sec), the angle-of-attack determined from rawinsonde winds is within 0.2 degree of that measured from the Q-ball and the fin angle-of-attack meters. From 100 to 115 seconds, the measured angle-of-attack and that calculated using rawinsonde winds agree within 0.5 degree. These parameters indicate good operation of the measuring devices in the region of substantial dynamic pressure.

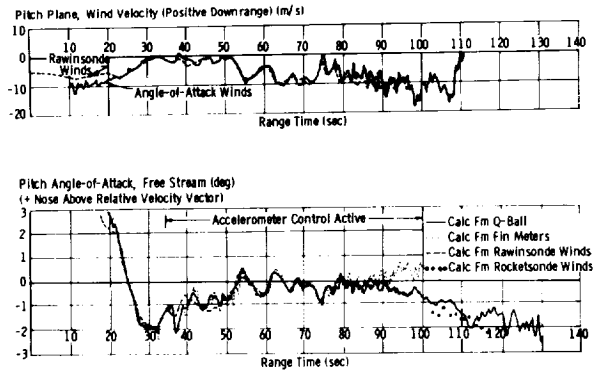

FIGURE 7-2. PITCH PLANE WIND VELOCITY COMPONENT AND FREE STREAM ANGLE-OF-ATTACK

The performance of the control system was satisfactory; however, there is evidence of a significant

disturbing moment in both the pitch and yaw planes. A six-degree-of-freedom (6-D) simulation of the telemetered values, made by using Q-ball angle-of-attack winds and an external nose down moment, is compared with the flight data in Figure 7-3. This moment has a maximum value of 698,000 N-m at 76 seconds and appears to have a shape related to the dynamic pressure. The cause of this moment is not known at this time. Agreement between the 6-D simulation and the telemetered values is within 0.2 degree in attitude error, 0.2 deg/s in angular rate, 0.15 degree in actuator position, and 0.2 degree in angle-of-attack during the max Q region.

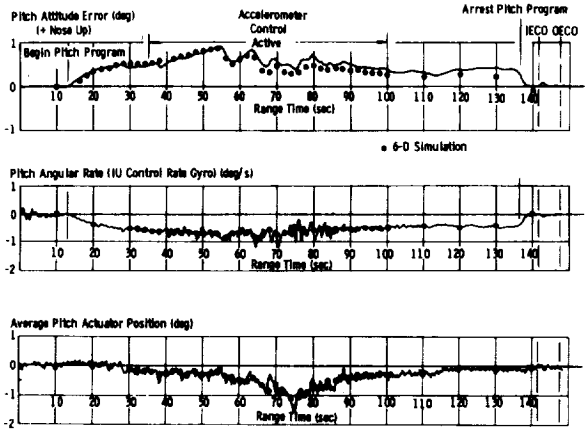

FIGURE 7-3. PITCH ATTITUDE, ANGULAR RATE AND AVERAGE ACTUATOR POSITION

7.3.1.2 YAW PLANE

The performance of the control system in the yaw plane was satisfactory. The maximum control values were:

Parameter	Magnitude	Range Time (sec)
Attitude (deg)	-0.6	72.1
Angle-of-Attack (free stream) (deg)	1.4	67.5
Angular Rate (deg/s)	-0.3	68.7
Normal Acceleration (m/s^2)	0.7	67.1
Actuator Position (deg)	-0.9	77.0
Angle-of-Attack Dynamic Pressure Product ($deg\text{-}N/cm^2$)	5.1	67.5

The rawinsonde and angle-of-attack yaw plane winds are shown in Figure 7-4. The maximum wind (15 m/s) is only about 1/5 of the 95 percent design wind.

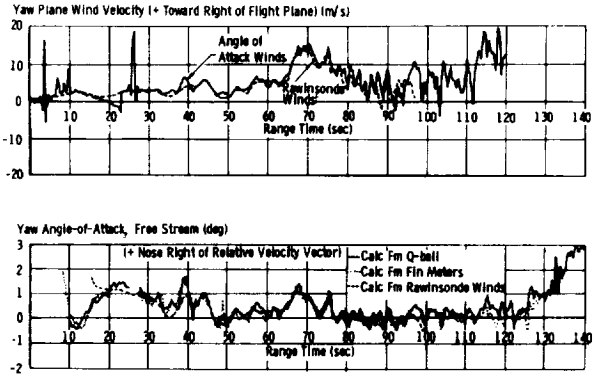

FIGURE 7-4. YAW PLANE WIND VELOCITY AND FREE-STREAM ANGLE-OF-ATTACK

The yaw attitude, angular rate, and average actuator position shown in Figure 7-5 indicate that perturbations in the yaw plane were very small. The peak yaw attitudes which occur during the max Q region are due to wind shears.

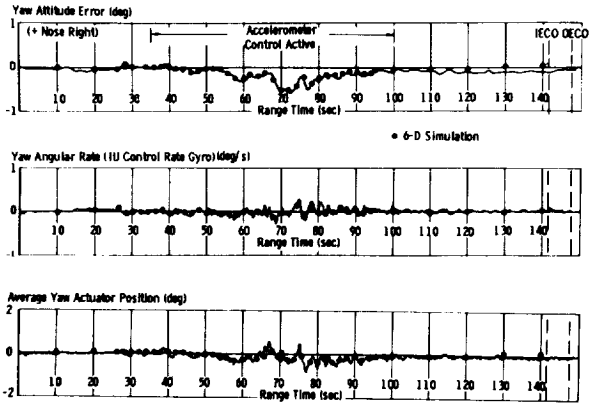

FIGURE 7-5. YAW ATTITUDE, ANGULAR RATE AND AVERAGE ACTUATOR POSITION

The vehicle appears to be trimming for a lateral CG offset towards Fin IV. At 140 seconds the attitude deviation is equivalent to a CG offset of 1.8 cm (0.7 in.), which is half the magnitude but in a direction opposite to that predicted. No explanation has been found for this minor deviation.

An external yaw moment is required in addition to the angle-of-attack winds to simulate the telemetered control deviations. This required external

moment has a maximum value of 420,000 N-m at 74 seconds. Agreement between the 6-D simulation and the flight data is within 0.1 degree in attitude, 0.1 deg/s in angular velocity, 0.1 degree in actuator position and 0.3 degree in angle-of-attack during the max Q region.

7.3.1.3 CONTROL DESIGN PARAMETERS

A comparison of total actuator deflection, angle-of-attack, and dynamic pressure angle-of-attack product between the flight results of SA-7 and Block II control system design criteria values is shown in Figure 7-6. The design value is based on a 95 percent non-directional wind velocity with 2σ shears and 11 percent variation in aerodynamics. Two σ variations in propulsion system performance and mass characteristics are also considered in arriving at the design values. The SA-7 data are similar to those of SA-5 and are well within the design values.

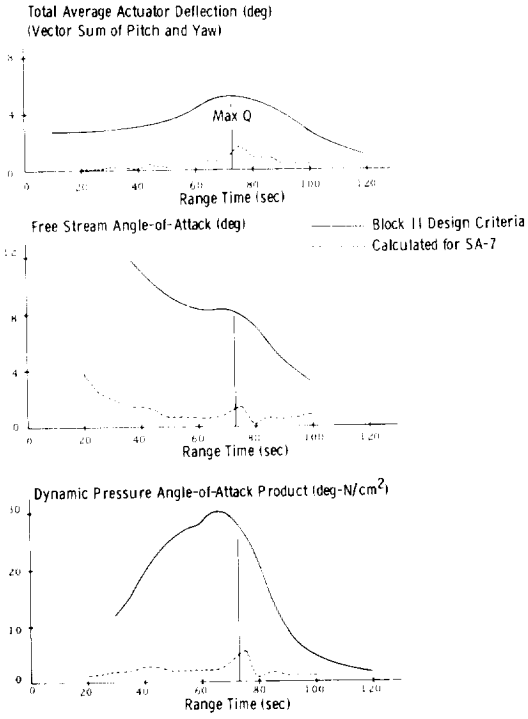

FIGURE 7-6. COMPARISON OF VEHICLE CONTROL PARAMETERS WITH DESIGN CRITERIA

7.3.1.4 ROLL PLANE

Immediately after liftoff SA-7 rolled counterclockwise to a steady state value of 0.2 degree (see Fig. 7-7). This indicates an S-I thrust misalignment in roll equivalent to 0.3-degree engine deflection for each control engine. At 11.35 seconds the required

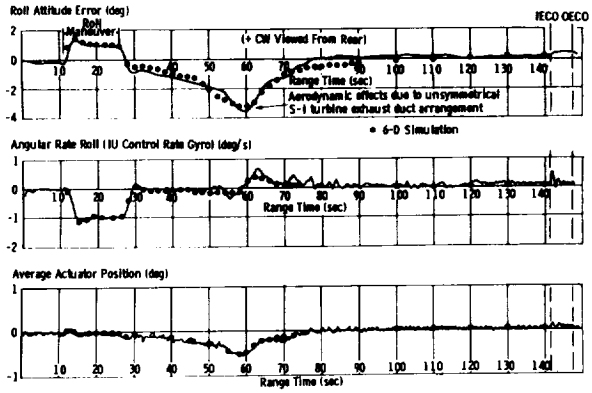

FIGURE 7-7. ROLL ATTITUDE, ANGULAR RATE AND AVERAGE ACTUATOR POSITION

launch-to-flight azimuth roll maneuver program began, rotating the vehicle's pitch and yaw axes into coincidence with the stabilized platform axes. The 15-degree roll program, executed at a rate of 1 deg/s, was completed at 26.4 seconds (Fig. 7-8). On previous Block II flights, the ST-90S stabilized platform was utilized to generate the roll attitude error signal to roll the vehicle from the 90-degree launch azimuth to the 105-degree flight azimuth. On SA-7, the digital computer issued a constant command rate to the χ_Y resolver to cause the ST-124 system to generate the roll attitude error signal used to accomplish the maneuver.

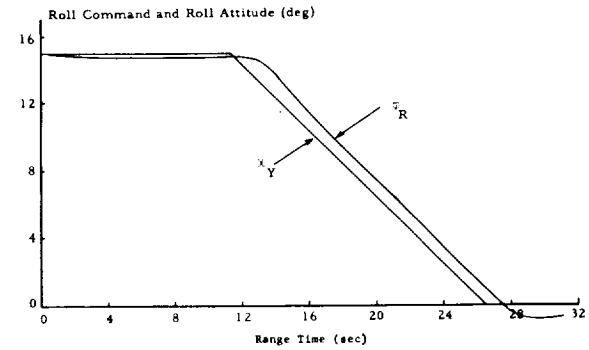

FIGURE 7-8. ROLL ATTITUDE DURING ROLL MANEUVER

The roll axis maximum control values measured during S-I propelled flight were:

Parameter	During Roll Maneuver (Magnitude)	(Range Time)	After Roll Maneuver (Magnitude)	(Range Time)
Attitude Error (deg)	1.3	13.9	-3.5	59.5
Angular Rate (deg/s)	-1.2	15.1	0.7	62.7
Engine Deflection Roll (deg)	-0.2	15.9	-0.5	60.0

The aerodynamic roll moment observed on all previous Block II flights was observed on SA-7. This moment is due to the aerodynamic flow effects associated with the turbine exhaust ducts at the tail of the S-I stage. The resulting attitude error reached a maximum value of 3.5 degrees CCW (viewed from rear) at 59.5 seconds. The comparison of the calculated roll moment coefficient with the wind tunnel measurements is generally consistent with the previous Block II flight results (Fig. 7-9).

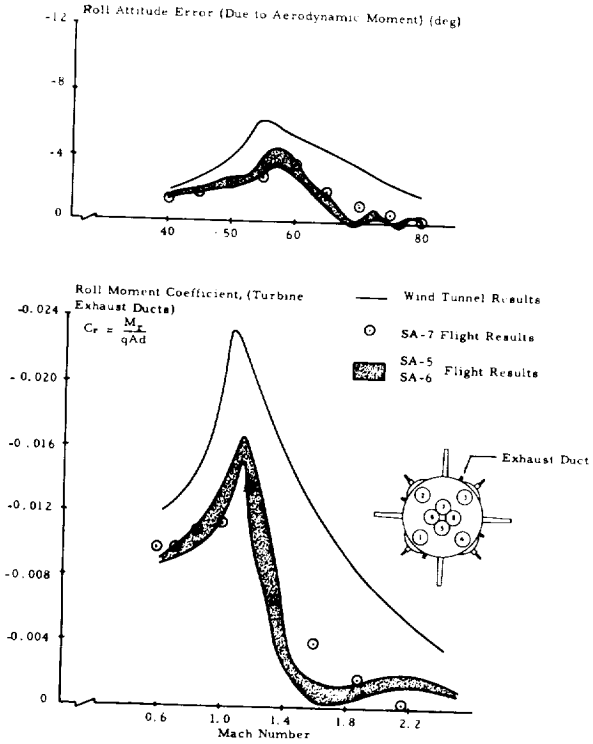

FIGURE 7-9. ROLL ATTITUDE ERROR AND ROLL MOMENT COEFFICIENT

At IECO the roll attitude error changed from 0.2-degree to 0.4-degree CW (viewed from rear) indicating an average thrust misalignment in roll of 0.06-degree CW per control engine and 0.03-degree CCW per fixed engine. These angles were only about 10 percent of the SA-6 values.

On SA-6 the roll gain coefficient was reduced by 50 percent after 110 seconds. After the flight data were analyzed, it was decided to keep the roll gain coefficient constant throughout S-I burn on SA-7 to prevent the possibility of the control system saturating under large roll moments. This 100 percent increase in the static roll moment capacity after 110 seconds reduced the roll angles on SA-7 by 50 percent.

7.3.2 S-IV STAGE FLIGHT CONTROL

The performance of the S-IV-7 flight control system was satisfactory. The pitch, yaw and roll plane parameters are presented in Figures 7-10, 7-11 and 7-12 respectively. A large roll deviation developed

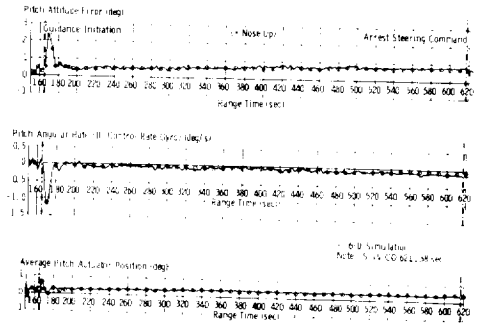

FIGURE 7-10. PITCH ATTITUDE ERROR, ANGULAR RATE AND AVERAGE ACTUATOR POSITION

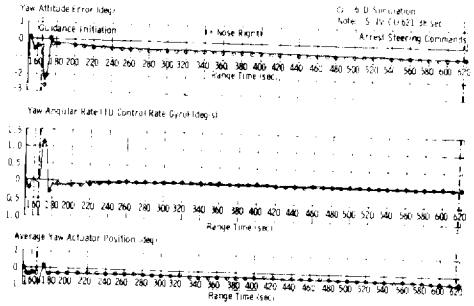

FIGURE 7-11. YAW ATTITUDE ERROR, ANGULAR RATE AND AVERAGE ACTUATOR POSITION

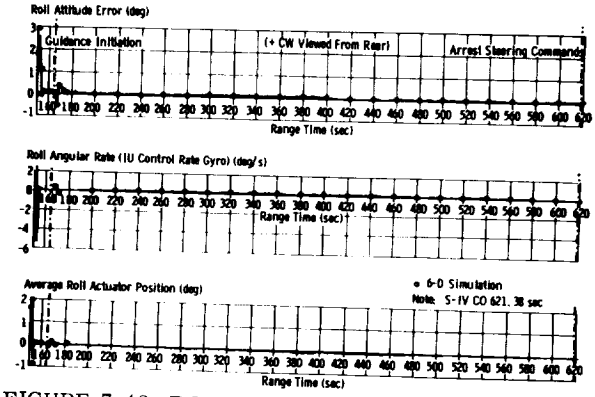

FIGURE 7-12. ROLL ATTITUDE ERROR, ANGULAR RATE AND AVERAGE ACTUATOR POSITION

immediately following S-I stage separation due to a large S-IV ullage rocket misalignment (see Section IX). During the 2-second period from separation until the S-IV stage control system became effective, the roll attitude error increased to 5.9 degrees CW (viewed from rear). The S-IV control system eliminated the roll attitude error rapidly, with very little overshoot, by introducing a maximum angular roll rate of -5.6 deg/s. No control disturbances resulted from LES tower jettison at separation plus 12 seconds.

The control system responded properly to guidance initiation. The initiation of yaw plane delta-minimum path guidance at 165.74 seconds caused the vehicle yaw attitude to build up to 5.6 degrees at 174.0 seconds and the roll attitude to reach 0.9 degree at 168.6 seconds (Fig. 7-13). These vehicle attitudes resulted from the control system's response to the χ_X and χ_Y steering commands which were generated by the digital computer to correct out the cross range velocity and displacement deviations of -12.2 m/s and -460 m which existed at guidance initiation. The peak attitude errors sensed by the ST-124 platform were -2.4 degrees in yaw at 168.4 seconds and 0.6 degree in roll at 168.9 seconds. The yaw plane steering commands were reduced to near zero about 85 seconds after guidance initiation.

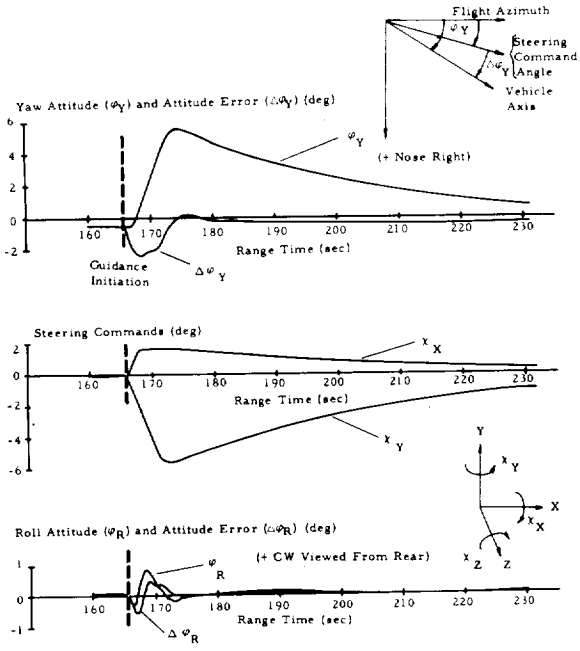

FIGURE 7-13. VEHICLE RESPONSE TO YAW PLANE GUIDANCE INITIATION

Due to the higher than predicted S-I stage propulsion system performance, the space-fixed velocity at guidance initiation was 32 m/s above nominal. The digital computer issued a pitch plane steering correction of 4.5 degrees (nose down) from nominal to adjust the flight path for the excess velocity condition. A maximum pitch attitude error of 2.3 degrees at 169.2 seconds resulted from guidance initiation (Fig. 7-14). At guidance initiation, the pitch steering command was 66.75 degrees; it then increased to 75 degrees at 188 seconds to generate the vehicle nose down steering correction maneuver. Some 6 seconds after the initiation of pitch plane path adaptive guidance, the steering misalignment correction term (χ_{Z_c}) was introduced to compensate for off-nominal conditions in the pitch plane (offset CG, thrust variations, etc.). The χ_{Z_c} term increased from about 1 degree at 175 seconds to 1.4 degrees at the end of path guidance. (The predicted maximum value for the steering misalignment correction term is about 2.5 deg).

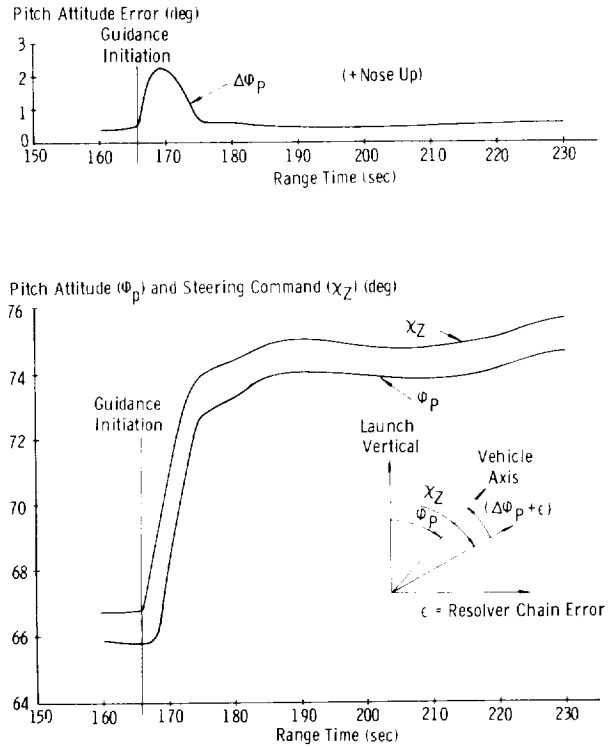

FIGURE 7-14. VEHICLE RESPONSE TO PITCH PLANE GUIDANCE INITIATION

The S-IV stage experienced maximum thrust vector misalignments of approximately 0.05 degree in

pitch and 0.02 degree in yaw. Due principally to the increasing CG offset during S-IV burn, the pitch attitude error increased from 0.45 degree nose up at 250 seconds to 0.85 degree nose up at S-IV cutoff; the mean yaw attitude error increased from 0.45 degree nose left at 250 seconds to 0.67 degree nose left at S-IV cutoff. These values agree very closely with the corresponding preflight predictions (based on CG offset and individual engine thrust levels) of 0.47 degree and 0.73 degree in pitch and 0.49 degree and 0.69 degree in yaw. Both the pitch and yaw attitude errors were larger than those experienced on S-IV-6; however, these increases were predicted because the removal of the backup helium bottles introduced larger than normal CG offsets. The mean roll attitude error was less than 0.1 degree through S-IV flight.

Engine deflections, except for the period required to damp out the roll deviation at separation, remained small throughout flight. After the guidance initiation transients were controlled out, the maximum engine gimbal angle required was only 0.5 degree.

Vehicle steering commands were arrested when the space-fixed velocity vector computed by the guidance system reached 7760 m/s (Fig. 7-15). This occurred about 2 seconds before S-IV guidance cutoff command. Due to the increasing yaw attitude error during S-IV burn, the measured cross range velocity reached a steady-stage value of -0.4 m/s (left of the reference trajectory plane) and the cross range displacement was about twice nominal at S-IV cutoff.

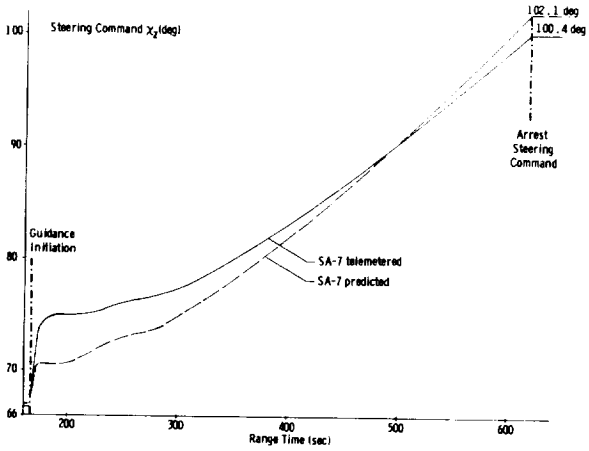

FIGURE 7-15. PITCH STEERING COMMAND

The angular rates resulting from steering arrest and S-IV engine shutdown were nearly zero. At the end of S-IV thrust decay the angular rates were -0.03 deg/s in pitch, -0.04 deg/s in yaw and 0.06 deg/s in roll.

7.4 FUNCTIONAL ANALYSIS

7.4.1 CONTROL SENSORS

7.4.1.1 CONTROL ACCELEROMETERS

Two body-fixed control accelerometers located in the Instrument Unit provided partial load relief in the pitch and yaw planes between 35 and 100 seconds. Peak lateral accelerations of 0.8 m/s^2 in pitch and 0.7 m/s^2 in yaw were measured near max Q. Figure 7-16 shows the measured lateral accelerations transferred to the vehicle CG. The following

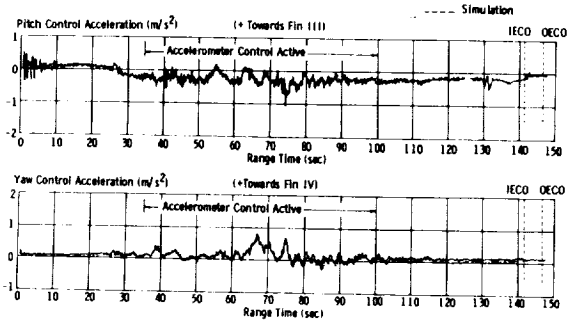

FIGURE 7-16. PITCH AND YAW CONTROL ACCELEROMETERS

frequencies were evident during some portion of S-I propelled flight when accelerometer control was active:

Frequency (Hertz)	Cause
1.2	S-I propellant sloshing
3.7 - 4.5	Vehicle second bending mode
5 - 6	Vehicle first torsional mode

The maximum RMS amplitude of the noise superimposed upon the signal was about 0.1 m/s^2. The accelerometers functioned satisfactorily throughout the flight.

7.4.1.2 ANGLE-OF-ATTACK SENSORS

Pitch and yaw angle-of-attack components were measured by a Model F16 Q-ball angle-of-attack meter mounted on the tip of the Launch Escape System (LES) and by fin mounted Edcliff angle-of-attack meters mounted on booms at the tips of Fins I and II. Both type meters indicated good comparisons with the computed angle-of-attack (Fig. 7-17). This comparison included pitch misalignments of 0.0 degree for Q-ball and 0.3 degree for the fin mounted meters and yaw misalignments of 0.45 degree for Q-ball and 0.25 degree for the fin mounted meters. After

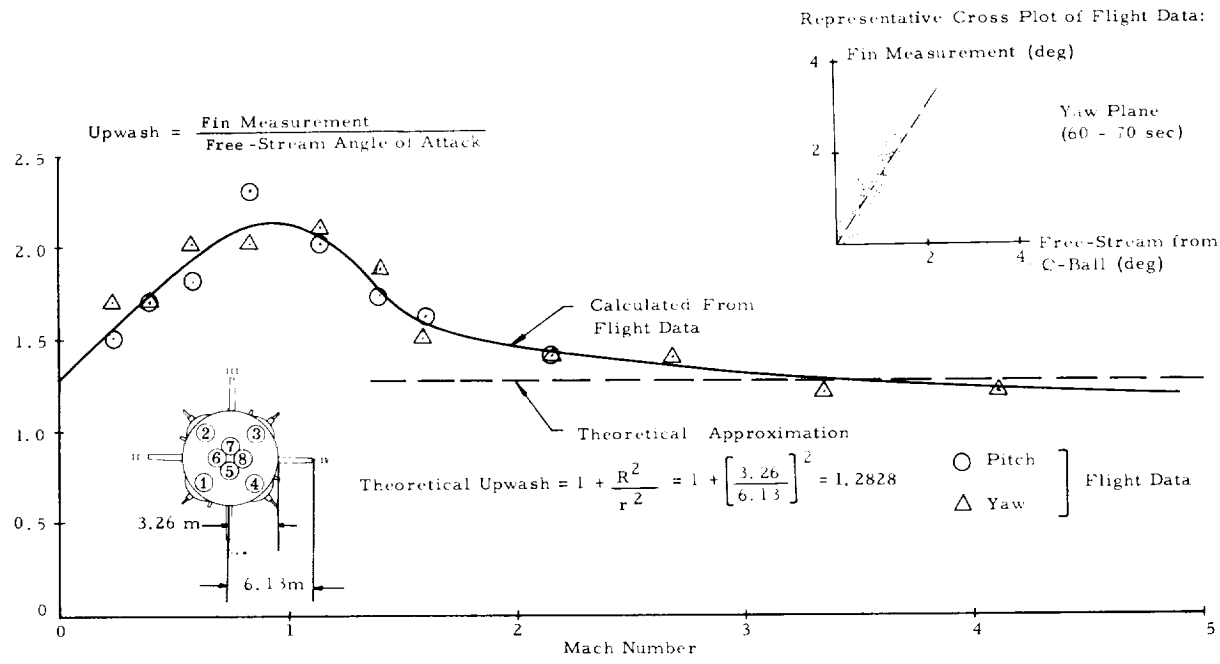

FIGURE 7-17. CALCULATED UPWASH FACTOR FOR FIN MOUNTED ANGLE-OF-ATTACK METERS

adjusting for the upwash factor, the fin mounted angle-of-attack data were in good agreement with the Q-ball from 20 to 92 seconds in pitch, and from 20 to 120 seconds in yaw. During the max Q region, the maximum pitch angles-of-attack indicated were -1.0 degree (Q-ball) and -0.9 degree (Fin Meters). Maximum yaw angles-of-attack indicated were 1.4 degrees (Q-ball) and 1.3 degrees (Fin Meters).

7.4.1.3 RATE GYROS

The SA-7 vehicle was instrumented with three rate gyro packages:

1. A ±10 deg/s range, 3-axis, control rate gyro package, located in the Instrument Unit, was used to provide pitch, yaw and roll angular rate information for vehicle control throughout flight. A control signal processor is used with the gyros to distribute ac and dc power to the gyro package and to demodulate the ac rate signals for input to both the flight control computer and the telemetry system.

2. The second rate gyro package is a 3-axis, ±10 deg/s range, self contained control type unit which is being flown for developmental purposes and is located in the thrust structure area of the S-I stage.

Analysis of the pitch and yaw rate gyros from both ±10 deg/s packages indicated that the vehicle was responding to the first four bending mode frequencies (2.0 to 2.2 Hz, 3.7 to 4.5 Hz, 4.1 to 5.3 Hz and 6.3 to 9.0 Hz) during S-I burn. The two roll rate gyros responded to the first torsional mode frequency (3.1 to 6.7 Hz) during S-I propelled flights. The rate gyros did not measure any appreciable bending or sloshing during S-IV burn. The performance of the rate gyro system used in controlling the vehicle was satisfactory.

The angular rate data telemetered from the control rate gyro system in the Instrument Unit were correct up to LOS at Pretoria, South Africa, (40 min). At Carnarvon, Australia, AOS, the angular rate information was no longer usable due to the depletion of the short life battery affecting the F6 telemetry system. See Section XII for the detailed analysis of this condition.

7.4.1.4 HORIZON SENSORS

Four horizon sensors were flight tested on SA-7. They were attached to the outside skin of the Instrument Unit and oriented as shown on the schematic in Figure 7-18. Except for a brief period during the first orbit, only sensor 1 performed satisfactorily. Sensors 3 and 4 oscillated randomly between 0 and 5 degrees and 0 and 1 degree respectively, while sensor 2 swept over to its stop at a 65-degree deflection angle and remained there throughout most of the flight. Sensor 1 locked on the horizon at 228.2 seconds and remained locked on until the horizon passed

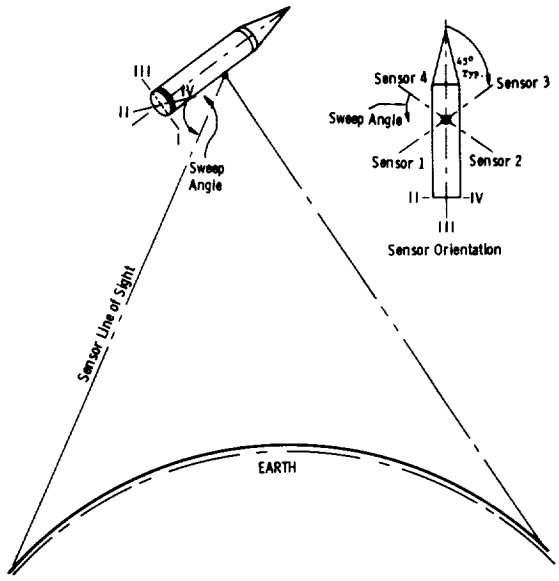

FIGURE 7-18. HORIZON SENSOR ORIENTATION AND SWEEP ANGLES

from its field of view at 794 seconds. Figure 7-19 compares the telemetered sensor angle from sensor 1 with the calculated angle for this sensor determined from the ST-124 attitude angles and the vehicle altitude.

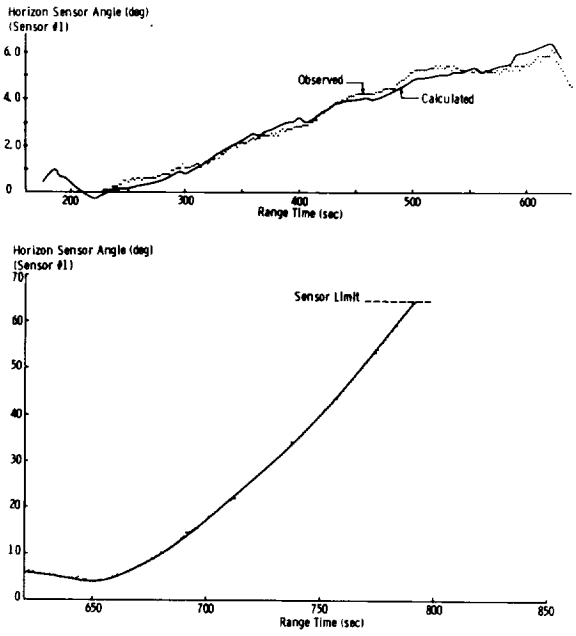

FIGURE 7-19. HORIZON SENSOR ANGLES

Figure 7-19 also shows the performance of sensor 1 immediately after orbital insertion. However, with only one sensor operating, the attitude angles cannot be determined.

Horizon sensor data were received at Ascension from 1230 to 1711 seconds. At 1689 seconds, sensors 1, 2, and 3 locked on and tracked the horizon until telemetry loss at 1711 seconds. Figure 7-20 shows the pitch and roll attitude angles computed from the horizon sensor angles. The rate of change of these angles agrees very well with rate gyro information during this time. The average calculated altitude from the sensors (Fig. 7-20) agrees with the altitude determined from orbital tracking.

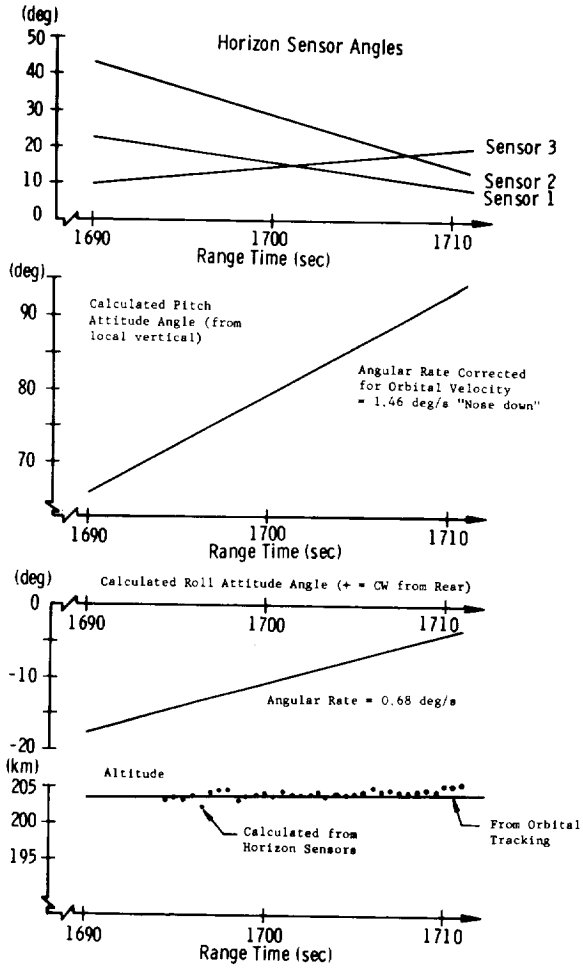

FIGURE 7-20. HORIZON SENSOR ANGLES AND CALCULATED ATTITUDE ANGLES AND ALTITUDE

7.4.1.5 RESOLVER CHAIN ERROR COMPARISON

The total resolver chain error in any axis is the angle difference between the output angle generated by the ST-124 and the input angle commanded by the digital computer.

A comparison between predicted and calculated pitch axis resolver chain error is shown as a function of the pitch command resolver angle (χ_Z) in Figure 7-21. The calculated resolver error was obtained by subtracting the calculated pitch attitude error from the telemetered attitude error. The calculated attitude error was obtained from a vector balance using the guidance system measured space-fixed acceleration, the body-fixed pitch and longitudinal accelerations, and the telemetered pitch steering command (χ_Z). Predicted and calculated values of pitch axis resolver error are in good agreement for both S-I and S-IV flight stages. The effects of this error on the guidance are discussed later in this section.

$\epsilon_{cal} = \Delta\varphi_{PT} - \Delta\varphi_{PC}$

$\Delta\varphi_{P_T}$ = Telemetered pitch attitude error

$\Delta\varphi_{P_C}$ = Calculated pitch attitude error

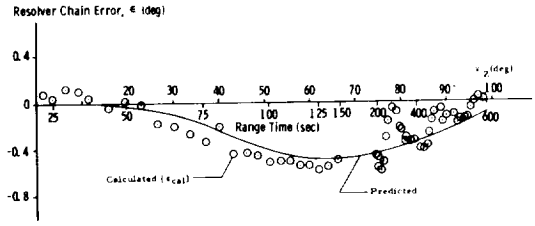

FIGURE 7-21. CALCULATED AND PREDICTED PITCH AXIS RESOLVER CHAIN ERROR

The maximum predicted resolver chain errors in the yaw and roll axis were less than 0.1 degree; therefore, a comparison between predicted and calculated errors is not practical.

7.4.1.6 FLIGHT CONTROL COMPUTER AND ACTUATOR ANALYSIS

The commands issued by the control computer to position the actuators were correct throughout the entire controlled flight period of both stages. These commands were well within the load, gimbal rate and torque capabilities of the S-I and S-IV actuators. Except for near maximum S-IV actuator deflections at separation, due to the roll deviation, the engine gimbal angles were quite small throughout flight.

The S-I stage telemetered attitude errors, angular velocities, and control accelerometer signals were analyzed with an open loop analog simulation of the control filters. The calculated values were within 0.2 degree of the telemetered data. This small error is within the range of telemetry errors.

The following tabulation presents a summary of the maximum measured gimbal actuator flight data:

S-I Stage (maximum actuator deflection was 1.7 deg)

Parameter	Type of Data	Liftoff	Event Max Q	OECO
Gimbal Rate (deg/s)	Measured	1.0	1.5	0.5
	Design Limit		17	
Torque (N-m)	Measured	6,200	9,400	15,500
	Design Limit		29,200	

S-IV Stage (maximum actuator deflection was 3.0 deg)

Parameter	Type of Data	Event Ignition	Cutoff
Gimbal Rate (deg/s)	Measured	4.5	0.5
	Design Limit	19	
Torque (N-m)	Measured	556	556
	Design Limit	1,180	

The performance of all S-I and S-IV stage actuators was satisfactory.

7.5 PROPELLANT SLOSHING

7.5.1 S-I POWERED FLIGHT PROPELLANT SLOSHING

S-I stage sloshing was monitored by means of differential pressure measurements in three of the nine propellant tanks (LOX tank 02, fuel tank F4, and center LOX tank) similar to the previous Saturn I vehicles. The maximum slosh amplitudes (peak to peak) observed on SA-7 were 15 cm in all the S-I tanks and 7 cm in the S-IV tanks during max Q (Figs. 7-22 and 7-23). All observed slosh frequencies followed the predicted first mode except the center LOX tank frequency which was slightly higher than predicted.

7.5.2 S-IV POWERED FLIGHT PROPELLANT SLOSHING

7.5.2.1 LOX SLOSHING

The LOX sloshing amplitude and frequency are shown in Figures 7-24 and 7-25. S-IV-7 LOX sloshing amplitudes correlate well with those calculated on previous flights, except for the buildup in amplitude during the latter portion of S-IV-5 flight. This difference resulted from the change of actuators that took place after the S-IV-5 flight. The nonlinearities in the actuators on S-IV-5 tended to excite the LOX second mode sloshing. This tendency resulted in a large amplitude indication, since the location of the PU probe makes it extremely sensitive to second mode sloshing.

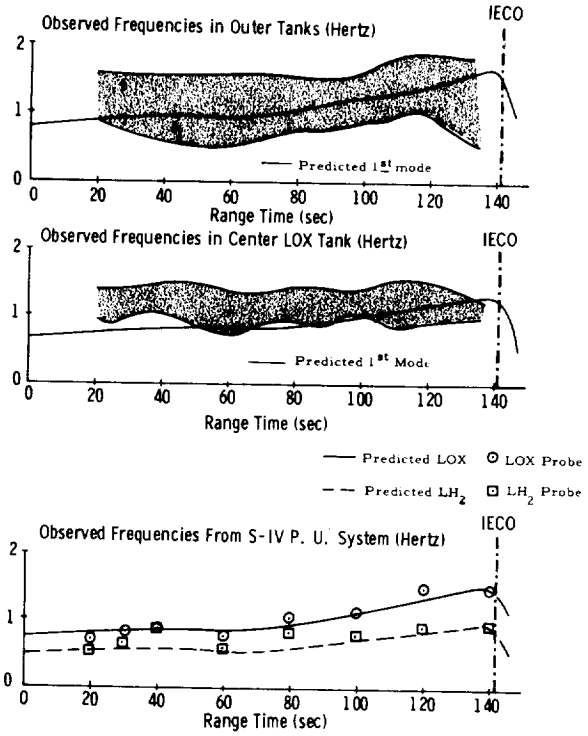

FIGURE 7-22. PROPELLANT SLOSH FREQUENCIES DURING S-I POWERED FLIGHT

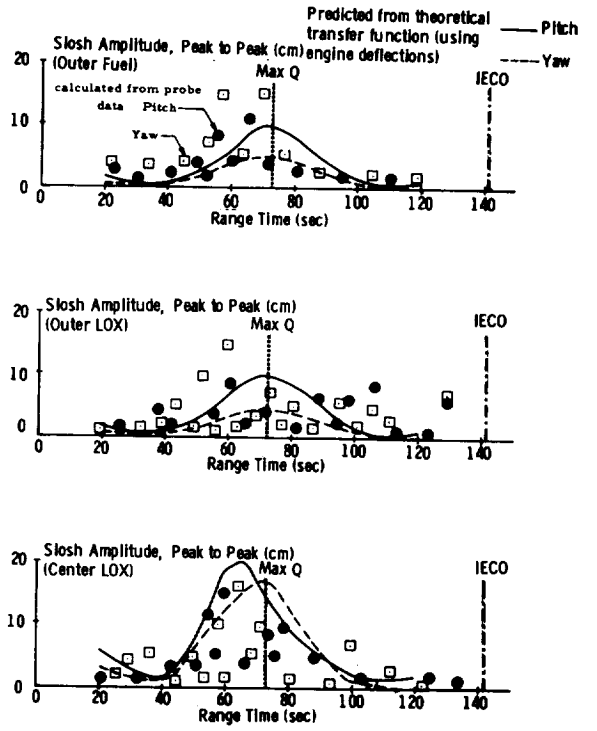

FIGURE 7-23. S-I SLOSH AMPLITUDES DURING S-IV POWERED FLIGHT

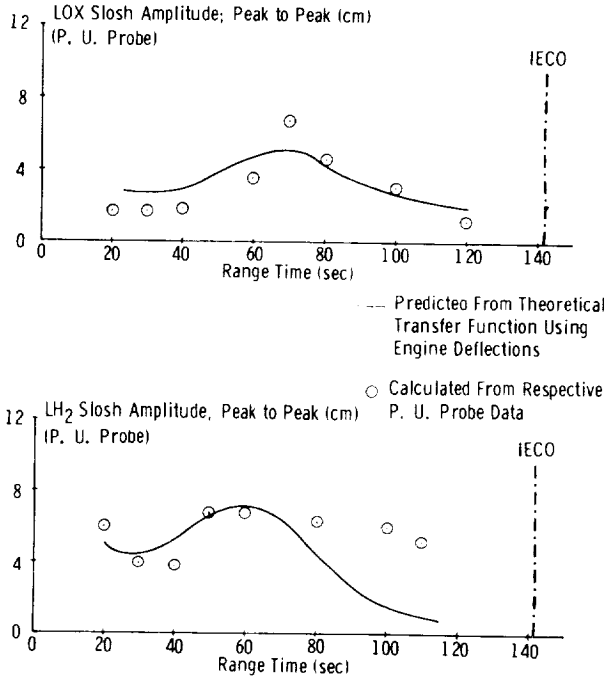

FIGURE 7-24. S-IV SLOSH AMPLITUDES DURING S-I POWERED FLIGHT

The LOX sloshing frequency data agreed well with the S-IV-6 flight first mode frequency data and with the theoretical first mode frequency curve. The higher frequencies seen on S-IV-5 as explained above, were a result of non-linearities in the actuators and in the location of the PU probe.

7.5.2.2 LH_2 SLOSHING

The S-IV-7 LH_2 sloshing amplitude and frequency are shown in Figures 7-24 and 7-25. The LH_2 sloshing amplitudes agree well with those observed on previous flights. The sloshing frequencies were nearly identical to S-IV-5, and S-IV-6 first mode flight data and to the theoretical first mode frequencies. The higher mode frequencies seen on the S-IV-6 flight were not evidenced on S-IV-7.

7.6 GUIDANCE SYSTEM PERFORMANCE

Although the overall performance of the ST-124 guidance system (ST-124 stabilized platform and electronic box, guidance signal processor and digital computer) was generally satisfactory, certain deviations were observed which required further investigation. Detailed analysis of the telemetered data from the guidance system revealed that:

1. The predicted and actual guidance intelligence errors were in wide disagreement.

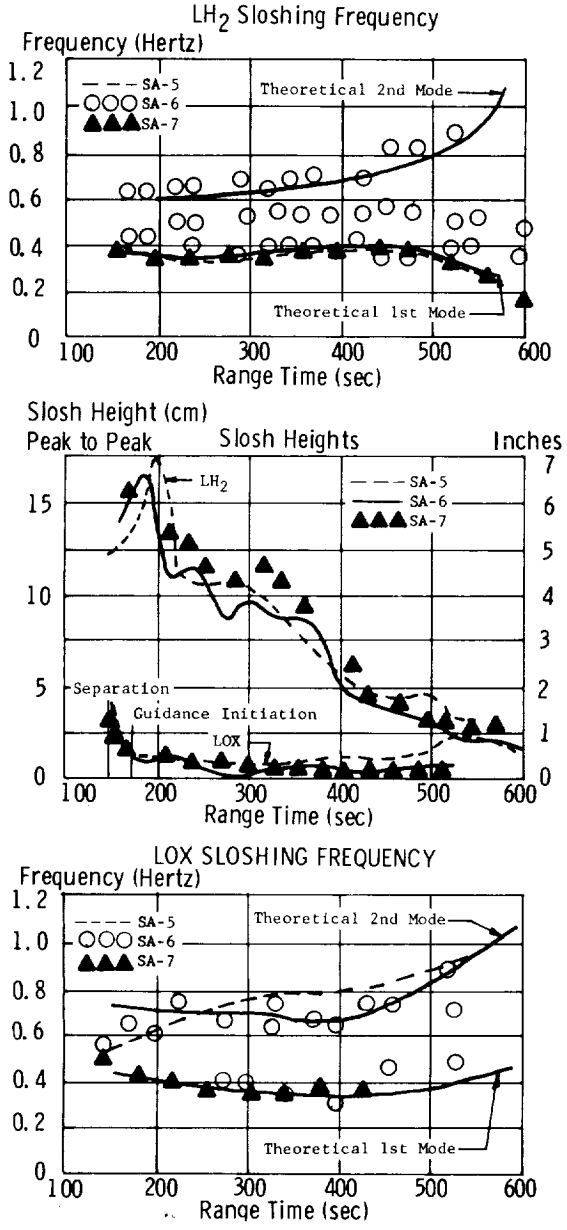

FIGURE 7-25. S-IV LOX AND LH_2 SLOSHING PARAMETERS

2. The actual space-fixed velocity vector at S-IV cutoff was 1.8 m/s larger than the digital computer value of 7806.0 m/s (identical to velocity presetting).

3. The digital computer's gravity term was slightly in error before liftoff.

4. The digital computer sequencing discretes were issued with a small time delay.

5. Minor velocity differences existed between the accelerometers and the digital computer.

The detailed analysis of these deviations are presented in subsequent parts of this section.

7.6.1 GUIDANCE INTELLIGENCE ERRORS

Guidance intelligence errors are defined as the differences between the range, altitude and cross range inertial velocity components measured by the ST-124 accelerometers and the corresponding parameters calculated from tracking data.

The sources of the guidance intelligence errors may be divided into two general categories, component errors and system errors. The component errors, scale factor and bias, are those which are attributed directly to the guidance accelerometers. The system errors (contributed by the stabilized element on which the accelerometers mount) are: gyro drift rates (constant and g dependent), platform leveling errors, nonorthogonality of the accelerometer measuring directions and misalignment of the platform flight azimuth. With the exception of the leveling and azimuth errors, the above data were obtained by laboratory measurements several weeks prior to launch. The leveling and azimuth deviations were determined from data which were available only at liftoff.

The predicted ST-124 inertial velocity errors for the SA-7 flight test were based on laboratory calibration of the ST-124 stabilized platform system (Table 7-I). Three σ deviation values for accelerometer leveling and azimuth alignment were used for the prediction. The ST-124 system 3σ tolerances were used to develop an error band for each velocity component to serve as a standard for comparison with the actual inertial velocity errors.

The ST-124 system error data used to calculate the predicted and actual SA-7 guidance intelligence errors are presented in Table 7-I. Note that there are two different values listed for platform leveling errors: the smaller values were calculated from telemetered accelerometer data prior to S-I ignition and the larger values were observed at liftoff.

The telemetered ST-124 accelerometer (inertial) velocities measured from vehicle first motion were compared with the corresponding velocity components determined from tracking. The differences between the telemetered velocity data and tracking are listed in Table 7-II for the principal event times. In each component, the velocity differences are much larger than those calculated from the ST-124 3 σ deviations.

TABLE 7-I. SIGNIFICANT GUIDANCE INTELLIGENCE ERRORS

Error Source	Units	Laboratory* Error Measurements	Pre-Liftoff Error Measurements	Errors Established From Trajectory Analysis	Inertial Velocity Errors at S-IV Cutoff (m/s) $\dot{X}_3$ Lab	$\dot{X}_3$ Traj	$\dot{Y}_3$ Lab	$\dot{Y}_3$ Traj	$\dot{Z}_3$ Lab	$\dot{Z}_3$ Traj
1. System Errors										
a. Platform Leveling	deg									
1) About X Axis			-0.050 ± 0.005	$-.054$						
2) About Z Axis			-0.027 ± 0.005	$-.0225$		-1.2		3.2		2.4
b. Azimuth Alignment	deg		0.004 ± 0.010	.012					0.5	1.6
c. Accelerometer Nonorthogonality	deg									
1) Attitude Accel. Rotated Toward - X Axis		0.0075		.0075			-1.0	-1.0		
d. Gyro Drift, Constant	deg/hr									
1) Yaw (X) Gyro (About X Axis)		0.05		.006					-0.1	0.0
2) Roll (Y) Gyro (About Y Axis)		0.03		.07					0.4	0.4
3) Pitch (Z) Gyro (About Z Axis)		0.04		.055	0.1	0.1	-1.1	-0.7		
e. Gyro Drift, g - Dependent	deg/hr/g									
1) Yaw (X) Gyro (About X Axis Due to $\ddot{X}$)		-0.15		-.125					0.2	0.2
2) Roll (Y) Gyro (About Y Axis Due to $\ddot{X}$)		-0.01		-.006					-0.1	-0.1
3) Roll (Y) Gyro (About Y Axis Due to $\ddot{Y}$)		-0.02		-.042					-0.2	-0.4
4) Pitch (Z) Gyro (About Z Axis Due to $\ddot{X}$)		-0.10		-.140	-0.1	-0.2	1.4	2.0		
2. Component Errors										
a. Accelerometer Bias	m/s^2			-0.097×10^{-3}						
1) Range Accel.		-0.63×10^{-3}		0.49×10^{-3}	-0.4	-0.1				
2) Cross Range Accel.		-0.96×10^{-3}		0.35×10^{-3}			0	-0.2	-0.3	-0.3
b. Accelerometer Scale Factor	g/g			0.31×10^{-4}						
1) Range Accel.		0.16×10^{-4}		0.23×10^{-4}	0.1	0.2	0	-0.1		
				Total Error	-0.3	-1.2	-0.7	3.0	0.4	4.6

*See Reference 10

TABLE 7-II. COMPARISON OF INERTIAL GUIDANCE VELOCITIES

Event	Type of Data	Total Velocity		Range Velocity		Altitude Velocity		Cross Range Velocity	
Range Time (sec)		Actual	Vel. Diff.	Actual	Vel. Diff	Actual	Vel. Diff.	Actual	Vel. Diff
	Accelerometer	3384.2		2282.3		2498.8		-10.5	
IECO	Tracking	3384.5		2283.3		2498.2		-13.4	
141.536	Precalculated	3332.8		2261.1		2448.4		-7.9	
	Accel - Track		-0.30		-1.0		0.6		2.9
	Track - Precal		51.7		22.2		49.8		-5.5
	Accelerometer	3558.6		2456.0		2575.2		-11.3	
OECO	Tracking	3559.0		2457.0		2574.7		-14.1	
147.636	Precalculated	3505.6		2434.8		2522.1		-8.4	
	Accel - Track		-0.3		-1.0		0.5		2.8
	Track - Precal		53.4		22.2		52.6		-5.7
	Accelerometer	3650.7		2546.7		2615.7		-12.3	
Guidance	Tracking	3651.1		2547.7		2615.2		-15.3	
Initiation	Precalculated	3600.5		2528.8		2563.0		-9.5	
165.740	Accel - Track		-0.4		-1.0		0.5		3.0
	Track - Precal		50.6		18.9		52.2		-5.8
	Accelerometer	8187.2		7629.1		2970.9		-0.4	
S-IV	Tracking *	8187.1		7630.2		2967.8		-5.1	
Cutoff	Precalculated	8186.9		7628.3		2972.3		-0.2	
621.375	Accel - Track		0.1		-1.1		3.1		4.7
	Track - Precal		0.2		1.9		-4.5		-4.9
	Accelerometer	8189.6		7631.9		2970.4		-0.4	
Orbital	Tracking *	8189.5		7632.9		2967.4		-5.1	
Insertion	Precalculated	8188.3		7629.9		2972.0		-0.2	
631.375	Accel - Track		0.1		-1.0		3.0		4.7
	Track - Precal		1.1		3.0		-4.6		-4.9

*Based on Orbital Tracking.

The guidance intelligence errors predicted from the laboratory data fall within the limits of the velocity errors calculated from the 3 σ tolerances. This indicates the ST-124 system errors much larger than those resulting from the 3 σ deviation must have developed prior to liftoff. Figure 7-26 also shows the residual velocity errors remaining after the telemetered accelerometer data were corrected for the following measured errors:

Attitude Accelerometer Non-orthogonality	-0.008 deg
Platform Azimuth Alignment	0.004 deg
Platform Leveling Errors	
About Z axis	-0.030 deg
About X axis	0.050 deg

The residual velocity errors ($\Delta \dot{X}_i = -0.5$ m/s; $\Delta \dot{Y}_i = 0.5$ m/s; $\Delta \dot{Z}_i = 0.2$ m/s) indicated by the

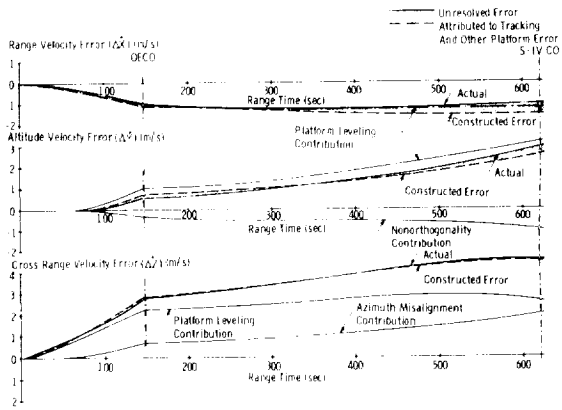

FIGURE 7-26. RESIDUAL INERTIAL VELOCITY COMPONENT DIFFERENCES (CORRECTED ACCELEROMETER - TRACKING)

cross-hatched area in Figure 7-26 are within the tracking data accuracy (± 0.5 m/s). Table 7-I lists additional corrections that would further reduce these residual velocity errors.

7.6.2 GUIDANCE SYSTEM PERFORMANCE COMPARISONS

The digital computer's measured space-fixed velocities at S-IV cutoff are compared with tracking and the precalculated trajectory data in Table 7-III. The same data, corrected for the ST-124 errors determined after flight and the computer initialization errors, are included in the comparison.

The difference between the total space-fixed vectors for the measured and adjusted computer values (-2.4 m/s) is about evenly divided between the range velocity and altitude velocity errors. Even though the magnitude of the cross range velocity error is large its effect on the total velocity is virtually zero. The computer's adjusted total velocity agrees with the tracking data within the tracking data tolerances of ± 0.5 m/s. The computer's measured space-fixed total velocity agrees exactly with the precalculated velocity (identical to cutoff velocity presetting) which indicates that the computer functioned as expected since the maximum predicted implementation scheme dispersion was ± 0.05 m/s. The total velocity difference between the measured computer data and tracking (1.8 m/s) is much larger than the maximum predicted error of 0.4 m/s (based on the laboratory measured ST-124 errors and the maximum predicted computer initialization errors) principally due to the large ST-124 leveling errors (see Ref. 9).

In Table 7-IV, the measured and the adjusted digital computer space-fixed velocities at orbital insertion are compared with the corresponding tracking and precalculated trajectory data. The adjusted computer data have the ST-124 system and the computer initialization errors removed.

The precalculated space-fixed velocity components and total velocity at orbital insertion were based upon a total velocity gain of 1.5 m/s due to S-IV thrust decay impulse from the start of S-IV engine shutdown signal. However, if the correct predicted cutoff impulse (from guidance cutoff command to the end of thrust decay) is used, the precalculated total velocity

TABLE 7-III. COMPARISON OF SPACE-FIXED VELOCITIES AT S-IV GUIDANCE CUTOFF (621.375 SEC RANGE TIME)

Data Source	Total Velocity (m/s)	Total Velocity Difference (m/s)	Range Velocity (m/s)	Range Velocity Difference (m/s)	Altitude Velocity (m/s)	Altitude Velocity Difference (m/s)	Cross Range Velocity (m/s)	Cross Range Velocity Difference (m/s)
Computer (measured)	7806.0		7291.7		-2785.2		-86.0	
Computer (adjusted)	7808.4		7293.4		-2787.4		-90.6	
Tracking *	7807.8		7292.5		-2787.9		-90.2	
Precalculated	7806.0		7297.3		-2770.5		-86.2	
Computer (meas-adjusted)		-2.4		-1.7		2.2		4.6
Computer-Tracking (adjusted)		0.6		0.9		0.5		-0.4
Tracking-Precalculated		1.8		-4.8		-17.4		-4.0

*Based on Orbital Tracking.

TABLE 7-IV. COMPARISON OF SPACE-FIXED VELOCITIES AT ORBITAL INSERTION (631.375 SEC RANGE TIME)

Data Source	Total Velocity (m/s)	Range Velocity (m/s)	Altitude Velocity (m/s)	Cross Range Velocity (m/s)
Computer (measured)	7808.7	7260.8	-2872.0	-85.2
Computer (adjusted)	7810.9	7262.3	-2874.2	-89.8
Tracking (Orbital)	7810.4	7261.6	-2874.7	-89.4
Precalculated	7807.5	7265.4	-2857.3	-85.5
Computer (meas-adjusted)	-2.2	-1.5	2.5	4.6
Computer-Tracking (adjusted)	0.5	0.7	0.5	-0.4
Tracking-Precalculated	2.9	-3.8	17.4	-3.9

would be 7808.8 m/s at orbital insertion; the predicted total velocity increase between cutoff and insertion (2.6 ± 0.4 m/s) would then agree favorably with the tracking velocity difference of 2.6 m/s.

Using this value for the velocity increase, the difference at insertion between the adjusted precalculated velocity and the tracking data is 1.8 m/s, which is in agreement with the corresponding difference at S-IV cutoff.

The performance of the yaw plane delta-minimum guidance scheme is shown in Figure 7-27. The cross range velocity and displacement (-12.2 m/s and -460 m) at guidance initiation were reduced to minimum values at about 400 seconds. The increase in all parameters (velocity, displacement, steering command, etc.) after this time is due to the rapidly increasing vehicle lateral CG offset (from -0.097 cm at 400 sec to -0.211 cm at S-IV cutoff). Due primarily to this condition, the cross range velocity and displacement increase to -0.3 m/s and -254 m at S-IV cutoff.

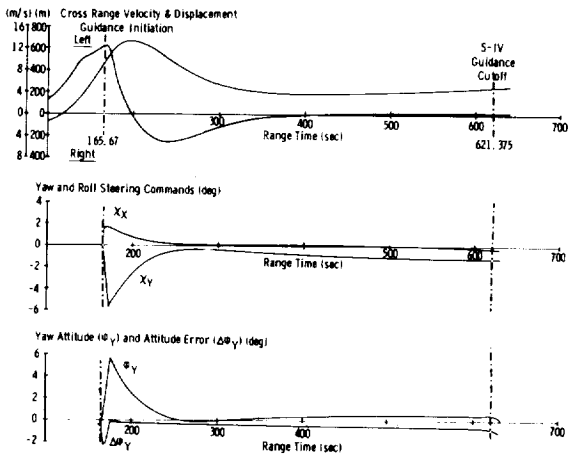

FIGURE 7-27. YAW PLANE DELTA MINIMUM GUIDANCE PARAMETERS

7.7 GUIDANCE SYSTEM HARDWARE

7.7.1 GUIDANCE SIGNAL PROCESSOR AND DIGITAL COMPUTER ANALYSIS

The overall performance of the guidance system hardware was satisfactory. However, the following minor deviations were observed:

1. Altitude Velocity Error

The time difference between physical liftoff of the vehicle (first motion) and the sensing of electrical liftoff command by the digital computer was 0.210 second. This time difference resulted in a computer inertial and gravitational altitude velocity error of 2.5 m/s throughout flight. However, the computer program is so written that any such error will not carry through to the space-fixed velocity and consequently guidance accuracy is not affected. The space-fixed altitude velocity is not affected because it is the algebraic sum of the inertial and gravitational velocity values both of which contain the 2.4 m/s error and the error cancels [$\dot{Y}_S = (\dot{Y}_i - \Delta\dot{Y}_i) - (Y_{gy} - \Delta Y_i)$].

2. Computer Initialization Errors

Small constant velocity differences exist between the accelerometer data and the inertial velocity values measured by the digital computer. The magnitudes of these errors are constant throughout flight at -0.2 m/s in $\dot{X}_i$; 0.3 m/s in $\dot{Y}_i$; and 0.1 m/s in $\dot{Z}_i$. The $\dot{X}_i$ and $\dot{Z}_i$ errors were the result of small and unpredictable (and, therefore, uncorrected) platform leveling errors of about -0.004 degree for the range accelerometer and -0.006 degree for the cross range accelerometer. Two-thirds of the total accumulated error in $\dot{Y}_i$ resulted from the computer gravity term used for pre-liftoff computations being slightly low (-9.788397 m/s^2 instead of -9.790552 m/s^2). The slight gravity term error has been corrected in the computer program for future flights. The remaining initialization errors (-0.2 m/s, -0.1 m/s and 0.1 m/s) all fall within the predicted range (see Ref. 9).

3. Bit-by-Bit Computer Data Analysis

The Bit-by-Bit comparison program was used to evaluate the operation of the ASC-15 digital computer equipment on SA-7 flight. This analysis is made

to confirm the correct operation of the computer and it does not check the validity of the flight program. Due to the nature of the Bit-by-Bit analysis program, all of the computer telemetry was not examined. All navigation and guidance quantities were examined. Minor loop telemetry data, which include accelerometer readings and mode codes, however, were not examined.

The total number of computer words telemetered between liftoff and entry into the cutoff loop was 54,883. Of this number, 53,250 or 97.25 percent were available for examination by the Bit-by-Bit program. The remainder was lost due to telemetry blackout during staging and second stage ignition. The Bit-by-Bit program examined 62 percent of the 53,250 telemetry words. The remaining information was minor loop telemetry. Thus, 60.5 percent of the total flight computer telemetry (54,883 words) during the time interval considered was examined in this analysis. An estimated 2.35 percent of the telemetry was lost due to dropouts. This number includes the data lost in the RF blackout during staging.

From this analysis, it was concluded that the ASC-15 flight computer and flight program operated correctly during flight.

4. Sequencing Time Errors

The digital computer issued all its sequencing command functions satisfactorily. However, there were slight time delays in these functions to both the S-I stage and IU flight sequencer systems. The total delay between the expected and actual sequencing function times were 0.078 second to the S-I stage and 0.084 second to the IU. The breakdown of the sources contributing to these total delay times is:

Source of Time Delay	Flight Sequencer (S-I Stage) (sec)	Flight Sequencer (IU) (sec)
Computer Senses Liftoff	0.014	0.014
Computer Program	0.040	0.052
Networks	0.010	0.010
Telemetry	0.014	0.008
Total Time Delay	0.078	0.084

The reason for these delays is that the computer cannot send out discrete signals except during a minor loop operation which is 0.100 second long. The computer program documentation did not consider this or the delay in sensing liftoff signal. On SA-9 and subsequent vehicles, the computer program documentation will reflect these considerations plus the electrical network constant delay time. The telemetry delay time is a function of telemetry channel assignment and will vary from about 0.005 to 0.015 second.

During the first orbit while the vehicle was over Ascension Island (LO + 1/2 hr) a test was made to demonstrate the capability of loading information into the digital computer via the digital command system. The telemetered computer information verifies that the loading operation was completely successful. Thirty 25 bit data words accompanied by 30 control words (16 bits each) were loaded into the computer and telemetered back to the ground correctly. The verification portion of the load-readout routine was then performed and the 30 data words telemetered correctly again.

7.7.2 ST-124 STABILIZED PLATFORM SYSTEM HARDWARE ANALYSIS

Although the ST-124 system functioned properly detailed analysis of hardware performance revealed the following deficiencies:

1. The stabilized platform developed large leveling errors about the pitch and yaw axes between S-I engine ignition and liftoff (Fig. 7-28).

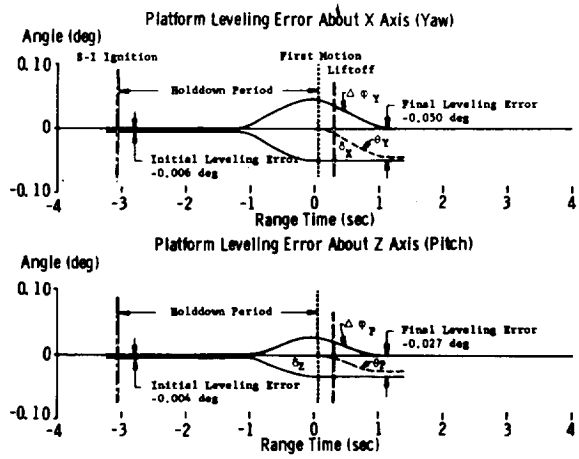

Notes:
1. $\Delta\Phi$ is the telemetered attitude error angle.
2. θ is the angle between the vehicle longitudinal axis and the local vertical.
3. δ is the angle between the platform Y axis and the local vertical

FIGURE 7-28. DEVELOPMENT OF PLATFORM LEVELING ERRORS DURING HOLDDOWN

The air bearing pendulums, which generate error signals used to maintain the stabilized element leveling prior to launch, were left in the erection loop until liftoff. The high vibration levels experienced during the last second of the holddown period caused the pendulums to drift, issuing erroneous leveling command signals. These signals caused the servos to drive the stabilized element (on which the guidance accelerometers are mounted) off level. These large leveling

errors were the main contributors to the guidance intelligence errors. This problem will be eliminated in future launches by switching the pendulum signals out of the loop prior to S-I ignition.

2. The stabilized platform also appeared to have an azimuth misalignment significantly larger than the calculated value of 0.004 degree. Detailed analyses of the cross range velocity errors strongly suggest that the azimuth error was in the range of 0.010 to 0.015 degree. This error contributed 2.0 m/s to the total lateral velocity error at S-IV cutoff. The cause of this error has not been identified as yet; therefore, it is possible that a similar effect may occur on future flights.

The three stabilizing servo loop pickup error signals indicated maximum values of 0.2 degree. These values, which agree with the corresponding data from the flights of SA-5 and SA-6, are satisfactory. The redundant gimbal servo error signal remained very near the null position as expected. The guidance accelerometer servo pickup signals were also very smooth and remained near null.

7.8 ST-124 GAS BEARING SUPPLY SYSTEM

The performance of the gas bearing supply system was completely satisfactory. The 0.028 m^3 (1 ft^3) GN_2 storage bottle was pressurized to 2137 N/cm^2 gauge (3100 psig) by the high pressure ground supply system before liftoff. This value is well within the specified launch requirement of 1793 to 2206 N/m^2 gauge (2600 to 3200 psig). From liftoff to S-IV cutoff, the ST-124 gas bearings consumed 1.1 SCM (38.8 SCF), or 21.6 percent of the total supply of 5.1 SCM (180 SCF). This value agrees with the predicted consumption rate of 0.1065 SCM/min (3.76 SCF/min) within one-half percent.

Before liftoff, the average temperature of the GN_2 supplied to the ST-124 gas bearings was 297°K (298 ± 5° K specified). Inflight, the average temperature of the GN_2 supplied to the ST-124 was also 297°K.

The preset regulator pressure differential between the gas bearing supply pressure and the specified Instrument Unit pressure was 12.5 N/cm^2 differential (18.1 psid). The regulator was set at this pressure to provide the specified differential pressure of 10.4 ± 0.4 N/cm^2 differential (15.0 ± 0.5 psid) at the ST-124 inlet manifold. Prior to liftoff the average regulated pressure differential (gas bearing supply pressure minus IU pressure) measured 13.2 N/cm^2 differential (19.2 psid); inflight, the average pressure differential was 13.0 N/cm^2 differential (18.8 psid). The differential pressure was three percent too high during prelaunch and one-half percent too high during inflight to meet the ST-124 gas bearing manifold supply pressure requirement of 10.4 ± 0.4 N/cm^2 differential (15.0 ± 0.5 psid). These small errors are within the measurement accuracy and, therefore, are not considered significant.

SECTION VIII ORBITAL ATTITUDE

8.1 SUMMARY

The S-IV-7 stage with Instrument Unit and Apollo Boilerplate Payload was inserted into orbit at 631.38-seconds range time. The attitude of the vehicle at that time was 99.8 degrees in pitch, 0.5 degree in yaw and 0.06 degree in roll. The angular rates observed at S-IV cutoff were -0.03 deg/s in pitch, 0.04 deg/s in yaw and 0.06 deg/s in roll. The greatest recorded changes in angular rates occurred between 11 and 12 minutes after liftoff. Records indicate that the main LH_2 vent opened 12 times during this period and that the main LOX vent valve did not open. At 20 minutes the roll angular rate had increased to 0.4 deg/s CW from rear and the vehicle was performing a precessional motion with a tumble (pitch/yaw) rate of 1.46 deg/s. The tumble rate reached a maximum of 1.65 deg/s at 25 minutes. The maximum roll rate observed was at 40 minutes with a rate of 1.03 deg/s CW from the rear. At loss of telemetry signal (40 min) the vehicle was essentially in a flat spin and was performing a gyroscopic precessional motion with a half cone angle of approximately 85 degrees and had a precessional period of 4 minutes (1.5 deg/s equivalent angular rate). At loss of rate gyro telemetry, the only direct measurement of vehicle angular rates, the observed angular rates were less than 2 deg/s in any axis. Analysis of radar signal strength records (AGC) after the end of residual propellant venting (approximately 24 hours), indicates a final tumble rate of approximately 6 deg/s.

A non-propulsive vent (NPV) system was flown for the first time on SA-7, in addition to the main pressure relief LOX and LH_2 vent systems used on SA-5 and SA-6, to obviate the excessive angular rates due to the venting of residual propellants after S-IV cutoff experienced on SA-5 and SA-6. The NPV system was designed to keep the vehicle angular rates below 6 deg/s, the maximum allowable on the Pegasus experiments. This system performed satisfactorily and all system components operated as expected although there was some indication that the final rates were approximately the maximum allowable.

8.2 VEHICLE ATTITUDE IN ORBIT

The vehicle was inserted into orbit at 631.38-second range time with a 99.8-degree pitch attitude, 0.5-degree yaw attitude, and 0.06-degree roll attitude.

The angular rates at S-IV guidance cutoff signal (621.38 sec range time) were -0.03 deg/s in pitch, 0.04 deg/s in yaw, and 0.06 deg/s in roll. At S-IV cutoff the non-propulsive LH_2 and LOX vents opened. No noticable changes in angular rates were noted from S-IV cutoff to the beginning of the tape recorder playback. These angular velocities were not telemetered during the period of tape recorder playback of S-I/S-IV separation data from 642.7 to 672.8 seconds.

At resumption of telemetry (672.8 sec), the angular rates had changed to -0.25 deg/s in pitch, -0.24 deg/s in yaw and 0.22 deg/s in roll. This indicates that the main LH_2 vents (propulsive) probably opened during this period which was void of telemetered data. The greatest recorded changes in angular rates occur between 674 to 720 seconds. During this time period, the main LH_2 vents opened 12 times and the main LOX vents did not open. These were the only recorded orbital openings of the main vent valves. Figure 8-1 shows the telemetered angular rate observed at Antigua through Pretoria.

At loss of signal from Antigua 14 minutes after liftoff, the angular rates were -0.76 deg/s in pitch, -0.57 deg/s in yaw, and 0.12 deg/s in roll. At acquisition of telemetry by Ascension (20 min) the roll angular rate had increased to 0.4 deg/s CW from rear and the vehicle was performing a precessional motion with a tumble (pitch/yaw) rate of 1.46 deg/s. This tumble rate reached a maximum of 1.65 deg/s at 25 minutes. The angular rates observed in the rate gyro telemetry at Ascension loss of signal were 1.38 deg/s in tumble (pitch/yaw) and 0.79 deg/s in roll. These telemetered rate gyro angular rates compare favorably with the angular rates defined by the horizon sensor at this time of 1.46 deg/s tumble and 0.68 deg/s roll. The roll rate changed from 0.79 deg/s at loss of signal by Ascension (28 min) to 0.92 deg/s at acquisition by Pretoria (32 min). At loss of signal by Pretoria (40 min), the vehicle was tumbling at 1.55 deg/s with a roll rate of 1.03 deg/s CW from rear. The vehicle was performing a gyroscopic precessional motion with a half cone angle of approximately 85 degrees and had a precessional period of 4 minutes (1.5 deg/s equivalent angular rate). Figure 8-1 presents the tumble and roll rates observed during the times of valid orbital telemetry.

From the observed angular rates, the body fixed moments acting on the orbiting vehicle were:

Time (sec)	Pitch	Yaw	Roll
674 - 720	139 N-m	132 N-m	7.75 N-m
720 - 860	15 N-m	27 N-m	1.53 N-m
1236 - 1690	32 N-m	12 N-m	1.25 N-m
1930 - 2400	10 N-m	7.5 N-m	1.11 N-m

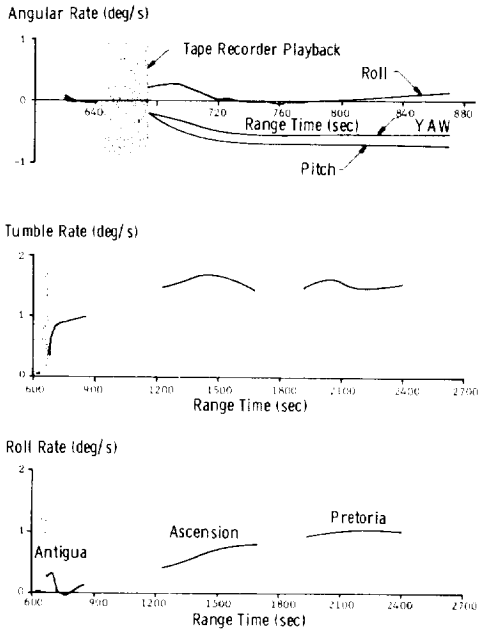

FIGURE 8-1. ANGULAR RATES DURING ORBITAL VENTING

Radar, Minitrack, and telemetry signal strength records (AGC) and radar operators comments were utilized in attempting to define the orbiting vehicle angular rates after loss of telemetry. Figure 8-2 shows the tumble rates observed in the orbital records.

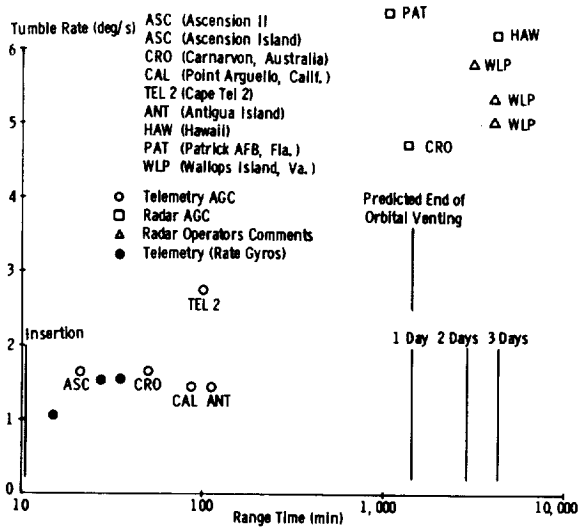

FIGURE 8-2. OBSERVED SA-7 TUMBLE RATES

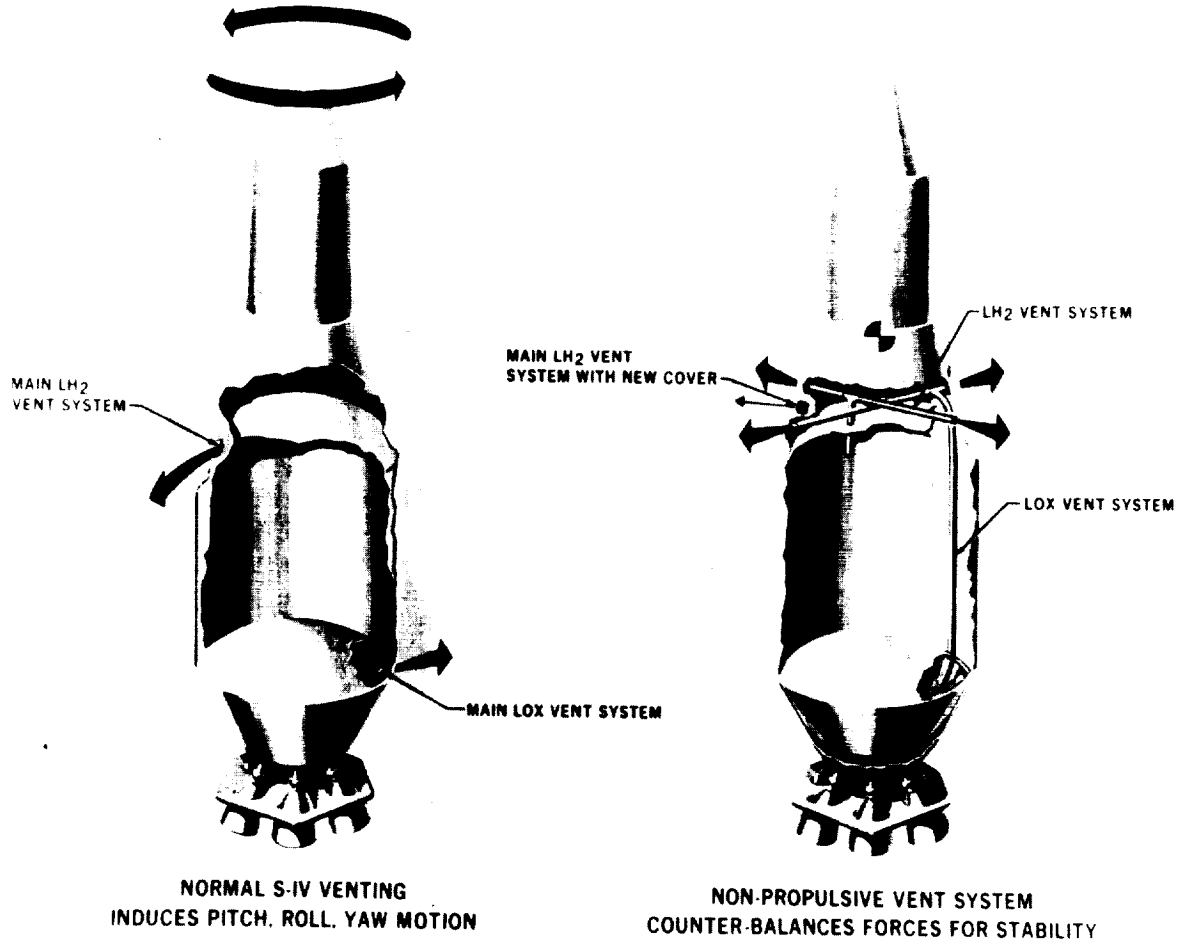

FIGURE 8-3. NON-PROPULSIVE VENT SYSTEM

During the period of active telemetry there is reasonable agreement between the telemetered angular rates and the angular rates indicated by AGC records. After the first three revolutions the only valid data available for rate analysis were skin track radar AGC and radar operator comments. Signal periodicity (equivalent angular rate) seen in radar skin track records can be interpreted only as a tumble indication. The vehicle tumble rate as indicated by this evidence would be approximately 6 deg/s at the end of orbital venting of residual propellants (approximately one day). Spin rate indications in the orbital records were extremely difficult to discern and the roll rate at the end of orbital venting could not be defined. Investigations are continuing in this area in an attempt to establish reliability of observations.

8.3 NON-PROPULSIVE VENTING SYSTEM PERFORMANCE

A non-propulsive vent (NPV) system was installed on SA-7, in addition to the main pressure relief LOX and LH_2 vent systems used on SA-5 and SA-6, to obviate the excessive angular rates due to the venting of residual propellants after S-IV cutoff experienced on SA-5 and SA-6 (See Fig. 8-3). The NPV system was designed to keep the angular rates below 6 deg/s, the maximum allowable on the Pegasus experiments.

The S-IV-7 non-propulsive vent system performed satisfactorily, as indicated by all available data, and system component operation was as expected. The two hydrogen and one oxygen non-propulsive vent valves opened at engine cutoff (621.38 sec), and the newly designed main hydrogen vent cover closed and latched as intended.

The main hydrogen vent (propulsive) did open, but the main oxygen vent (propulsive) did not open after S-IV engine cutoff.

The total impulse of the hydrogen vented through the main vent valve was determined to be approximately 8,896 N-s (2000 lb_f-s) based on the following data evaluations:

1. After a time lag of approximately 5 seconds, the LH_2 tank pressure rose sharply from 25.1 N/cm^2 (36.5 psi) at 626 seconds to 30.3 N/cm^2 (44.0 psi) at 643 seconds, at which time there was a loss of data because of the onboard recorder playback.

2. After the period of data dropout, which occurred from 643 to 674 seconds, the LH_2 tank vented through its main vent system. All recorded vent periods occurred between 685.5 and 720 seconds. The No. 2 vent valve opened nine times. The No. 1 vent valve opened three times. However, the LH_2 vent pressure recording, shown in Figure 8-4, indicates possible pilot flow up to 805 seconds.

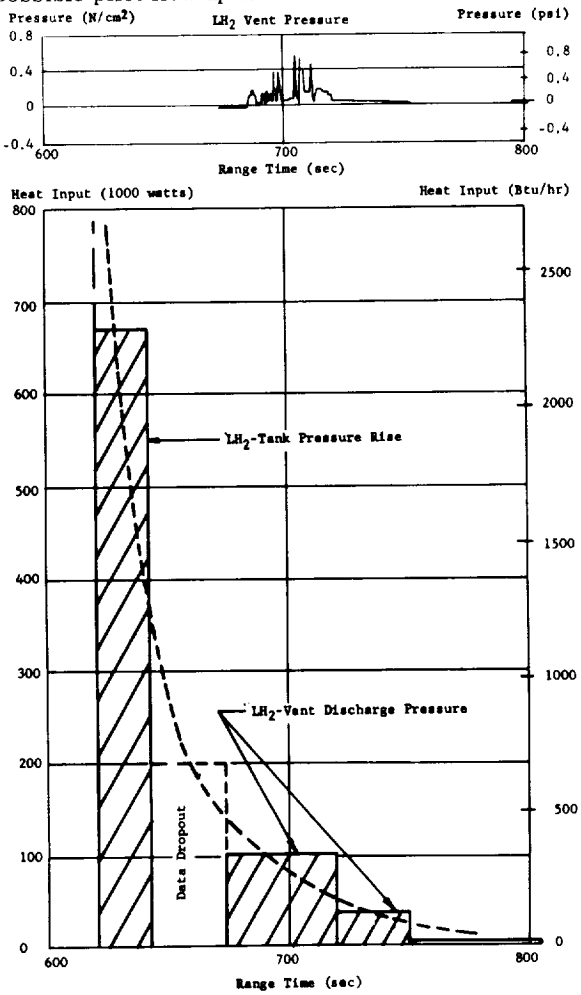

FIGURE 8-4. LH_2 VENT PRESSURE AND HEAT INPUT

3. The area under the recorded LH_2 vent pressure curve (Fig. 8-4) has been integrated. The result indicates a vented total impulse of 5,227 N-s (1,175 lb_f-s).

4. In order to make a deduction of the vented total impulse during the data dropout period, the heat input into the LH_2 tank has been evaluated. This evaluation is shown in Figure 8-4. The evaluation was based on the following events:

a. The LH_2 tank pressure rise prior to the data dropout period.

b. Total vented impulse after the data dropout period. Thus, a heat input rate during the recorder playback period was interpolated.

The equivalent vented total impulse during this period, derived from the above procedure, was 3,684 N-s (820 lb_f-s).

5. The combination of the conclusions reached in 3 and 4 above indicates a vented total impulse of 8,874 N-s (1,995 lb_f-s) or 7.3 kg (16.2 lbm) of GH_2 vented through the hydrogen main vents.

Based on analytical evaluation of the S-IV-7 flight, the following residuals at S-IV stage all engines cutoff command were considered to be accurate for this analysis:

205 kg (451 lbm) of LH_2
986 kg (2174 lbm) of LOX

The equivalent total impulses are:

338,065 N-s (76,000 lb_f-s) LH_2 tank
386,995 N-s (87,000 lb_f-s) LOX tank

Table 8-I gives the possible angular rates based on maximum tolerances of the NPV system plus hydrogen venting through the main vents. At the end of orbital venting a maximum of 5 deg/s in roll and 3 deg/s in tumble is predicted. Figure 8-5 shows the predicted LH_2 and LOX tank pressures versus time during orbital venting as functions of the nominal residual propellants. The pressure history curves would change negligibly if the actual residual propellant masses were used in the analysis. The Tel 2 data of the first orbital pass indicate a LOX tank pressure of 13.8 N/cm^2 (20 psi) and an LH_2 tank pressure of 19.0 N/cm^2 (27.5 psi), at approximately 1.5 hours from orbital insertion. The predicted tank pressures at this time are 13.8 N/cm^2 (20 psi) in the LOX tank (assuming 907 kg or 2000 lbm LOX residual at S-IV cutoff) and 11.7 N/cm^2 (17 psi) in the LH_2 tank (assuming 136 kg or 300 lbm residual at S-IV cutoff).

TABLE 8-I. PREDICTED ANGULAR RATES AT THE END OF ORBITAL VENTING

Venting Parameters	Roll Rate deg/s	Tumble (Pitch/Yaw) Rate deg/s
205 kg (451 lbm) LH_2 - residual	2.1	0.8
986 kg (2174 lbm) LOX - residual	2.4	1.1
8,896 N-s (2000 lb_f-s) total impulse vented through the LH_2 main vents	0.7	0.8
Totals	5.2	2.7*

*The pitch-yaw velocities are added algebraically. A summation of the velocity vectors would reduce the quoted pitch-yaw velocity by approximately 10%.

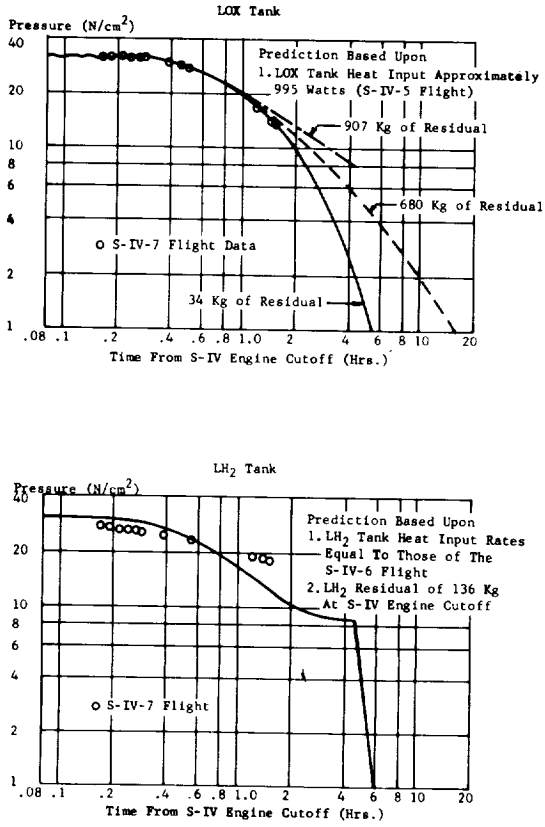

FIGURE 8-5. PREDICTION OF LOX AND LH_2 TANK VENTING

These data are in the expected range if it is recognized that the LH_2 tank venting is dependent on the heat input into the tank. The predicted heat input is shown in Figure 8-6.

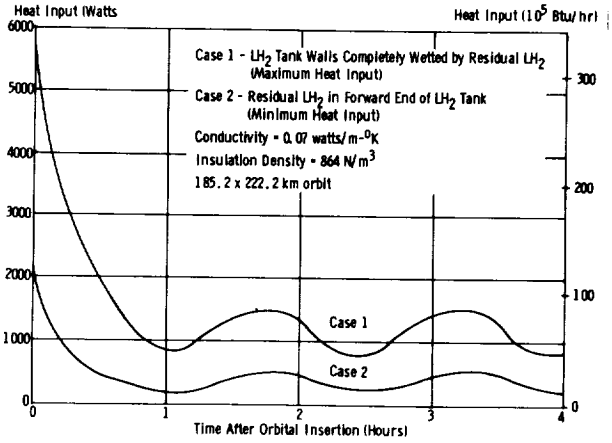

FIGURE 8-6. LH_2 ORBITAL HEATING RATE

SECTION IX. SEPARATION

9.1 SUMMARY

Separation of the first and second stage of the SA-7 vehicle was accomplished in the same manner as SA-6. The separation scheme is discussed in Reference 3. The only major difference between SA-6 and SA-7 was the delay time between OECO and separation command. This delay time was 0.4 second for SA-6 and 0.8 second for SA-7.

All elements of the separation system operated properly and the first relative motion between stages was observed within 0.09 second of separation command. Only 12 percent (0.09 m or 3.4 in) of the available lateral clearance (0.74 m or 29 in.) was used during the separation period.

At S-IV engine ignition command the exit plane of the S-IV engines was 10.1 m (33 ft) forward of the lip of the interstage; this is 7.0 m (23 ft) greater than the minimum design requirement of 3 m (10 ft).

The vehicle had attitudes and angular rates considerably less than design values at separation; however, angular rates for the separated S-I stage increased during the separation period. Only the roll angular rate of the S-IV stage increased significantly during the separation process. The roll excursion, while not affecting separation, did produce a large transient at the time the S-IV stage thrust reached a value large enough to restore the vehicle to the proper attitude. The cause of the roll deviation was primarily a total ullage rocket misalignment of 1.2 ± 0.2 degrees or some equivalent value distributed among all four ullage rockets.

9.2 SEPARATION DYNAMICS

9.2.1 TRANSLATIONAL MOTION

The actual separation sequence for the SA-7 vehicle is depicted in Figure 9-1. The separation command was issued at 148.44 seconds. The first motion between the two stages was observed from telemetry (simulation) to have occurred at 148.53 seconds. Two extensometers mounted on the S-IV stage indicated a first motion time of 148.55 seconds (30.48 cm extensometer) and 148.58 seconds (475.2 cm extensometer).

Figure 9-2 shows the separation distance between the S-I stage and the S-IV stage. Shown for comparison is the SA-6 separation time history. The S-IV stage engines cleared the interstage 0.06 second earlier than predicted. Figure 9-2 shows the velocity

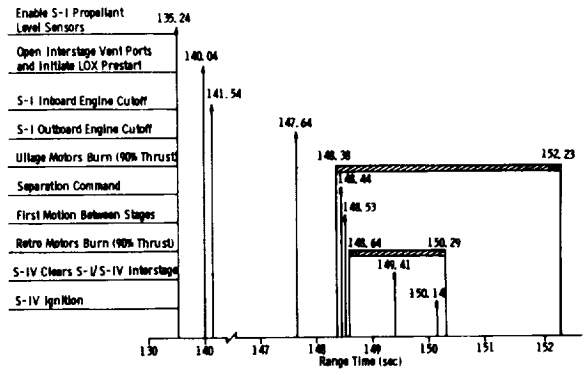

FIGURE 9.1. SEPARATION SEQUENCE

increment for both stages plus the total relative velocity between stages. The two stages had separated by 10.1 m (33 ft) at S-IV stage ignition, which is 7.0 m (23 ft) greater than the specified minimum clear-

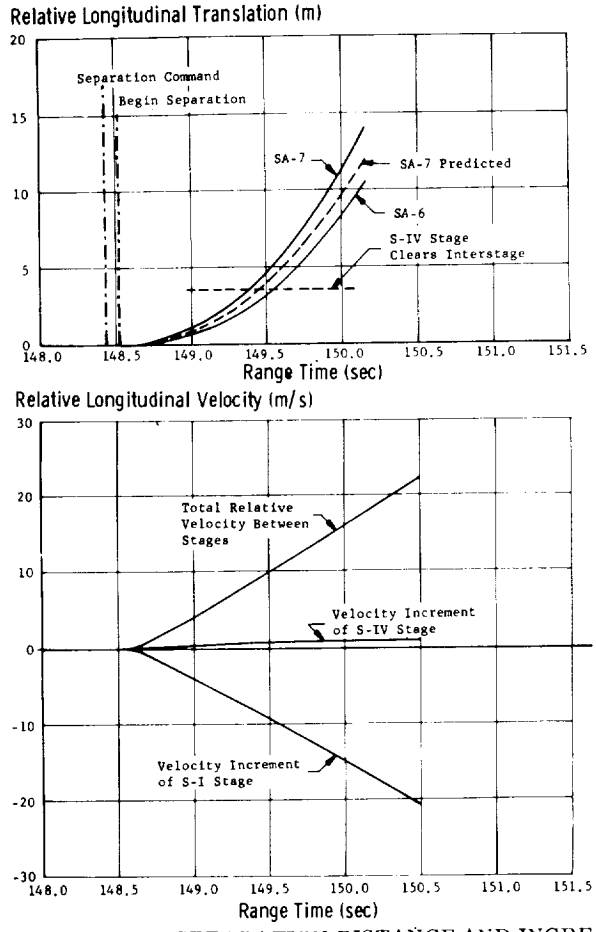

FIGURE 9-2. SEPARATION DISTANCE AND INCREMENTAL VELOCITIES

ance. The increased clearance is attributed to the later separation time (0.8 sec) from OECO, resulting in a higher negative booster acceleration at separation.

The lateral clearance analysis on SA-7 indicated that separation required 0.09 m (3.4 in.) of the 0.74 m (29 in.) available lateral clearance, corresponding to a probability of 0.75.

9.2.2 ANGULAR MOTION

At the start of separation the vehicle had the following attitudes and angular rates: (design values are listed for comparison)

Parameter	Actual	Design
Pitch Attitude (deg)	0.1 (nose up)	1.0
Yaw Attitude (deg)	-0.1 (nose left)	1.0
Roll Attitude (deg)	0.4 (CW from rear)	-
Pitch Rate (deg/s)	0	1.0
Yaw Rate (deg/s)	0	1.0
Roll Rate (deg/s)	0.1 (CW from rear)	-

Angular rates experienced by the S-I stage were considerably larger than the S-IV stage with the exception of roll (Fig. 9-3). The roll angular rate was practically the same on both stages, for the first two seconds after separation.

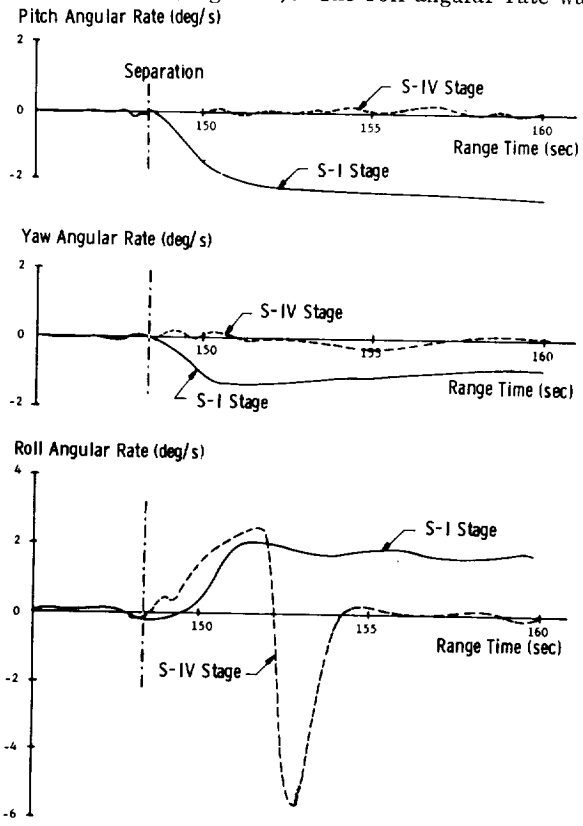

FIGURE 9-3. ANGULAR VELOCITIES DURING BOOSTER SEPARATION

The observed angular motion of the S-I stage would require the total angular impulse presented below. This total angular impulse is equivalent to the retro rocket misalignment and CG offset indicated.

Observed Angular Impulse (N-m-s)	147,483	88,729	12,554
Total Retro Rocket Misalignment (deg)	-0.22	-0.14	0.13
S-I Stage CG Offset (m)	0	-0.01	0

The retro rocket misalignment is nearly the same magnitude as observed on previous flights.

Figure 9-4 shows the telemetered and simulated attitude error transients of the S-IV stage which resulted from separation disturbances. The simulation includes the inflight engine thrust buildup and mass characteristics, and also includes an approximation to the preflight predicted CG offset history. In the yaw plane, the CG offset is to the left of center when looking forward and varies linearly from 1.8 cm

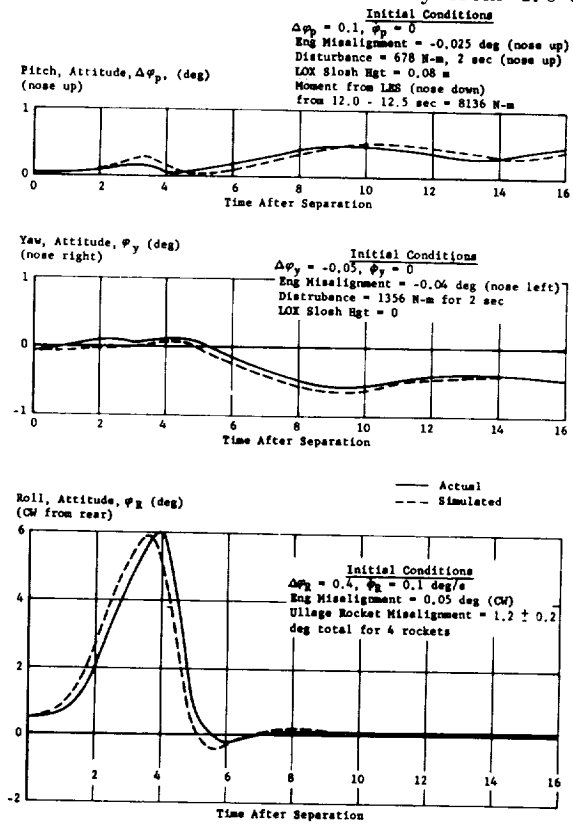

FIGURE 9-4. S-IV ATTITUDE DURING SEPARATION

(0.73 in.) at separation to 4 cm (0.7 in.) at cutoff. In the pitch plane, the CG offset is above center and varies linearly from 2.1 cm (0.84 in.) at separation to 5 cm (2 in.) at cutoff. The correlation between the simulated attitude errors and the actual attitude errors indicates that the vehicle CG offsets and thrust vector misalignments were close to those assumed. The large separation transient in roll is attributed to 1.2 ± 0.2 degree total ullage rocket misalignment. Initial disturbing moments of 678 N-m (500 ft-lb) and 1356 N-m (1000 ft-lb) are estimated to have acted on the S-IV stage in the pitch and yaw planes, respectively, for the first two seconds after separation. These moments are attributed to the cooldown exhaust vent.

The alignment tolerance of each S-IV stage ullage rocket is 0.7 degree (3σ). Root sum squaring this value would give an upper limit of 1.4 degrees of expected misalignment. This misalignment includes both angular and translational effects. The 1.2 ± 0.2 degrees determined to explain the roll deviation are near the upper expected limit. However, from a control standpoint the vehicle could control a misalignment of approximately 2.7 degrees without saturating the attitude error signal of 15 degrees and the angular rate of 10 deg/s, assuming no other disturbances exist that would add to the roll maneuver. Using the design values of 1 degree attitude in pitch and yaw, 1 deg/s rates and an angle-of-attack of 4 degrees the misalignment that could be tolerated is 2.0 degrees. No relaxation of the ullage rocket alignment tolerances should be considered if other disturbances existed and the roll error signal should not be saturated.

SECTION X. STRUCTURES

10.1 SUMMARY

The maximum pitch bending moment experienced during the flight of SA-7 occurred at 74.7 seconds and indicated a maximum of approximately 30 percent of the design moment and 39 percent of the maximum moment experienced on SA-6.

The structural flight loads were somewhat lower than on previous flights.

The bending oscillations observed were identical to those observed during the flight of SA-6. The vibratory force during the starting sequence of the engine pairs was determined to be 13 percent of the static thrust, which is well within the 20 percent allowable.

The flight vibration levels on the S-I stage were among the lowest ever exhibited by the Saturn vehicle. The structural vibration levels were mild except for the holddown, Mach 1 and max Q periods of flight. The vibration levels measured in the Instrument Unit were approximately one-third those measured during the SA-6 flight.

The bending observed on the second flight stage of SA-7 indicated frequencies near the second bending mode frequency in the yaw plane for four seconds following separation. The frequency then decreased to very near the first bending mode frequency until LES jettison. The pitch bending amplitude during this time was much lower than in yaw. Following LES jettison, bending in yaw was not observed. However, first mode bending in pitch was excited, probably by the LES exhaust blast.

The vibration levels observed on the S-IV stage of SA-7 were very near those observed on previous flights.

10.2 RESULTS DURING S-I POWERED FLIGHT

10.2.1 MOMENTS AND NORMAL LOAD FACTORS

10.2.1.1 CALCULATED VALUES

The maximum pitch bending moment experienced by the Saturn SA-7 vehicle occurred at 74.7 seconds of flight. The distribution of this moment is presented in Figure 10-1, together with the normal load factor obtained from the accelerometer readings from the IU measurements. The slope of this load factor line indicates the rotational acceleration of the vehicle. This maximum moment is 30 percent of the design moment and 30 percent of the maximum moment experienced by SA-6.

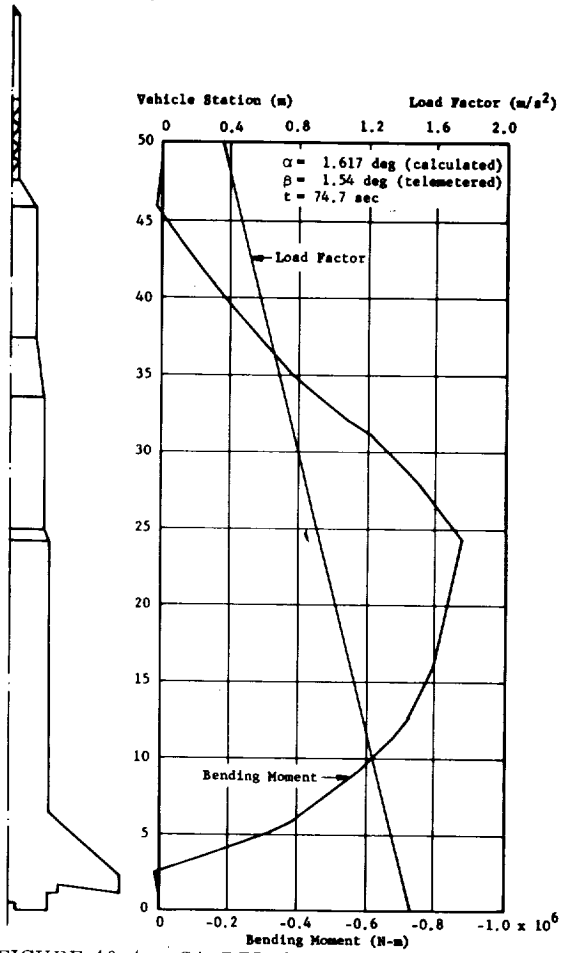

FIGURE 10-1. SA-7 PITCH BENDING MOMENT AND NORMAL LOAD FACTOR

The calculated angle-of-attack (α) and telemetered gimbal angle (β) which produced the depicted normal load factor when nominal aerodynamic and weight data were considered, were used for the bending moment distribution. The calculated angle-of-attack necessary to produce the normal load factor observed is 0.6 degree higher than the measured angle-of-attack if nominal aerodynamics are used. Time points on either side of this maximum loading point were investigated. The resulting angles-of-attack were approximately 0.6 degree higher than those measured, while the gimbal angles coincided. The control analysis (Section VII) indicated that an aerodynamic moment was acting on the vehicle; however, this is not supported by the structural analysis.

10.2.1.2 MEASURED VALUES

Station 23.9 m (942 in.) is the location of the eight LOX stud and sixteen tension tie measurements at the lower side of the spider beam. The vehicle body loads can be measured at this station with the exception of that portion of the load carried in the center LOX tank. The maximum bending moments at 75 seconds estimated on the basis of the strain data were: -286,000 N-m in yaw, 550,000 N-m in pitch with a resultant of 620,000 N-m. These values do not include the 15 percent of the total moment which is carried by the center LOX tank. Inclusion of this contribution yields a total resultant bending moment of 730,000 N-m at 75 seconds of flight.

10.2.2 LONGITUDINAL LOADS

10.2.2.1 ACCELEROMETER DATA

An investigation was made to compare the calculated response of the system, using the observed thrust forces, to that observed during the thrust buildup period. The buildup period is defined as the the time interval from ignition of the first engine to vehicle liftoff. The engines were scheduled to ignite in pairs, with a 100 ms delay between pairs to limit the vibratory force to 20 percent of the static thrust. Figure 10-2 shows the engine staggering times (ignition delay) to the erratic; however, the maximum response was only 13 percent of the static thrust.

Oscillations of aproximately ± 0.1 g were observed on the Instrument Unit accelerometer during the time interval between 40 and 80 seconds range time. An attempt was made to correlate peak amplitude frequencies of LOX and fuel pump inlet pressures, engine chamber pressures, and longitudinal accelerations. No similarity was evident and, as was shown in the flight of SA-6, the existence of POGO oscillations was not apparent.

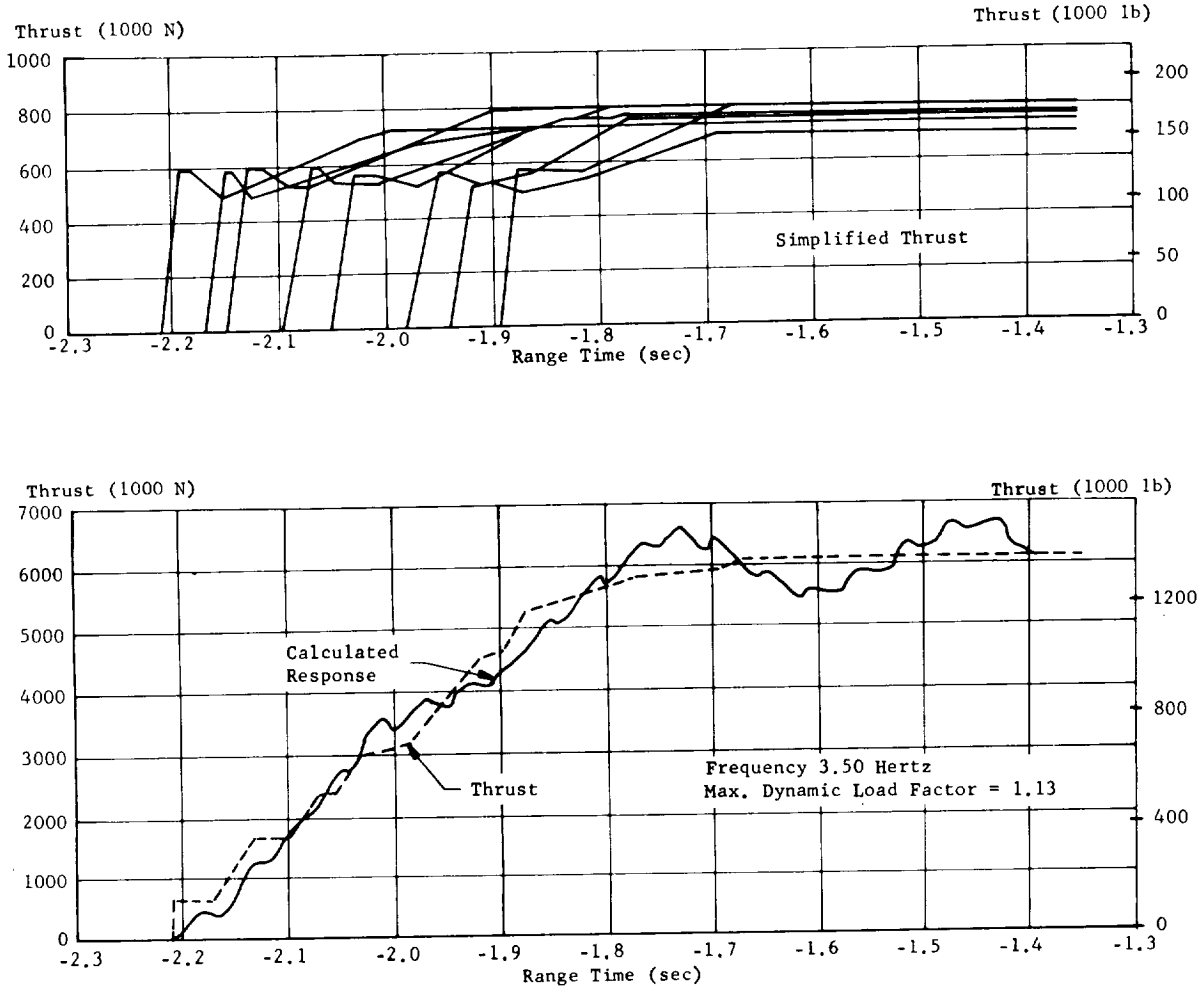

FIGURE 10-2. MAXIMUM DYNAMIC RESPONSE

The vibration acceleration level measured in the Apollo capsule was in good agreement with the calculated accelerations, and the frequency agrees with that observed on the holddown arms.

10.2.2.2 STRAIN DATA

The axial load at Sta. 23.9 m (942 in.) compared very well to the predicted values, and those obtained on vehicles SA-5 and SA-6. The axial load distribution on SA-7 follow the same general trends as observed in the longitudinal accelerations shown in Section V.

10.2.2.3 FUEL TANKS SKIRT LOADS

The fuel tank skirts were instrumented with 32 strain gauges. Eight of the gauges are equally spaced around each tank at Sta. 6.63 m (261 in.). The data received from SA-7 were in agreement with corresponding data received from SA-5 and SA-6. This agreement was expected since the skirts are not affected by body bending moments, but only by axial forces which remain nominally the same during each flight. The apparent load relief that occurred on SA-5 and SA-6 during the time interval between ignition and liftoff was difficult to see on SA-7 because of the scatter in the data. The apparent cooling of the strain gauge, located on fuel tank number one above stub fin I, from 80 to 110 seconds was repeated. This same occurrence was experienced on SA-5 and SA-6 and must be considered an actual structural response.

10.2.3 BENDING OSCILLATIONS

10.2.3.1 BODY BENDING

The SA-7 flight data showed no significant difference from the SA-6 flight test vehicle. A filter bandwidth of 0.667 Hz was used on the telemetered data for this evaluation. The response amplitude was low in the frequency range of 0 to 10 Hz, with a maximum of 0.3 g single amplitude.

Figure 10-3 represents a comparison of SA-7 flight frequencies with SA-6 dynamic test frequencies. In Figure 10-4 the amplitude response for the pitch and yaw accelerometers, located at the nose cone and escape tower, are presented. This figure shows peak amplitudes which occur in the regions of Mach 1 (55.3 sec) and max Q (73.0 sec).

All accelerometers appeared to function normally and the data received were within the range of expected results.

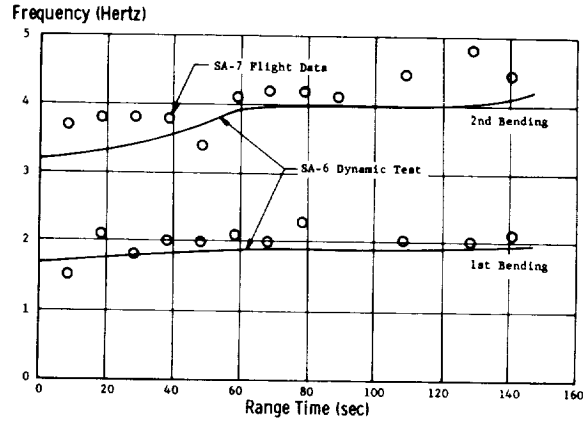

FIGURE 10-3. VEHICLE BENDING FREQUENCIES

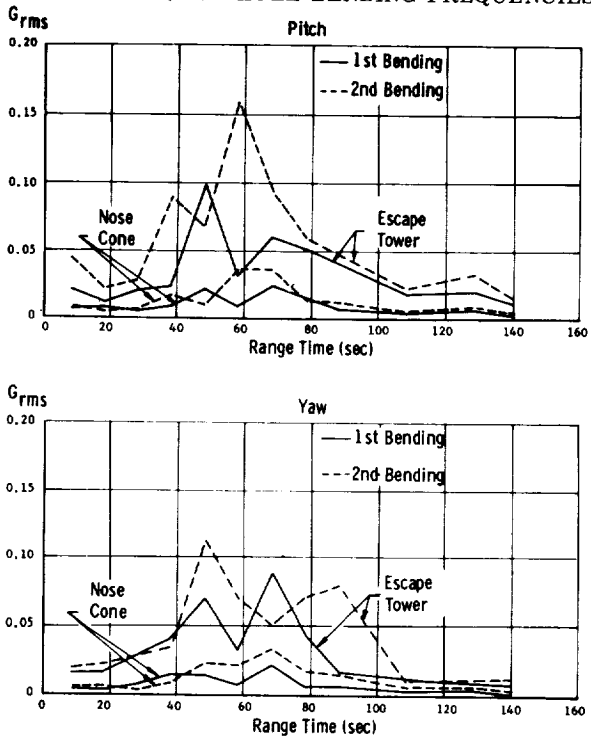

FIGURE 10-4. SA-7 ESCAPE TOWER AND NOSE CONE ENVELOPE

After separation of the S-I stage and jettisoning of the LES, oscillograph records indicate a frequency response level of negligible value.

10.2.3.2 FIN BENDING

For the SA-7 flight, three of the six fin accelerometers were changed in range from ± 1 g to ± 5 g's, but some of the data were still slightly clipped at Mach 1.0 and maximum dynamic pressure.

Slice times at 20 seconds, Mach 1.0, and maximum dynamic pressure were analyzed over the frequency span of 0 - 60 Hz. The predominant frequencies were 30, 37, and 44 Hz. These predominant frequencies showed very little change over the various slice times and, therefore, coalescence of the predominant frequencies or any flutter trend was not indicated. The frequency content of the data were approximately the same as recorded on previous flights.

10.2.4 S-I VIBRATIONS

10.2.4.1 STRUCTURAL MEASUREMENTS

Thirteen accelerometers were located on the S-I booster to measure structural vibration. All telemetered data appeared to be valid, including that obtained from four retro rocket measurements questioned during previous flights. With the exception of shear panel measurement, all data exhibited normal or expected levels throughout S-I powered flight. Envelopes of the structural vibration levels are presented in Figure 10-5.

Four of the five shear beam and shear panel measurements indicated expected vibration increases during the critical flight periods. The overall envelope of the recorded levels from these measurements correlated closely, but was slightly lower than the SA-6 envelope. The fifth measurement, located in the center of the shear panel between Fins III and IV, showed an unexpected decrease in level during the Mach 1/max Q period. Although this structure appears to be predominantly affected by excitation from the engines, the maximum level experienced during mainstage was not influenced by engine vibrations.

Shroud panel vibration levels were typical of thin, lightly braced structure. Anticipated increases in vibration were observed during critical flight periods; however, the amplitudes during holddown and Mach 1/max Q were approximately 15 percent lower on SA-7 than on SA-6.

There were three orthogonally oriented measurements of structural vibration on the spider beam spoke at Fin Line I. Compared with the SA-6 G_{rms} envelope,

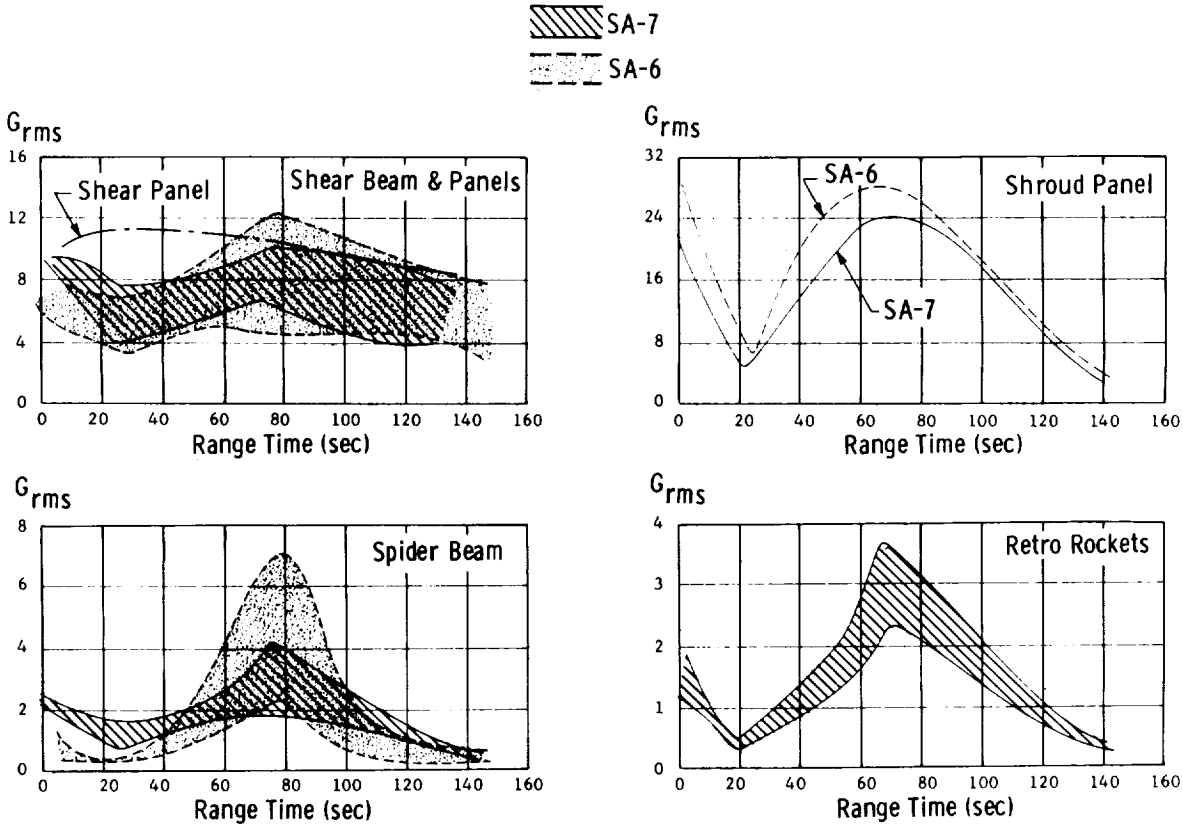

FIGURE 10-5. VIBRATION ENVELOPES OF S-I STRUCTURE

the SA-7 envelope exhibited higher levels during ignition and mainstage, but indicated a considerable reduction in level during the Mach 1/max Q period of flight. These differences in vibration amplitude are attributed to the difference in angle-of-attack. This conclusion is substantiated by the close comparison between the levels on SA-7 and SA-5, which had similar angles-of-attack.

There were four accelerometers located on the support brackets for retro rockets 1 and 3. This structure, which is most susceptible to aerodynamic excitation, showed expected increases in vibration during the Mach 1/max Q period of flight. The max Q vibration was three times higher than the holddown vibration.

10.2.4.2 ENGINE MEASUREMENTS

Four accelerometers located on the combustion chamber domes of engines 1, 3, 5, and 7 measured vibration in the longitudinal (flight) direction. All four accelerometers measured vibration levels that were inconsistent with previous static and flight test history. Consequently, the validity of the SA-7 data was questioned. An investigation of the SA-7 data revealed that there was a large discrepancy between the telemetered data received during holddown and the landwire data obtained from the combustion stability monitor (CSM) measurements. The CSM and flight measurements are located side by side and should provide comparable data. Therefore, it was concluded that the SA-7 flight combustion chamber dome data were unreliable. Figure 10-6 shows a comparison of the data from SA-7 to that of SA-6.

Four accelerometers were located on the combustion chamber domes of engines 2, 4, 6, and 8 to measure vibration in the lateral direction. The SA-7 vibration was normal throughout S-I flight and the time history correlated well with previous flight history (see Fig. 10-6).

Four accelerometers measured the vibration of the turbine gear box on each of the outboard engines. In general, the vibration levels were lower than those measured on SA-6 flight (Fig. 10-6). The vibration of engine 3 gear box was higher than the other three after the max Q period. The SA-7 vibration levels were as expected.

A series of vibration measurements were made on the engine components to determine the levels associated with these components. Figure 10-7 presents the envelopes of the vibration levels determined for the engine components compared to the levels for SA-6.

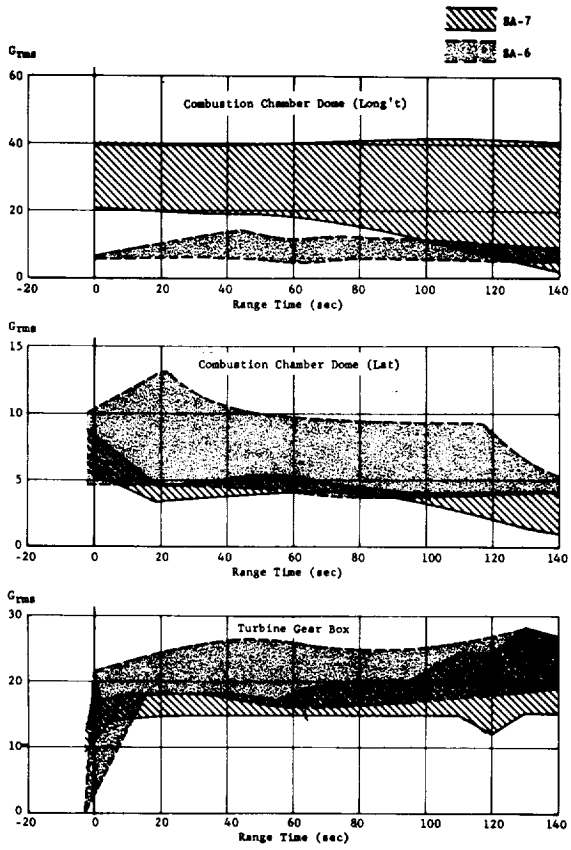

FIGURE 10-6. VIBRATION ENVELOPES OF S-I ENGINE MEASUREMENTS

Three accelerometers measured the vibration of yaw actuator of engine 4. The SA-7 vibration levels were normal. Compared to SA-6, the SA-7 vibrations were approximately 30 percent lower. As expected, the vibrations in the longitudinal (flight) direction were higher throughout flight than the yaw measurements.

Six accelerometers measured the vibration of the fuel suction line of engine 6 at both the inlet and outlet flanges. The SA-7 vibration was normal and correlated well with the previous flight history. As expected, the vibration at the outlet flange of the fuel suction line was 50 percent higher than the vibration at the inlet flange in the longitudinal direction.

Three accelerometers measured the vibration at the outlet flange of the engine 6 heat exchanger. The SA-7 vibration levels were normal and were about 25 percent lower than the levels measured during SA-6.

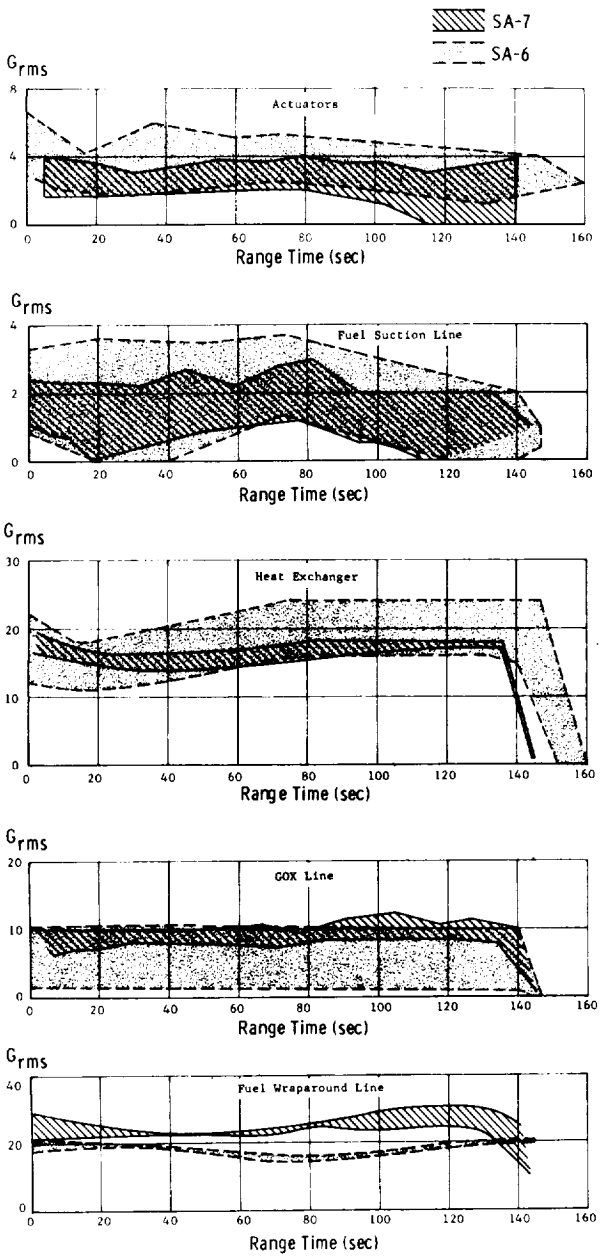

FIGURE 10-7. VIBRATION ENVELOPES OF S-I ENGINE COMPONENTS

Six accelerometers measured the vibration of the engine 6 GOX line. The SA-7 vibration levels were as expected. Compared to SA-6, the SA-7 vibrations were lower during the first half of the flight including max Q, but slightly higher during the remainder of the flight.

Two accelerometers measured the vibration of the fuel wraparound line of engine 6 near the line outlet to the turbopump. The highest vibration levels occurred after max Q. Compared to SA-6, the SA-7 levels were 20 percent higher; however, the SA-7 levels are comparable to those measured on SA-3 flight.

10.2.4.3 COMPONENT MEASUREMENTS

Eight accelerometers were located in the forward and aft skirt regions of the fuel tanks. Six of these transducers measured vibration on the instrument compartment panels in the forward skirt region of fuel tanks 1 and 2, and the remaining two measurements were made in the aft skirt region of fuel tank 1 adjacent to the 9A3 distributor mounting bracket. Envelopes of the vibrations observed on these measurements are presented in Figure 10-8

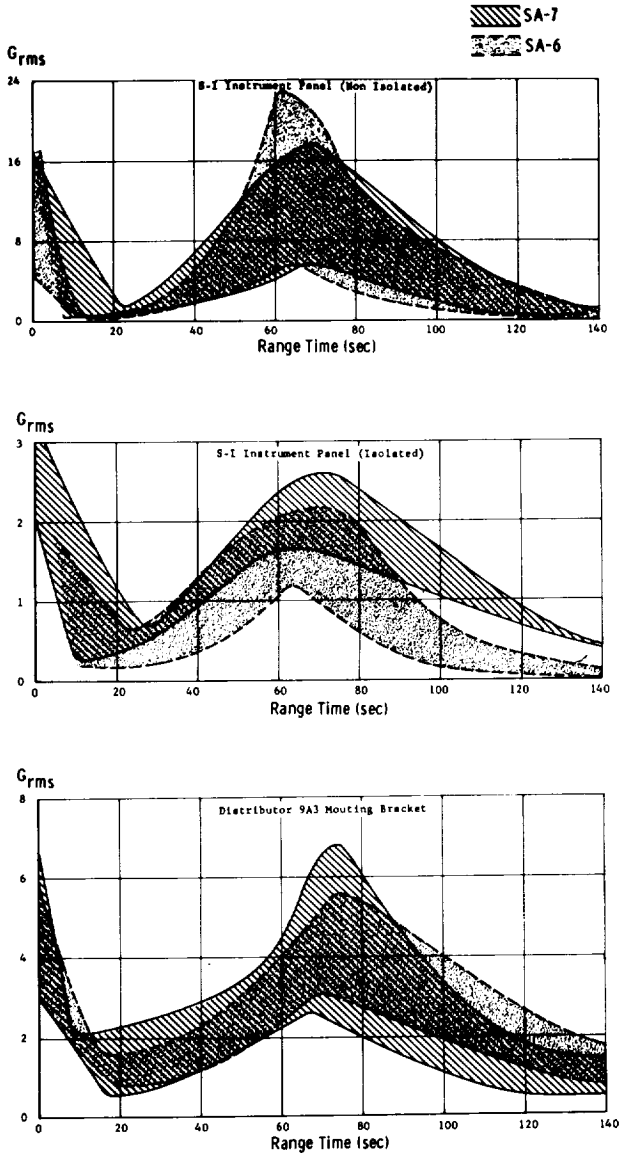

FIGURE 10-8. VIBRATION ENVELOPES OF S-I COMPONENT MEASUREMENTS

A hard mounted instrument panel was located in fuel tank 2 and exhibited typical increases in vibration during the holddown and Mach 1/max Q regions of flight. The composite G_{rms} envelope was equal to the SA-6 envelope during holddown and mainstage, and slightly lower during Mach 1/max Q.

The vibration levels of the shock mounted instrument panel, located in the forward skirt region of fuel tank 1, were consistent with expected amplitudes. Levels measured on the isolated instrument panel were approximately 84 percent lower than those on the non-isolated (hard mounted) panel. The SA-7 composite vibration was slightly higher than the SA-6 vibration during holddown and Mach 1/max Q; however, due to the relatively low amplitudes involved, this difference was not considered significant.

Two accelerometers located adjacent to the distributor 9A3 mounting bracket measured vibration on the fuel tank skirt ring frame. As expected, an increase in vibration occurred during holddown and Mach 1/max Q. The vibration perpendicular to the ring frame was slightly lower during SA-7 flight than during SA-6. Compared to SA-6, the SA-7 vibration parallel to the ring frame was higher from ignition through max Q. From max Q to engine cutoff, the amplitude was lower than that recorded during SA-6. The overall SA-7 envelope of the vibration input to the 9A3 distributor mounting bracket correlated closely with past flight history.

10. 2. 5 S-IV VIBRATIONS

10. 2. 5. 1 STRUCTURAL MEASUREMENTS

Nine vibration measurements were taken on the S-IV-7 stage thrust structure and LH_2 tank. Envelopes of the composite time histories are shown in Figure 10-9. Envelopes of thrust structure measurements from the SA-5 and SA-6 flights are also shown for comparison. The vibration levels measured during the SA-7 flight fell within the envelopes established from SA-5 and SA-6 flight measurements. The vibrations on the thrust structure exhibited expected characteristics during the S-I stage powered flight, and the levels did not present any problems to the S-IV stage thrust structure.

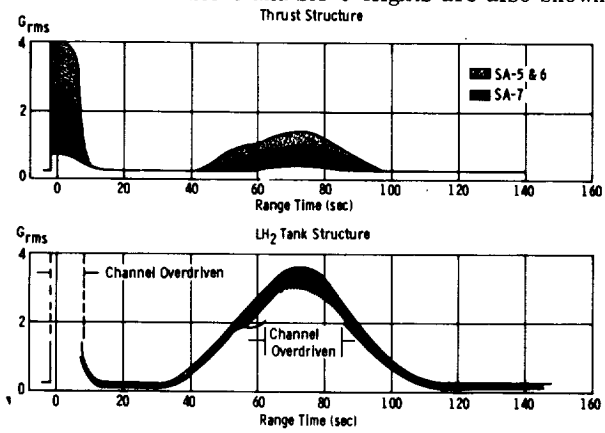

FIGURE 10-9. ENVELOPES OF S-IV STRUCTURAL VIBRATIONS DURING S-I STAGE POWERED FLIGHT

The measurements on the LH_2 tank structure showed levels that were higher than expected during holddown, liftoff, and max Q; data were lost during these periods due to over driving of the telemetry channel. Calibration range changes will be made on future flights to insure that valid data can be obtained.

10. 2. 5. 2 ENGINE MEASUREMENTS

Measurements of each engine were taken on the thrust chamber dome in the thrust direction and on the gear case housing in the radial direction. The vibration levels during S-I stage powered flight were below the noise level of the telemetry system and were considered negligible at these locations.

10. 2. 5. 3 COMPONENT MEASUREMENTS

The component measurements were separated into components in the aft skirt and thrust structure, in the LH_2 tank, and in the forward interstage. The aft skirt and thrust structure measurements were taken on the helium heater, at the base of the inverter, sequencer, PU computer and ullage rocket. The LH_2 tank measurements were taken at the cold helium sphere attach point to the LH_2 tank skin (three directions). The forward interstage measurements were located on the telemetry rack, including both the input to the rack and to the command destruct receiver mounted on the rack. Envelopes of the composite time histories are shown in Figure 10-10. Also shown are SA-5 and SA-6 flight envelopes for the thrust structure and forward interstage components.

The components on the aft skirt and thrust structure showed a high upper envelope which is attributed to the measurement at the ullage rocket. This measurement was exposed to the direct impingement of the acoustic and aerodynamic environments during boost and max Q periods of flight and reflected the high excitation which these periods induced. The vibration level on the other components (on thrust structure) fell below the environment established during the SA-5 and SA-6 flights. The vibrations on the thrust structure components exhibited the expected characteristics during S-I stage powered flight.

The overall vibration levels at the cold helium spheres, located in the LH_2 tank, were consistent in

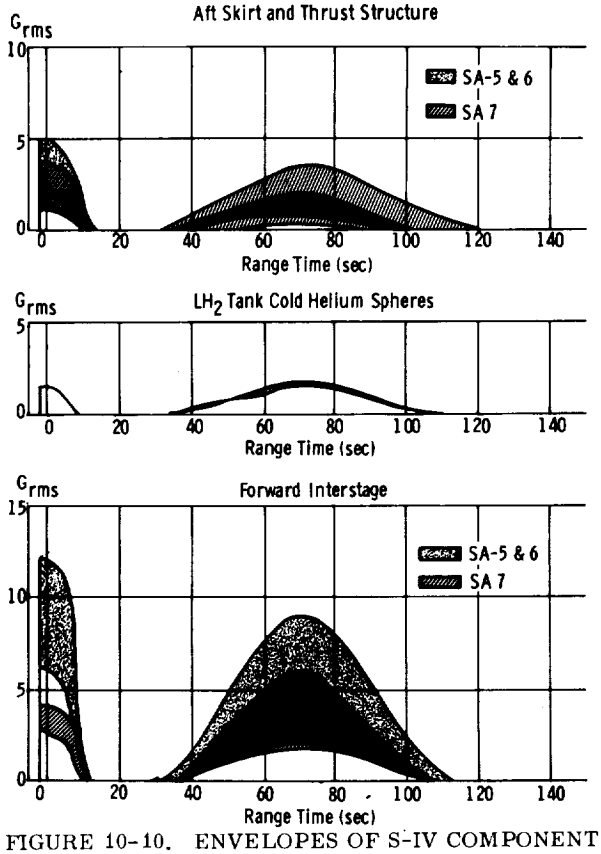

FIGURE 10-10. ENVELOPES OF S-IV COMPONENT VIBRATIONS DURING S-I STAGE POWERED FLIGHT

three directions (thrust, normal and tangential) during S-I stage powered flight. Overall levels of approximately 1.5 G_{rms} at liftoff and max Q were lower than expected. There were no previous flight measurements to refer to for comparison purposes.

The forward interstage envelopes in Figure 10-10, representing the environment during flight, were formed by the data from the command destruct receiver measurement (lower band) and from the measurement at the base of the telemetry rack (upper band). The SA-7 envelope indicates that the vibration amplitude was attenuated by the isolated panel to which the command destruct receiver was mounted. The SA-5 and SA-6 flight levels were considerably higher due to differences in the direction of the measurements and angle-of-attack. The vibrations at the telemetry rack exhibited the expected characteristics during S-I stage powered flight.

10.2.6 INSTRUMENT UNIT VIBRATIONS

10.2.6.1 STRUCTURAL MEASUREMENTS

The Instrument Unit structure vibrations shown in Figure 10-11 were monitored by ten accelerometers located on the Instrument Unit mounting ring and the Apollo mounting ring, and by one accelerometer located on the skin. The skin vibration amplitude was 50 percent higher than the highest mounting ring vibration during the Mach 1/max Q period of flight.

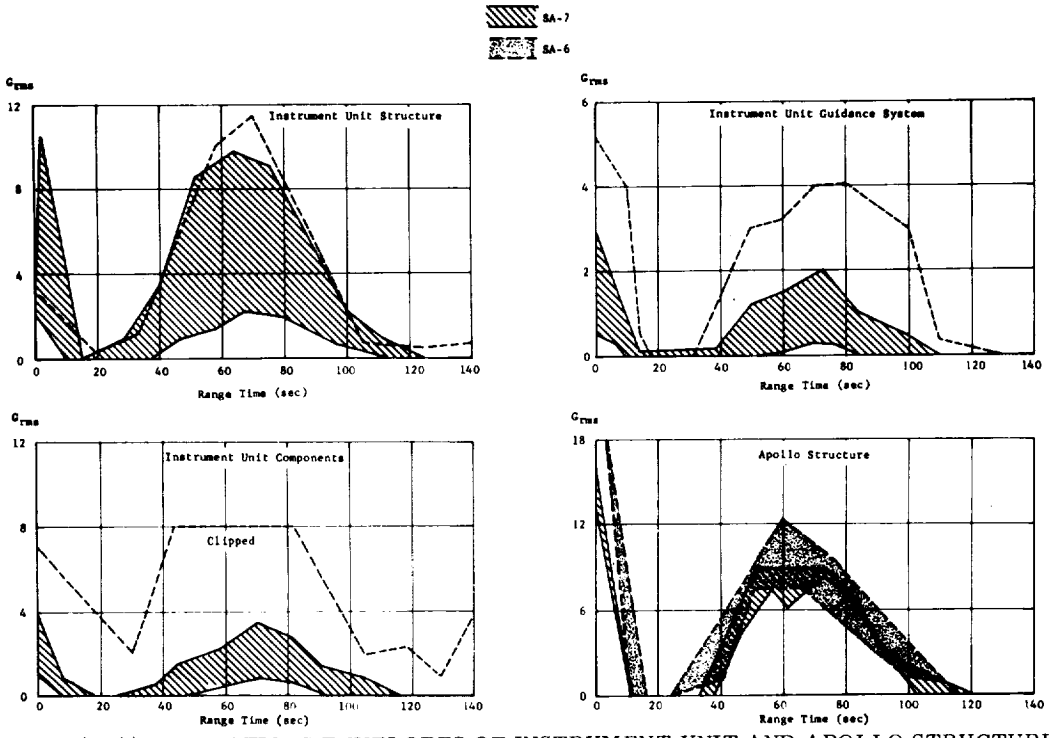

FIGURE 10-11. VIBRATIONS ENVELOPES OF INSTRUMENT UNIT AND APOLLO STRUCTURE

The SA-7 skin vibration was 20 percent lower than SA-6. The mounting ring vibration was lower by approximately the same percentage. This was as expected due to the lower angle-of-attack.

10.2.6.2 COMPONENT MEASUREMENTS

The vibration input to various Instrument Unit components was monitored by 12 accelerometers located on support bases, panels, brackets, etc. The vibration environment of the various components was minor except during the holddown and Mach 1/max Q periods of flight (see Fig. 10-11). Maximum amplitudes during holddown and max Q were lower than expected. Some previous flight data were clipped, making overall comparisons impossible.

The ST-124 guidance system vibration was monitored by nine accelerometers. The vibration of the system was mild except during the critical flight periods (see Fig. 10-11). The SA-7 vibrations were lower than SA-6 by approximately 50 percent due to the programmed flight trajectory having a lower angle-of-attack.

10.2.7 APOLLO VIBRATIONS

The Apollo structural vibration was measured with two accelerometers located on the reinforced "boilerplate" structure at Sta. 39.9 m (1570 in.). One measurement was at Fin Position I and the other was at Fin Position III. The SA-7 vibration was minor except during the holddown and Mach 1/max Q periods, as expected. The vibration during holddown was 1.5 times higher than the vibration during max Q. At S-I OECO, vibrations exceeding twice the max Q levels lasted for 50 to 100 milliseconds. At IECO, the vibrations were minor. Compared to SA-6, the SA-7 vibrations were 20 percent lower during the critical flight periods.

It was noted that vibration at the Fin I and Fin II locations had very dissimilar time histories. The vibration at Fin I (lower part of band in Fig. 10-11) rose to a maximum twice during the Mach 1/max Q period. This phenomenon was attributed to the passage of two shock waves over the structure, the first wave being stronger than the second. It was expected that this phenomenon would be less apparent during SA-7 flight because of the "zero" angle-of-attack. However, this was not the case.

10.2.8 STRUCTURAL ACOUSTICS

The acoustic environments of SA-7 were compared with predicted values rather than measured data because of the change in the programmed angle-of-attack. This change resulted in different aerodynamic flow characteristics which affected the acoustic environment.

10.2.8.1 S-I STAGE

The S-I stage acoustic environment was measured at four locations. Two of these measurements were internal and two were external. All of the acoustic data appeared normal and agreed well with the predicted acoustic time histories. The two internal measurements, at Sta. 21.5 m (845 in.) were in good agreement with the predicted environments, particularly at the critical periods of holddown, Mach 1 and max Q. The highest levels measured during these times were 148 db during holddown and 130 db during Mach 1/max Q. The two external measurements, at Sta. 23.5 m (925 in.) were also in good agreement with predicted time histories. The overall acoustic levels at each location were comparable during holddown and Mach 1/max Q periods. The levels during mainstage were considerably lower and difficult to estimate due to the lower calibration limit of the microphone. The time history of the measurement 22.5 degrees off Fin IV toward Fin I exhibited separate peaks in the time history at Mach 1/max Q and were slightly higher than the adjacent measurement 24 degrees off Fin Line IV toward Fin Line I. Figure 10-12 presents a time history of the S-I stage acoustic measurements.

10.2.8.2 S-IV STAGE

Acoustic measurements on the S-IV stage were taken at the engine 4 gimbal block and between the sequencer and PU computer inside the thrust structure. The measurement at the gimbal block provided no data. Because of time sharing, the measurement next to the sequencer provided data only during the period from 7 to 10 seconds after S-I stage engine ignition. During this period, the level was low (131 db), and the data were below the noise level of the telemetry system for the remainder of powered flight. Calibration range changes will be made on future flights.

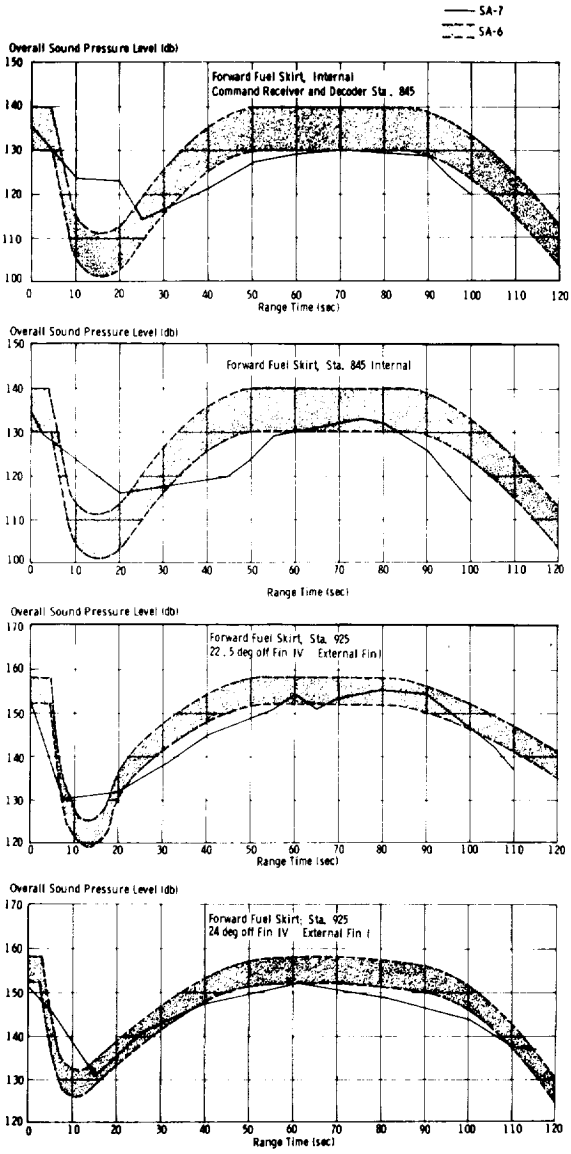

FIGURE 10-12. FORWARD FUEL SKIRT ACOUSTICS

10.2.8.3 INSTRUMENT UNIT

Two external measurements were made of the acoustic environment on the skin surface of the Instrument Unit. One measurement located at Sta. 38.4 m (1512 in.) measured the acoustic environment 20 db lower than the predicted levels while the other measurement, located in the same radial direction at Sta. 37.2 m (1464 in.), was in very good agreement with predicted values (see Fig. 10-13). It is not felt that the difference in the locations of these two measments is sufficient to account for this change in the acoustic environment. Therefore, these data are not

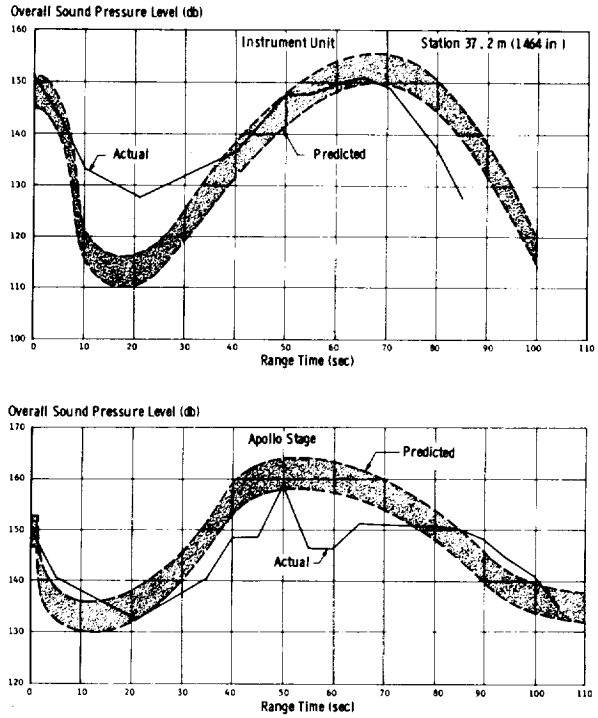

FIGURE 10-13. INSTRUMENT UNIT AND APOLLO ACOUSTICS DURING S-I FLIGHT

considered valid. The acoustic levels during the hold-down and Mach 1/max Q periods were 151 db and 155 db respectively, which agree well with the predicted values.

10.2.8.4 APOLLO STAGE

One external measurement of the acoustic environment was made on the Apollo stage. This measurement was located at Sta. 45.74 m (1800.9 in.) on Fin Line III. Figure 10-13 presents a time history of this measurement. This time history indicated that the levels were generally within the predicted levels. However, between 2 and 14 seconds and 85 and 100 seconds the environment did exceed these limits by approximately 3 db. The levels later in the flight are the result of the aerodynamic turbulence and shock interaction peculiar to this location.

10.3 RESULTS DURING S-IV POWERED FLIGHT

10.3.1 S-IV LOADS

Data from the S-IV-7 stage indicated that all major structural components functioned as designed. Because of the limited camera coverage, however, it was not possible to determine if there was a recurrence of the opening or loss of the air conditioning door of the aft interstage, as was the case with S-IV-5 and

S-IV-6. For the same reason, the effectiveness of the 10 grain primacord used to open the blowout panels could not be determined.

10.3.2 BENDING

At separation, body bending was excited in yaw. For the first four seconds after separation, the predominant frequency was 10 Hz, which is very close to the predicted SA-7 second mode frequency of 10.2 Hz. From four seconds after separation to LES jettison, the predominant frequency was 4 Hz, which is slightly higher than the predicted S-IV-7 first mode frequency of 3.6 Hz. During this time period, bending in the pitch plane was of much smaller magnitude than in the yaw plane.

Following LES jettison, bending in yaw was not observed. However, first mode bending in pitch was excited, probably by the LES exhaust blast. The frequency of this oscillation was 11 Hz, compared to 1.4 Hz predicted for S-IV-7 first mode after LES jettison. The pitch oscillations damped out quickly after LES jettison.

10.3.3 S-IV VIBRATIONS DURING S-IV POWERED FLIGHT

10.3.3.1 STRUCTURAL MEASUREMENTS

The structural measurements were located on the thrust structure and LH_2 tank. Five structural measurements were taken on the thrust frame assembly (pitch and yaw directions), and on the engine 4 thrust structure at the gimbal block (thrust and yaw directions) and actuator B attach point (parallel to center line of actuator). The envelopes of the overall time histories are shown in Figure 10-14. The SA-5 and SA-6 flight envelopes of the gimbal point measurements are also shown in this figure. Vibration levels during the SA-5 and SA-6 flights were considerably higher at the gimbal point. These higher levels are attributed to differences in measurement locations and to a high thrust environment on engine 4 during the SA-6 flight. The SA-5 and SA-6 flight measurements were located on the structure next to the gimbal block, while the SA-7 flight measurements were mounted directly on the block. The vibration levels on the thrust frame were lower than expected, in comparison to the static test levels. Although the amplitudes were low, the G_{rms} values were constant during S-IV stage powered flight.

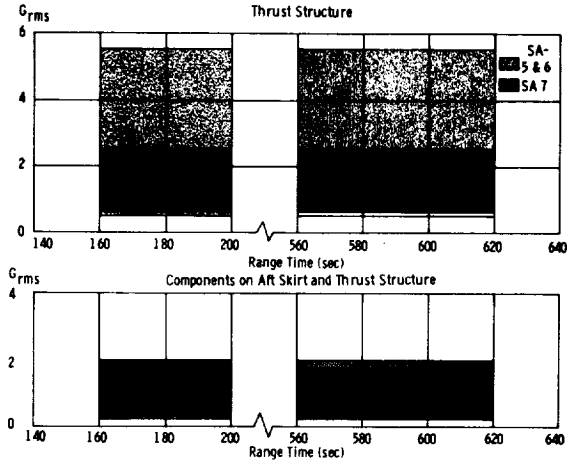

FIGURE 10-14. ENVELOPES OF S-IV STRUCTURAL AND COMPONENT VIBRATIONS DURING S-IV STAGE POWERED FLIGHT

The vibration levels on the LH_2 tank were below the noise level of the telemetry system and therefore were considered negligible during S-IV stage powered flight.

10.3.3.2 ENGINE MEASUREMENTS

Measurements were taken for each engine on the thrust chamber dome in the thrust direction and on the gear case housing in the radial direction. Figure 10-15 shows a composite vibration time history plot for each engine.

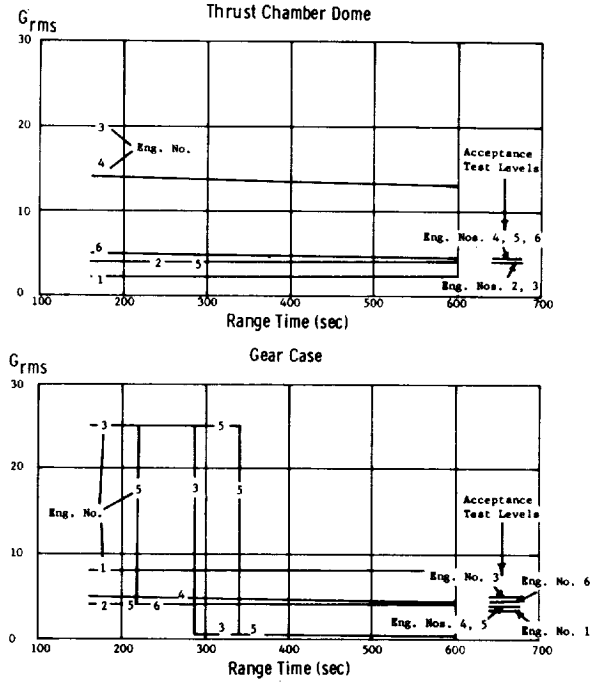

FIGURE 10-15. VIBRATIONS ON ENGINES DURING S-IV STAGE POWERED FLIGHT

The vibration levels measured on the gear case housing of engines 2, 4 and 5 were approximately the same as those measured during the S-IV-7 stage acceptance firing, and were as expected. At 220 seconds the vibration levels from engine 5 exceeded the

calibration limits of the telemetry channel (24 G_{rms}). After 342 seconds the vibration levels dropped to zero indicating that either the engine experienced electrical problems or that the transducer mounting block became debonded from the gear case housing. Since all engine operating parameters were nominal, it is reasonable to conclude that the high vibration levels measured between 220 and 342 seconds were caused by a malfunction of the measuring system and, therefore, are not valid engine vibration levels.

The vibration levels on the gear case housing of engine 3 also exceeded the calibration limits of the telemetry system (24 G_{rms}) from S-IV ignition until 273 seconds. After 273 seconds the level dropped to zero, indicating problems similar to those experienced by the engine 5 gear case measurement. Although the vibration levels measured on the engine 6 gear case appeared normal (4 G_{rms}), the data contained square waves and must be considered invalid. The data from the engine 1 gear case show a 6 G_{rms} overall level which is slightly higher than the other engines. It appears that the higher overall level was caused by a low frequency shift in the data. The low frequency shift (5 Hz) is not valid data because it is impossible for the engine to move at the displacement indicated (± 10 cm) by the data.

The vibration levels measured on the thrust chamber dome of engines 2, 5, and 6 were about the same as measured during the S-IV-7 stage acceptance firing. Engine 1 indicated levels lower than expected. An explanation of these low levels cannot be made at present. The vibration levels measured on the thrust chamber dome of engines 3 and 4 were unusually high (20 and 15 G_{rms}, respectively) during S-IV stage powered flight; these levels are considered questionable. The data exhibited the same characteristics as the data from the case housing of engines 3 and 5, and are considered invalid for the same reasons of possible debonding or electrical problems.

Past experience of battleship and acceptance firing testing indicates that the thrust chamber dome and gear case transducer mounting blocks are susceptible to debonding after several engine firings. The number of measurements lost during flight could be reduced by the removal and careful rebonding of each gear case and thrust chamber dome measurement just prior to flight.

10.3.3.3 COMPONENT MEASUREMENTS

A total of 11 component measurements were taken on the S-IV forward interstage, LH_2 tank, and the aft skirt and thrust structure. The aft skirt and thrust structure measurements were located on the helium heater and at the base of the inverter, sequencer, PU computer and ullage rocket. The LH_2 tank measurements were located at the attach point between the cold helium sphere and the LH_2 tank skin. The forward interstage measurements were confined to the telemetry rack, specifically at the base of the telemetry rack and at the base of the command destruct receiver mounted on the rack.

Envelopes of the composite time histories for components on the aft skirt and thrust structure are shown in Figure 10-14. Envelopes of the SA-5 and SA-6 flight measurements are also shown in this figure. The envelopes show that the component vibrations of the three flights varied less than 2 G_{rms}. The vibration levels were nominal throughout S-IV stage powered flight.

The vibration levels for the components in the LH_2 tank (cold helium sphere) and forward interstage (T/M rack) were below the noise level of the telemetry system. They are considered to have been negligible throughout S-IV stage powered flight. The vibration levels at the cold helium sphere were lower than expected.

10.3.4 INSTRUMENT UNIT VIBRATIONS

There was no significant instrument unit vibration during S-IV powered flight. The vibration amplitude during this period was of the same order of magnitude as the vibration amplitude during the mainstage period of S-I powered flight.

10.3.5 APOLLO VIBRATION

The Apollo boilerplate structure vibration was negligible during S-IV powered flight.

10.4 S-I/S-IV INTERSTAGE

Recovered camera data (see Section 14.8.2) revealed debonding of the interstage similar to that on SA-5. However, the apparent deflection of the interstage on SA-7 was approximately two times that of SA-5. The information available was not sufficient to determine the actual cause of this failure. An attempt is being made to instrument future flights in order to better explain this phenomenon.

SECTION XI. ENVIRONMENTAL TEMPERATURES AND PRESSURES

11.1 SUMMARY

No unexpected environments were indicated for the SA-7 flight. Surface pressures and temperatures on the S-I-7 and S-IV-7 stages were in good agreement with past results.

S-I stage base thermal environment was similar to previous flight results indicating maximum heating to the outer region. Simulation (postflight) of the flame shield total heat rate indicated a level of 30-40 watts/cm^2 after approximately 70 seconds. This verified that no convective cooling is present in this area as would be expected. Engine compartment temperatures indicated that no fires existed in the S-I-7 base.

Compartment pressures and loading on SA-7 were in good agreement with expected levels.

11.2 S-I STAGE ENVIRONMENT

11.2.1 SURFACE PRESSURES

Surface pressure environments on the forward and aft S-I-7 tank skirts showed no unusual deviations from those measured on previous Saturn I flights.

A maximum pressure loading of 2.4 N/cm^2 (surface pressure minus internal pressure) was measured across the spider beam fairing at 60 seconds. This measurement was flown for the first time on SA-7 and the maximum pressure was approximately 0.8 N/cm^2 below design value.

11.2.2 FIN TEMPERATURES AND HEATING RATES

In general, the S-I-7 fin temperatures and heating rates agreed with the previous two flights. The influence of plume radiation on the fin skin temperatures increased slightly but this influence, as with the previous flights, was not considered critical.

Fin Base Heating Rates

Fin base heating rates on S-I-7 were similar to the rates for S-I-5 and S-I-6 (see Fig. 11-1). However, erratic data were obtained between 1 and 15 km (40-70 sec) for the total calorimeter measurement for the SA-7 vehicle.

11.2.3 S-I STAGE SKIN TEMPERATURES

Good agreement was indicated for the thermal environment at the forward end of the 1.78 m (70 in.) LOX tank between the SA-5, SA-6, SA-7 environments and with predicted as shown in Figure 11-2. However, much higher temperatures were indicated at the same location 180 degrees around the 1.78 m (70 in.) LOX tank. These higher values appear to be a measurement of the ambient temperature and not the LOX tank skin temperatures. A large difference (approximately 60°K) exists between SA-7 and the previous SA-5 and SA-6 flights for the LOX tank temperatures at Sta. 14.5 m (569 in.) during the portion of flight when LOX is against the tank wall. During the remainder of flight the agreement between the three flights becomes better with a discrepancy of approximately 15°K remaining by engine cutoff.

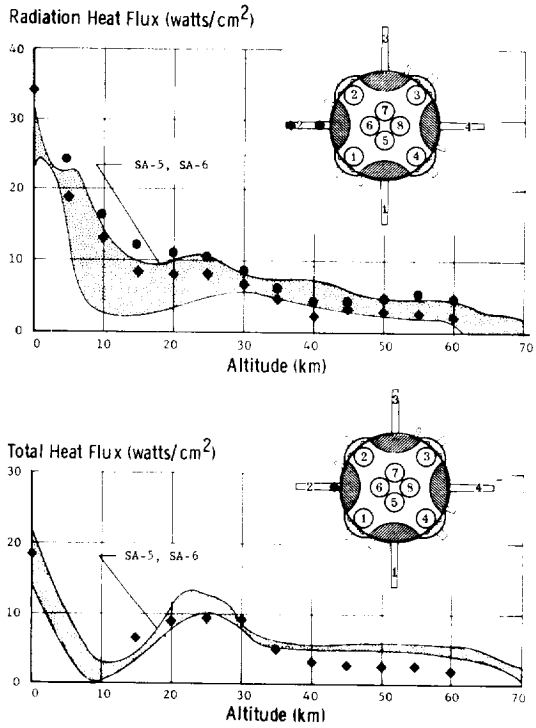

FIGURE 11-1. FIN BASE HEATING RATES

Skin temperatures on the S-I-7 60-degree fairing were higher than on the previous flights as shown in Figure 11-3. The reasons for the higher temperatures are due to the hotter SA-7 launch day and to the fact that the Thermo-lag had been removed from the S-I-7 fairing.

Tail shroud temperatures for SA-7 and SA-6 are shown in Figure 11-3. Thermal environment for this area can be closely approximated considering only aerodynamic heating effects, indicating little or no effects from exhaust radiation.

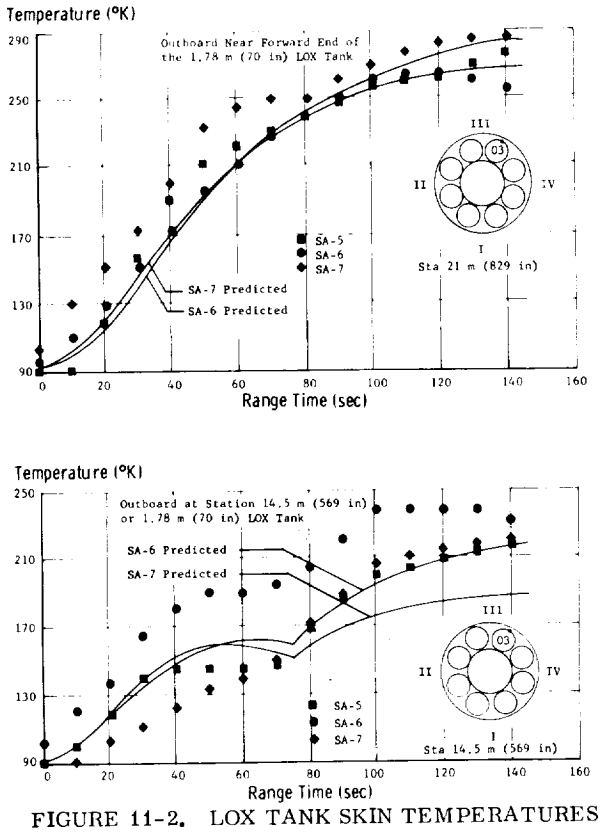

FIGURE 11-2. LOX TANK SKIN TEMPERATURES

Hydrogen vent pipe temperature on the forward end reached a maximum value of 320°K and a new measurement on the leading edge of the vent protruding from the stub fin reached a maximum value of 360°K (Fig. 11-3). These maximum temperatures were reached by approximately 110 seconds at which time hydrogen venting occurred.

Inboard engine turbine exhaust duct temperatures were measured for the first time on SA-7 (Fig. 11-4). Maximum values measured were within design limits.

11.2.4 BASE PRESSURES

Measured pressures on the S-I-7 base were consistent with SA-5 and SA-6 results except at the higher altitudes where the two SA-7 flame shield measurements indicated higher pressures (see Fig. 11-5). At approximately 35 km, the pressure level on the center of the flame shield rose to a maximum value of 2.2 N/cm^2 above ambient compared to 1.8 N/cm^2 above ambient on SA-6. Wind tunnel hot-jet tests have shown an increase in flame shield pressure when the ambient (free-stream) pressure is lowered.

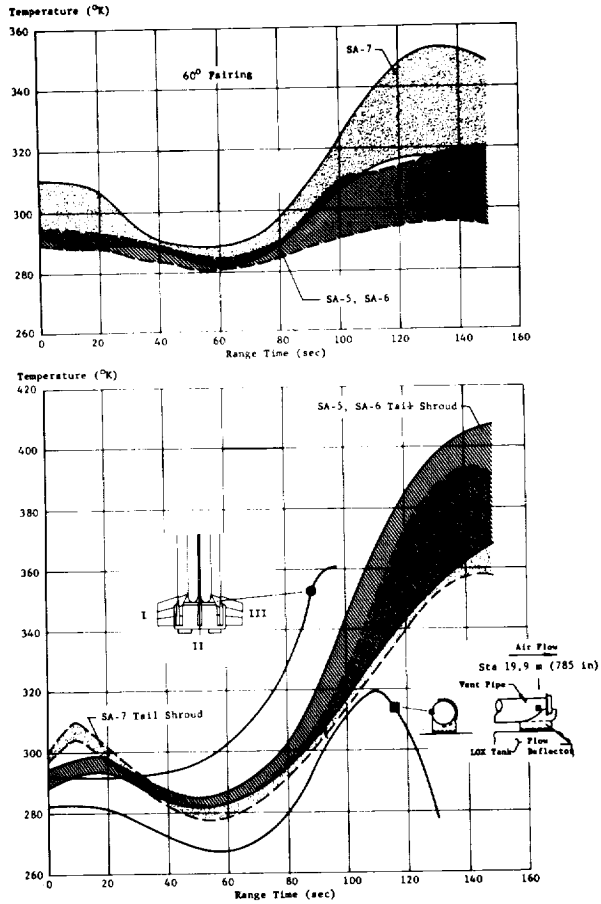

FIGURE 11-3. TEMPERATURE ON SIXTY DEGREE FAIRING, TAIL SHROUD AND HYDROGEN VENT PIPE

Measured heat shield pressures were consistent to those obtained on SA-5 and SA-6; however, two of the five measurements on the SA-7 heat shield appear to have failed after 11 km.

11.2.5 BASE TEMPERATURES

Inner and outer region gas temperatures on S-I-7 were in good agreement with the majority of measurements on previous flights as shown in Figure 11-6. Maximum temperature in the inner region was approximately 1160°K at 60 km while for the outer region a value of approximately 1150°K was reached at 25 km.

Engine shroud gas temperature, flown for the first time on SA-7, is compared to outer region gas temperature (see Fig. 11-7). Good correlation between the two sets of data is attained after 15 km.

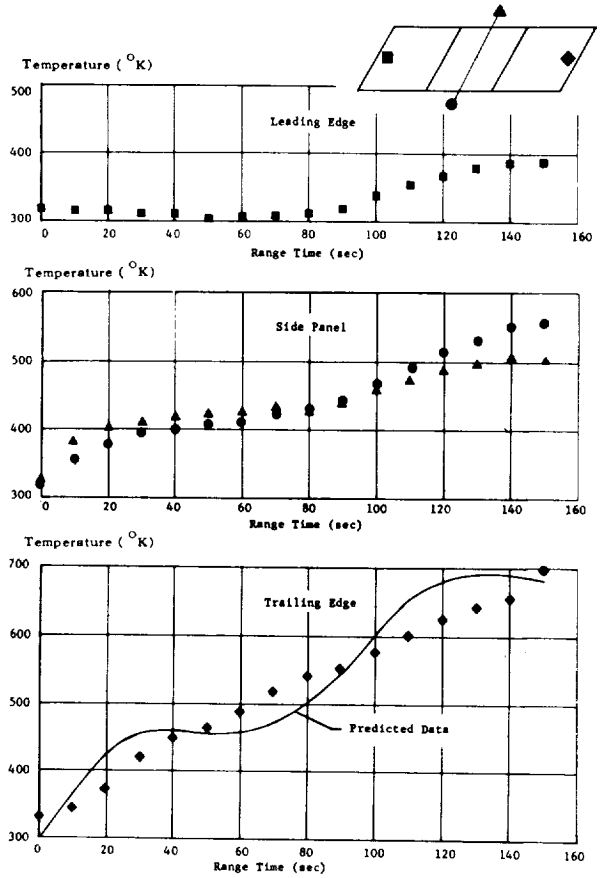

FIGURE 11-4. TURBINE EXHAUST FAIRING TEMPERATURE

Good correlation was indicated for the fin base gas temperature on SA-7 to previous flights. A maximum value of approximately 1050° K was obtained at 30 km on SA-7.

Flame shield gas temperature was in good agreement with past flights (see Fig. 11-7). Maximum values of 2000° K (5.5 cm aft of surface) and 1600° K (flush with surface) were measured in the flame shield region.

11.2.6 BASE HEATING RATES

Generally, the S-I-7 base heat rates, both total and radiation, agree with the S-I-5 and S-I-6 base environments.

Inner and outer region radiation and total heat rates fell within the SA-5 and SA-6 data band (see Figs. 11-8 and 11-9).

The high radiation to the engine shroud experienced on the previous flights was not indicated on S-I-7, although an unexplained rise did occur around 50 km (see Fig. 11-10).

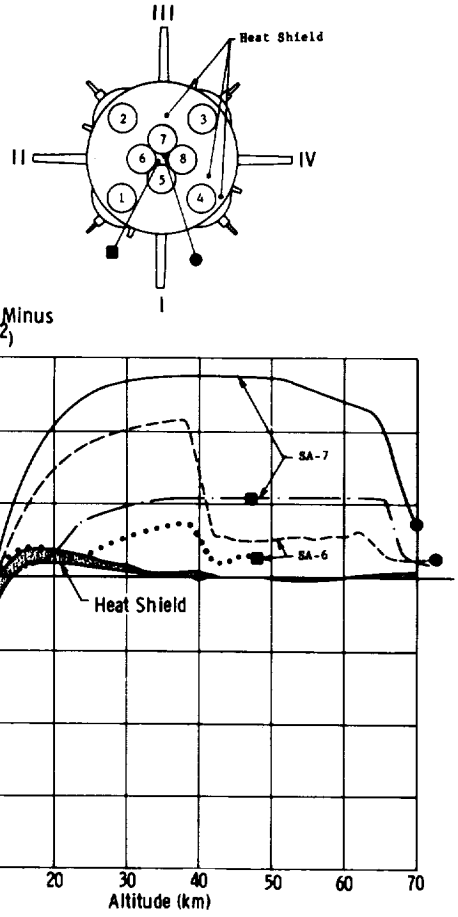

FIGURE 11-5. S-I STAGE BASE PRESSURES

Total S-I-7 heat rates on the engine shroud correlates well with the S-I-5 and S-I-6 data band (Fig. 11-10). Radiation heat rates on the shroud during S-I-7 were initially 26 watts/cm² and dropped off to approximately 6 to 8 watts/cm² between 12 and 48 km rising to 12 watts/cm² at 58 km before finally decreasing. Radiation heating to the shroud from SA-5 and SA-6 does not agree with the SA-7 results but no explanation for this deviation is available at this time.

Previous flame shield total calorimeter surfaces have been coated with a platinum black coating and following flow reversal this coating has deteriorated to the point that data reduction of this measurement has not been accurate. To circumvent the surface deterioration, the SA-7 gauge had the coating removed leaving a bright copper surface. Because the actual surface emissivity and absorptivity values were unknown a parametric study was performed that essentially brackets the postflight simulated values of the heat rates (see Fig. 11-11). Fair agreement was obtained with the analytical results for a surface emissivity (ϵ) of 0.6 and a surface absorptivity (A) of 0.4 to 0.6.

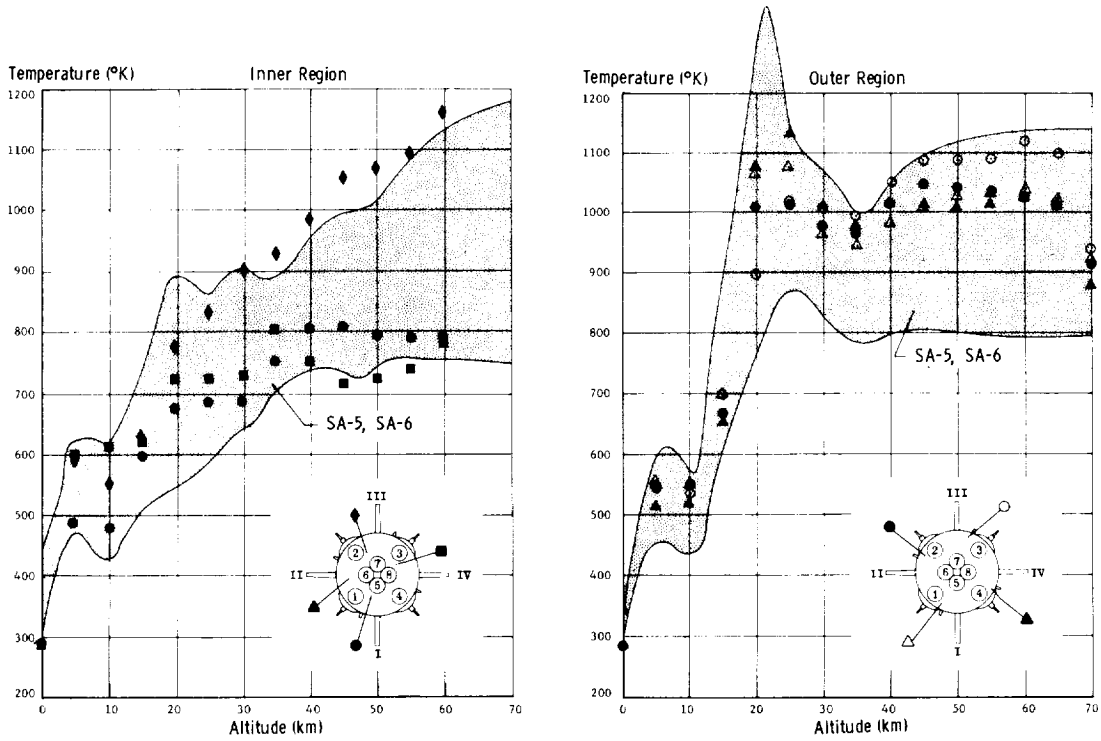

FIGURE 11-6. BASE GAS TEMPERATURE

Also shown are the radiation heat rates to the flame shield surface. Contrary to past results, convective heating is indicated late in flight instead of the previously unexplained convective cooling.

11.2.7 ENGINE COMPARTMENT ENVIRONMENT

Temperatures

Gas temperatures in the engine compartment remained normal throughout flight indicating that no excessive temperatures or fires existed for S-I-7.

Forward side heat shield structural temperatures again indicated the presence of water or ice as they followed the trend of the saturation temperature of water.

Access chute structural temperature on SA-7 was much lower than on previous Block II flights. There is no apparent reason for this difference and since the previous flights are consistent they are considered more reliable.

Engine Compartment and Thrust Frame Compartment Pressures

Pressure environments in the thrust frame compartment above the firewall and in the engine compartment below the firewall were nearly uniform, as in SA-6 (see Fig. 11-12). On the average, a general compartment pressure increase of 0.3 N/cm^2 over SA-6 is observed in SA-7.

A maximum pressure difference of 0.93 N/cm^2 was observed between the engine compartment and the heat shield at 60 seconds of flight. This localized rearward loading on the heat shield agrees well with previous SA-5 and SA-6 results shown for comparison.

Loading on the 60-degree tank fairing and on the shroud below the firewall was less than measured on SA-6 (see Fig. 11-13).

11.2.8 S-I/S-IV INTERSTAGE PRESSURES

Aft Interstage Compartment Pressures

Pressures in the aft interstage area were monitored during S-I flight by the helium heater chamber pressure sensor. It should be noted that the interstage ambient pressure transducer (0-2 N/cm^2) that was installed for the SA-6 flight was not available for SA-7.

Interstage pressure, in the form of its difference from free-stream static pressure, is presented in

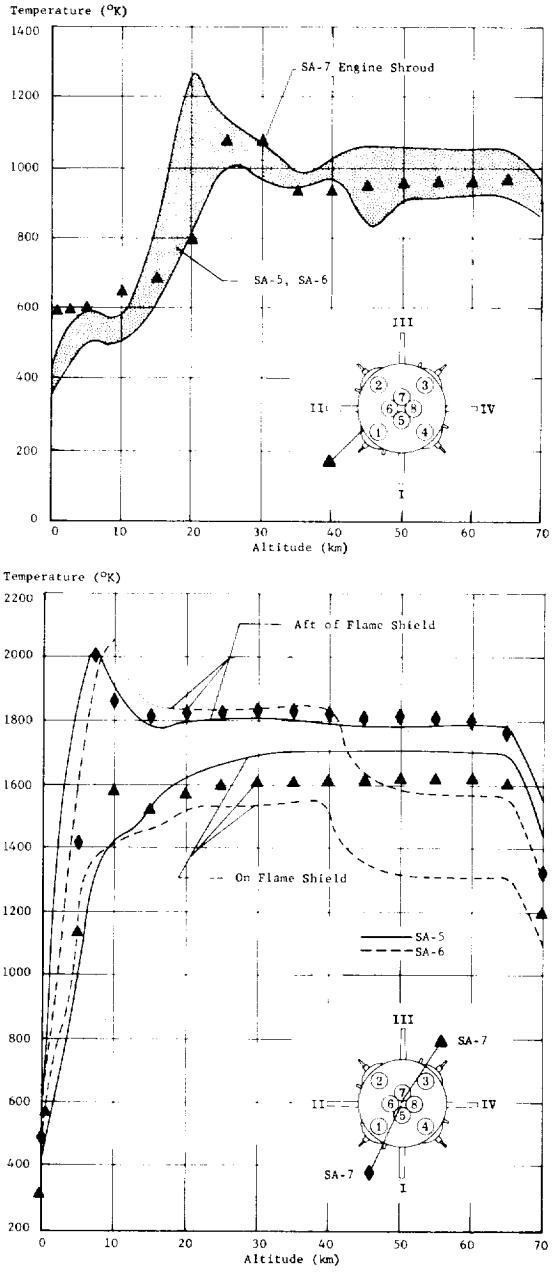

FIGURE 11-7. ENGINE SHROUD GAS AND FLAME SHIELD TEMPERATURES

Figure 11-14, along with two predicted curves. Analytical predictions were made by assuming two different interstage vent exit conditions. The first prediction considered the external flow to have no influence on the discharging air, except in providing a base pressure behind the air conditioning vent fairing. The second prediction was based on the assumption that the external flow not only created a base pressure be-

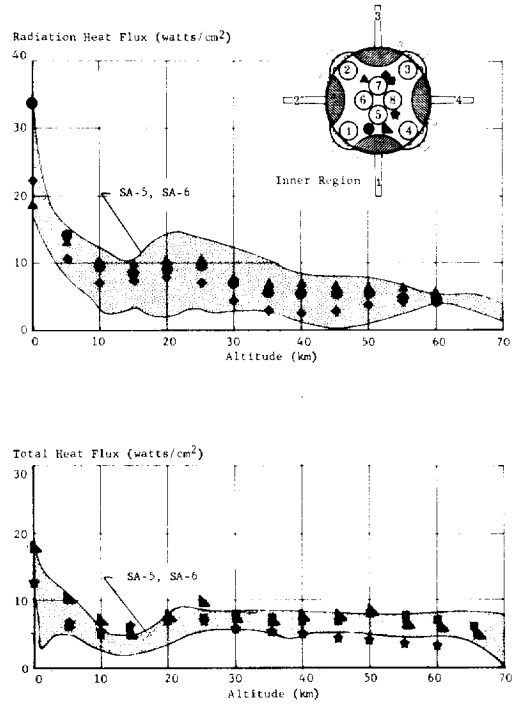

FIGURE 11-8. INNER REGION HEATING RATES

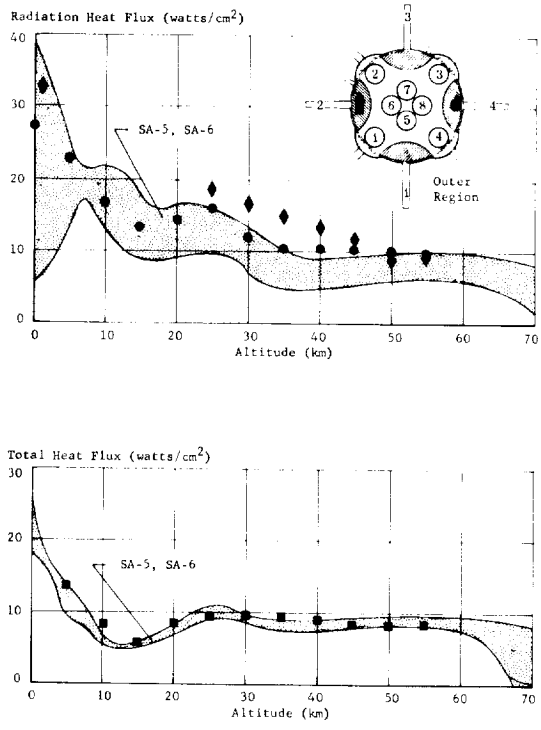

FIGURE 11-9. OUTER REGION HEATING RATES

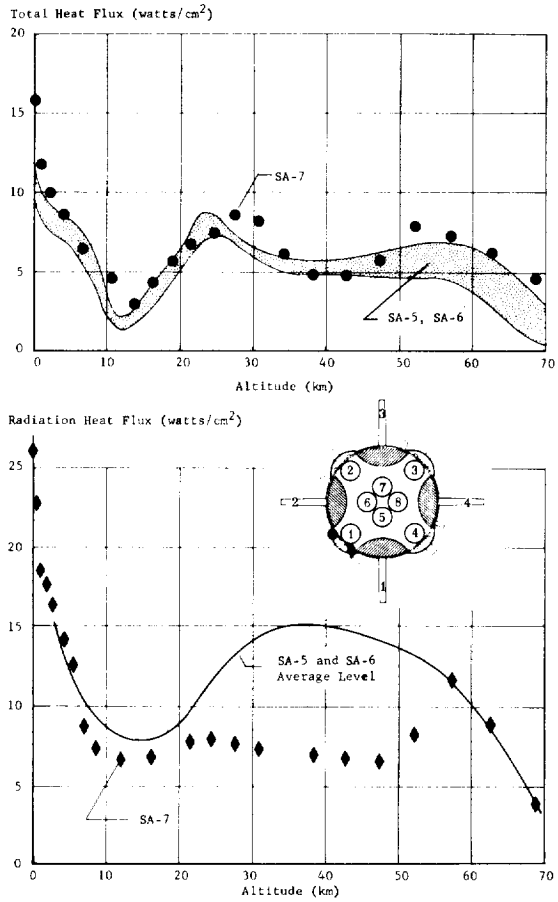

FIGURE 11-10. ENGINE SHROUD HEATING RATES

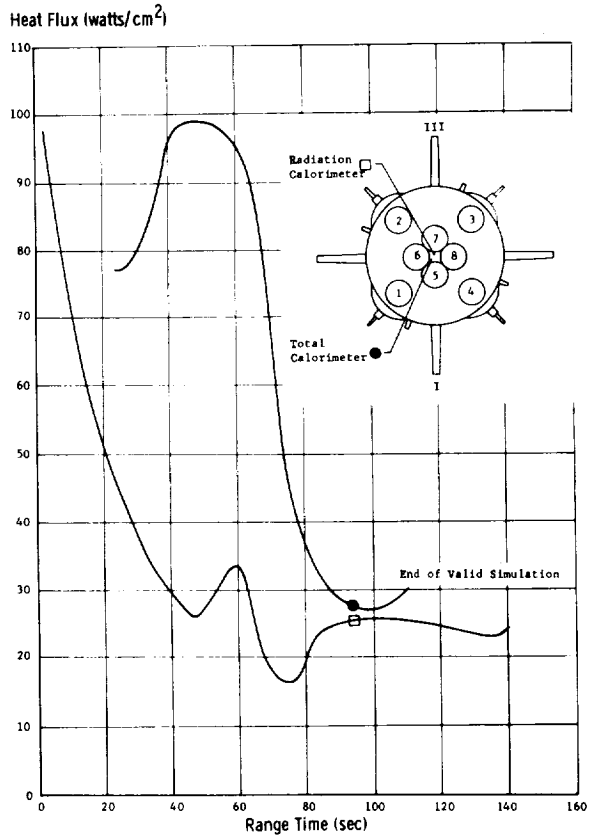

FIGURE 11-11. FLAME SHIELD TOTAL AND RADIATION HEATING RATES

hind the air conditioning fairing, but also interacted with the exhausting air to create a higher local external pressure. The flight results are not in very good agreement with either assumption.

Detonation Pressures

The detonation pressure switches located near the separation plane showed no indication of detonation or over-pressurization of the aft interstage area during separation.

11.3 S-IV STAGE ENVIRONMENT

11.3.1 SURFACE TEMPERATURES

Forward Interstage Temperatures

External skin temperatures on the S-IV forward interstage for SA-7 were in good agreement with predicted and S-IV-6 flight results (see Fig. 11-15). However, temperatures measured at Sta. 35.9 m (1414 in.) deviated after 100 seconds due to apparent debonding of the sensor. Interior skin temperatures for the forward interstage were in good agreement with predicted and S-IV-6 results until 115 seconds where the SA-7 flight temperature level became lower than predicted.

LH_2 Tank Temperatures

LH_2 tank temperatures at Sta. 32.8 m (1290 in.) were in better agreement with predicted than those recorded for S-IV-6 (see Fig. 11-15). Good agreement for the initial slopes and general data trends were observed on S-IV-7 with a maximum deviation of approximately 14° K occurring at 115 seconds. However, for the tank measurement Sta. 30.8 m (1211 in.) good agreement with predicted was obtained until approximately 70 seconds. Flight data leveled off at this time while the predicted temperature continued to rise due to aerodynamic heating. Therefore, data for this location is not considered reliable after 70 seconds.

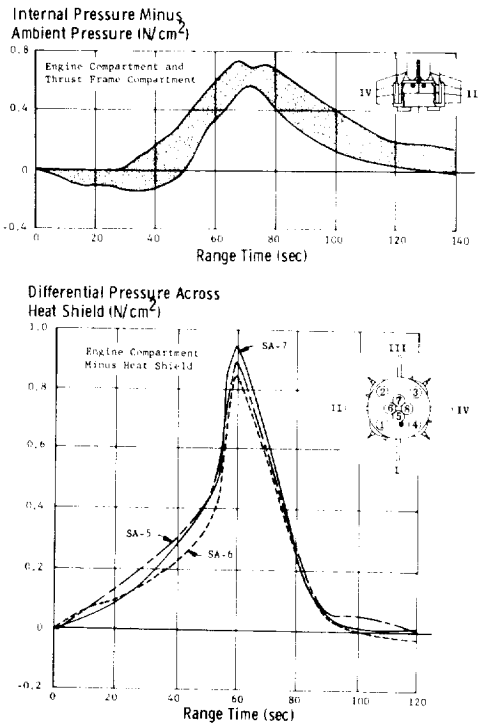

FIGURE 11-12. S-I STAGE INTERVAL AND HEAT SHIELD PRESSURE DIFFERENTIAL

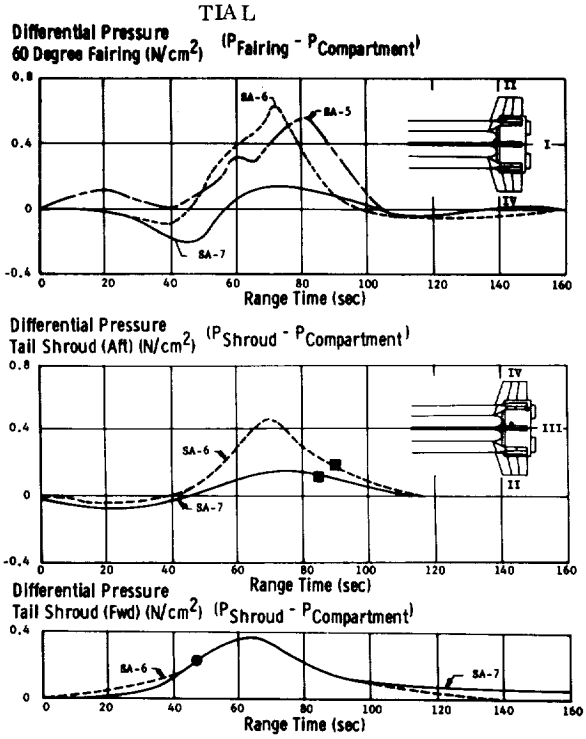

FIGURE 11-13. DIFFERENTIAL PRESSURES ACROSS TANK FAIRING AND SHROUD

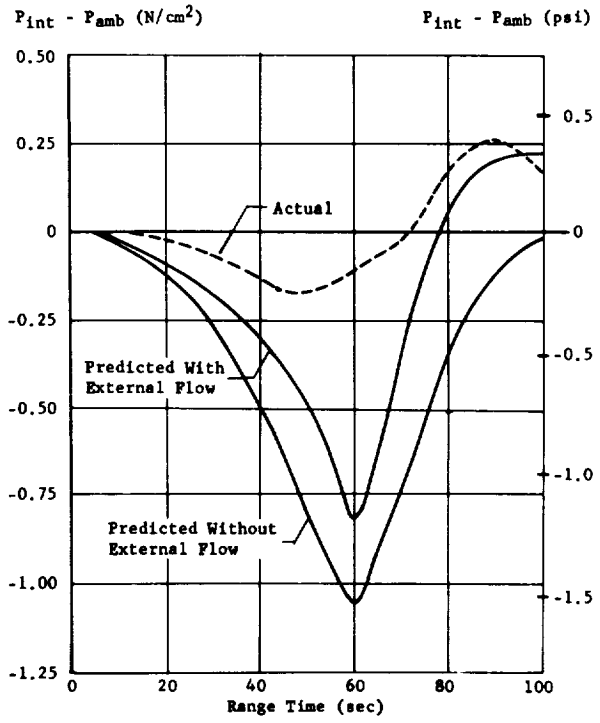

FIGURE 11-14. S-IV AFT INTERSTAGE PRESSURE DIFFERENTIAL HISTORY

Aft Skirt Temperatures

Interior and exterior temperature measurements were flown at Sta. 29.4 m (1156 in.) for the first time on S-IV-7. Correlation of the external temperature with predicted was good until approximately 100 seconds when the measured values began to decrease slowly (see Fig. 11-15). Interior surface temperatures were in good agreement with predicted with a maximum deviation of approximately 8.5° K occurring at 140 seconds.

Ullage Rocket Fairing Temperatures

Ullage rocket fairing number 2 was instrumented for the first time on S-IV-7 on the internal surface. During the early portion of flight, until approximately 80 seconds, measured levels were slightly lower than predicted (see Fig. 11-15). During the period between 80 and 100 seconds an increase in heat rate was encountered which is undefined at this time.

Structural Temperatures During Orbit

Predicted and measured orbital temperature histories of the forward interstage, LH_2 tank, and aft skirt are shown in Figure 11-16. Measured temperatures are derived from Ascension Island and Pretoria data (10 to 30 min after insertion) and from Tel 2 data (86.6 to 97.2 min after insertion). No data were ob-

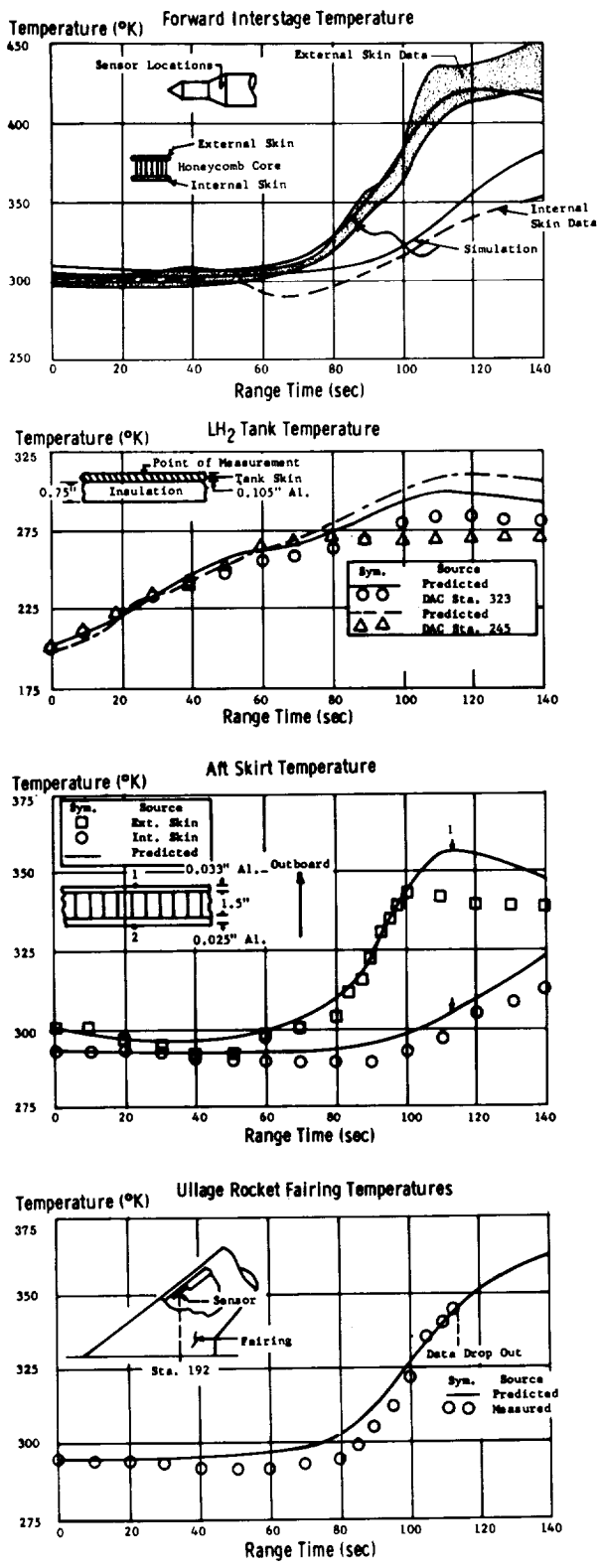

FIGURE 11-15. S-IV STAGE SURFACE TEMPERATURES DURING BOOST

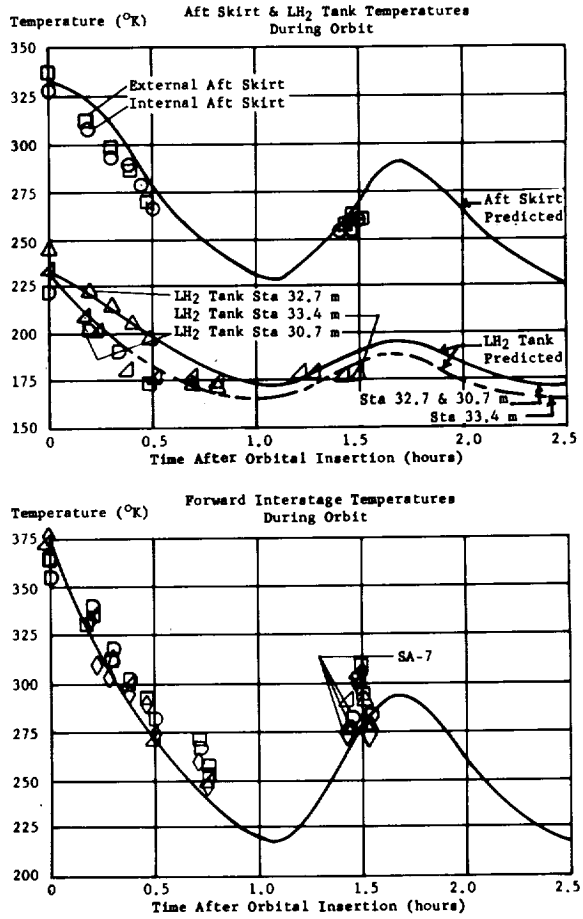

FIGURE 11-16. S-IV TEMPERATURES DURING ORBIT

tained from the sensors located at Sta. 32.8 m (1290 in.) and 30.8 m (1212 in.) on the LH_2 tank during the Tel 2 sampling period.

In general, the data showed good correlation with the predicted temperature histories as shown in Figure 11-16. However, the data sample from Tel 2 shows a sharp rise and fall over a span of approximately 6 minutes. This sharp deviation from the predicted is believed to be the transient response of partially debonded sensors to a changing solar input. The solar input is changing because of the roll and tumble rates experienced by the stage.

11.3.2 BASE TEMPERATURES

Base Thrust Structure Temperatures

S-IV stage thrust structure temperatures located in Stiffner No. 26 were in good agreement with predicted levels as well as S-IV-5 and S-IV-6 flight results (see Fig. 11-17) for the initial 150 seconds of flight. As on S-IV-5 and S-IV-6, however, the temperature decreased at a more rapid rate for the two forward locations than was predicted.

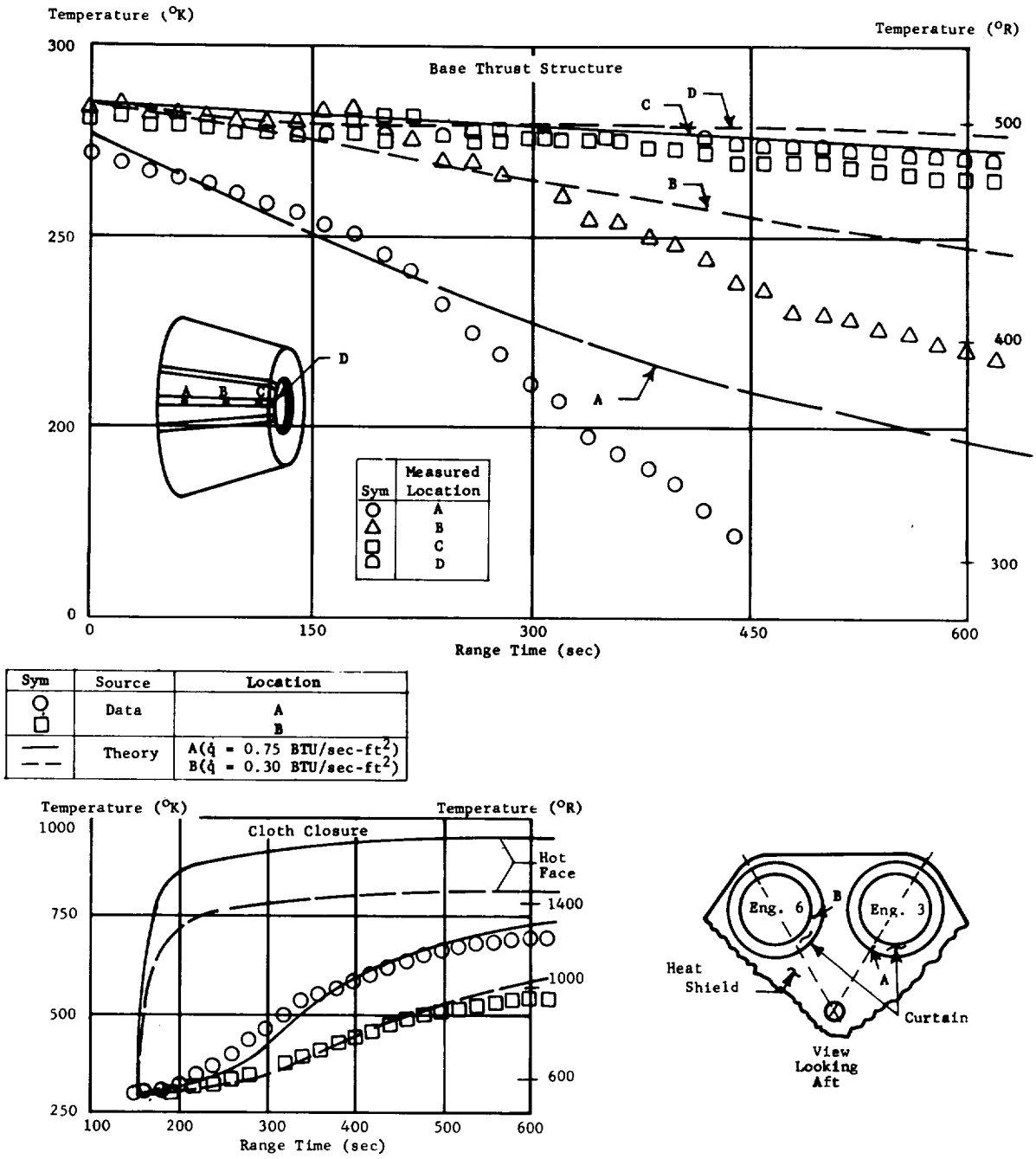

FIGURE 11-17. BASE REGION TEMPERATURE

Cloth Closure Temperature

Cloth closure temperatures about engine 3 and 6 were recorded for the first time on S-IV-7. Flight temperature histories compare well with theoretical temperature histories which were computed using a two dimensional heat transfer model of the cloth closure (see Fig. 11-17). The heat rate inputs for the theoretical calculations were 0.85 and 0.34 watts/cm^2 for locations A and B respectively.

These heat rates compare to the S-IV-6 heat rate values of 1.13 and 0.68 watts/cm^2 for locations on the heat shield of 0.86 m (33.85 in.) and 1.52 m (59.90 in.) radii respectively. On the basis of these data, a flux of 0.85 watts/cm^2 at location A is reasonable,

while a flux of 0.34 watts/cm^2 at location B seems somewhat low.

Maximum temperature levels for the cloth closures were 695°K at location A for the sensor temperature which corresponds to a value of 945°K for the hot face at the same location. The average hot face temperature for the cloth curtain was approximately 850°K. Average cold side cloth closure temperature determined from the heat transfer model was approximately 625°K between locations A and B.

11.3.3 AERODYNAMIC PHENOMENON

Observation of TV films taken during SA-7 flight revealed an interesting aerodynamic phenomenon. A "halo" of ice crystals formed just aft of the Apollo nose cone, at approximately Mach = 1, and existed for about 4 seconds.

The visual "halo" occurred when the SA-7 entered a layer of high humidity air starting at 6.9 km and ending at 8.4 km. The ambient air temperature at the respective altitudes was 262°K and 253°K. Occurrence of high humidity air coincidental with flight in the transonic flow regime (Mach = 1) resulted in this visual effect. A Prandtl-Meyer expansion at the junction of the nose cone and the cylindrical section created an area of low pressure and low temperature just aft of the junction. Moisture in the atmosphere condensed and froze in this region, and thereby formed the visible "halo."

11.4 EQUIPMENT TEMPERATURE AND PRESSURE ENVIRONMENT

11.4.1 S-I STAGE

Two instrument compartments located immediately above S-I stage fuel tanks F1 and F2 contained instruments which were maintained within satisfactory operating limits. To maintain this environment within limits, preflight cooling was provided from a ground source. Listed below are the preflight temperatures and the required operating limits for the two compartments.

	Preflight		Operation Limit	
	Max	Min	Max	Min
F2 Instrument Compartment Temp. (°K)	296	295	313	293
F1 Instrument Compartment Temp. (°K)	301	299	323	273

11.4.2 S-IV STAGE

Temperature

S-IV forward interstage (outside the pressurized Instrument Unit) temperature varied between 298°K and 287°K during S-I stage flight. Liftoff (also S-I stage flight maximum) temperature was 298°K or approximately 5°K below ambient air temperature. The minimum inflight temperature of 287°K occurred at 70 seconds range time. The foregoing trends were similar to those for the SA-6 flight.

Pressure

Pressure in the S-IV forward interstage decayed from ambient at liftoff to 0.4 N/cm^2 (0.5 psi) at the end of S-I stage powered flight.

11.4.3 INSTRUMENT UNIT

Temperature

All Instrument Unit component temperatures were within the operating limits prior to and during flight. These temperatures were close to those experienced during SA-6 flight except for the telemetry ambient temperature. SA-7 telemetry ambient temperature did not vary as much on SA-7 as observed on SA-6.

Pressure (Conditioned Area)

Pressure was maintained at a satisfactory level (between 11.1 and 11.8 N/cm^2) prior to liftoff. At liftoff the pressure rose to 11.8 N/cm^2 which was approximately 0.15 N/cm^2 below the effective inflight cooling lower limit to 14 seconds flight time. However, during the SA-6 flight, this same phenomenon occurred but lasted for a longer period.

Pressure (Unconditioned Area)

A maximum internal pressure of nearly 0.8 N/cm^2 above ambient was observed inside the unpressurized portion of the Instrument Unit at 58 seconds (see Fig. 11-18). Previous SA-6 data show values about 0.2 N/cm^2 higher than SA-7 which may be attributed to the measurement being on the windward side of the relative air velocity vector for SA-6.

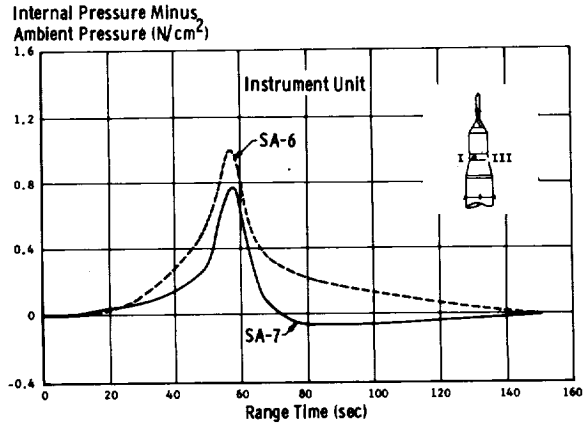

FIGURE 11-18. INSTRUMENT UNIT PRESSURE

SECTION XII. VEHICLE ELECTRICAL SYSTEM

12.1 SUMMARY

The SA-7 vehicle electrical systems operated satisfactorily during the boost and orbital phase of flight. All mission requirements were met, except the failure to monitor the three rate gyro measurements (F42-802, F43-802, and F44-802) for one orbit. These measurements failed after 41 minutes of flight. This apparent failure was caused by having the "inflight control" relay (K25) in the F6 telemeter on the "short life" battery. When it became deenergized, the F6 telemeter switched from the "intelligence mode" to the "calibrate mode" of operation.

On the Saturn IB and Saturn V programs the telemeter calibrator will have the "inflight control" relay deenergized during flight. Until the new calibrator is implemented into the design the calibrator "inflight control" circuit has been placed on the "long life" battery.

12.2 S-I STAGE ELECTRICAL SYSTEM

The electrical system for SA-7 booster was essentially the same as SA-6. The main differences were the addition of two fuel depletion sensors, removal of the X1 telemeter from area 9, the addition of the P2 telemeter in area 12, computer backup for outboard engine cutoff, removal of the TV camera in area 2, the addition of inflight fire detection, engine cutoff due to rough combustion after cutoff arm, and revision of the thermal probe circuitry.

The electrical power source for the booster consisted of two identical 28-volt zinc silver oxide batteries, designated as 1D10 and 1D20. The capacity of the batteries was 2650 ampere-minutes.

During the boost phase of flight the booster electrical system operated satisfactorily. The 1D10 battery current varied from 89 to 122.8 amperes and the 1D11 bus voltage varied from 27.7 to 29.2 vdc. The 1D20 battery current varied from 94 to 100 amperes and the 1D21 bus voltage varied from 28.5 to 28.9 vdc. Figure 12-1 shows the current and voltage profiles for the S-I stage.

The output of the eight 5 vdc measuring supplies located, one each, in the measuring distributors delivered a nominal 5 vdc. The master measuring supply was not telemetered, but could be monitored from the calibration voltage. The master measuring supply was nominally 5 vdc.

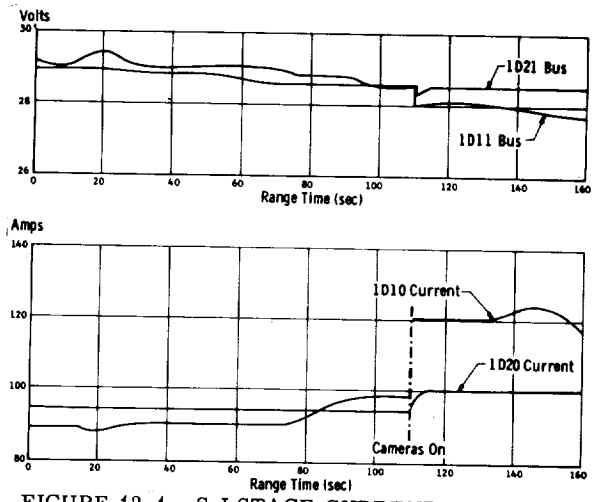

FIGURE 12-1. S-I STAGE CURRENT AND VOLTAGE

All EBW firing units used to blow the vent ports, initiate separation, and fire the retro rockets operated satisfactorily. The average charging time was 1.4 seconds with a nominal charge of 2400 vdc.

12.3 S-IV STAGE ELECTRICAL SYSTEMS

All S-IV electrical systems functioned normally. All power requirements were satisfactorily met, and all sequenced commands were received and executed at the correct time.

The electrical power system consisted of five major subsystem components: battery 1 (control battery), battery 2 (engine battery), instrumentation battery 1, instrumentation battery 2, and the static inverter.

The voltage and current profiles for battery 1 and 2 are shown in Figure 12-2 along with the voltage profile for the static inverter. The performance of batteries 1 and 2 were satisfactory and the current and voltages were within the expected ranges. The operation of the instrumentation batteries was normal, with 28 volts output and a total current of 16.2 amperes. At launch and at S-IV cutoff, the respective currents of instrumentation battery 1 were 10.8 and 10.3 amps, and the respective currents of instrumentation battery 2 were 5.4 and 5.9 amps. The difference was expected because the design power levels of the two batteries were not identical. The performance of the inverter was satisfactory. During separation, the output voltage dropped, as shown, to 108.8 volts.

A similar voltage drop was observed in the data from the S-IV-6 flight. It is believed that the pins, which are connected to the umbilical during GSE preflight monitoring of inverter voltage, were shorted by an ionizing of the area around the pins by the ullage rockets. This ionization-shorting phenomenon in no way impaired the operation of the inverter.

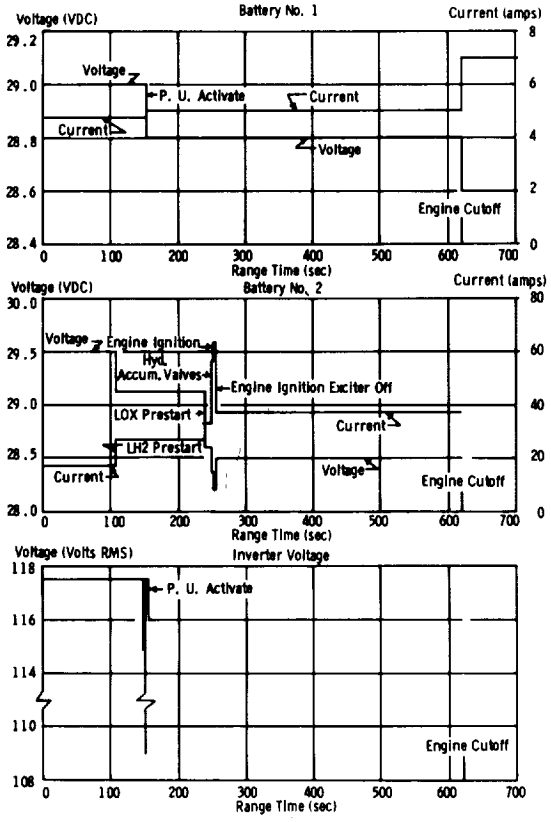

FIGURE 12-2. S-IV STAGE CURRENT AND VOLTAGE

The helium heater exciter ignited the helium heater at 150.19 seconds. Its operation was normal, and was verified by proper helium heater ignition.

All monitored EBW firing units functioned properly in response to their respective commands. Ullage rocket ignition charge command was given at 141.6 seconds. The ignition command was given at 148.36 seconds.

The Ullage rocket jettison charging command was given at 155.04 seconds. The monitored firing unit charged at 155.17 seconds. The ullage rocket jettison command was given at 160.44 seconds. The ullage rocket jettison EBW firing units fired at 160.46 seconds, at which time all four ullage rockets jettisoned.

12.4 IU STAGE ELECTRICAL SYSTEM

The electrical system for SA-7 Instrument Unit was essentially the same as SA-6; the main difference was the replacement of the program device with the guidance computer for sequence of events timing. An additional 270 multiplexer and measuring distributor were added on SA-7 to handle the added DDAS requirements.

The electrical power source for the Instrument Unit consisted of two 28-volt zinc silver oxide batteries, designated as 8D10 and 8D20. The 8D10 battery was the "long life" battery and was rated at 2650 amp-minutes. The 8D20 battery was the "short life" battery and was rated at 1850 amp-minutes.

During the boost and orbital phase of flight the Instrument Unit electrical system operated satisfactorily, except for the failure to monitor the 3 rate gyro measurements. The 8D10 battery current varied from 46 to 52 amperes, and the battery life was 133 minutes. The 8D11 bus voltage varied from 28.2 to 28.4 vdc. The 8D20 battery current varied from 73.6 to 80.1 amperes, and the battery life was 38 minutes. The 8D21 bus voltage varied from 28.2 to 29.1 vdc. Figure 12-3 shows the current and voltage profiles for the Instrument Unit batteries. The changes in load caused by the cycling of the ST-124 heater at liftoff and after 10 minutes of flight are shown in the performance of the 8D20 battery.

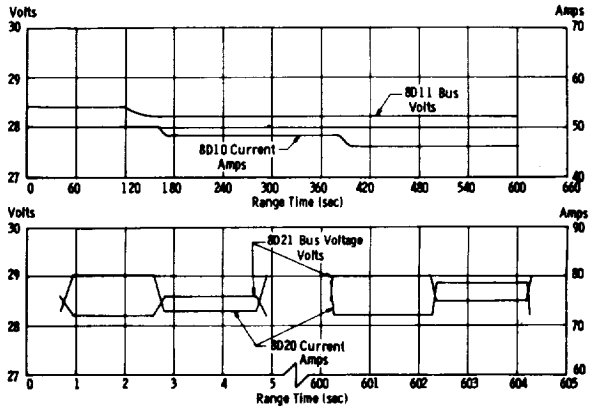

FIGURE 12-3. INSTRUMENT UNIT CURRENT AND VOLTAGE

The 5-volt measuring supply operated satisfactorily during flight with a nominal 5 vdc.

The failure of the three rate gyro measurements was apparently caused by having the "inflight control" relay (K25) in the F6 telemeter on the "short life" battery. This relay is normally energized during flight. It became deenergized when the bus voltage

dropped below the hold-in voltage of the relay. This phenomenon occurred at approximately 41 minutes of flight. This time is based on the discharge characteristics for the "short life" battery at a load of 75 amperes because the signal was lost over Pretoria after 40 minutes of flight. The telemeter calibrator was on the short life battery. With F6 in the "calibrate mode" and the calibrator on the short life battery the characteristic output on the three rate gyro telemeter channels between 41 minutes and 57.73 minutes of flight was a voltage slowly drifting towards zero. When the 28-volt battery became less than the 5 vdc measuring voltage at 57.73 minutes there was a step in the outputs of the three rate gyro telemeter channels. This step dropped the output voltage to 0.6 vdc. This output voltage remained constant until the measuring supply became inoperative or until the 5-volt supply was unable to maintain its output voltage.

All measurements on channels 2 through 15 of the F6 telemeter were lost after 41 minutes of flight, but those of prime importance were the three rate gyro measurements which were on the long life battery.

13.1 SUMMARY

Because of the relatively small angles-of-attack and resulting engine deflections encountered during the SA-7 flight, it was not possible to make valid analyses of aerodynamic stability parameters.

Fin leading edge pressure distribution plots at various Mach numbers indicate the expected higher pressures at mid-span and tip relief effects.

The base drag coefficient agreed well with SA-6 results, falling generally below predicted. The flight determined axial force coefficient was higher than predicted in the subsonic regime and fell, on the average, about 20 percent lower than predicted after Mach 1.4.

13.2 FIN PRESSURE DISTRIBUTION

To measure localized loadings and pressure distribution on the Saturn I fins, four pairs of measurements were located on opposite sides of Fin II. The same number of measurements were flown on SA-5 and SA-6, but at different locations. Because of the small angles-of-attack encountered during the flight of SA-7, it was impossible to obtain the pressure loading per unit angle-of-attack with reliable accuracy. Lower and upper surface pressure distribution plots shown in coefficient form, $(P_{surface} - P_{ambient})/Q$, indicate the highest pressures occurring near the leading edge, as expected (see Fig. 13-1). SA-5 data from additional measurements at Mach numbers and pitch angles-of-attack similar to SA-7 are also shown to obtain a more complete leading edge pressure distribution. In the transonic and low supersonic regime, these plots clearly indicate the expected higher pressures at mid-span with a dropoff occurring near the tips (tip relief effect).

13.3 DRAG

Because of two apparent measurement failures on the heat shield, data from only three measurements were used in determining the base drag coefficient. Nevertheless, results agree well with SA-6 with values falling generally below predicted (see Fig. 13-2). As in SA-6, a maximum peak value of 0.2 was observed at Mach 1.1. Because of recirculation of hot exhaust gases, an expected positive pressure thrust was observed beginning around Mach 1.7.

The axial force coefficient was obtained from flight simulation analyses of propulsion performance (see Fig. 13-2). A maximum value near 1.08 was observed at around Mach 1.1 which is in excellent agreement with predicted. Flight results were higher than predicted in the subsonic regime and fell, on the average about 20 percent lower than predicted after Mach 1.4.

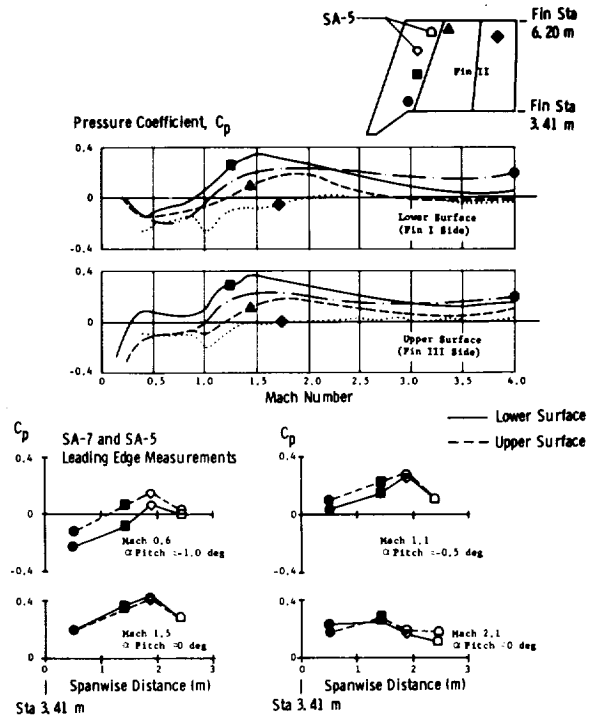

FIGURE 13-1. FIN PRESSURE DISTRIBUTIONS

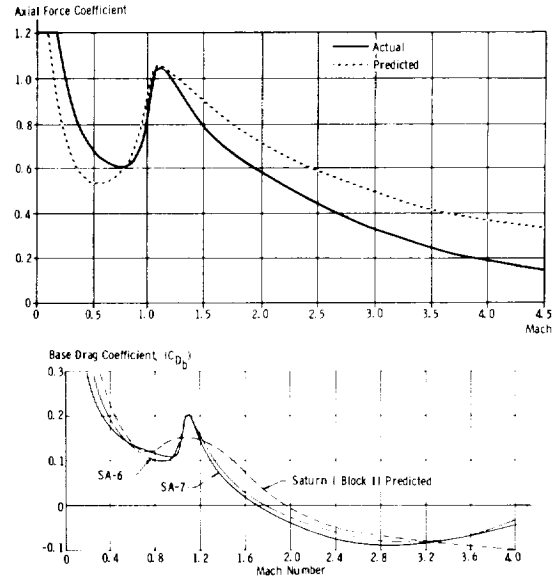

FIGURE 13-2. AXIAL FORCE AND BASE DRAG COEFFICIENTS

SECTION XIV. INSTRUMENTATION

14.1 SUMMARY

Overall reliability of the SA-7 measuring system was 99.35 percent; this includes 8 measurement malfunctions that resulted in total loss of information. Only measurements active at liftoff were considered in the above percentage. A total of 14 measurements were scrubbed before launch.

Transmitter radio frequency power on all links was sufficient to produce desired data coverage of all planned flight periods. This includes the IU stage telemetry during orbit. However, continuous channels from link F6 were terminated prematurely due to a wiring error. The lost data included IU rate gyro information.

The passenger fire detection system, flown for the first time on SA-7, operated satisfactorily. No fires were indicated.

All preflight and inflight calibrations were normal and satisfactory.

All onboard RF systems performed as expected. Effects of flame attenuation due to retro rocket firing were similar to SA-5 and SA-6 and resulted in lost data from those links not associated with a playback recorder. Operation of the three airborne tape recorders (one in the S-I, one in the IU and one in the S-IV stage) was very satisfactory. The playback records were free of retro rocket flame attenuation effects.

Ninety-one cameras provided optical coverage for launch of SA-7. Nine of the instruments failed due to a power failure on camera station 4.

Immediate recovery of the 8 onboard cameras was impossible because of Hurricane Gladys. However, two of the eight cameras were discovered approximately 50 days after launch on San Salvador and Eleuthera Islands. Good coverage was obtained from these cameras.

14.2 S-I STAGE MEASURING ANALYSIS

14.2.1 MEASUREMENT MALFUNCTIONS

A total of 653 inflight measurements was scheduled for the S-I stage of SA-7. Seven of the 653 total were scrubbed prior to launch. Two of the 646 measurements active at launch failed completely; six measurements were only partially successful. Table 14-I lists the S-I stage measurement malfunctions.

14.2.2 MEASURING RELIABILITY

Reliability of the S-I stage measuring system was 99.7 percent, considering only those measurements active at liftoff compared with complete failures.

One of the combustion chamber pressure measurements, D1-3, was termed as a partial success (Table 14-I) because of damage sustained to the vibrotron caused by a high vibration level at ignition. The remaining seven combustion chamber measurements were considered to be successful, but only one of the seven, D1-4, was within the 0.5 percent measuring error limit. The partially successful measurement, D1-3, contained a 14.85 percent calibration shift. The next highest percent shift was observed on D1-7 and was 1.91 percent. Two of the measurements, D1-6 and D1-8, contained shifts that were only slightly in excess of the error limit; the shifts were 0.71 percent and 0.54 percent respectively.

14.3 S-IV STAGE MEASURING ANALYSIS

14.3.1 MEASUREMENT MALFUNCTIONS

Five measurements were complete failures on the S-IV stage during powered flight of the SA-7 vehicle. There were 17 measurements on the S-IV stage from which acceptable data could be retrieved during only portions of the flight. However, these data were in sufficient enough quantity to permit a proper evaluation of the environment to be measured. Table 14-II lists those specific measurements which failed and those which were only partially successful, along with comments concerning particular malfunctions. Other than transducer problems, only one instrumentation system component malfunction occurred. The long-dwell commutator clock, which controls the sampling duration of channels 9, 10, 17 and 18 on FM system 3, malfunctioned from liftoff through separation. The malfunction caused the sample period for each channel to vary from 3 to 21 seconds. The normal sample period is 3.0 ± 0.15 seconds per channel. The data channel duration time is controlled by a resistance-capacitance timed unijunction oscillator circuit contained in block module A1 of the commutator assembly. It has been established that the leakage resistance between emitter and base of the transistor tends to decrease and/or vary in many cases, allowing an alternate path to ground, and preventing the capacitor's normal charge buildup. This, in turn, results in the noted lengthening of the sampling time. A production change, incorporated in later models, places a transistor in an emitter-follower circuit

TABLE 14-I. S-I AND IU MEASUREMENT MALFUNCTIONS

Meas. No.	Title	Remarks
	Scrubbed Before Launch	
E271-4	Vibration Actuator	Cancelled because the actuator was changed and transducers were not reinstalled.
E272-4	Vibration Actuator	Same as above
E273-4	Vibration Actuator	Same as above
D31-4	ΔP Actuator	Same as above
D30-2	ΔP Yaw Actuator	Meas. Inoperative, inaccessible for replacement.
E114-18	Vibration Rear Spar Flange	Meas. Inoperative, inaccessible for replacement.
E342-18	Vibration Holddown Point Fin II Longt.	Meas. Inoperative, inaccessible for replacement.
	Complete Loss of Data	
E338-9	Vibration Tank 02 Support Longt.	Output motor boating, probably moisture in connector at gauge.
E301-9	Strain Comp. F2 Skirt	Gauge Balance shifted off scale.
L68-801	Sound Intensity Instr. Unit	Gauge diaphram was damaged during checkout resulting in the loss of mechanical coupling to the crystal.
	Partial Success	
E116-6	Vibration GOX Line	Probable open cable at 89 seconds.
	Functioning But Not Valid	
D1-3	Pressure Combustion Chamber	Vibrotron gauge appears to have been damaged by an extremely high vibration level at ignition.
C3-1	Temperature H.S. Pinion Bearing #5	Apparent reversed thermocouple
C5-1	Temperature Turbine Shaft #7	Reads much lower than measurements on other engines.
C9-6	Temperature Gas Generator	Extremely noisy with different temperature from other measurements. Discrepancy was in gauge circuit.
C1-6	Temperature LOX Pump Bearing #1	Very little change in reading compared to measurements on other engines.

TABLE 14-II. S-IV STAGE MEASUREMENT MALFUNCTIONS

Meas. No.	Title	Remarks
	Scrubbed Before Launch	
C671-400	Temp. Aft Interstage Skin	Measurements covered by S-I Stage Fairings.
C672-400	Temp. Aft Interstage Skin	Same as above.
D643-404	Engine 4 Actuator A Differential Pressure	Transducer Malfunction during checkout. Sufficient time not available to replace prior to launch.
D643-406	Engine 6 Actuator A Differential Pressure	
C606-406	Engine 6 LOX Pump Housing Temperature	Same as above.
C620-409	Cold Helium Bottle Gas Temperature #2	Same as above.
C625-401	Engine 1 Thrust Chamber Out Skin Temperature	Same as above.
	Failures	
A600-405	LOX Pump Speed-Engine 5	Possible failure of 1) the frequency oscillator, 2) pickup failed to sense rotation 3) open circuit in multicoder input.
D642-407	Acoustic Pickup S-I/S-IV Interstage Internal	Circuitry discontinuity
E668-409	Vibration - Forward Dome Pitch Axis	Possible failure of 1) averaging amplifier, 2) the coaxial cable, 3) the accelerometer pickup
F613-410	Ring Mode Accel. Sta. 1250 Fin Plane 2	Failure reason unknown
L604-409	LH_2 Point Level Sensor-Location A	Sensor did not activate
	Partial Success	
D604-401	LOX Injector Differential Pressure - Eng. 1	Potentiometer Wiper failure
D604-402	LOX Injector Differential Pressure - Eng. 2	Same as above
D604-403	LOX Injector Differential Pressure - Eng. 3	Same as above
D604-405	LOX Injector Differential Pressure - Eng. 5	Same as above
D604-406	LOX Injector Differential Pressure - Eng. 6	Same as above
D604-407	S-I/S-IV Extensiometer	Cable prematurely separated
E624-403	Vibration-Gear Case Engine 3	Under investigation for:
E624-405	Vibration-Gear Case Engine 5	1) Coaxial cable discontinuity
E624-406	Vibration-Gear Case Engine 6	2) Amplifier malfunction
E623-403	Vibration-Thrust Chamber Dome Engine 3	3) Transducer debonding
E623-404	Vibration-Thrust Chamber Dome Engine 4	
C603-405	LH_2 Pump Housing Temperature Engine 5	Open circuit in temp sensing leg of temp bridge
C668-412	Temp-Ullage Rocket Fairing No. 2	Transducer malfunction
C677-409	Temp-LH_2 Tank External Skin	Improper contact of bridge module connector pins
C623-417	Temp-Helium Heater Combustion	Transducer failed in the open circuit condition
C603-404	Temp-LH_2 Pump Housing-Engine 4	Transducer partially debonded
C600-402	Turbine Inlet Temperature Engine 2	Trend Only (cause of failure under investigation)
	Questionable - Under Investigation	
C664-410	Ext. Skin Temp-Forward Interstage-Sta 448	Probable transducer debonding
C674-407	Ext. Skin Temp-Aft Skirt-Sta 190	Same as above
C675-409	Ext. Skin Temp-LH_2 Tank-Sta 245	Same as above

configuration between the timing capacitor and emitter of the unijunction transistor, effectively insulating the capacitor from alternate discharge paths.

The malfunction did not actually result in any loss or degradation of data. It did, however, prevent equal time-sharing of the input channels. The problem cleared up after separation, and the sample durations returned to near nominal, varying from 3 to 5-seconds duration for the remainder of the flight. The most likely explanation of this return to normal is that the malfunctioning circuit is temperature-sensitive, and that the increased thrust structure temperature encountered during S-IV powered flight caused a fortunate shift in circuit operation. Investigation of this entire problem is continuing.

14.3.2 MEASURING RELIABILITY

The flight performance of the S-IV-7 instrumentation system was very good. A total of 401 measurements was attempted. By launch time, seven measurements had developed problems which were impossible to resolve within launch schedule limitations and were therefore officially deleted. Consequently, there were 394 active measurements aboard S-IV-7 at launch. Of these, five were complete failures in that they provided no usable data. This loss resulted in a measurement efficiency of 98.7 percent.

14.4 INSTRUMENT UNIT MEASURING ANALYSIS

14.4.1 MEASUREMENT MALFUNCTIONS

A total of 187 inflight measurements was scheduled to be flown on the IU of SA-7. No IU measurements were scrubbed prior to launch and only one measurement failed. The IU sound intensity measurement L68-801 had a loss of mechanical coupling to the crystal. This failure was caused by damage during checkout (see Table 14-I).

14.4.2 MEASURING RELIABILITY

Reliability of the IU measuring system was 99.5 percent. Only one out of 187 measurements failed.

14.5 AIRBORNE TELEMETRY SYSTEMS

14.5.1 TELEMETRY LINKS

Data transmission for flight testing Saturn vehicle SA-7 was effected by thirteen radio telemetry system links on the combined S-I, S-IV and IU. An additional three links (MSC responsibility) were on the Apollo Spacecraft (see Section XV for Spacecraft Instrumentation). The following systems were utilized on SA-7:

S-I Stage

Link	Modulation	Link	Modulation
F1	PAM-FM-FM; FM-FM	S1	SS/FM
F2	PAM-FM-FM; FM-FM	S2	SS/FM
F3	PAM-FM-FM; FM-FM	P2	PCM/PM

S-IV Stage

Link	Modulation
D1	PDM-FM-FM
D2	PDM-FM-FM
D3	PDM-FM-FM

Instrument Unit

F5	FM-FM; FM-FM-FM	S3	SS-FM
F6	FM-FM; FM-FM-FM; PAM-FM-FM	P1	PCM-FM

Links P1 and P2, PCM systems, also functioned as Digital Data Acquisition Systems (DDAS) for their respective stages. The DDAS function was digital encoding and transmission of the model 270 commutator outputs of Links F1, F2, F3 and F6 at reduced sampling rates. The primary purpose of the link P2 DDAS was preflight checkout of the S-I-7 stage; the link P1 DDAS was used primarily for preflight checkout of the IU. DDAS information was also available from links P1 and P2 during flight. Insertion of digital data into the PCM output format worked very satisfactorily.

14.5.2 DATA ACQUISITION

Transmitted radio frequency power on all S-I and IU stage telemetry links was sufficient to produce the desired data coverage of all planned flight periods.

Battery life was sufficient to give the orbital telemetry coverage planned. No inflight telemetry calibrations were executed during orbital flight. An inflight relay within the F6 telemetry package was inadvertently overlooked and was connected to the short life battery. When the short life battery voltage decayed to the dropout point, the relay became deenergized causing all continuous data channel relays to go

to the calibration bus position and therefore data inputs were invalid from this time on. This occurred at a range time of approximately 41 minutes (extrapolated time).

PCM data acquisition by means of the predetection recording system at sites having this capability produced excellent data results.

The passenger fire detection system was flown for the first time. Operation of the modules was normal with no fires indicated. Scattered momentary indications did appear in some channels. This problem was also encountered during checkout.

Transmission of all three S-IV links was good throughout the flight. All transmitters, multicoders, and VCO's were operational up to 108 minutes after liftoff. The last recorded data were from Antigua at that time.

14.5.3 INFLIGHT CALIBRATION

All inflight calibrations were normal and satisfactory. There were no inflight telemetry calibrations on the IU stage airborne tape recorder playback record, nor during orbital telemetry coverage. Present configuration of the telemetry for SA-9 calls for the same conditions.

14.5.4 PREFLIGHT CALIBRATION

All preflight calibrations were normal and satisfactory.

14.6 AIRBORNE TAPE RECORDERS

14.6.1 S-I RECORDER

The airborne tape recorders used for the SA-7 flight were dual-track recorders capable of recording the mixer-amplifier outputs of two telemeters. The S-I stage contained one recorder which recorded the output of telemeter F2. The Instrument Unit contained one recorder which recorded the outputs of telemeters F5 and F6. During the playback mode the transmitter is switched from the mixer amplifier to the recorder. The purpose of the recorder is to record data during the periods when RF dropout is anticipated due to flame attenuation, retro and ullage firing, look angle, etc.

The telemeter F2 (S-I stage link) airborne received the signal to record at 39.34 seconds and to stop recording at 173.44 seconds range time. Recorder transfer signal to playback mode was initiated at 173.44 seconds. An elapsed time of 1.46 seconds was required for the transfer from record mode to playback mode. The recorder began playback of data at 174.90 seconds and completed data playback at 309.0 seconds. At completion of recorder playback, modulation was removed from telemeter F2.

Operation of this airborne recorder was satisfactory and data contained in the playback record is free of the effects of retro flame attenuation.

14.6.2 S-IV RECORDER

The S-IV tape recorder operation was entirely satisfactory. The malfunction noted during the flight of S-IV-6 did not occur. Telemetry measurements were taken on S-IV-7 to record vehicle reception of the following commands: record, stop record, playback, and stop playback. The tape recorder received these commands and responded to them as planned. However, the playback command was not actually recorded; but since operations occurred as planned, the command was received. This measurement, which is on PDM, effectively destroys its own record by causing systems 1 and 2 to stop the sending of real time data and to commence the transmission of recorded data. Had playback not been effected by this command, it would have been observed in the data and could have been used in malfunction analysis.

The S-IV recorder received signal to record at 139.64 seconds and to stop at 169.64 seconds, range time. Playback of S-IV recorder information occurred between 642.72 and 672.79 seconds.

14.6.3 IU RECORDER

The telemeter F5 and F6 (Instrument Unit links) airborne recorder received the signal to record at 139.54 seconds and to stop recording at 169.64 seconds, range time. Recorder transfer signal to playback mode was initiated at 642.72 seconds. An elapsed time of 1.62 seconds was required for the transfer to the playback mode. The recorder began playback of data at 644.34 seconds and completed data playback at 672.79 seconds.

Operation of this airborne recorder was good and data contained in the playback record are free of the effects of retro flame attenuation.

14.7 RADIO FREQUENCY ANALYSIS

All onboard RF systems performed as expected. Effects of flame attenuation were more severe on this flight than previous flights and resulted in lost data for the Apollo and S-I stage links.

14.7.1 TELEMETRY

Telemetry signals were received from liftoff through orbital insertion, by the stations listed in the telemetry summary chart, Figure 14-1.

14.7.2 TRACKING

Azusa/GLOTRAC

The new antenna system produced improvement

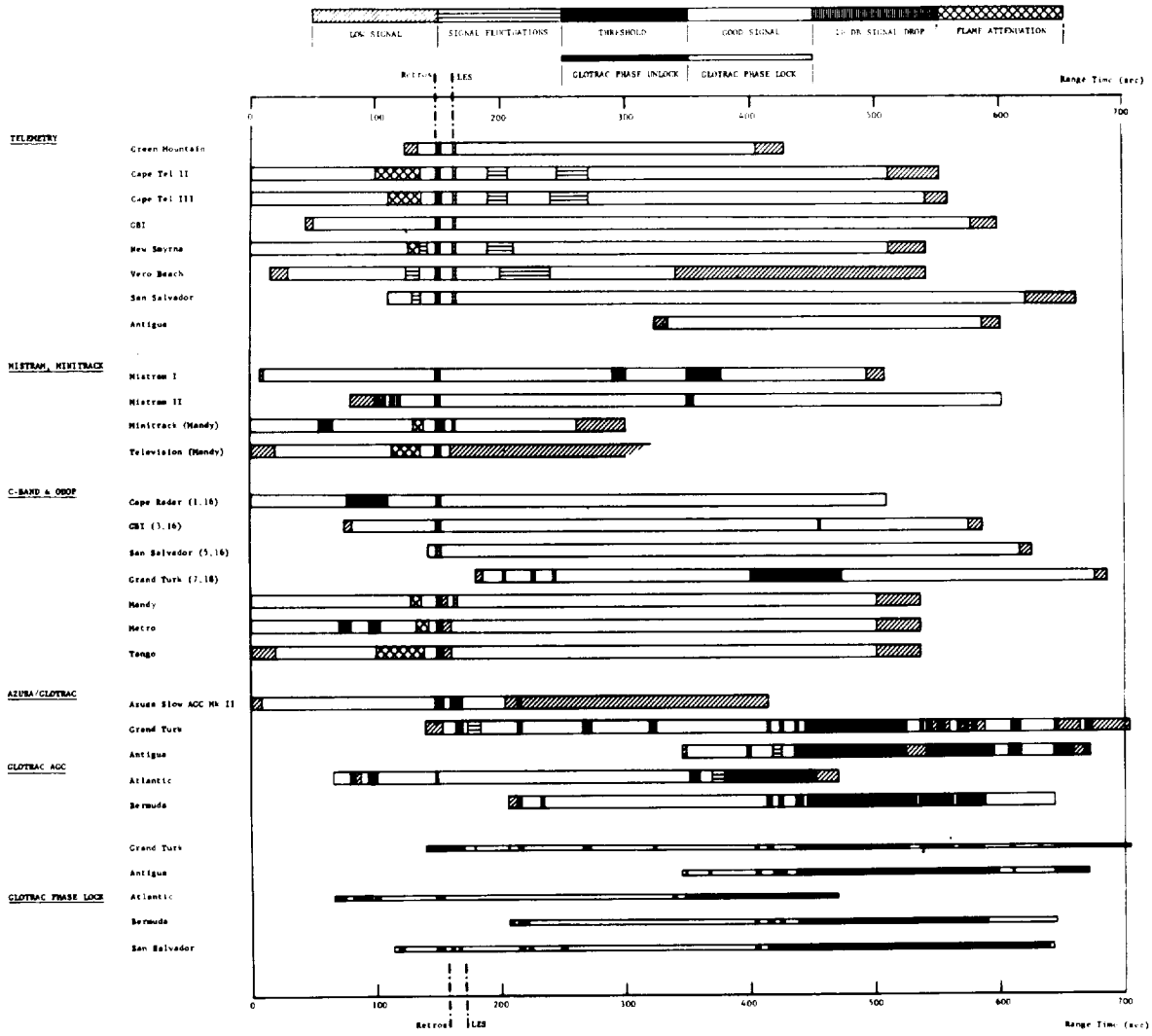

FIGURE 14-1. RF SYSTEM PERFORMANCE

All stations experienced signal dropout at retro rocket ignition as expected. Flame attenuation was quite severe at all uprange telemetry sites. Cape Tel 2 experienced approximately 40 seconds of attenuation with the signal dropping to threshold level during part of this period for the Apollo and S-I stage links.

Unexplained signal fluctuations were observed at Cape Tel 2, Cape Tel 3, New Smyrna and Vero Beach between 190 and 290 seconds.

All stations saw signal fluctuations resulting from Launch Escape System (LES) jettison.

in some regions while failing to meet expectations in others. An Azusa/GLOTRAC summary is shown in Figure 14-1. It is observed that the Mk II and Atlantic sites suffered phase unlocks at retro rocket firing but experienced no noticeable main engine flame effects. Simultaneous three-station tracking was obtained from 165 until 437 seconds and from 598 until 645 seconds, giving about 319 seconds of usable tracking data.

The signal threshold levels and corresponding phase unlocks between 440 and 590 seconds were a result of improper handover techniques at the San

Salvador transmitter. Steps have been taken to prevent this happening on future flights.

14.7.3 MISTRAM

MISTRAM AGC data was much improved over previous flights (a summary is shown in Fig. 14-1). As with all RF systems, a dropout occurred at retro rocket ignition and lasted about 3 seconds at MISTRAM I. MISTRAM II had large attenuation spikes at retro ignition and termination. The signal between these spikes was attenuated but usable. This same phenomenon occurred with the C-band radar systems.

Handover at 350 seconds resulted in a 20 db drop at MISTRAM II lasting 5 seconds. MISTRAM I dropped to threshold and remained until re-acquisition at 375 seconds. Good signal levels were observed until 598 seconds.

14.7.4 C-BAND RADAR

AGC data received from the operating radar stations were excellent. Cape radar had a signal dropout from 77 to 110 seconds attributed to a polarization null, and Grand Turk experienced a dropout from 400 to 472 seconds. The latter resulted when another radar station interfered with the Grank Turk interrogations.

Retro rocket effects were similar to MISTRAM II, i.e., attenuation spikes at ignition and termination with normal (10 db down) signal between. A summary of C-band AGC is shown in Figure 14-1.

14.7.5 ODOP

The ODOP system operated as expected and provided useful data until approximately 500 seconds with intermittent losses occurring during the flame and retro rocket periods. An ODOP AGC coverage summary is shown in Figure 14-1.

14.7.6 ALTIMETER

The data from the altimeter were excellent. Good data were received from 167 to 795 seconds with intermittently usable data prior to 167 seconds.

14.7.7 MINITRACK

Mandy Minitrack operated satisfactorily during powered flight and in orbit. Minor flame attenuation was noted from 100 to 137 seconds and retro rocket ignition caused a 6.5-second dropout period at 148.46 seconds. LES jettison was also observed at this site. Summary coverage is shown in Figure 14-1.

14.7.8 TELEVISION

The television AGC curves indicate that good data were received between 20 and 115 seconds. At 115 seconds, flame attenuation caused a signal drop of about 20 db which recovered at 136 seconds. Retro rocket firing resulted in a 2.5-second signal dropout period. A summary is shown in Figure 14-1. Picture quality throughout the flight coverage was excellent except during retro rocket burning and separation when the picture was momentarily blacked out. One of the camera lenses (screw on type) came loose at separation, but did not greatly affect the picture quality.

14.7.9 COMMAND

The guidance command experiments performed at the Cape and at Ascension Island were performed successfully.

Destruct command systems performed as expected.

14.7.10 RF SYSTEMS ANALYSIS (S-IV)

The RF performance of S-IV-7 was satisfactory. Data from link 3 of Tel 2 were noisy from approximately 350 seconds until loss of signal. Links 1 and 2 were satisfactory during this time. However, Antigua data showed no appreciable noise after 410 seconds on link 3. Forward and reflected power measurements were steady throughout flight except at staging. It was apparent from tape recorder data that the forward power dropped and the reflected power increased, indicating that the plume from the retro and ullage rockets seriously affected the antenna impedances. Based upon limited orbital data information (Tel 2 and Tel 3), it is evident that the recorded signal strengths were substantially improved over those of S-IV-6. From a launch phase plot of link D2 (Tel 2), a serious drop occurred at approximately 125 to 140 seconds. This drop was caused by main engine flame attenuation.

14.8 OPTICAL INSTRUMENTATION

An optical instrumentation system consisting of 91 instruments was installed through the Air Force Eastern Test Range to provide a film recording of the performance and operation of the SA-7 vehicle during liftoff and through powered flight. Visual inspection of the vehicle and ground support equipment furnished information that substantiates findings of the other methods of instrumentation and also reveals pertinent facts that cannot be recorded by other means.

The overall coverage obtained for SA-7 was satisfactory. Out of 91 instruments, 9 failed to operate due to a power failure on camera station 44. Timing from camera start was recorded on all film except one sway camera. Usable time indexing (time displacement between an exposed frame and its related timing mark) was only recorded on the tracking cameras.

14.8.1 ENGINEERING SEQUENTIAL CAMERAS

Seventeen instruments were located on the launch pedestal to observe the launcher ground support equipment (GSE) and the aft section of the vehicle prior to and during liftoff. The GSE observed were the eight holddown arms, short cable mast II and IV, and the LOX fill and drain mast.

All eight holddown arms appeared to operate normally. However, the cap on the shoe pivoted on the end of the holddown arm at stub fins I-II, and III-IV fell after arm retraction. Cameras viewing the holddown arms were unrestrained and vibrated excessively prior to liftoff.

Short cable masts II and IV appeared to retract normally.

The LOX fill and drain mast appeared to retract normally, but was obscured by smoke and ice when released from the vehicle.

No movement of the heat shield during engine ignition was perceptible. The aft section of the vehicle (engines and heat shield) appeared to operate satisfactorily with no damage seen.

First motion of the vehicle liftoff was defined by the records received from two cameras positioned for this purpose.

In addition to the launch pedestal cameras, twelve cameras located on the umbilical tower viewed the upper ground support equipment of the launch complex and forward section of the vehicle. Cameras were located at the 14.6 m level to view the fuel fill and drain mast, and at the 36 m level to view the vehicle interstage. These two camera groups obtained excellent film coverage of this area and the latter was used to determine vehicle vertical displacement for the first 5.8 m of flight, even though the camera operated at three-quarters its programmed speed.

Seven cameras on the umbilical tower were oriented to cover the four swing arms. Three arms functioned properly; arm number three did not. The LH_2 vent line on this arm did not disconnect when the umbilical connector pneumatic system operated, but was disconnected when the mechanical release was actuated by the swing arm rotation.

Complete 360-degree surveillande of the launch facility and vehicle was provided by a system of 44 fixed cameras at various sites within the proximity of the launch facility. Of these 44 cameras, 35 operated properly. The failure of the nine cameras to operate was caused by power failure on station 4. Vehicle liftoff was recorded by the fixed cameras for a distance of three vehicle lengths. No malfunctions during this time were observed.

14.8.2 ONBOARD CAMERAS

Eight onboard optical cameras were on the SA-7 vehicle. All eight cameras operated as programmed and were ejected. Immediate recovery of these cameras was impossible because of Hurricane Gladys in the impact area. However, two of the cameras were recovered on San Salvador and Eleuthera Islands. Good coverage was obtained from these cameras.

14.8.3 TRACKING CAMERAS

Sixteen long focal length, ground based tracking telescopes recorded operation of the vehicle from launch through jettison of the launch escape system tower. Cameras within this system were used to record the exhaust flame pattern. A change in the flame pattern of the outboard engines was observed approximately 15.7 seconds after liftoff. Prior to this, a dark area in the flame pattern extended downward approximately 1.5 m from the engine nozzles. This dark area decreased to approximately 0.3 m in length at 15.8 seconds range time. A similar dark area has been observed on previous flights and attributed to the presence of fuel rich turbine exhaust gases introduced by the outboard engine aspirators. This same condition occurred again for this flight.

Retro rocket ignition and burning were observed by the tracking telescopes. All rockets appeared to ignite simultaneously and burn for 3.33 seconds. Separation was also observed, as well as the trajectory of the S-IV stage through jettison of the Launch Escape System tower.

14.9 ORBITAL TRACKING AND TELEMETRY SUMMARY

14.9.1 TRACKING

Orbital tracking of the SA-7 was conducted by the NASA Space Tracking and Data Acquisition

Network (STADAN) and the Manned Space Flight Network (MSFN), composed of the global network of Minitrack stations and Minitrack optical tracking stations (MOTS). The MSFN, supported by elements of DOD, is a global network of radar tracking stations. Additional tracking support was provided by the Smithsonian Astrophysical Observatory (SAO), and the North American Air Defense (NORAD).

The last beacon track of the orbiting vehicle was 4.5 hours after liftoff by Hawaii. All subsequent radar tracking was skin-track. It can be seen that the skin track mode was successful on SA-7 as it was on SA-6. The last skin track of the vehicle was at 11:18:53 U.T., September 22, 1964, by Wallops Island, Virginia.

During the first day of orbital flight there were six Minitrack passes. After the first day there was an average of nine Minitrack passes per day for the vehicle lifetime. The last vehicle contact was a Minitrack beacon signal received on 136 mc telemetry by Kano, Nigeria, on revolution 59 at 11:33:39 U.T., September 22, 1964.

There were four optical observations (Baker-Nunn Camera) reported by SAO and two optical observations (MOTS) reported by STADAN. No comments have been received concerning the stellar magnitude of the orbiting vehicle. Thirteen NORAD observations were reported.

14.9.2 TELEMETRY

Link F5 telemetry was the first link out and ceased transmitting between Pretoria, South Africa, and Carnarvon, Australia. The last link to be recorded was the spacecraft Channel A at South Point, Hawaii, more than seven hours after liftoff.

SECTION XV. SPACECRAFT

15.1 SUMMARY

This was the second Saturn flight to carry a Boilerplate Apollo spacecraft (BP-15). A description of the BP-15 spacecraft, as flown, is given in Appendix A and in Reference 5. The purpose of this flight test was to demonstrate the compatibility of the spacecraft with the launch vehicle, to determine the launch and exit environmental parameters for design verification, and to demonstrate the alternate mode of escape tower jettison, utilizing the launch escape and pitch control motors. Primary differences between the BP-15 spacecraft and the BP-13 spacecraft, flown on the SA-6 mission, were the installation of an instrumented simulated reaction control motor quad on the service module, relocation of some sensors, and the installation of live launch escape and pitch control motors in the launch escape subsystem. All mission test objectives were fulfilled.

15.2 SPACECRAFT PERFORMANCE (Ref. 5)

All mission test objectives were fulfilled by the time of orbital insertion, and additional data were obtained by telemetry through the Manned Space Flight Network until the end of effective battery life during the fourth orbital pass. Radar skin tracking was continued by the network until the spacecraft reentered over the Indian Ocean during its 59th orbital pass.

During the countdown, there were no holds caused by the spacecraft. All spacecraft subsystems fulfilled their specified functions throughout the countdown and the planned flight test period. Engineering data were received through telemetry from all but two of the 133 instrumented spacecraft measurements for the full flight test period of the mission.

The instrumentation subsystem was successful in determining the launch and exit environment, and telemetry reception of the data was continuous through launch and exit except for a short period during vehicle staging. Battery life exceeded the launch plus one orbit requirement, with main battery A providing at least 7 hours and 38 minutes of useful power, and main battery B providing at least 5 hours and 20 minutes of useful power.

The launch escape tower jettison by the alternate mode was successful. Positive ignition of the pitch control motor could not be determined; however, the general trajectory indicated that it operated properly. The launch escape motor, together with the pitch control motor, carried the tower structure safely out of the path of the spacecraft. On the basis of design values, the maximum tumbling rate (approximately 675 deg/s) observed during the launch escape motor burning period indicated possible yielding of the LES ballast mounting plate but no separation.

All strain gauge, pressure, and accelerometer measurements indicated that the spacecraft performed satisfactorily in the launch environment. Command module conical surface static pressures correlated closely with wind tunnel data, and the product of angle-of-attack and dynamic pressure (αq) did not exceed 4.78 deg N/cm^2 (1000 deg lb$_f$/ft^2). The venting system of the service module performed satisfactorily.

A 1.8 g, peak-to-peak, 10 Hz vibration was noted during holddown. Other vibration modes were similar to those experienced during the BP-13 spacecraft flight. One of the simulated reaction control subsystem quad assemblies was instrumented for vibration on the BP-15 spacecraft flight. The measured vibration levels were above the design limit.

The strain measurements in the command module and service module indicated that all bending moments are within the design limits.

The launch heating environment of the BP-15 spacecraft was similar to that encountered by the BP-13 spacecraft. Peak values at most points for the two flights were approximately equal; however, the influence of surface irregularities, as well as circumferential variations in heating, was somewhat different for the two flights because of differences in trajectory and angle-of-attack. Both command and service module heating rates were within the predicted range. The heat protection equipment on the launch escape subsystem (LES) was subjected to temperatures much lower than the design limits which were established on the basis of an aborted mission.

Flight data from the instrumented simulated RCS quad assembly differed from the values issued for design criteria for the RCS. Additional investigation and analysis will be necessary to complete the design and flight data criteria.

Satisfactory engineering data, covering designated parameters of spacecraft environment for a Saturn V type launch trajectory, were obtained for use in verifying launch and exit design criteria.

SECTION XVI. SUMMARY OF MALFUNCTIONS AND DEVIATIONS

The flight test of Saturn SA-7 did not reveal any malfunctions or deviations which could be considered a serious system failure or design deficiency. However, a number of deviations did occur and are summarized.

Corrective measures were recommended by the MSFC Laboratory concerned for some of the items listed. These are marked with an asterisk. Each item is listed in the area where the deviation and/or malfunction occurred.

Launch Operations

1. Inadvertent Firex System activation on the service structure during air conditioning duct removal (Para. 3.4.1).

2. S-I hydraulic pump temperature OK interlock malfunction (Para. 3.4.1).*

3. Problems with Eastern Test Range Instrumentation (ETR) (Table 3-II).

4. Swing Arm 3 was disconnected by mechanical release instead of umbilical connector pneumatic system operation (Para. 3.7.3).

Propulsion

1. S-I stage combustion stability monitor on engine 3 indicated large pressure disturbances during ignition (Para. 6.2.3).

2. The flight fuel and LOX specific weights are significantly different from predicted due to temperature change (para. 6.2.3).

3. Higher than predicted S-IV cutoff impulse (Para. 6.7.3.4).*

4. Minimum required LH_2 pump inlet conditions were not achieved for approximately 30 seconds (Para. 6.8.1.1).

Guidance and Control

1. Some evidence for an external moment acting in both pitch and yaw planes with a shape related to dynamic pressure was noted (Para. 7.3.1.1 and 7.3.1.2).

2. Large stabilized platform leveling and azimuth alignment errors caused the actual space-fixed velocity vector at S-IV cutoff to be 1.8 m/s larger than the digital computer value (Para. 7.6.1 and 7.6.2).*

3. The digital computer's gravity term was slightly in error before liftoff (Para. 7.7.1).*

4. The digital computer sequencing discretes were issued with a small time delay (Para. 7.7.1).*

Orbital Attitude

1. Radar skin tracking signal strength analysis, though inconclusive, indicates a vehicle tumble rate of approximately 6 deg/s at the end of orbital venting (Para. 8.2).

Separation

1. Evidence indicates that there was a large total misalignment (1.2 deg ± 0.2 deg) of the ullage rockets (Para. 9.1 and 9.2.2).

Structures

1. The measured vibrations for combustion chamber domes of engines 1, 3, 5 and 7 were inconsistent with previous static and flight test history (Para. 10.2.4.2).

2. Debonding of aft interstage after separation (Para. 10.4).

Vehicle Electrical Systems

1. An inflight control relay for link F6 was connected to the short life battery instead of the long life battery (Para. 12.4).*

2. S-IV inverter output voltage dropped momentarily at separation (Para. 12.3).

Instrumentation

1. A total of 8 measurement malfunctions resulted in total loss of information (Para. 14.1).

2. A total of 14 measurements were scrubbed before launch (Para. 14.1).

3. The long-dwell commutator clock malfunctioned from liftoff through separation (Para. 14.3.1).

APPENDIX A

VEHICLE DESCRIPTION

A.1 SUMMARY

The flight of Saturn SA-7 was the third flight test of a Block II Saturn I research and development vehicle, and involved the second consecutive successful orbiting of the Boilerplate Apollo command and service modules. The vehicle, which measured approximately 58 m (190.4 ft) in length, consisted of four distinct units: the uprated S-I stage, S-IV stage, Instrument Unit, and Boilerplate Apollo command and service modules (Fig. A-1). The changes which distinguish this vehicle from the SA-6 flight vehicle include:

1. Elimination of the S-IV LOX tank backup pressurization system.

2. Addition of non-propulsive venting system on S-IV stage.

3. Elimination of ST-90S stabilized platform system and supporting equipment.

4. ST-124 system and control rate gyros active in vehicle control from liftoff.

5. Live launch escape and pitch control motors used to eject launch escape system.

The following is a description of the four major components of the vehicle.

A.2 S-I STAGE

A cluster of eight uprated H-1 engines powered the S-I stage (Fig. A-2) producing a total sea level thrust of 6.67 million Newtons (1.5 million lb). The four outboard engines were gimbal mounted to provide pitch, yaw, and roll control. All engines were canted to minimize the disturbing moments that would be induced by an engine failure at critical dynamic pressure. Propellants were supplied to the engines through suction lines from an arrangement of nine propellant tanks. These tanks consisted of four 1.78 m (70 in.) diameter fuel tanks, four 1.78 m (70 in.) diameter LOX tanks and a 2.67 m (105 in.) diameter center LOX tank. Each outboard tank (LOX and fuel) supplied propellants to one inboard and one outboard engine. The center LOX tank supplied the outboard tanks through the LOX interchange system. Thrust and longitudinal loads were carried by the pressurized LOX tanks. The propellant tanks were retained at the forward end of a structural member called a spider beam. Four 151,240 N (34,000 lb) thrust solid propellant retro rockets on the spider beam decelerated the S-I stage for inflight separation from the S-IV stage.

Four large fins and four stub fins were attached to the base of the S-I stage to provide flight stability plus support and holddown points at launch. Each large fin projected an area of approximately 11.24 m^2 (121 ft^2) and extended radially about 2.74 m (9 ft) from the outer surface of the thrust structure. Four stub fins were attached midway between the main fins. Stub fins II, III and IV also provided enclosure and attachment for the three 0.0348 m (12 in.) diameter ducts used to exit chilldown hydrogen from the S-IV stage. Four fairings between the larger fins and stub fins enclosed the inboard engine turbine exhaust ducts.

A.3 S-IV STAGE

Six gimbal mounted RL10A-3 engines, providing 400,340 N (90,000 lb) total thrust at an altitude of 60,960 m (200,000 ft), powered the vehicle during the S-IV stage portion of powered flight. The engines were mounted on the thrust structure with a six-degree outward cant angle from the vehicle longitudinal axis. Each engine had a gimbal capability of a plus or minus four-degree square pattern for pitch, yaw, and roll control. The S-IV stage (Fig. A-3) carried approximately 45,359 kg (100,000 lb) of usable liquid hydrogen and liquid oxygen.

The LH_2 (fuel) system consisted of a cylindrical container with a bulkhead at each end. LH_2 flowed from the container through six suction lines, each of which connected to one RL10A-3 engine.

The LOX system consisted of a 35.74 cubic meters (1262 cubic ft) container. Vacuum-jacketed suction lines transferred the LOX from the container through the antivortex screen, filter assembly and sump cone. The lower suction line flange ends were connected to the LOX inlet flange on each engine.

The thrust structure provided engine thrust transfer to the LH_2 and LOX container.

Four 15,125 N (3400 lb) thrust solid propellant ullage rockets provided proper positioning of the propellants prior to the S-IV stage ignition.

A.4 INSTRUMENT UNIT

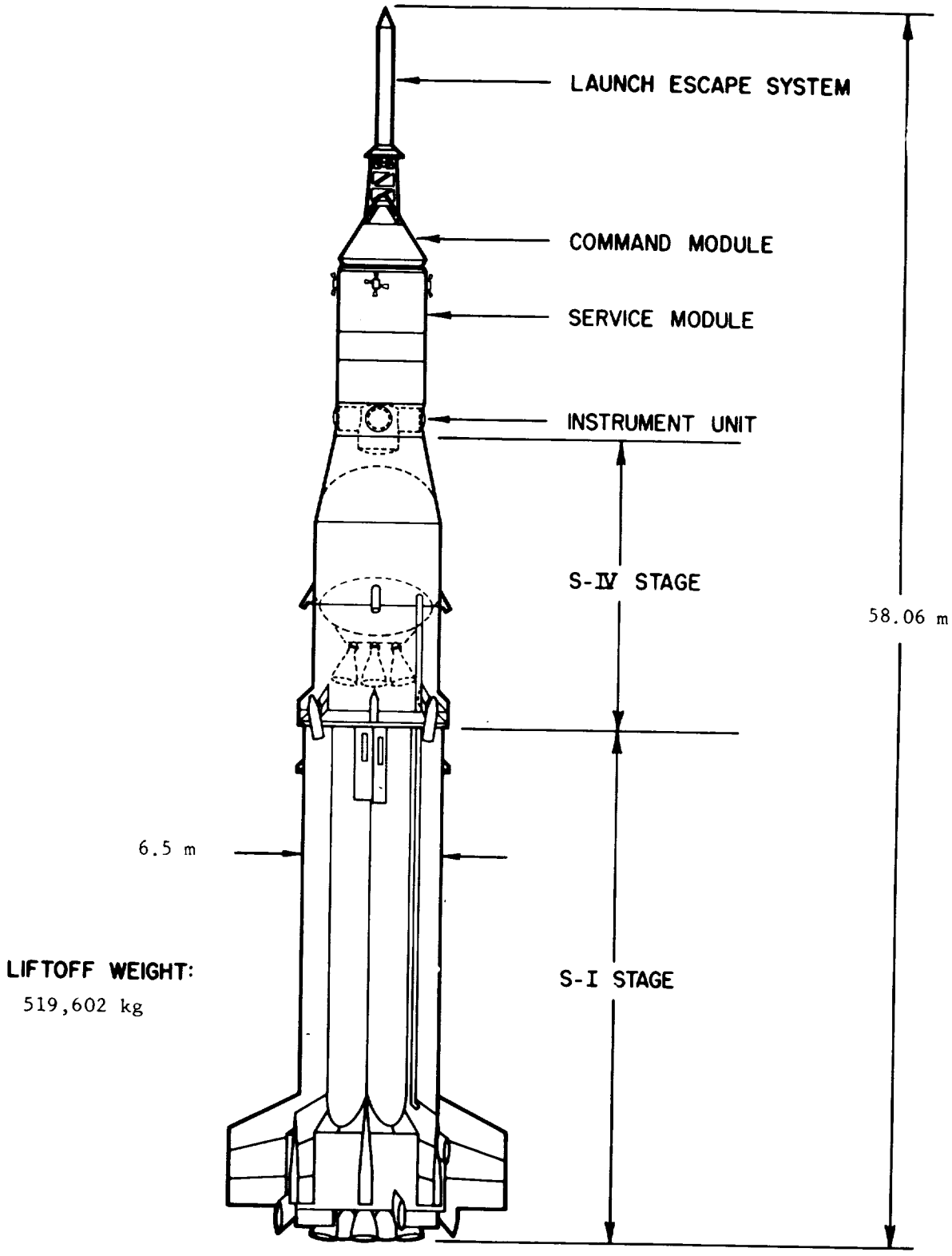

FIGURE A-1. SA-7 VEHICLE CONFIGURATION

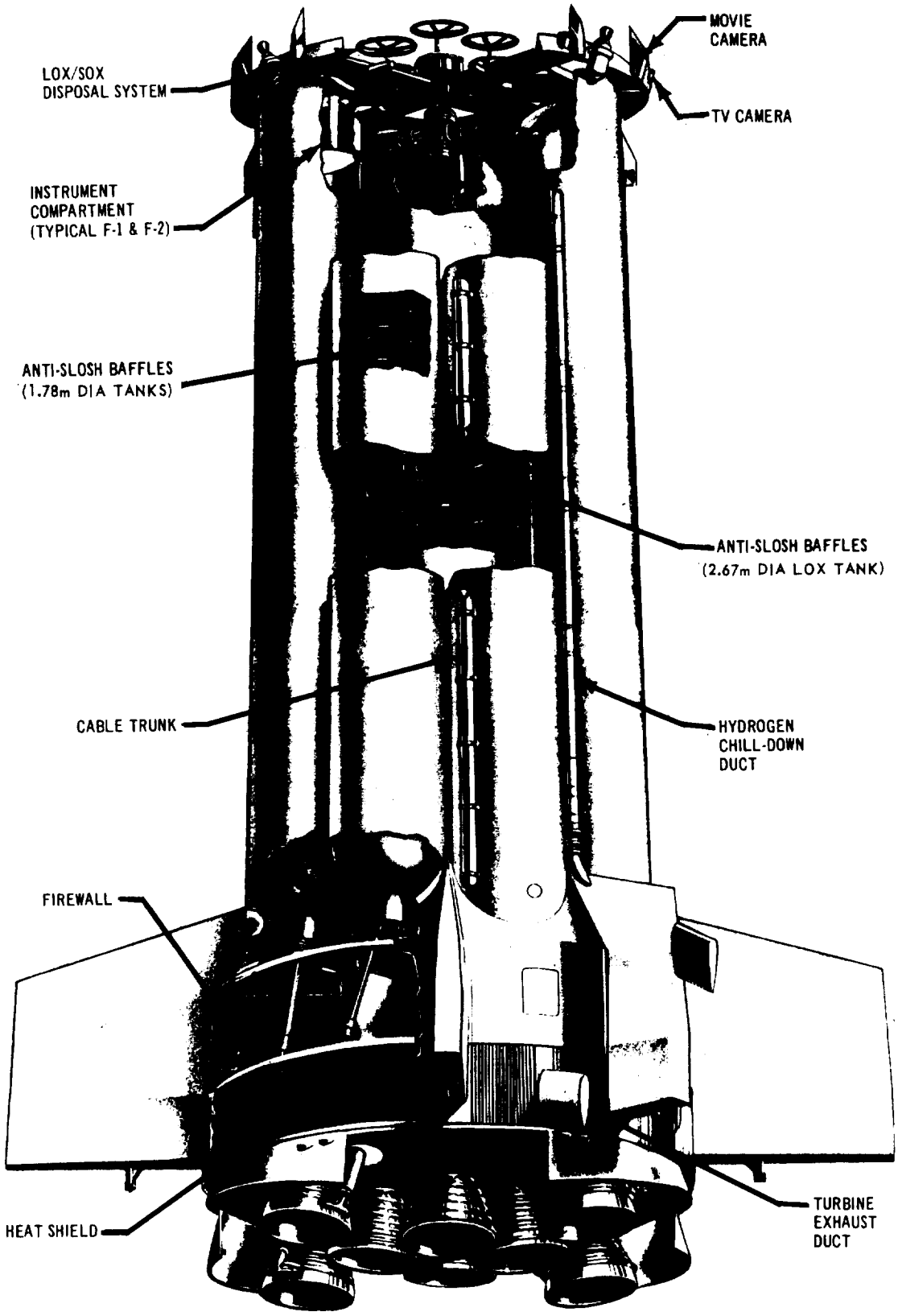

FIGURE A-2. S-I STAGE

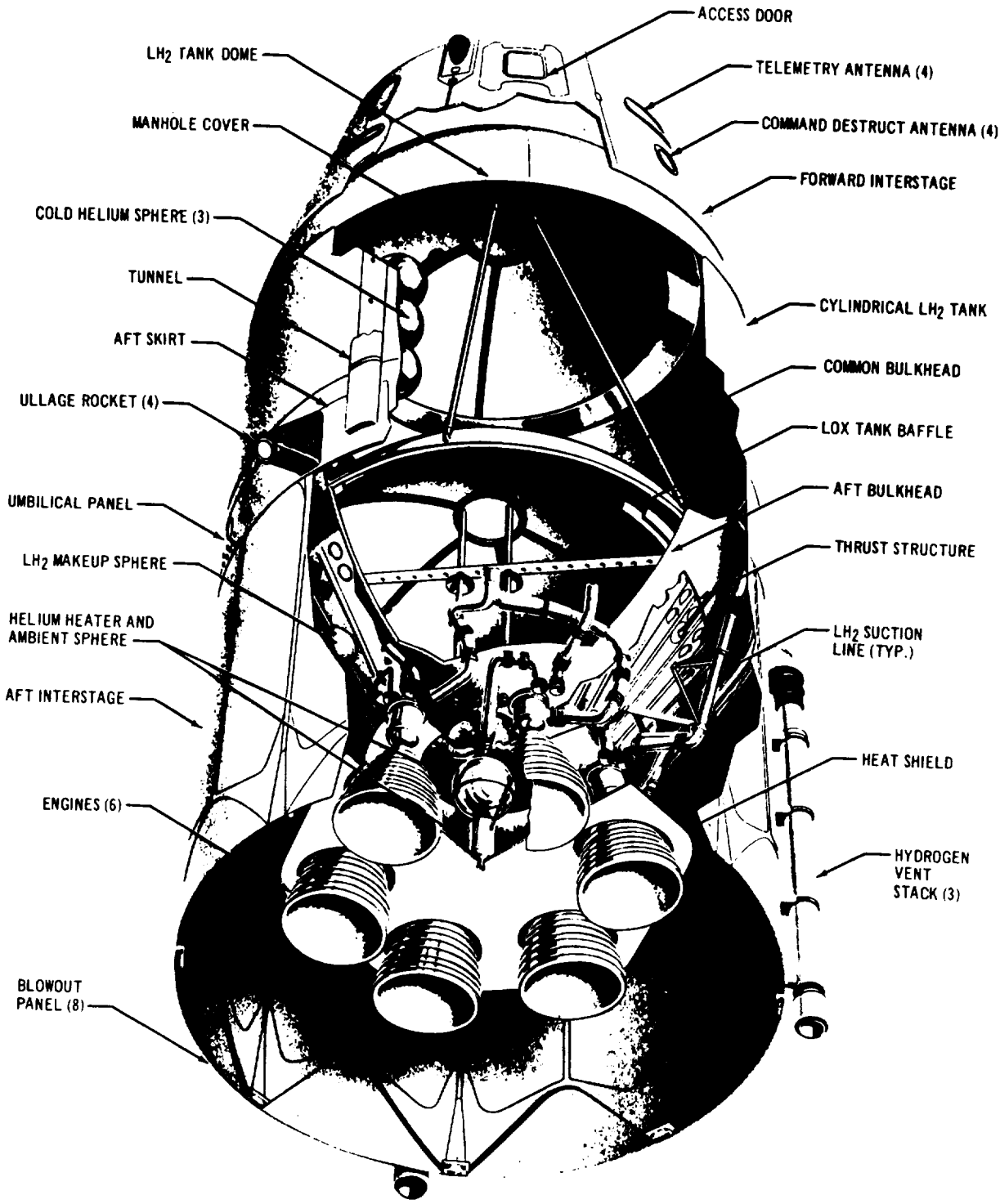

FIGURE A-3. S-IV STAGE

The Instrument Unit (Fig. A-4) located between the S-IV stage and the payload, provided an environmentally conditioned compartment to house electronic equipment. Structurally, this unit consisted of four 1.02-meter-diameter (40 in.) tubes extending radially from a 1.78-meter-diameter (70 in.) center tube. The overall diameter and length were 3.91 m (154 in.) and 2.31 m (91 in.) respectively. The equipment installation included guidance and control, telemetry, tracking, electrical power sources, and distributors. The ST-124 system and control rate gyros were active in vehicle control from liftoff.

A.5 PAYLOAD

The Apollo Boilerplate 15 (BP-15) spacecraft, shown in Figure A-5, was of a configuration essentially the same as that of the BP-13 spacecraft flown on SA-6 (Ref. 6 and 7). The primary differences were as follows:

The LES motors for pitch control, tower jettison, and launch escape were live. However, there were no initiators installed in the jettison motor, and the wiring circuit from the sequencers to this motor was purposely not completed so as to simulate a jettison motor failure. The alternate mode of tower jettison (by firing only the launch-escape and pitch-control motors) was used.

Four simulated RCS quad assemblies were attached to the upper portion of the SM exterior, 90 degrees apart. In order to duplicate the aerodynamic characteristics of the production units, the simulated units were similar in size and shape and were arranged on the SM in the same location as they would be found on the production spacecraft. The RCS quad assembly located near the Fin I axis was instrumented to provide temperature and vibration measurements.

The spacecraft weight when inserted into orbit was 7816 kg (17,231 lbm); the spacecraft weight at liftoff was 10,813 kg (23,838 lbm). The BP-15 spacecraft weight was greater than that of BP-13 spacecraft by 94.3 kg (208 lbm) at orbit insertion and 134 kg (295 lbm) at liftoff.

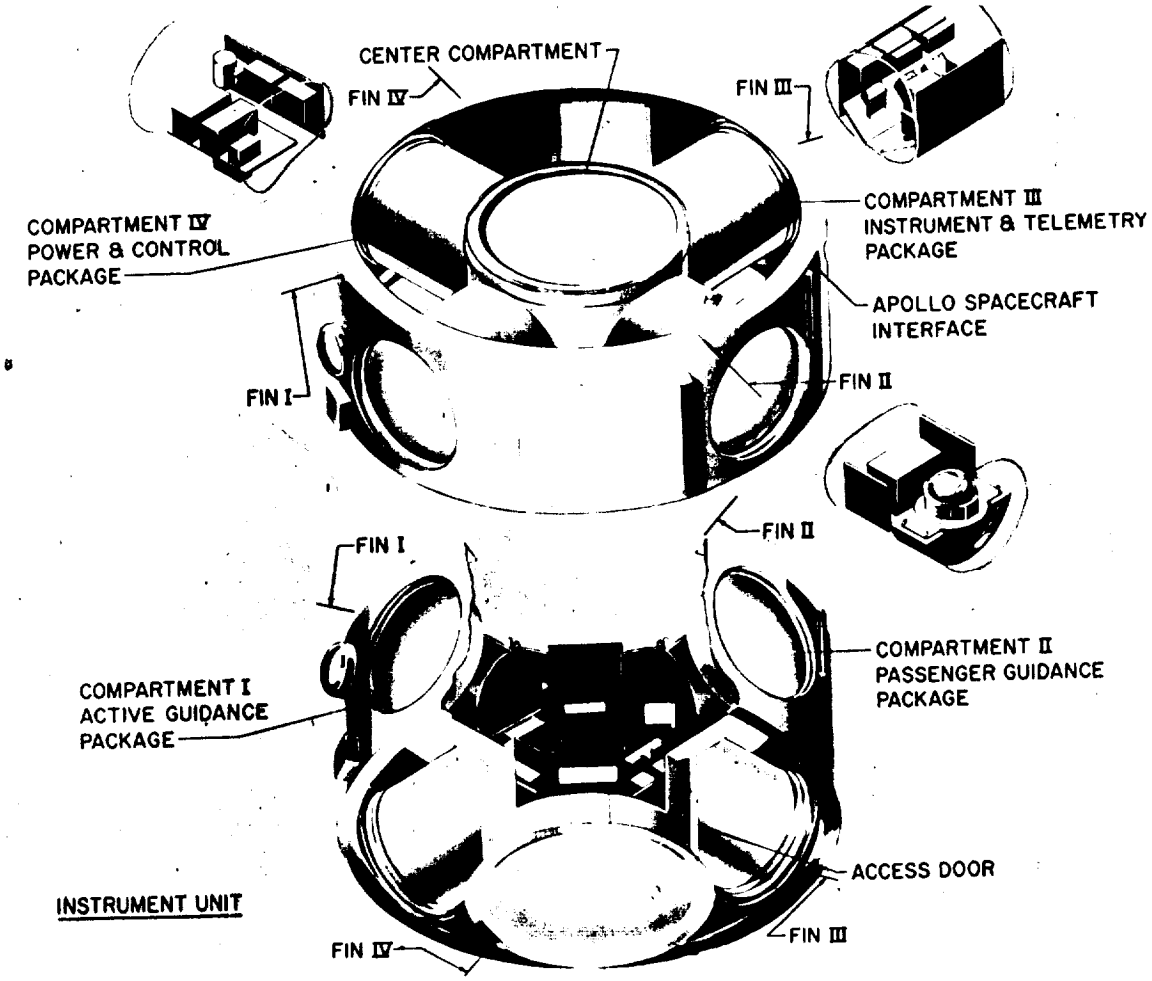

FIGURE A-4. INSTRUMENT UNIT

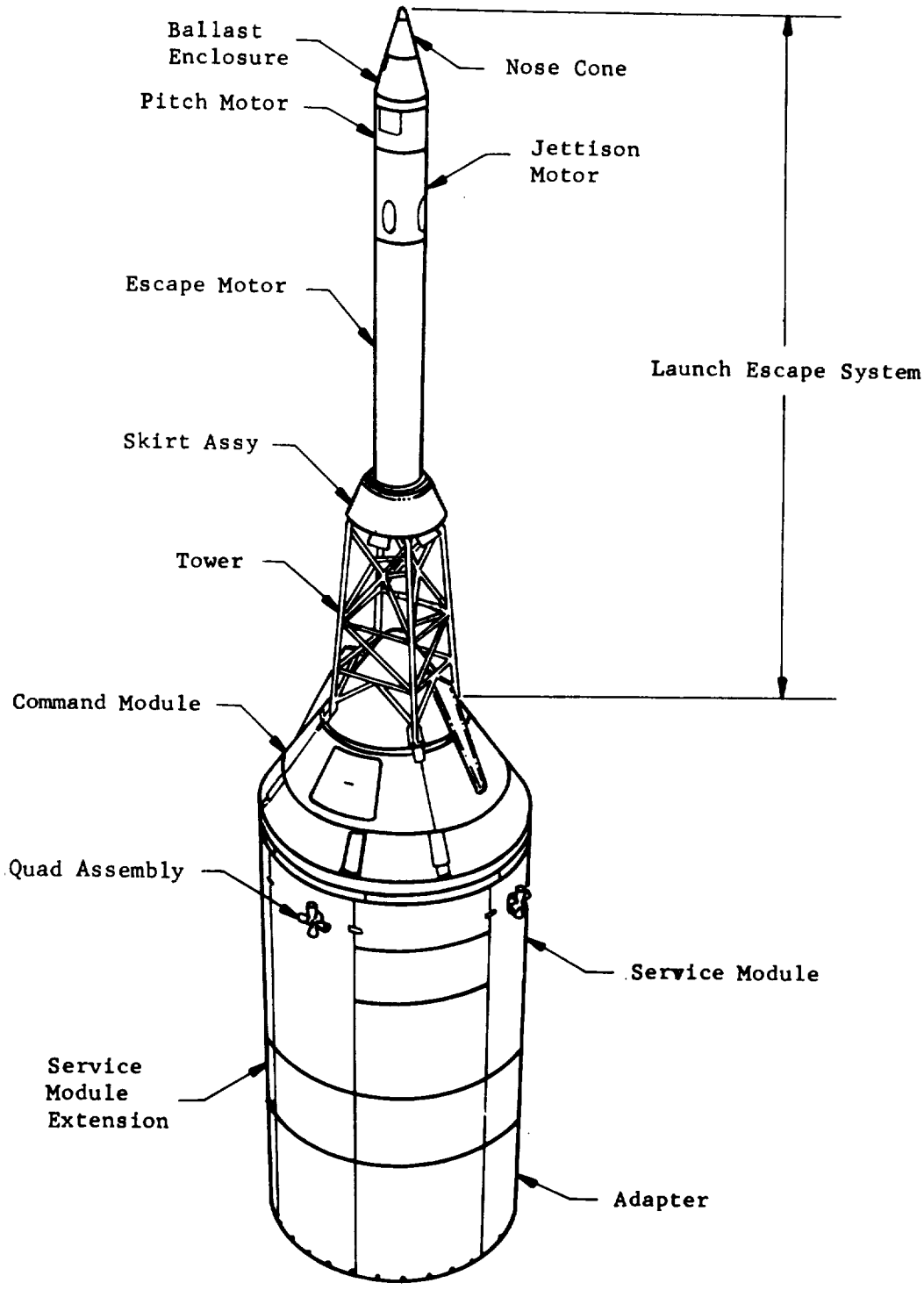

FIGURE A-5. SA-7 PAYLOAD

REFERENCES

1. Memo: R-P&VE-VAW-64-103, August 5, 1964, (Confidential), "Final Predicted Mass Characteristics of the Saturn I, SA-7, Vehicle," J. C. Glover.

2. NASA TM X-53120, August 13, 1964, (Confidential), "Final Predicted Trajectory and Dispersion Study for Saturn I Vehicle SA-7," by J. D. Weiler and O. M. Hardage, Jr.

3. MPR-SAT-FE-64-16, August 7, 1964, (Confidential), "Results of the Sixth Saturn I Launch Vehicle Test Flight," by Saturn Flight Evaluation Working Group.

4. MSC-R-A-64-2, June 18, 1964, (Confidential), "Post Launch Report for Apollo Mission A-101 (BP-13)."

5. MSC-R-A-64-3, October 10, 1964, (Confidential), "Post Launch Report for Apollo Mission A-102 (BP-15)."

6. MTP-M-S&M-E-61-2, May 12, 1961, (Confidential), "Saturn Block II Design Criteria," Vehicle Systems Integration Office, Propulsion and Vehicle Engineering Laboratory.

7. "SA-7 Saturn Vehicle Data Book," July 15, 1963, (Confidential), Vehicle Engineering Branch, Propulsion and Vehicle Engineering Laboratory.

8. MPR-SAT-FE-64-15, April 1, 1964, (Confidential), "Results of the Fifth Saturn I Launch Vehicle Test Flight," by Saturn Flight Evaluation Working Group.

9. Memo: R-ASTR-NG-102, September 15, 1964, (Confidential), "The Effect of Known Guidance Errors on SA-7 Flight Performance," J. L. Mack.

10. Memo: R-ASTR-G-263-64, August 11, 1964, (Confidential), "Test Data From Serial Number 4, ST-124 Platform System for SA-7," Carl H. Mandel.

11. Memo: R-ASTR-G, November 8, 1962, (Confidential), "ST-124 Instrument Errors," C. H. Mandel.

A

B

C

D

E

I

J

L

V

W

U

V

W

DISTRIBUTION

DIR
Dr. von Braun

DEP-T
Dr. Rees

DEP-A
Mr. Gorman

AST-S
Dr. Lange

E-DIR
Mr. Maus

I-DIR
Gen. O'Connor
Dr. Mrazek

I-I/IB-MGR
Col. James

I-I/IB-T
Mr. Fikes (21)

I-V-MGR
Dr. Rudolph

R-DIR
Mr. Weidner

R-AS
Mr. Williams

R-SA
Dr. Kuettner
Mr. Dannenberg

R-AERO-DIR
Dr. Geissler
Mr. Jean

R-AERO-A
Mr. Dahm

R-AERO-AT
Mr. Wilson

R-AERO-D
Mr. Horn

R-AERO-F
Dr. Speer (35)

R-AERO-FF
Mr. Lindberg

R-AERO-G
Mr. Baker

R-AERO-P
Mr. McNair

R-AERO-Y
Mr. Vaughan

R-AERO-YT
Mr. O. E. Smith

R-ASTR-DIR
Dr. Haeussermann

R-ASTR-E
Mr. Fichtner

R-ASTR-F
Mr. Hosenthien

R-ASTR-I
Mr. Hoberg
Mr. Powell

R-ASTR-IE
Mr. Price

R-ASTR-IMD
Mr. Avery

R-ASTR-N
Mr. Moore

R-ASTR-NGI
Mr. Nicaise

R-ASTR-S
Mr. Noel

R-COMP-DIR
Dr. Hoelzer

R-COMP-R
Mr. Prince

R-COMP-RR
Mr. Cochran

R-ME-DIR
Mr. Kuers

R-ME-D
Mr. Eisenhardt

R-ME-M
Mr. Orr

R-ME-T
Mr. Franklin

R-ME-X
Mr. Wuenscher

R-P&VE-DIR
Mr. Cline
Mr. Palaoro

R-P&VE-A
Mr. Goerner

R-P&VE-M
Dr. Lucas

R-P&VE-P
Mr. Paul (2)

R-P&VE-PPE
Mr. McKay (2)

R-P&VE-S
Mr. Kroll
Mr. Hunt

R-P&VE-SVM
Mr. Gassaway

R-QUAL-DIR
Mr. Grau

R-QUAL-A
Mr. Henritze

R-QUAL-P
Mr. Brooks

R-QUAL-PI
Mr. Corder

R-QUAL-QVS
Mr. Peck

R-QUAL-R
Mr. Brien
Mr. Smith

R-RP-DIR
Dr. Stuhlinger

R-TEST-DIR
Mr. Heimburg
Mr. Tessmann

R-TEST-C
Mr. Grafton

R-TEST-I
Dr. Sieber

R-TEST-M
Mr. Edwards

R-TEST-S
Mr. Driscoll

R-TEST-SB
Mr. Reilman

MS-H
Mr. Akens

MS-IP
Mr. Remer (2)

MS-IL
Miss Robertson (15)

LVO-DIR
Dr. Gruene

LVO-G
Mr. Rigell

LVO-M
Mr. Pickett

KSC-ED
Dr. Burns

KSC-ED4
Mr. Jelen

KSC-ET
Mr. Collins

EXTERNAL

Headquarters, National Aeronautics & Space Administration
Washington, D. C. 20546
Assistant Deputy Administrator: Dr. G. L. Simpson, Jr.
Office of Policy Planning: Dr. G. L. Simpson, Jr.
Office of Technology Utilization: Breene M. Kerr
Scientific & Technical Information Division Director: Melvin S. Day
Office of the Associate Administrator: Dr. Robert C. Seaman, Jr.
Office of Industry Affairs
Reliability & Quality Assurance Office: John E. Condon

Office of Manned Space Flight
Associate Administrator: Dr. G. E. Mueller
Apollo Program Director: Maj. Gen. S. C. Phillips (USAF)
MSF Field Center Development Director: Capt. Robert Freitag (USN)

Office of Space Science and Applications
Associate Administrator: Dr. Homer E. Newell
Director of Engineering: Robert F. Garbarini
Launch Vehicle & Propulsion Programs Director: Vincent L. Johnson (10 copies)
Meteorological Programs Director: Dr. Morris Tepper

Office of Advanced Research and Technology
Associate Administrator: Dr. Raymond L. Bisplinghoff
Chemical Propulsion Division Director: Adelbert Tischler

Director, Ames Research Center: Dr. Smith J. DeFrance
National Aeronautics & Space Administration
Moffett Field, California 94035

Director, Flight Research Center: Paul F. Bikle
National Aeronautics & Space Administration
P. O. Box 273
Edwards, California 93523

Goddard Space Flight Center
National Aeronautics & Space Administration
Greenbelt, Maryland 20771
Attn: Herman LaGow, Code 600

John F. Kennedy Space Center
National Aeronautics & Space Administration
Kennedy Space Center, Florida 32899
Attn: Technical Library
Mrs. L. B. Russell

Director, Langley Research Center: Floyd L. Thompson
National Aeronautics & Space Administration
Langley Station
Hampton, Virginia 23365

Director, Lewis Research Center: Dr. Abe Silverstein
National Aeronautics & Space Administration
21000 Brookpark Road
Cleveland, Ohio 44135

Manned Spacecraft Center
National Aeronautics & Space Administration
Houston, Texas 77058
Attn: Director: Dr. Robert R. Gilruth
Robert Smith, Code EC6 (5)
Robert E. McKann, Code PT6 (3)
Charles M. Grant, Code BF3 (2)

Director, Wallops Station: R. L. Krieger
National Aeronautics & Space Administration
Wallops Island, Virginia 23337

Director, Western Operations Office: Robert W. Kamm
National Aeronautics & Space Administration
150 Pico Blvd.
Santa Monica, California 90406

Scientific and Technical Information Facility
P. O. Box 5700
Bethesda, Maryland 20014
Attn: NASA Representative (S-AK/RKT) (25)

Jet Propulsion Laboratory
4800 Oak Grove Drive
Pasadena, California 91103
Attn: Irl Newlan, Reports Group
H. Levy, CCMTA (4)

Office of the Asst. Sec. of Defense for Research & Engineering
Room 3E1065
The Pentagon
Washington, D. C. 20301
Attn: Tech Library

Director of Guided Missiles
Office of the Secretary of Defense
Room 3E131
The Pentagon
Washington, D. C. 20301

Central Intelligence Agency
2430 E. Street, N. W.
Washington, D. C. 20037
Attn: Liaison Div. OCD (2)

Director, National Security Agency
Ft. George Mead, Maryland 20755
Attn: C3/TDL

U. S. Atomic Energy Commission, Sandia Corp.
University of California Radiation Lab.
Technical Information Division
P. O. Box 808
Livermore, California 94551
Attn: Clovis Craig

U. S. Atomic Energy Commission, Sandia Corp.
Livermore Br, P. O. Box 969
Livermore, California 94551
Attn: Tech Library

Commander, Armed Services Technical Information Agency
Arlington Hall Station
Arlington, Virginia 22212
Attn: TIPCR (Transmittal per Cognizant Act Security Instruction) (5)

Commanding General
White Sands Proving Ground
New Mexico 88002
Attn: ORD BS-OMTIO-TL (3)

Chief of Staff, U. S. Air Force
The Pentagon
Washington, D. C. 20330
1 Cpy marked for DCS/D AFDRD
1 Cpy marked for DCS/D AFDRD-EX

Commander-in-Chief
Strategic Air Command
Offutt AFB, Nebraska 68113
Attn: Director of Operations, Missile Division

Commander
Arnold Engineering Development Center
Arnold Air Force Station, Tennessee 37389
Attn: Tech Library (2)

Commander
Air Force Flight Test Center
Edwards AFB, California 93523
Attn: FTOTL

Commander
Air Force Missile Development Center
Holloman Air Force Base
New Mexico 88330
Attn: Tech Library (SRLT)

Commander, AF Missile Test Center
Patrick AFB, Florida 32925
Attn: Technical Information Intelligence Office, MTGRY (3)

DISTRIBUTION (Cont'd)

Headquarters
6570th Aerospace Medical Division (AFSC)
U. S. Air Force
Wright Patterson Air Force Base, Ohio 45433
Attn: H. E. Vongierke

Systems Engineering Group (RTD)
Attn: SEPIR
Wright-Patterson AFB, Ohio 45433

Director
U. S. Naval Research Laboratory
Washington, D. C. 20390
Attn: Code 2027 (2)

Chief of Naval Research
Department of Navy
Washington, D. C. 20390
Attn: Code 463

Chief, Bureau of Weapons
Department of Navy
Washinton, D. C. 20390
1 Cpy to RESI, 1 Cpy to SP,
1 Cpy to AD3, 1 Cpy to REW3

Commander
U. S. Naval Air Missile Test Center
Point Mugu, California 93041

AMSMI-RBLD; RSIC (3)
Bldg. 4484
Redstone Arsenal, Alabama

Aerospace Corporation
2400 East El Segundo
El Segundo, California 90245
Attn: D. C. Bakeman

Aerospace Corporation
Reliability Dept.
P. O. Box 95085
Los Angeles, California 90045
Attn: Don Herzstein

Bellcomm, Inc.
1100 Seventeenth St. N. W.
Washington, D. C. 20036
Attn: Miss Scott, Librarian

The Boeing Company
Saturn Booster Branch
P. O. Box 26088
New Orleans, Louisiana 70126
Attn: R. H. Nelson (3)

Chrysler Corporation Space Division
Michoud Operations
Dept. 2812
P. O. Box 29200
New Orleans, La. 70129
Attn: Mr. Leroy Smith (8)

Chrysler Corporation Space Division
Huntsville Operations
Dept.4800
1312 N. Meredian St.
Huntsville, Alabama 35801
Attn: H. Bader, Jr. (3)

Douglas Aircraft Company, Inc.
Missile and Space Systems Engineering
3000 Ocean Park Blvd.
Santa Monica, California 90405
Attn: T. D. Smith (1)
A. J. German (5)
D. A. Petty (2)

Douglas Aircraft Company, Inc.
Marshall Space Flight Center
Bldg. 4481, Room 61
Huntsville, Alabama 35812
Attn: R. A. Ammons (5)

Grumman Aircraft Engineering Corp.
Apollo Space Program Office
Bethpage, Long Island, N. Y. 11714
Attn: Jack Small (3)

International Business Machine
System Design, Dept. 229
150 Sparkman Dr. NW
Huntsville, Alabama 35808
Attn: R. E. Poupard (2)

Martin Company
Space Systems Division
Baltimore, Maryland 21203
Attn: W. P. Sommers

North American Aviation
Space & Information Division Systems
12214 S. Lakewood Blvd.
Downey, California 90241
Attn: A. Shimizu (2)
W. F. Parker (1)

Pratt & Whitney Aircraft
Suite 4, Holiday Office Center
Huntsville, Alabama 35801
Attn: J. C. Hammond, Jr. (2)

Radio Corporation of America
Defense Electronic Products
Data Systems Division
8500 Balboa Blvd.
Van Nuys, California 91406

Rocketdyne
6633 Canoga Avenue
Canoga Park, California 91303
Attn: O. I. Thorsen (3)